HIGH-RESOLUTION SEQUENCE STRATIGRAPHY OF THE GALLUP SYSTEM

HIGH-RESOLUTION SEQUENCE STRATIGRAPHY, FACIES ANALYSIS, AND SEDIMENT QUANTIFICATION OF THE CRETACEOUS GALLUP SYSTEM, NEW MEXICO, U.S.A.

By WEN LIN, B.Sc., M.Sc.

A Thesis Submitted to the School of Graduate Studies in Partial Fulfillment of the Requirements for the Degree Doctor of Philosophy

McMaster University Doctor of Philosophy (2018)

Hamilton, Ontario, Canada (Geography and Earth Sciences)

TITLE: High-Resolution Sequence Stratigraphy, Facies Analysis, and Sediment Quantification of the Cretaceous Gallup System, New Mexico, U.S.A.

AUTHOR: Wen Lin

Bachelor of Science in Geology

China University of Geosciences, 2005

Master of Science in Petroleum Geology

China University of Geosciences, 2008

SUPERVISOR: Dr. Janok P. Bhattacharya, Professor

NUMBER OF PAGES: 255

ABSTRACT

The quantification of sediment budget in a well-defined ancient source-to-sink (S2S) system is vital to understand Earth history and basin evolution. Fulcrum analysis is an effective approach to estimate sediment volumes of depositional systems, given total mass balance throughout source areas to basins. The key to this approach is to quantify sediment in a closed S2S system with time controls. We analyzed Allomember E of the Cretaceous Dunvegan Alloformation in the Western Canadian Sedimentary Basin to test this sediment estimation approach. The results indicate that the sediment transported by the trunk-river generically matches the sediment estimated to be deposited in the basin. The upper-range estimate may suggest mud dispersal southward by geostrophic currents.

Deciphering the relationships between traditional lithostratigraphy and sequence stratigraphy is the key to correctly understanding time-stratigraphic relationships. High-resolution sequence stratigraphic analysis of the Cretaceous Gallup system documents the high-frequency depositional cyclicity using detailed facies analysis in extensively exposed outcrops in northwestern New Mexico, US. We identified thirteen stratigraphic sequences, consisting of twenty-six parasequence and sixty-one parasequences. Shoreline trajectories are evaluated based on the geometry of the parasequences. The results show the previously identified sandstone tongues are equivalent to high-frequency sequence sets. The depositional duration estimates of respective sequence stratigraphic units, associated with the estimated changes in relative sea level, imply that Milankovitch-cycle-dominated glacio-eustasy may be the predominant control on the high-frequency sequence stratigraphy.

Shoreline processes are more dynamic and complicated with mixed-energy dominance. The re-evaluation of the depositional environments of the Gallup system and the reconstructions of the paleogeography with temporal controls help to examine the depositional evolution in space and time. Paleogeographic reconstructions at parasequence scales allow for the documentation of the process-based lateral facies variations and the depositional evolution. The distinction between different wave-dominated facies associations is proposed based on this process-based facies analysis.

ACKNOWLEDGEMENTS

First I would like to express my sincere gratitude to my academic advisor, Dr. Janok P. Bhattacharya for his tremendous help and continuous guidance. My Ph.D. study could not be completed without an advisor like him: always supportive, knowledgeable, passionate, and positive. I thank him for his patience, encouragement, and endless editing on my writing.

I would like to thank my Ph.D. supervisory committee members, Dr. Andrew Miall, Dr. Joe Boyce, and Dr. Carolyn Eyles for their great help, valuable suggestions, and positive feedback through my research. I thank them for being there and guiding me through all four years.

I am grateful to Monica Wiercigroch, Sean Karner, and Andrew Stockford for their tremendous assistance in the field. It always feels good and safe to have someone to talk to in the desert. Thanks are also given to my labmates, especially Logan Jung-Ritchie, Curtis Ferron, Rachel Nelson, Matt Leung, Zach Waller, and Madison Macandrew, who volunteered to be my field assistants, even for only one day. I appreciate all the discussions, supports, and fun I got from my lab.

Funding for the projects constituting this dissertation was generously supplied by NSERC Discovery Grant RPG IN05780-14 to Dr. Bhattacharya, by sponsors of the McMaster University Quantitative Sedimentology Laboratories (QSL) including BP and Inpex, and by the Susan Cunningham Research Chair in Geology. This work was also partially supported by AAPG "Martin D. Hewitt" Named Grant and GSA Graduate Student Research Grant.

I am also grateful to the Navajo Nation for permitting the fieldwork and to the Navajo people for allowing us to work on their lands—some outcrops are legitimately in their backyards. I thank the family who fixed our flat tire and the people who directed the ways to outcrops. Thank for their curiosity that allows me to practise explaining my research in plain language.

Special thanks are given to Dr. Henry Posamentier, my mentor for life. I thank Henry for his great support at different stages of my life and for the countless reference letters he wrote for me, including the one that got me in my Ph.D. program. He is my role model, the one whom I designed my own career path according to.

I would like to mention Zhiyang Li, who did his Masters with Dr. Bhattacharya. We met at a field trip in Utah and became best friends since then. I know I have someone whom I can talk to, even complain to during the hard time of my Ph.D. study, and who always understands and supports.

I am also grateful to all the people I met at the conferences for their positive feedback to my work, valuable suggestions, and encouragement. I thank all the editors and reviewers for my journal papers too. Their help takes my work to the public.

Last but not least, I would like to express my deepest gratitude to my family: my wife, my son, my daughter, my parents, and my parents-in-law. I thank my wife for her infinitive support, her understanding, and her encouragement. Thank her for her firmness and decisiveness that made my Ph.D. decision happen. She is my soul mate, whom I always rely on in many aspects. I thank my son, Nicholas for his existence and his love, which is always my motivation to move forward, and for listening to me talking about

rocks and fossils. I cannot forget the moment that he made me explain what a sequence boundary is to him. I am encouraged whenever he says he wants to be an earth scientist in the future. I thank my daughter, Alice for her kindness and happiness, for saying “alright” whenever I turned her down for playing because I was busy, and for making me laugh and refreshed. I would like to thank my parents for their forever love, understanding, support, care, and encouragement. Although they do not express much, I know what they feel. Also, I thank my parents-in-law for their tremendous support and understanding and for allowing their son-in-law to enjoy school life without worrying too much. Dear family, you all should know how much I love you.

PREFACE

This Ph.D. dissertation is composed of five chapters. Chapters 2, 3, and 4 constitute the main body of the dissertation; each of these three chapters is written as a peer-viewed journal paper. Chapter 2 tests a fulcrum approach in the Dunvegan Formation of the Alberta Basin to estimate sediment budget from source areas and volumes of sediment accumulated in sink areas with the assumption of mass balance. Chapter 3 documents the high-frequency regional sequence stratigraphy of the Cretaceous Gallup system and establishes the high-resolution sequence stratigraphic framework. The study deciphers time relationships between lithostratigraphy and sequence stratigraphy and proposes a possible Milankovitch-cycle-dominated glacio-eustatic control. Chapter 4 documents facies associations, describes facies variations, and reconstructs the paleogeography at parasequence scales on the basis of sedimentary processes. The study denotes the depositional evolution in space and time in mixed-process dominated shoreline environments.

Declaration of Academic Achievement

Chapter 2:

Lin, Wen, and Bhattacharya, Janok P. (2017) Estimation of source-to-sink mass balance by a fulcrum approach using channel paleohydrologic parameters of the Cretaceous Dunvegan Formation, Canada. *Journal of Sedimentary Research,* 87 (1), p. 97–116.

Wen Lin (the dissertation author) is the first author, corresponding author, and main researcher of this paper. Wen Lin collected 70% of the data for the research, and Dr. Janok P. Bhattacharya provided 30% of the data. Wen Lin reconciled and analyzed all the

data, and did all the calculations. Wen Lin drafted the text and prepared all the figures. Dr. Bhattacharya edited the manuscript and provided thoughtful input.

Chapter 3:

Lin, Wen, Bhattacharya, Janok P., and Stockford, Andrew. (2018) High-resolution sequence stratigraphy of the Late Cretaceous Gallup system, New Mexico, U.S.A. *Journal of Sedimentary Research,* in revision.

Wen Lin is the first author, corresponding author, and main researcher of the paper. Wen Lin measured 69 sedimentological sections from outcrops, and Andrew Stockford provided two measured sections. Wen Lin took the main responsibility to draft all the measured sections, correlate the sections, and analyze the data. Dr. Janok P. Bhattacharya guided the fieldwork and the analysis of the data. Wen Lin drafted the text and prepared all the figures, and Dr. Bhattacharya edited the manuscript.

Chapter 4:

Lin, Wen, and Bhattacharya, Janok P. (2018) Depositional facies of a mixed-process influenced deltaic system in a stormy ramp setting: the Cretaceous Gallup system, New Mexico, U.S.A. *Sedimentology,* to be submitted.

Wen Lin is the first author, corresponding author, and main researcher of the paper. Wen Lin measured all the sedimentological sections for the study and took the main responsibility to analyze the data. Wen Lin drafted the text and prepared all the figures, and Dr. Bhattacharya edited the manuscript.

TABLE OF CONTENTS

LIST OF FIGURES

LIST OF TABLES

CHAPTER 1

INTRODUCTION

1.1 Overview

Sequence stratigraphy is considered to be one of the most revolutionary concepts in the field of sedimentary geology. It correlates stratigraphic units on the basis of their genetic relationships and chronological orders rather than lithologies (Van Wagoner *et al.*, 1988). This discipline is an powerful analytical technique to understanding Earth history (Steel and Milliken, 2013; Miall, 2013). Applications of sequence stratigraphy tackle problems ranging from denoting the record of sedimentary processes of the Earth's surface, to guiding petroleum exploration and production.

Sequence stratigraphy was originated based on seismic reflection (Mitchum *et al.*, 1977); the resolution has significantly increased with studies on well logs, cores, and especially outcrops. High resolution analysis has revealed high-frequency sequence stratigraphic cyclicity; however, the controlling mechanisms of the cyclicity are the key questions. Milankovitch cycle has proved to be a dominant control on such high-frequency stratal variation in deep times (Sageman et al., 1997). Although the orbitally-driven mechanism has been well studied in the Quaternary period owing to the high-frequency glaciation (Hilgen et al., 2015), whether Milankovitch cycle-dominated high-frequency eustasy can control the stratigraphic cycles of greenhouse age (e.g., Cretaceous) remains debatable (Miller, 2005; Vakarelov et al., 2006).

Shallow marine environments that occupy continental margins are the most critical depositional and ecological continuum in the world: these depositional environments link

the land and the ocean as sediment transporting conduits or storages, and they are classified as key elements in source-to-sink (S2S) systems (Allen, 2008). Ancient shallow marine deposits, including fluvial–delta systems and marine shorefaces, have been proven to be the most common reservoir types of hydrocarbon and aquifer (i.e., Niger Delta holds 34.5 Billion barrels of recoverable oil and 93.8 TCF of recoverable gas; Bridge, 2002; Tuttle et al., 1999; Tyler and Finley, 1991). Nonetheless, comprising the most depositional sub-environments, they are thought to be the most complicated realms that have not been thoroughly understood regarding depositional dynamics and processes, controlling elements, and temporal and spatial variations (Wright and Coleman, 1975; Miall, 1985; Bhattacharya, 2010; Plint, 2010).

Process-based facies analysis is designated to deciphering complicated sedimentary evolution and origin of depositional systems, particularly the shallow marine shoreline environments that are under the governance of mixed processes (wave, tide, and river; Ainsworth *et al.*, 2011). Intrinsic relationships between facies and developments of stratigraphic sequences have been discussed, showing that the deposition of sedimentary facies is most likely controlled by sequence stratigraphic evolution (Yoshida *et al.*, 2007). Only three-dimension paleogeographic reconstructions of finely-mapped stratigraphic units restricted by time slices can allow for the investigation of the controls of sedimentary processes on depositional systems (Van Cappelle *et al.*, 2018).

The source-to-sink (S2S) concept integrates the various components of depositional systems from source areas, through transfer systems, and then to sedimentary basins (Sømme and Jackson, 2013). Studies of ancient S2S systems help to understand the

dynamic evolution of Earth's surface and the related questions (e.g., tectonic movements). In addition, the advance of S2S analysis centres at that the quantification of a given section of a S2S system can be applied to predict upstream controls or downstream limits of the system. Such quantitative predictions of sediment budgets of sedimentary systems can shed information about the size and scale of potential hydrocarbon reservoirs and thus have significant economic value. However, this work requires stratigraphic controls to ensure that the quantitative analysis is confined within a well-defined time-stratigraphic framework. An accurate sequence stratigraphic analysis allows depositional systems to be correlated and mapped, such that upstream source elements (e.g., fluvial) can be linked to downstream sink components (e.g., shorelines, shelf, and deep-water deposits; Bhattacharya *et al.*, 2016).

The Cretaceous North American Western Interior Seaway, formed as an epicontinental sea from an active foreland basin, provides an ideal geological setting to test the various questions described above. This relatively narrow seaway is considered to be a semi-closed to closed and mixed-energy-dominated depositional system (Kauffman and Caldwell, 1993). The extensive and well-exposed outcrops of the clastic wedges developed along the west margin of the Western Interior Seaway provide excellent data to the analyses of sequence stratigraphy, facies architecture, and sedimentary evolution (see the numerous examples of the Book Cliffs). Nevertheless, along with the advance of theories and analytical tools, a significant number of those previous studies need to be re-visited and re-interpreted.

This dissertation is devoted to solving some key scientific problems using examples from the Cretaceous Western Interior Seaway. The studies composed in this dissertation aim to: 1) quantify sediment budgets using sequence stratigraphic archives of S2S systems; 2) decipher time-relationships between lithostratigraphy and sequence stratigraphy, evaluate high-frequency sequence stratigraphic cyclicity, and investigate the primary controls on high-frequency stratigraphy; and 3) document facies temporal and spatial variability, reconstruct paleogeography with chorological restriction, and denote the dominant controlling sedimentary processes of the depositional system.

1.2 Dissertation Contents

The dissertation is composed of five chapters; Chapters 2, 3, and 4 constitute the main body of the dissertation. Chapter 2 tests a fulcrum approach in the Dunvegan Formation of the Alberta Basin using the paleohydrological parameters of trunk rivers to estimate sediment budget derived from source areas and volumes of sediment deposited in sink areas. The results demonstrate that the sediment from the source area and transported through the trunk river matches the sediment volume in the sink and implies sediment escape as a result of oceanic geostrophic currents. Chapter 3 documents the high-frequency regional sequence stratigraphy of the Gallup system, based on facies, key surfaces, shoreline trajectory, and parasequence stacking pattern analysis. The results decipher time relationships between lithostratigraphy and sequence stratigraphy. It also discusses controls on high-frequency cyclicity and proposes a possible glacio-eustatic origin that supports the hypothesis of an ephemeral ice sheet covering Antarctica during the Late Cretaceous greenhouse age. Chapter 4 documents facies associations and

describes facies variations at parasequence scales. It also evaluates sedimentary processes that dominate the depositional system. The results show a mixed-process dominated environment with periodic intense storm influence. Paleogeographic constructions of the Gallup system show the evolution of the shoreline and depositional system along sequence stratigraphic cycles. The 3D paleogeographic maps with well-defined chorological controls also help us to examine lateral facies variabilities. The distinction between waves-dominate delta and shoreface deposits has also been discussed. Chapter 5 summarizes conclusions from Chapters 2, 3, and 4, and also suggests future work that is related to the studies described above.

CHAPTER 2

ESTIMATION OF SOURCE-TO-SINK MASS BALANCE BY A FULCRUM APPROACH USING CHANNEL PALEOHYDROLOGIC PARAMETERS OF THE CRETACEOUS DUNVEGAN FORMATION, CANADA

Abstract

Trunk rivers transport the bulk of the sediment in a source-to-sink (S2S) system, and total mass passing through any cross section (i.e., fulcrum) of a trunk-river over geologic time should allow matching of source-area sediment delivery budgets to downstream sediment volumes deposited in the basin. We analyze the paleohydrology of ancient trunk channels and link downstream deltaic strata of Allomember E of the Cretaceous Dunvegan Alloformation in the Western Canadian Sedimentary Basin to test the total mass-balance fulcrum approach. Bankfull channel depth and width, grain size, paleoslope, velocity, and discharge are derived from outcrop, core, and well logs. Some parameter estimates use multiple methods, providing a range of values and serve as a cross check of independent methods. Estimates of annual flood frequency and paleodischarge, associated with long-term geologic- time estimates, are derived from chronostratigraphic analysis and allow calculation of cumulative sediment discharge. Isopach maps are used to measure sink-area sediment volumes. The results indicate that the trunk river of Allomember E was 10–15 m deep and 150–250 m wide, carried fine- to medium-grained (, 200 microns) sand, and flowed over a low-gradient paleoslope of 4.1–6.1310–5. Annual total sediment discharge is estimated to have ranged from 5.4 to 123106 m3. Within 25,000 years, the river is estimated to have transported 135–307 km3 of sediment into the basin. This is

consistent with the 130 km3 of sediment mapped in the study area. However, the upper-range estimate of sediment delivered into the sink is 2.5 times the measured sediment volume in the map area, which, if accurate, suggests significant sediment escape. This supports the hypothesis that in Dunvegan time, mud was widely dispersed southward, along the Alberta Foreland Basin by geostrophic currents associated with storm processes and counterclockwise oceanic gyres in the Cretaceous Seaway.

2.1 Introduction

The source-to-sink (hereinafter referred to S2S) concept encompasses source sediment denudation from the initial catchment area, transportation or transient storage through the system, and ultimate deposition in the basinal sink (Castelltort and Van Den Driessche 2003; Sømme et al. 2011; Romans and Graham 2013; Jaeger and Koppes 2015; Leithold et al. 2015; Bhattacharya et al. 2016). The S2S concept has been increasingly applied to assess sediment budgets of both modern and ancient systems (Allen 2008b; Sømme et al. 2009; Carvajal and Steel 2012; Sømme and Jackson 2013). Given an ideally closed S2S system, the total sediment volume produced from the catchment should match the volume accumulated in downstream sinks (Paola 2000; Strong et al. 2005; Covault et al. 2011; Sømme et al. 2011; Hajek and Wolinsky 2012; Paola and Martin 2012; Allen et al. 2013; Matenco et al. 2013; Michael et al. 2013; Petter et al. 2013; Holbrook and Wanas 2014; Sadler and Jerolmack, 2015).

In estimating total mass balance, it is assumed that the total sediment volume passing through any cross section of a longitudinal trunk fluvial system in the transfer zone during a certain time interval should match both the sediment volume delivered from the source

area and the sediment volume passing through that cross section. This point in a cross section in the sediment routing system serves as a "fulcrum" that can be used to balance the total mass between source and sink (Holbrook and Wanas 2014). The largest-scale incised trunk rivers transport the bulk of the sediment in a S2S system, and best serve as key fulcrum points (Blum et al. 2013; Romans and Graham 2013; Romans et al. 2015). The fulcrum approach requires calculating the instantaneous paleodischarge and other paleohydraulic parameters of trunk rivers and integrating this over the duration of the associated stratal record of a given S2S system. The fulcrum approach can be applied without knowing source area properties, although knowledge of the catchment climate regime can be very useful, and does not require a closed downstream basin (Asselman 1999; Bhattacharya and Tye 2004; Hutton and Syvitski 2008; Parker et al. 2008; Whittaker et al. 2010; Blum et al. 2013; Holbrook and Wanas 2014; Bhattacharya et al. 2016). The fulcrum approach enables estimates of catchment areas and relief, amount of sediment transported in the systems, and the volume of sediment accumulation in the basins. These estimates also can be compared to those made from other approaches, such as the BQART method (see Syvitski and Milliman 2007), the use of regional climate curves (see Davidson and North 2009), other numerical models (Paola and Mohrig 1996; Paola 2000; Lee et al. 2002; Fedele and Paola 2007; Duller et al. 2010; Whittaker et al. 2011; Hajek and Wolinsky 2012; Allen et al. 2013; Liang et al. 2014), volumetric calculations from the stratigraphic record (Carroll et al. 2006; Carvajal and Steel 2012; Petter et al. 2013), and thermochronometric data (Michael et al. 2014).

Fig. 2.1.–Cretaceous Cenomanian paleogeographic map of North America showing delta complexes of the Dunvegan Formation in Alberta (modified after Bhattacharya and MacEachern, 2009).

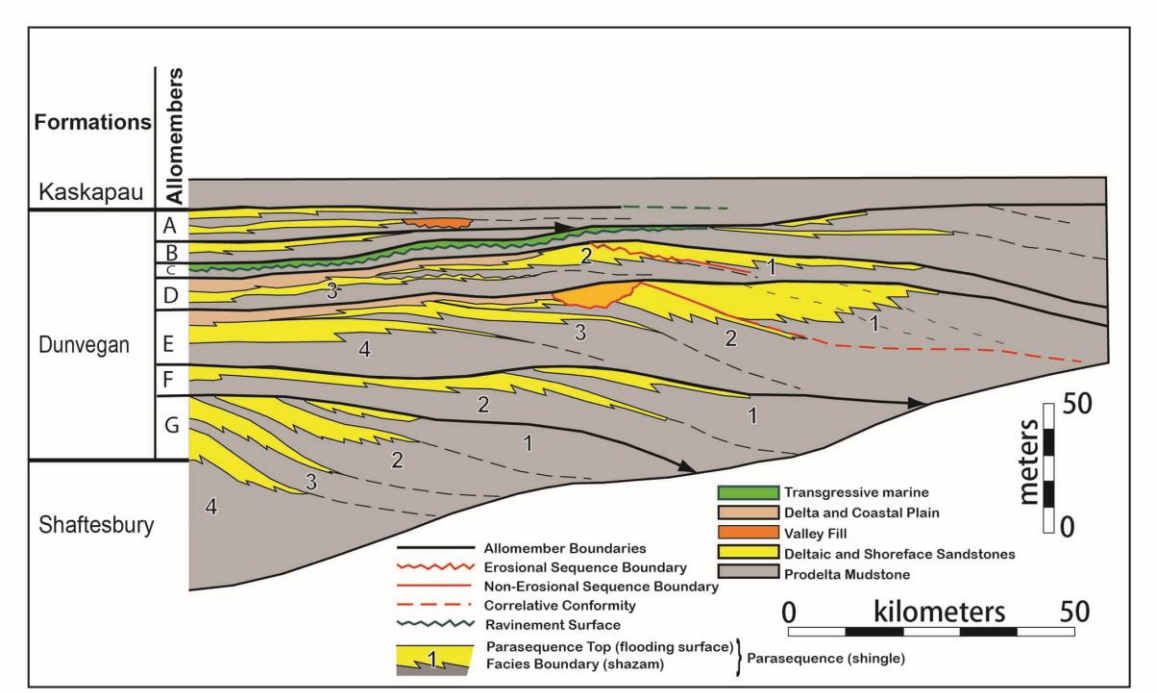

Fig. 2.2.–Regional cross section across the Alberta Foreland Basin, illustrating the allostratigraphic interpretation of the Upper Cretaceous Dunvegan Formation. The Dunvegan comprises several stacked allomembers (A to G). Each allomember is bounded by a regional transgressive flooding surface. Each allomember internally consists of several smaller-scale, offlapping, shingled parasequences that map as sandy delta lobes and their associated prodelta mudstones. Many delta lobes can be correlated into their updip feeder valleys, such as in Parasequence E1 (Bhattacharya and MacEachern, 2009).

The purpose of this paper is to estimate total mass balance by calculating long-term sediment flux through fulcrum analysis of trunk-river deposits, with mapped downstream sediment accumulations in the Upper Cretaceous Dunvegan Alloformation, in the Alberta Foreland Basin, Canada, using a combination of outcrop and subsurface data (Fig. 2.1). The Dunvegan Formation has been extensively studied, incorporating extensive outcrop and subsurface data to develop a high-resolution allostratigraphic and chronostratigraphic framework (Bhattacharya and Walker 1991a, 1991b; Bhattacharya 1992; Bhattacharya

1993; Gingras et al. 1998; McCarthy et al. 1999; Plint 2000; Plint et al. 2001; Plint 2002; McCarthy and Plint 2003; Plint and Wadsworth 2003; Plint and Wadsworth 2006; Plint and Kreitner 2007; Plint et al. 2009). The Dunvegan Alloformation has been subdivided into 10 allomembers, labelled J to A in ascending order, and these allomembers have been correlated and mapped on the basis of regional transgressive surfaces (Fig. 2.2). In sequence stratigraphic terms, each allomember represents a flooding-surface-defined genetic stratigraphic sequence (cf. Galloway 1989), each of which contains several parasequences (cf. Van Wagoner et al. 1990) that prograded towards the SE into the Cretaceous Interior Seaway. Eight of the allomembers contain recognizable paleovalley systems that can be linked to their downdip shoreline deposits (Bhattacharya and Walker 1991a; Plint 2000). These valleys define unconformity-bounded lowstand systems tracts within the genetic stratigraphic sequences (cf. Van Wagoner et al. 1990; Bhattacharya 1993; Plint and Wadswoth 2003). The Dunvegan is thus an ideal candidate for fulcrum analysis owing to the ability to identify and characterize the trunk rivers within a specific incised-valley system and correlate these to the downdip lowstand deltaic and offshore shelf systems tracts (Bhattacharya and Walker 1991a; Plint 2002; Plint and Wadsworth 2006) (Fig. 2.3). More importantly, these Dunvegan lowstand system tracts are smaller-scale features than modern continental-scale rivers, and are entirely confined to the Western Interior Seaway. Therefore the Dunvegan represents a potentially closed system (Bhattacharya et al. 2016). In this study, Allomember E was selected for more detailed fulcrum analysis because it has the clearest linkage between the tributary drainage system and its lowstand delta deposit (Bhattacharya 1993; Plint and Wadsworth 2006).

Allomember E also comprises a river-dominated delta system, with minimal tidal influence and limited wave reworking (Bhattacharya and Walker 1991a; Bhattacharya 1993) (Fig. 2.4). Previous mapping of the lowstand river-dominated delta lobes (Bhattacharya 1993) enables volumetric estimation of the downstream sediment accumulation (Bhattacharya and MacEachern 2009) (Fig. 2.3).

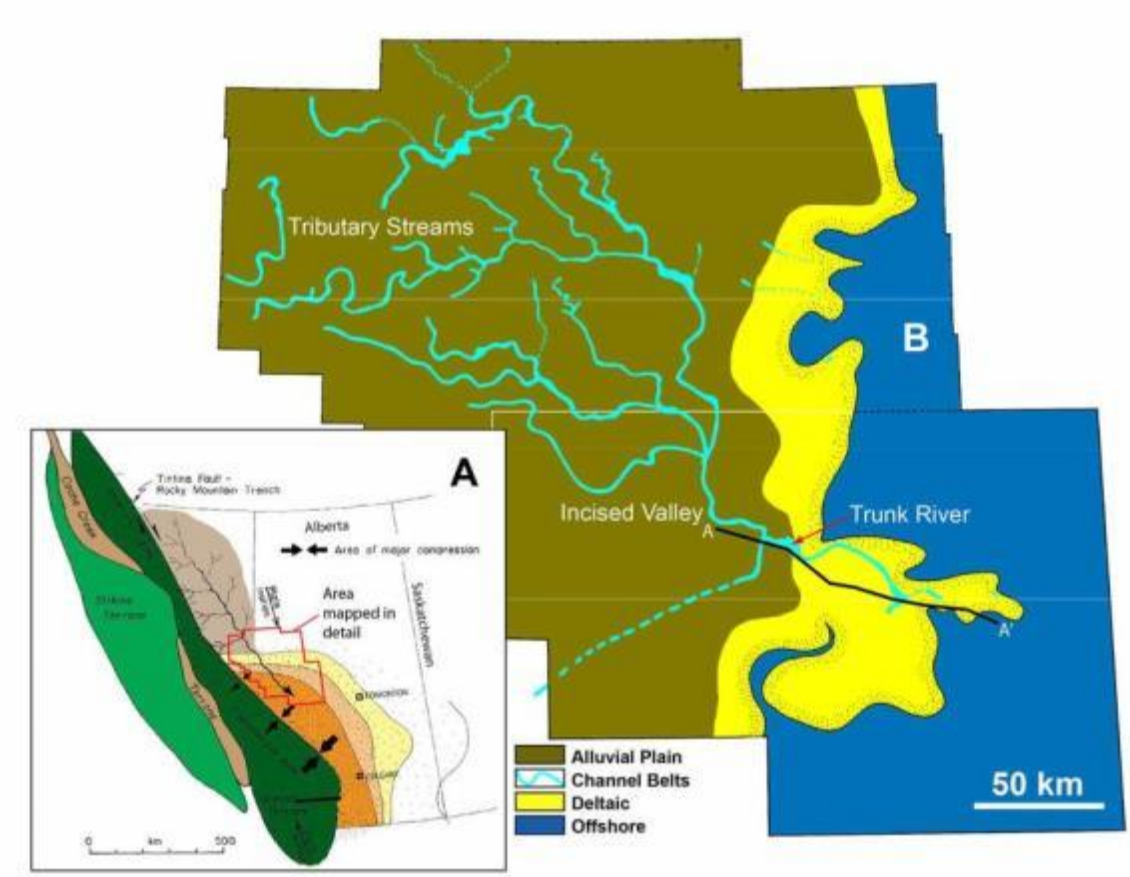

Fig. 2.3.–Paleogeographic map of valleys and lowstand deltas in Allomember E of the Dunvegan Formation (modifed after Bhattacharya and MacEachern, 2009).

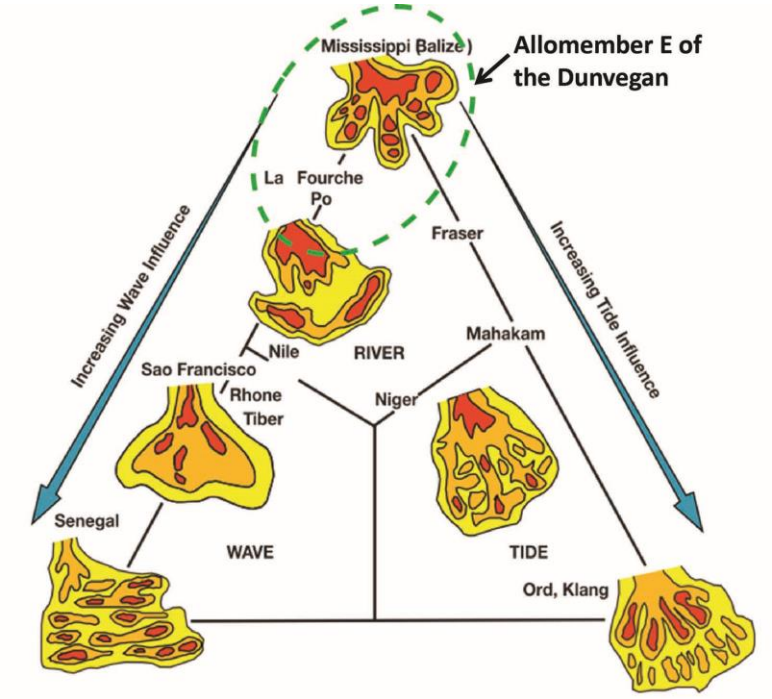

Fig. 2.4.–Allomember E, with a well identified trunk-river, is the most river-dominated delta with the least tidal influence. This allows accurate paleohydrological parameter estimates without tidal landward reworking (modified after Bhattacharya, 2006, which was modified based on Galloway, 1975).

2.2 Methods

The workflow for testing this fulcrum approach includes: 1) identifying the trunk river and estimating trunk-river dimensions and attributes for further paleohydrologic estimates, 2) calculating instantaneous bankfull paleodischarge and sediment load; 3) estimating annual sediment discharge using paleoclimate proxies (e.g., floodplain paleosol and paleobotanical data) and appropriate modern climatic analogs; and 4) determining total duration of the river and its valley from stratigraphic analysis; 5) evaluating total mass delivered to and through the trunk river over this geological time period; 6) measuring sediment volumes in the sink; and 7) reconciling sediment volumes delivered to the

fulcrum point from the source area to measured sediment accumulations in the sink area (Fig. 2.5).

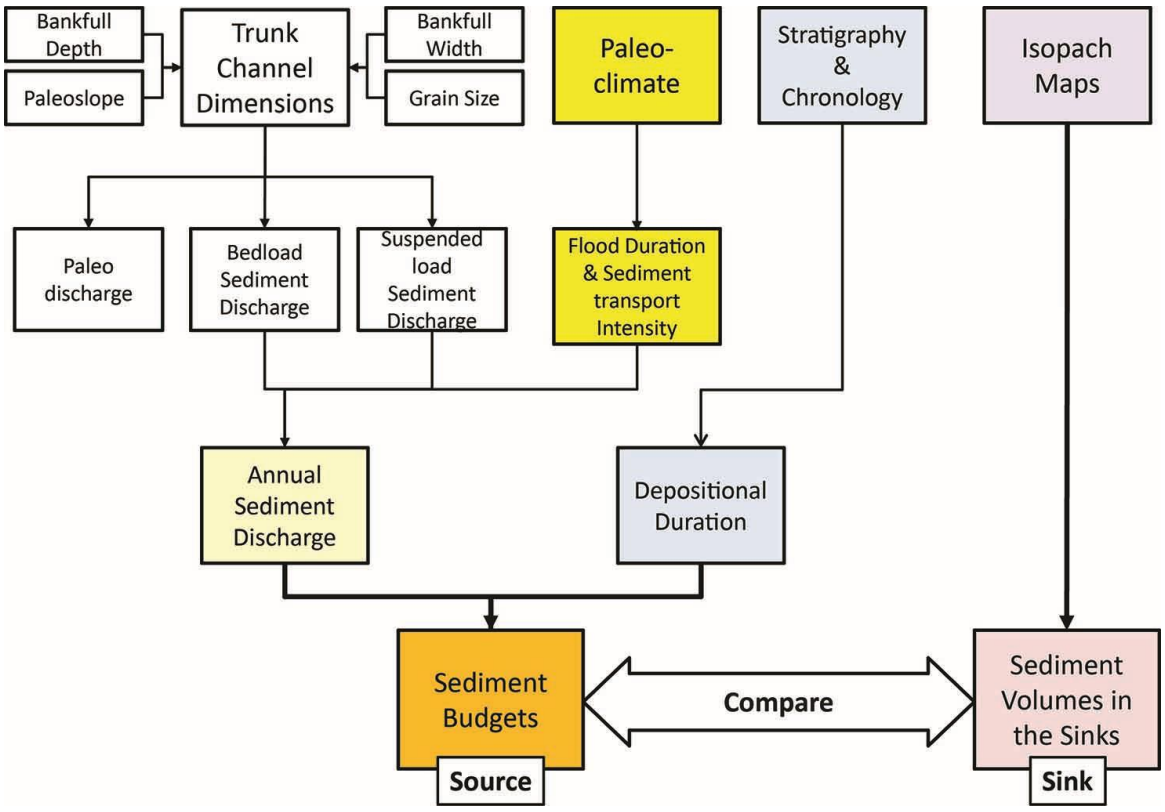

Fig. 2.5.–Work flow for fulcrum analysis.

2.2.1 Dimension Analysis of Trunk Rivers

The criteria for identification of trunk rivers in ancient deposits have been reviewed by Olariu and Bhattacharya (2006) and Bhattacharya et al. (2016). In this study, regional outcrop and subsurface mapping (e.g., Fig. 2.3) has identified both tributive and trunk valleys in the Dunvegan (Plint 2002, Plint and Wadsworth 2003). To estimate trunk-river paleohydraulics, dimensional information regarding the trunk rivers is required, including average bankfull channel depth (*dm*) and bankfull channel width (*Wc*). Grain size (*D*) and channel depth can be used to estimate paleoslope (*S*), and average flow velocity (*U*).

Trunk-river Bankfull Depth.--- Bankfull channel depth can be estimated on the basis of the thickness of fully preserved fining-upward facies successions (stories) as measured in outcrops, cores, or well logs with a small correction for compaction (Bridge and Tye 2000; Bhattacharya and Tye 2004; Adams and Bhattacharya 2005; Miall 2006; Allen 2008b; Davidson and Hartley 2010, 2014; Whittaker et al. 2011; Hajek and Heller 2012; Hajek and Wolinsky 2012; Blum, et al. 2013; Hampson et al. 2013; Petter et al. 2013; Bhattacharya et al. 2016).

Sedimentary structures, such as dune-scale cross-bedding, and bar accretion deposits, can also be used to estimate channel depth, independently of story thickness (Leclair and Bridge 2001; Bhattacharya and Tye 2004; Davidson and Hartley 2010; Foreman et al. 2012; Hajek and Wolinsky 2012; Holbrook and Wanas 2014). Dune height can be estimated from thickness of dune-scale cross-set using certain empirical equations, which have been shown to scale to channel depth (see LeClair and Bridge 2001, Reesink et al. 2015). Thickness measurements have an error of about 10% (i.e., 10 cm per meter) and estimates of channel depths can have uncertainties of up to 60% using the LeClair and Bridge (2001) method, and about 25% using measurements of story thickness.

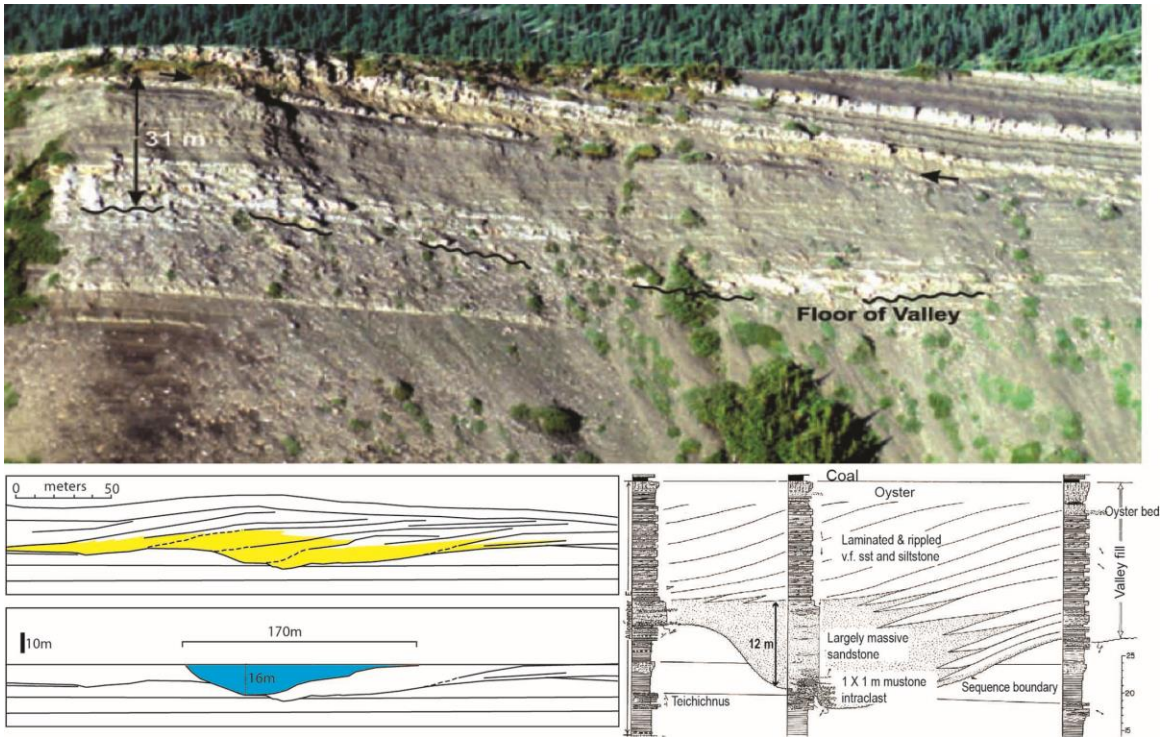

Fig. 2.6.–Large-bar-scale lateral accretion observed from outcrops allowing facies bedding analysis, which can further infer channel dimensions (modified after Bhattacharya et al., 2016 and Plint and Wadsworth, 2003).

Trunk-river Width.--- Channel and channel-belt width were measured from the previously published outcrop studies (e.g., Plint, 2002, Plint and Wadsworth 2003) oriented perpendicular to the flow direction. In subsurface, or areas of limited exposure, channel width was estimated based on various empirical equations depending on the fluvial style (e.g., single-thread meandering channel vs. braided channels; as presented in Leopold and Maddock 1953; Bridge and Mackey 1993; Hampson et al. 2013; and Holbrook and Wanas 2014). Large-scale lateral-accretion sets in point-bar deposits in Dunvegan outcrops show that the trunk river of the Allomember E valley was a single-thread meandering channel (Plint and Wadsworth 2003) (Fig. 2.6). Uncertainties of length

measurements of accretion beds are about 10%, and uncertainties in converting point-bar accretion length to channel width have an uncertainty of about 25%. As a consequence, width estimates based on outcrops exposures of meander belts have an uncertainty of about 35%.

Other scaling relationships of channel dimension are also applied to estimate channel width and constrain the results. For example, based on Gibling's (2006) channel width/thickness ratio classification, trunk rivers within valley fills typically have a width/thickness ratio ranging from 5 to 50 (see Blum et al. 2013), depending on tectonic uplift and climate. The entrenchment ratio, defined as valley width over bankfull channel width (Rosgen 1997), was also used to evaluate estimates of channel width.

Grain Size.--- Grain size can be used to estimate shear stress on the bed, which is determined by flow depth and relief, and controls the sediment transport mode (bedload vs. suspended load) and capacity, coupled with velocities of water flow and sediment transport (Hajek and Wolinsky 2012). The median grain size (D_{50}) value was used to estimate water discharge and to estimate paleoslope (Holbrook and Wanas 2014), and the suite of grain size distribution values (D_{50}, D_{90}, D_{84}, and D_{16}) are used to estimate total instantaneous sediment discharge. Grain size was derived directly from core and thin-section data, and used to generate cumulative distribution plots. The grain-size measurements, made with a standard grain-size card, have an error of about 1/2 phi (about 30%).

Paleoslope.--- Paleoslope is represented by the longitudinal profile of a sedimentary system (Posamentier and Vail 1988; Blum and Törnqvist 2000) and can be estimated

using multiple approaches, such as the use of empirical equations, stratigraphic stacking patterns, and lap-out relationships, including measurement of the onlap distance of coastal prisms versus the thickness mapped on regional dip-oriented cross sections (e.g., Blum and Tornqvist 2000), elevation drop of channel bases along a valley long profile (e.g., Bhattacharya et al. 2016), and paleohydrologic data (i.e., backwater and bayline length) (Blum et al. 2013).

We used the empirical equation of Holbrook and Wanas (2014):

$$\tau^*_{bf50} = (d_m S)/(PD_{50}) = \text{constant} \quad (1)$$

where S is slope, P is submerged dimensionless density of sand-gravel sediment (ρ_s- ρ_w), and D_{50} is grain size. An assumed sediment density of 2.65 g/cm^3 yields a dimensionless submerged density (P) of 1.65. The bankfull Shields number for dimensionless shear stress (τ^*_{bf50}) is 1.86 (also see Parker 1978; Dade and Friend 1998; and Parker et al. 1998).

Backwater length is defined as the landward limit that downstream effects can propagate upstream (Paola and Mohrig 1996; Hajek and Wolinsky 2012; Blum et al. 2013) (Fig. 2.7), which can be used to estimate slope associated with channel depth, and may determine the gravel/sand boundary in the upstream reaches of fluvial systems (Bhattacharya et al. 2016). The Backwater length is expressed as

$$L_b = d_m/S \quad (2)$$

where L_b is backwater length. Slope estimates are considered to be uncertain by a factor of 2.

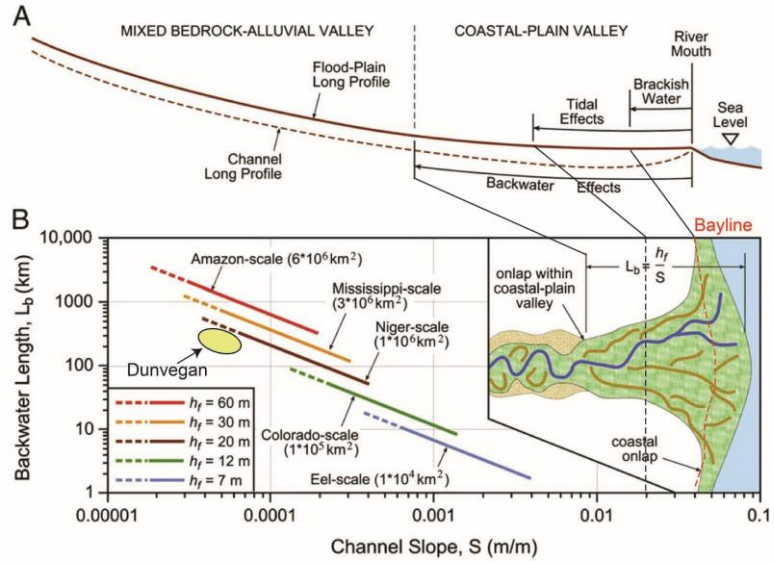

Fig. 2.7.–Backwater and Bayline length concept. A) longitudinal profile of sedimentary system illustrating Backwater length, defined as upstream limit of sea water, and bayline length, controlling tidal and brackish water limits. B) Backwater length vs. slope and channel scales with Dunvegan fluvial system plotted, as well as plan view of Backwater and Bayline concept (modified after Blum et al., 2013).

Flow Velocity.--- Flow velocity ($\bar{U}$) was estimated using 3D bedform-phase diagrams of Rubin and McCulloch (1980) (Bhattacharya and Tye 2004; Bhattacharya and Maceachern 2009; Bhattacharya et al. 2016), as bedforms are a function of flow velocity, depth, and grain size. Sedimentary structures and grain-size data are directly observed from outcrop and core. It is assumed that the dominant bedforms record bedload transport during flood events. In the Dunvegan, dune-scale cross beds are the dominant sedimentary structure observed in the cores and outcrop, and higher-flow-regime bedforms, such as upper plane bed, were not observed. Lower flow regimes are reflected by ripple cross lamination in upper parts of channel stories and likely reflect waning, lower flow stages of the river hydrograph. Flow depth is estimated from channel-story thickness. Flow velocity was

also estimated independently, based on hydraulic equations. Here we used the Chézy coefficient, hydraulic radius, and estimated slope to calculate the bankfull flow velocity (Holbrook and Wanas 2014), and compare this to the value estimated using the bedform-phase-diagram method. The bankfull flow velocity is a function of basal shear stress, and is determined by gradient and flow depth. The mean flow velocity of the trunk river of Allomember E was estimated using the equation:

$$\bar{U} = C_f(RS)^{1/2} \quad (3)$$

where C_f is the Chézy Coefficient ($C_z = (g)^{0.5}8.1(d_m/k_s)^{1/6}$, where d_m is mean bankfull water depth, and k_s is roughness element ($k_s = 3D_{90} + 1.1\Delta(1 - e^{-25\psi})$), where Δ = bedform height = d_m / 8 (after LeClair and Bridge 2001); $\psi = \Delta/\lambda$, where λ = bedform wavelength = 7.3 d_m (see Equation 4b), R is hydraulic radius, and S is paleoslope.

2.2.2 Paleodischarge Estimation

Paleodischarge was calculated using the flow velocity and channel dimensions estimated using the methods described above. Paleodischarge of rivers was also estimated by integrating drainage-basin area with paleoclimatic parameters (e.g., Davidson and North 2009), and these are in turn compared to estimates based on the flow velocity and channel dimensions, as explained above (Bhattacharya et al. 2016). Combining estimation of flow velocity with the channel dimensions allows calculations of bankfull paleodischarge (Q_{bf}), bedload sediment discharge (Q_{tbf}), suspended-load sediment discharge (Q_{ss}), and total sediment discharge using the following equations presented in Holbrook and Wanas (2014):

$$C_f\,[(Q_{bf}^{\,2})/(w_c^{\,2}d_m^{\,2})] = g\,d_m\,S \quad (4a)$$

where C_f is the dimensionless Chézy friction coefficient, estimated by Equation (4b), w_c is channel width, Q_{bf} is bankfull paleodischarge, and S is paleoslope.

$$C_f^{-1/2} = (8.32)(d_m / k_s)^{1/6} \quad (4b)$$

where $k_s = 3D_{s90} + 1.1\Delta(1 - e^{-25\psi})$, and Δ= bedform height = d_m / 8 and $\psi = \Delta/\lambda$, where λ is bedform wavelength = 7.3 d_m (after Van Rijn 1984).

$$Q_{tbf} = w_c q_{tbf} = w_c (RgD_{50})^{1/2} D_{50} \alpha_t [\varphi_s \tau^*_{bf50} - \tau^*_c]^{nt} \quad (5)$$

$$\alpha_t = \alpha_{EH}/C_f,\ \alpha_{EH} = 0.05,\ n_t = 2.5,\ \varphi_s = 1,\ \tau^*_c = 0 \quad (5a)$$

where R is hydraulic radius, calculated by Equation (6).

$$R = A/P = (w_c \times d_m)/(2 \times d_m + w_c) \quad (6)$$

For estimation of bankfull suspended-load discharge, the Van Rijn (1984) equation is used, which employs entrainment thresholds derived from grain-size distribution of bed load to determine suspended-load concentrations averaged over depth across a unit of channel width (see Holbrook and Wanas 2014). The method comprises 13 steps with 12 equations, which constrain variables in the final Equation (8) (see Appendix 2). The reader is referred to Holbrook and Wanas (2014) and Van Rijn (1984) for more detailed description of the calculation method. The suspended-load discharge per unit width (q_s) is multiplied by estimated channel width (w_c) to estimate total suspended-sediment discharge (Q_{ss}) (Equation 9).

$$q_s = F\bar{u}d_m c_a \quad (7)$$

$$Q_{ss} = q_s (w_c) \quad (8)$$

where F is the suspension factor, correcting for the concentration at the given depth to the full water column, $\bar{u}$ is mean flow velocity, d_m is mean bankfull flow depth, and c_a is the

concentration of suspended sediment at the reference depth. Two alternative methods were introduced to estimate suspended-load discharge (see Garcia and Parker 1991; Wright and Parker 2004); however, with the condition of low gradient and fine-grained sediment, the Van Rijn (1984) method is considered the most applicable in the Dunvegan (Holbrook and Wanas 2014).

2.2.3 Estimation of Annual Sediment Discharge

The values of bedload and suspended-load sediment discharge derived from the equations and methods discussed above were used to evaluate the volume of sediment passing through any river cross section per second, defined as an instantaneous discharge rate. This rate effectively characterizes flow conditions at the time of migration of the dominant dune bedforms, which are interpreted to reflect the flood stage of the river. Nevertheless, the fulcrum approach aims to quantify mass balance over a longer geological period of time. In order to estimate the total sediment volume delivered by the river during the given time period of stratal formation, mean annual sediment discharge rate and long-term time scales that represent the duration of trunk-river deposition are required. Mean annual sediment discharge can be estimated from rating curves of sediment discharge in analog modern systems; this is, however, not typically possible for stratigraphic systems. Mean bankfull discharge for various climate regions can be estimated as a function of bankfull depth and drainage-basin area (Simon et al. 2004; Davidson and North 2009). Nevertheless, few attempts have been made to estimate bankfull discharge on a yearly basis for deep-time systems.

In this study, we use modern analogs which show that the main proportion of the total annual sediment load is transported by rivers typically in a short-term period. These periods may reflect rainfall or seasonal climate events, resulting in flood-intensified peak flow periods, which typically occur over hours to days (Sadler 1981; Dott 1996; Clark 1998; Alexander et al. 2001; Meybeck et al. 2003; Vandenberghe 2003; Jerolmack and Sadler 2007; Kettner and Syvitski 2008; Fatorić and Chelleri 2012; Miall 2014; Cramer et al. 2015). The hydrological term "annual flood" refers to the period of maximum discharge for each year, regardless of whether the river has actually over topped its banks (Arora and Boer 2001). Compilations of annual flood durations in modern rivers show that they typically vary from a few days to a few weeks, but normally are on the order of one week (Wolman and Miller 1960; Andrews 1980; Nolan et al. 1987; Meybeck et al. 2003; Powell et al. 2006). From such statistical compilations, the following empirical equation has been obtained:

$$Q_{mas} = Q_{tbs} \times D / b \quad (9)$$

where Q_{mas} is annual discharge, Q_{tbs} is bankfull discharge, D is peak flood duration (days), and b represents the percentage of total sediment transported during peak flood. The flood duration and the proportion of sediment volume transported during flood events were estimated by reconstructing paleoclimate conditions and classifying paleoclimate regimes on the basis of modern analogs. The reconstructed paleoclimate conditions are compared to the Köppen-Geiger climate classification for modern systems, which will allow for application of a modern climatic-zone analog (Kottek et al. 2006).

2.2.4 Evaluation of Cumulative Sediment Load

In order to estimate total sediment budget in the system, the total depositional duration must be integrated with estimate of annual discharge. The total depositional duration of individual parasequences of Allomember E was estimated by previous sequence stratigraphic analysis. The number of parasequences identified in each allomember is variable but ranges from 2 to 4, and the extent and maturity of paleosols related to valley incision cycles can be used to estimate durations of individual valleys (Bhattacharya 1992; McCarthy and Plint 1999). The total sediment load passing through the trunk-river fulcrum point in the Dunvegan Allomember E can be calculated by integrating the paleohydrologic parameters over the total duration.

2.2.5 Sediment Accumulation in the Sink

The total sediment volume deposited downstream of the trunk river was estimated using isolith maps of Allomember E (Bhattacharya 1993). The total isopach map of Allomember E was digitized in ArcGIS and converted to a vector grid comprising geographic coordinates, which enabled accurate estimates of sediment volume. Similarly, digitizing a sandstone isolith map of a single parasequence E1 of Allomember E, in ArcGIS allowed sand sediment volume to be estimated. The sandstone isolith map of Parasequence E1 shows a lobate geometry, interpreted as a discrete delta lobe (Bhattacharya 1992). The map shows closure of the 4 m contour line, but the 0 and 2 m contour lines are not closed to the southwest due to loss of data in the thrust-fold-belt uplift. Isopach contours of the entire Allomember E, which include the shaly facies, thin uniformly basinward from a maximum of 65 m, in the delta lobe center, down to about 20

m. The zero edge of downlapping shales was mapped by Plint et al. (2009). Where appropriate, we manually closed contour lines by assuming uniform geometric trends. These maps provide values of area and thickness that are used to calculate sediment volumes.

2.3 Results

Allomember E of the Dunvegan Formation was deposited during a lowstand and includes an extensive tributary incised-valley system and a trunk valley that converged to feed a river-dominated progradational delta deposit (Figs. 2.3) (Bhattacharya and MacEachern 2009). In order to reflect uncertainties, we estimated a range of reasonable parameters instead of a single value.

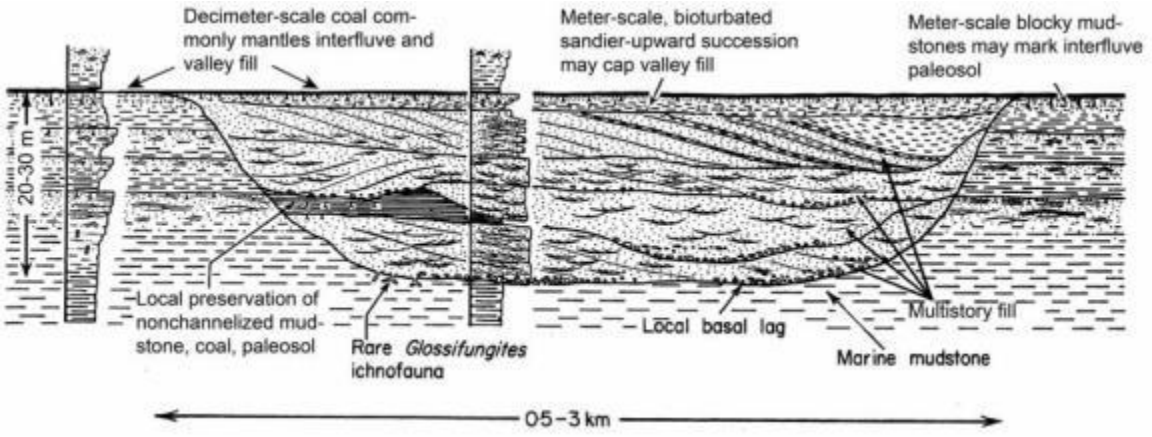

Fig. 2.8.–Paleovalley of the Dunvegan Formation characterization and architecture correlation from outcrop indicating valley-fill elements and individual channel-fill thickness (Plint and Wadsworth, 2003).

2.3.1 Trunk-river Dimensions

Trunk-river Bankfull Depth.--- Plint and Wadsworth (2003) showed that individual channel-fill thickness in the valley systems range from 3 m to 10 m, with an average of 8

- 10 m. The isolith map of sandy valley fill associated with Parasequence E1 does not exceed 16 m thick, although some postdepositional truncation by the overlying transgressive surface is observed. Sand-filled valleys range from 0.5 km to 2 km wide (Fig. 2.8). Maximum thalweg channel depth in the Allomember E valley was estimated to be about 16 m, as measured from the thickness of fining-upwards channel stories in core in the valley fill (Fig. 2.9). In outcrop, inclined heterolithic stratification (IHS) of point-bar deposits in the valleys indicates a 12 m deep channel that is about 100 - 150 m wide (Plint and Wadsworth 2003) (Fig. 2.6). Similarly, based on the data of Plint and Wadsworth (2003), Bhattacharya et al. (2016) estimated a large tributary channel that feeds the Allomember E trunk river, to be about 16 m deep and 150 m wide, based on heights of lateral-accretion bar from outcrop (Fig. 2.6). Statistics from well-log data, shown by Plint (2002), indicate that tributary channels of Allomember E are 10 m deep on average. Nonetheless, theoretically, trunk-river depth should increase downstream following a confluence of tributary channels.

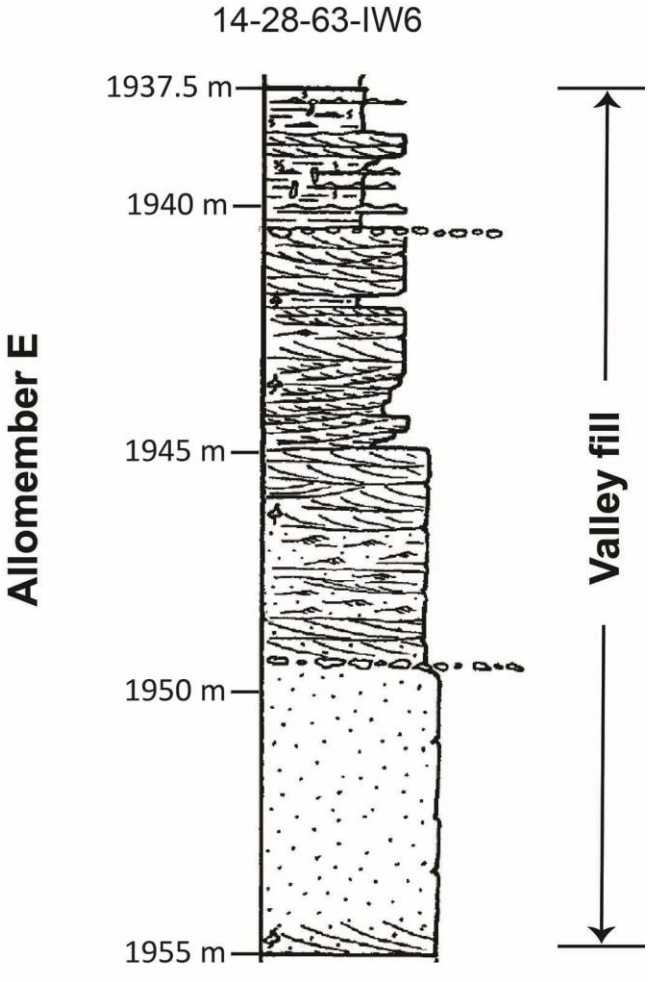

Fig. 2.9.–Core description of Allomember E illustrates multiple-story fluvial architecture and sedimentary structures in valley-fill succession. Single-channel depth can be estimated to be about 10 m. Cross-set is about 0.5 m thick (modified after Plint and Wadsworth, 2003).

Plint and Wadsworth (2003) documented the average cross-set thickness in the Dunvegan valley systems to be about 0.5 m (Fig. 2.9). This suggests bankfull channel depths ranging from 7 m to 18 m. Compilation of these channel-depth values, estimated from multiple methods, suggests mean bankfull channel depth values of about 10 - 15 m.

Trunk-river Width.--- Trunk-river width should be a small fraction of valley width (Gibling 2006; Blum et al. 2013; Hampson et al. 2013); thus the channel widths should be

less than 500 m, given the valley widths of 0.5 - 2 km. Single-thread meandering characteristics and a low gradient suggest that the entrenchment ratio should be greater than 2.2 (see Rosgen 1997), and accordingly the channel width should be less than 230 m. Plint and Wadsworth (2003) inferred that upstream tributary channels are about 100 - 150 m wide, and Bhattacharya et al. (2016) suggested that the trunk river of Allomember E must be somewhat wider than this. Therefore, we estimated trunk-river channel width to range from 150 to 230 m.

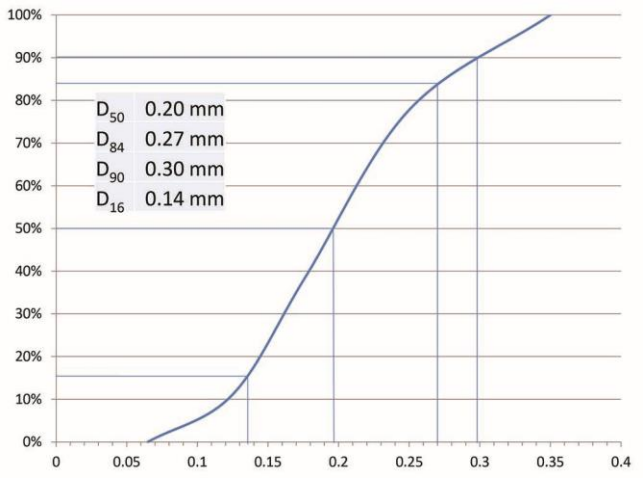

Fig. 2.10.–Sediment grain-size distribution. It is plotted based on the core data from nine wells presenting Parasequence E1 of Allomember E.

Grain Size.--- Compilation of core data from nine wells (see appendix 1) shows the overall sediment grain-size distribution of the Allomember E valley, from which key grain-size values (D_{50}, D_{90}, D_{84}, and D_{16}) were derived (Fig. 2.10). Grain sizes of the trunk river varies from very fine to medium grained, with a D_{50} grain-size value of 0.20 mm (~ 200 microns), categorized as fine-grained sandstone. The relatively small and well-sorted grains suggest a low paleoslope.

Paleoslope.--- Paleoslopes, estimated from Equation 1, are 4.1 - 6.1 $\times 10^{-5}$. In contrast, Plint et al. (2009) used qualitative reasoning to estimate paleoslopes of the Dunvegan alluvial and coastal plain to be in the range of 2 - 3 $\times 10^{-4}$, which are an order of magnitude steeper than the slopes calculated using the empirical equation herein.

Regional mapping of the Dunvegan Formation shows that conglomeratic facies are restricted to about 600 km inland (Stott 1982), which supports a low-gradient system. In addition, the bayline limit may also help characterize the slope. The bayline is defined as the boundary between the upper and lower delta plain, and its limit equals the tidal range divided by slope (Bhattacharya et al. 2016). Rare tidal deposits in the Dunvegan suggested a microtidal to low mesotidal regime (Plint 2003), suggesting a tidal height of < 2 m. The two different paleoslope estimates yield the estimated bayline limits as high as 36-54 km, for the lower slope, or 4-10 km for the higher slope. Paleogeographic maps illustrated that the bayline limit (from the lower delta plain to river mouth) of Allomember E should be on the order of tens of kilometers. Additionally, Plint and Wadsworth (2003) suggested a 30 km tidal backwater length for the Dunvegan. The paleoslope estimated using this longer tidal backwater length would be on the order of 10^{-5}, which is more consistent with the lower paleoslopes calculated above using the empirical equation. Combining the estimates from various approaches suggests that the paleoslope estimated from the empirical equation is more reasonable than the steeper gradient originally hypothesized by Plint and Wadsworth (2003). The estimated lower slope is also in agreement with the dominant fine sand grain size observed in the valley fills.

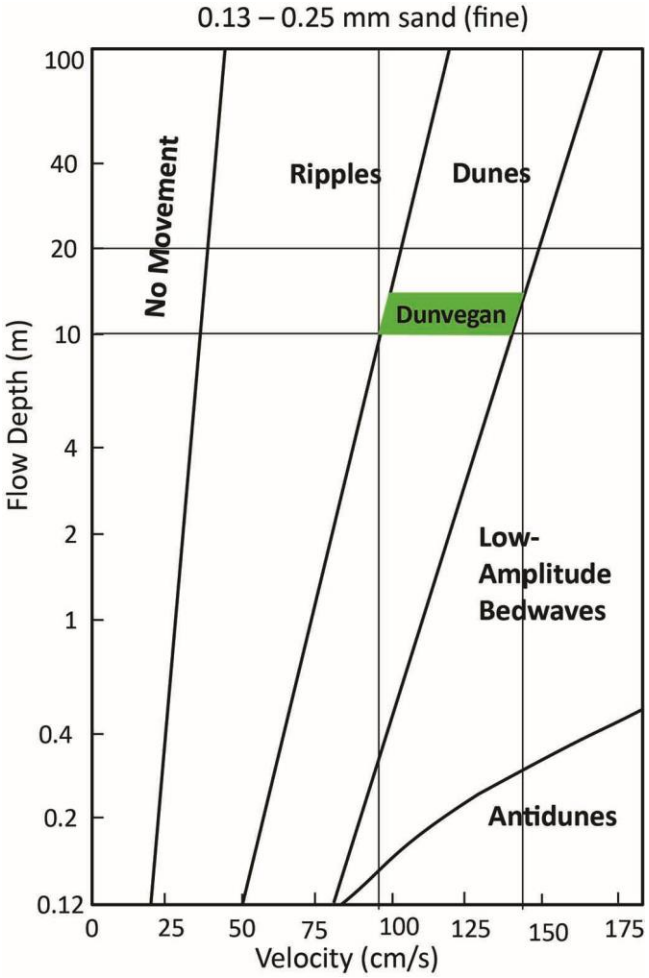

Fig. 2.11.– Bedform phase plot illustrating correlation between flow velocity and flow depth for various bedforms under certain sediment grain size (0.13-0.25 mm). The estimated grain size of the Dunvegan trunk-river is in the range of 0.15-0.25 mm. The estimated bankfull flow depth of 10-20 m, coupled with dune bedforms interpreted from cross-bedding sedimentary structure, approximated the Dunvegan velocity into the range of 0.9-1.4 m/s (modified after Rubin and McCulloch, 1980).

Flow Velocity.--- The flow velocity, estimated using the Chézy equation, is about 1.0 m/s. Using the estimated bankfull channel depth of 10 – 15 m, observation of predominantly upper-fine sandstone from cores, and the abundance dune-scale cross-bedding observed from both core and outcrops (Plint and Wadsworth 2003) (Figs. 8 - 10), the velocity

estimated from the bedform phase diagram is in the range of 0.9 - 1.4 m/s (Fig. 2.11). The flow velocity estimated from the Chézy Equation (Equation 4) thus falls into the same velocity range as approximated from the bedform-phase diagram but plots on the lower side of the range.

2.3.2 Discharge Estimation

The bankfull discharge (Q_{bf}) of the E1 trunk river is estimated to be 1.6 - 3.7 $\times 10^3$ m^3/s; the bedload sediment discharge (Q_{tbf}), estimated by the Chézy Coefficient method, ranges from 0.08 m^3/s to 0.12 m^3/s; and the suspended-load sediment discharge (Q_{ss}) estimated by the Van Rijn equations ranges from 2.1 m^3/s to 4.8 m^3/s (Table 1).

2.3.3 Estimation of Annual Sediment Discharge

In the Cenomanian, the Dunvegan deltaic complex was located in the Northern mid-latitude warm humid climate zone (NMW) (Fig. 2.12; Hay and Floegel 2012), which is equivalent to the warm temperate fully humid warm summer (Cfb) climate zone in the Köppen-Geiger climate classification. Geographically, the climate should be similar to northwest North America or Western Europe in modern times (Köppen-Geiger climate classification map). This is in agreement with the climate classification of the Dunvegan Formation, according to Davidson and North (2009).

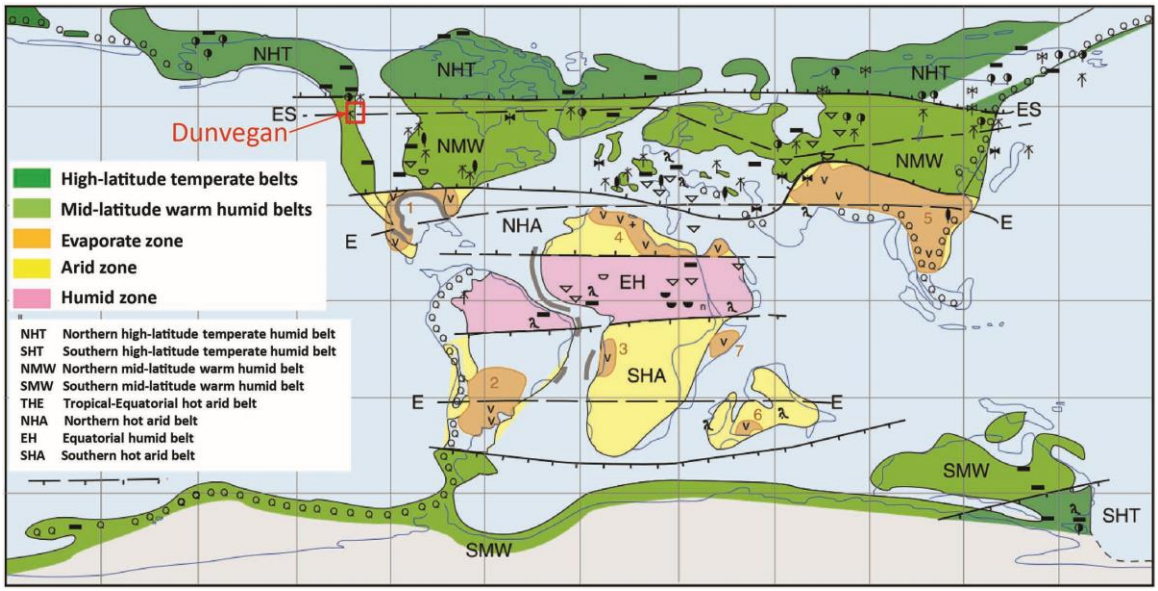

Fig. 2.12.–The global climate-zone classification of the Cenomanian period. The Dunvegan deltaic complex was located in the northern mid-latitude warm humid zone (NMW) (modified after Hay and Floegel, 2012).

Meybeck et al. (2003) discussed the sediment-flux variability and flood duration by synthesizing global river data in a variety of basin areas and climate regimes. The percentage of sediment transported within 2% of the total time is suggested to be correlated to drainage-basin area; thus, based on the estimated drainage-basin area of the Dunvegan Formation (on the order of 10^5 km^2, according to Plint and Wadsworth 2006), the trunk river may transport 10 – 40% (average 25%) of the total suspended sediment within 2% of the discharge time (Fig. 2.13). Additionally, research on the Rhine River, which is considered as a modern counterpart of the Dunvegan river based on Davidson and North (2009), also suggested that peak flow transports about 25% of the sediment. In this study, we similarly assume that 25% of the total sediment is transported within 2% of

one year (7.3 days) as the bankfull discharge duration. Therefore, Equation 10 can be written as

$$Q_{mas} = Q_{tbs} \times 7.3 / 25\%$$

Based on these parameters, the calculated annual bedload volume ranges from 1.9 to 3.0 $\times 10^5$ m^3, and the calculated annual suspended-load volume ranges from 5.2 $\times 10^6$ to 1.2 $\times 10^7$ m^3 (Table 1.1).

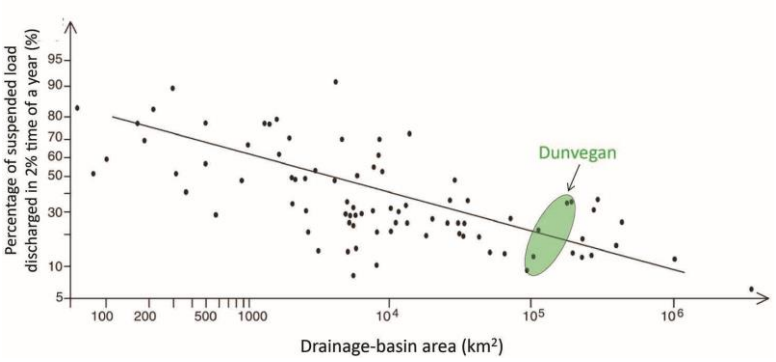

Fig. 2.13.–Plot of percentage of total suspended-load discharged within 2% time of a year by rivers with various drainage areas and in different climate regimes (modified after Meybeck et al. 2003).

2.3.4 Duration of Deposition

Previous work shows that the entire Dunvegan Alloformation was deposited in about 2 million years (Plint and Wadsworth 2006; Bhattacharya et al. 2016). Each of the ten Allomembers should thus be deposited in no more than 200,000 years. Plint and Wadsworth (2006) documented four paleovalley systems, and suggested that each paleovalley system may be formed within 100,000 - 200,000 years. McCarthy et al. (1999) and Plint et al. (2001) also estimated that each Dunvegan allomember represented 150,000 to 200,000 years. Moreover, Plint et al. (2001) inferred that the offlap pattern of

marine parasequences, and the maturity of interfluve paleosols, might represent as much as half of that time (Kraus 1999). They suggested that river entrenchment began early and continued throughout the falling-stage systems tract, resulting in sediment starvation due to incision on the interfluves and delivery of all available sediment to the delta front. Thus, each valley system might record half of the depositional duration of the allomembers of river entrenchment. Allomember E was further divided into four parasequences, and the individual trunk river parasequence likely represent deposition in less than 25,000 years (Bhattacharya et al. 2016).

2.3.5 Evaluation of Cumulative Sediment Load

The paleodischarge of the trunk river in Allomember E, as well as the total sediment load passing through the trunk-river fulcrum point, can now be calculated using the estimated paleohydrologic parameters and total duration. The results and estimated parameters are summarized in Table 1. The results indicate that the trunk river of Allomember E was 10 – 15 m deep and 150 – 230 m wide, carried mainly fine-grained (< 200 microns) sand and flowed over a low-gradient paleoslope of 4.1 – 6.1 $\times 10^{-5}$. Annual total sediment load is estimated to be in the range of 5.2 $\times 10^{6}$ – 1.2 $\times 10^{7}$ m^3/yr, including both bedload and suspended load. Within 25,000 years, the river is estimated to have transported 1.4 $\times 10^{11}$ m^3 – 3.1 $\times 10^{11}$ m^3 (135 – 307 km^3) of sediment into the basin (Table 1).

Table 2.1 Estimates of paleohydrologic parameters and discharge from the Dunvegan Formation Allomember E

Channel		Bankfull Channel Width (m)	Average bankfull depth (m)	Slope	Grain size (D_{16}, D_{50}, D_{84}, D_{90}) (mm)	Q_{bf} Water (m^3/s)	Q_{tbf} Bedload (m^3/s)	$\bar{u}$ Avg. Velocity (m/s)	Bankfull Suspended-Load Discharge, Q_{ss} (Van Rijn, 1984) (m^3/s)	Mean Annual Bedload Q_{sb} (m^3)	Mean Annual Suspended Sediment Q Van Rijn (m^3)	Total Bedload Q_{tsb} (km^3)	Total Suspended load Q_{tss} (km^3)	Total sediment load Q (km^3)
E1	Min.	150	10	6.1×10^{-5}	0.14, 0.20, 0.27, 0.30	1.6×10^3	0.08	1.0	2.1	1.9×10^5	5.2×10^6	4.8	130	135
	Max.	230	15	4.1×10^{-5}	0.14, 0.20, 0.27, 0.30	3.7×10^3	0.12	1.0	4.8	3.0×10^5	1.2×10^7	7.4	300	307

2.3.6 Sediment Accumulation in the Sink and Mass Balance

An isopach map of Allomember E (Bhattacharya 1993) was used to assess total sediment volume deposited downstream of the trunk river (Fig. 2.14). The volume of mapped deposits in the basin, down-dip of the fulcrum point, is approximately 4.3×10^{11} m^3, assuming 20% average porosity (Plint et al. 2009), thus the total volume of sediment deposited in the basin is about 3.4×10^{11} m^3, including both sandstones and mudstones. A 10% compaction factor (Holbrook and Wanas 2014) is also used to reconcile the original uncompacted sediment volume prior to compaction that subsequently approximates the sediment volume of 3.8×10^{11} m^3 (380 km^3). This sediment volume is estimated from the whole of Allomember E, whereas the lowstand delta fed by the trunk river was deposited only during the time represented by Parasequence E1. Four parasequences were mapped in Allomember E in total (Bhattacharya 1993); the sediment volume of Parasequence 1 is very likely greater than the other three parasequences, based on the paleogeographic maps of Bhattacharya (1993) and an approximate thickness estimate from Figure 2.2. Therefore, here we assume that the sediment volume of Parasequence E1 accounts for one third of the total estimated sediment volume of Allomember E, which is 1.3×10^{11} m^3 (130 km^3). A sandstone isolith map of Parasequence E1 delineates sandstone distribution and shows a lobate geometry (Bhattacharya 1993) (Fig. 2.15). The estimated sandstone volume is approximately 3.2×10^{10} m^3 (32 km^3) beyond the fulcrum point. Assuming 20% average porosity yields a sand sediment volume of ca. 2.6×10^{10} m^3 (26 km^3).

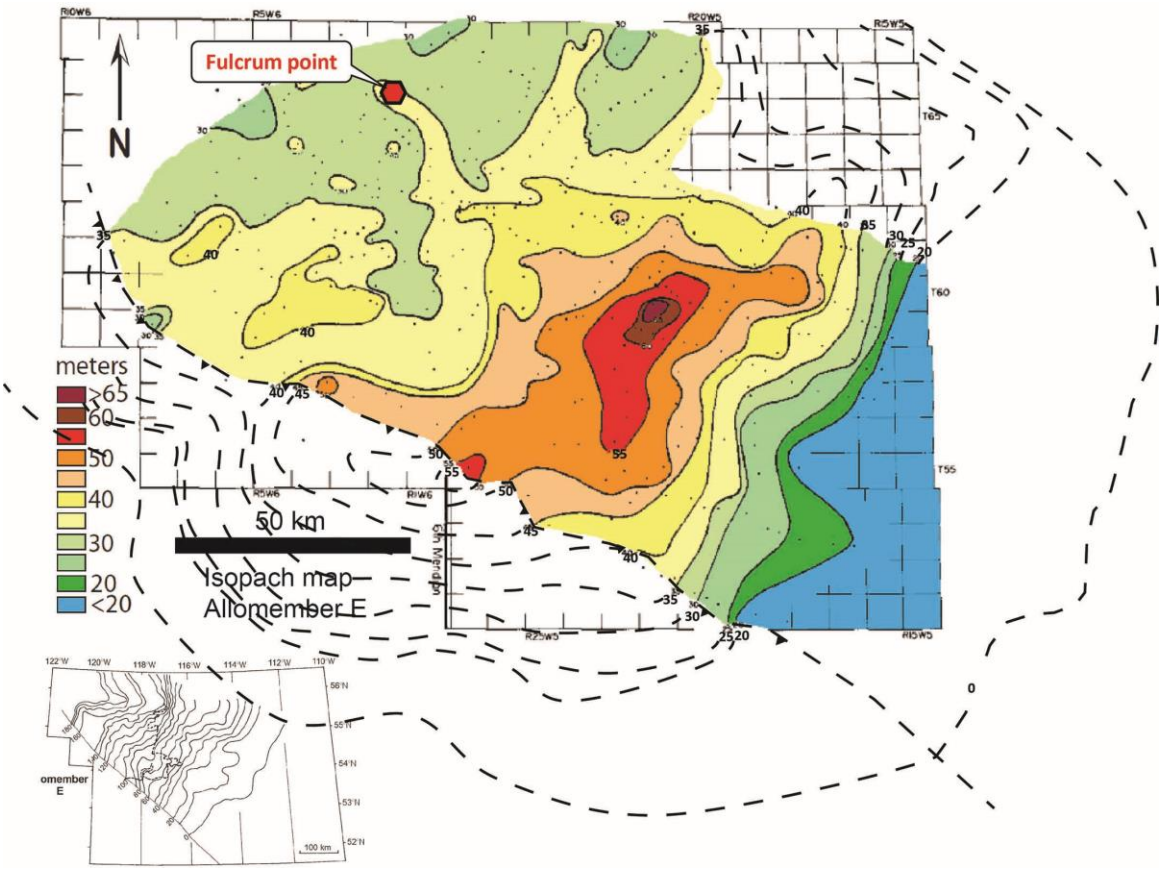

Fig. 2.14.–Isopach map of Allomember E in the Dunvegan Formation, Alberta, Canada. This well depicts depositional configuration and progradational characteristics of Allomember E. The map is used for volumetric assessment of sediment accumulation down-dip to the fulcrum point. Dashed lines were extended to close contours based upon geometric trend (modified after Bhattacharya, 1993).

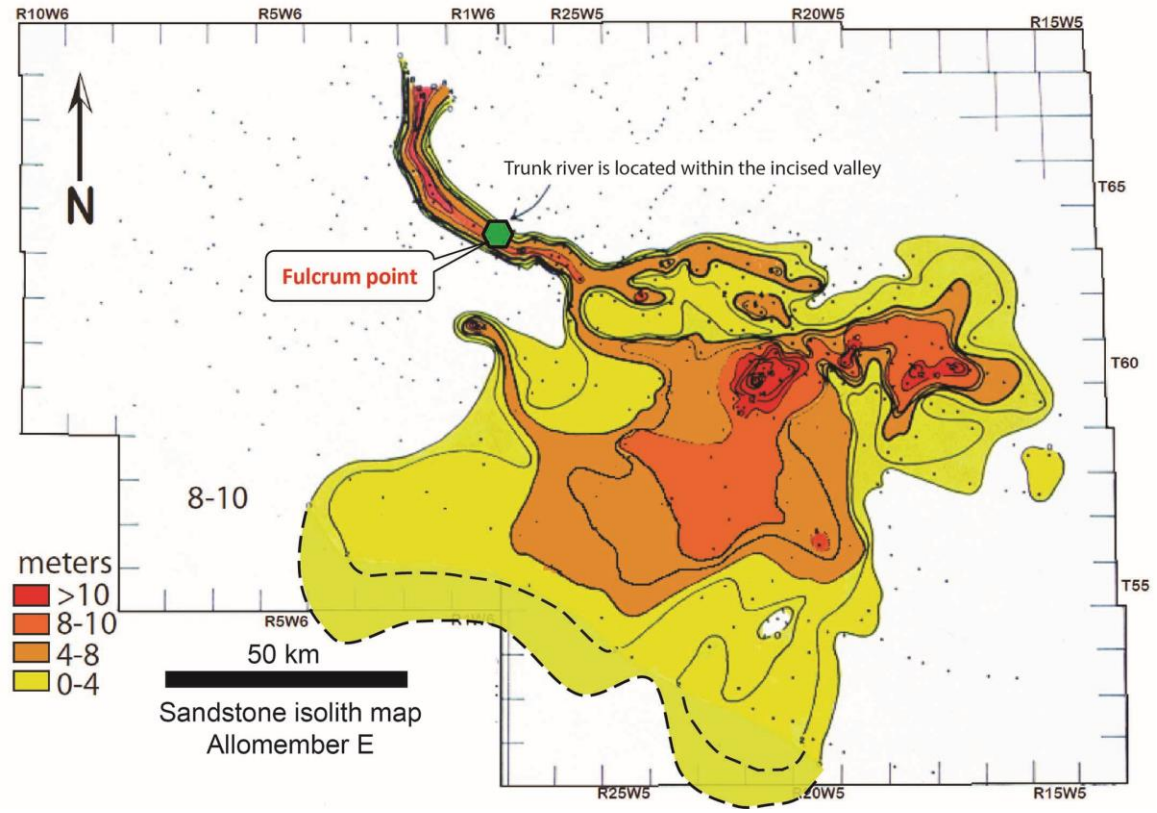

Fig. 2.15.–Isolith map of Parasequence E1 in Allomember E, Dunvegan Formation. The map well portrayed the lobate feature of river-dominated deltaic deposition. Sand-prone distributary system and deltaic lobes are depicted from the map. The map also allows sandy sediment volume calculation of the Dunvegan delta deposited in Parasequence E1. Dashed lines were extended from original contours based upon deltaic lobate geometric trend (modified after Bhattacharya, 1993).

The estimated sediment volume delivered and passed through the fulcrum based on the paleohydrologic evaluation of the trunk river is ca. 1.4×10^{11} m^3 – 3.1×10^{11} m^3 (135 - 307 km^3), while the documented sediment volume transported through the trunk river and accumulated in the sink area is about 1.3×10^{11} m^3 (130 km^3). The sediment budget and accumulation volumes are on the same order of magnitude, whereas the upper-range estimate is 2.5 times greater than the sediment mapped in the study area. This indicates

minimal sediment balance between source and sink, although the higher values indicate a possibly underbalanced system (Fig. 2.16).

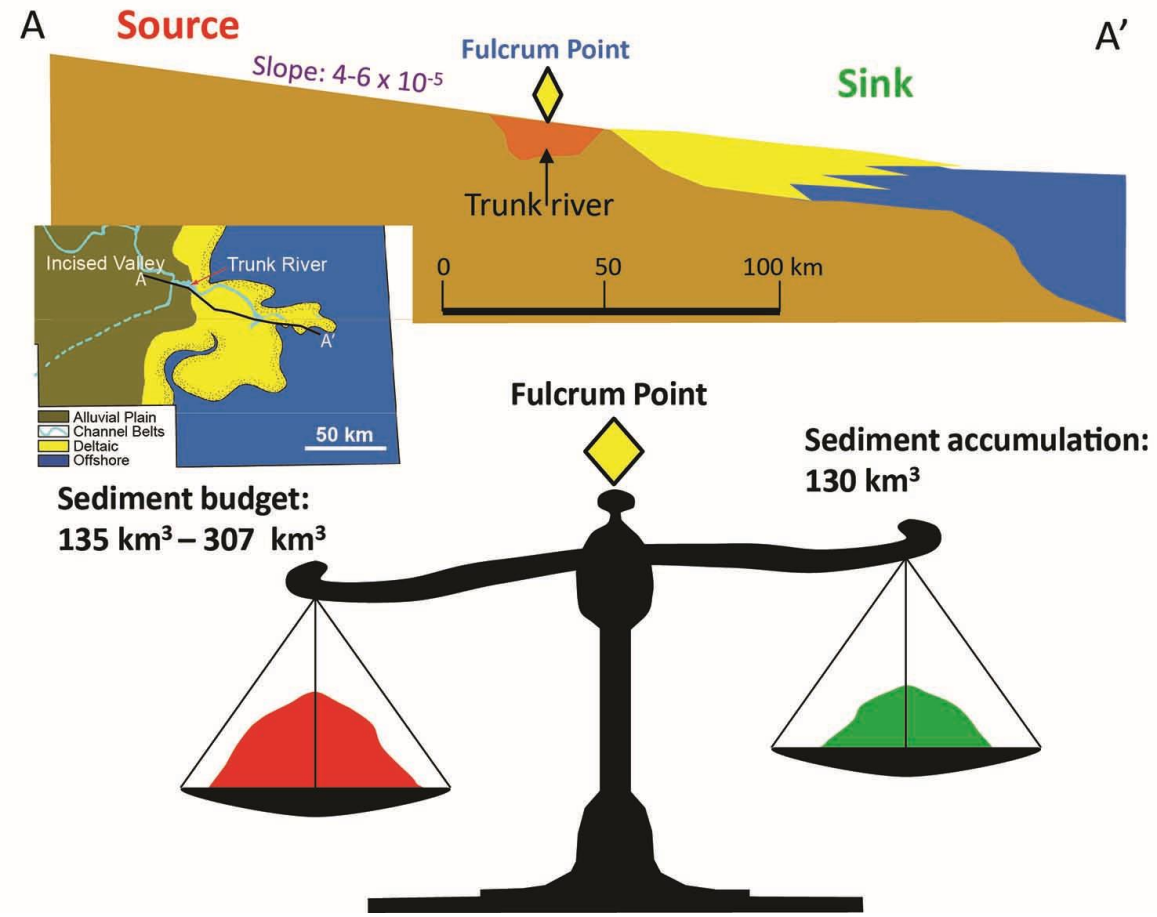

Fig. 2.16.–Cross section of the S2S system and mass-balance diagram. A-A' profile is sketched cross sectional view of trunk-river longitudinal profile of Parasequence E1 in Allomember E, referred to inset map of Parasequence E1 paleogeography. The trunk-river serves as a fulcrum connecting source and sink. The estimated sediment volume delivered and passed through the fulcrum is ca. 130 - 300 km3, while the documented sediment volume transported through the trunk-river and accumulated in the sink area is about 100 km3. The sediment budget and accumulation volumes are in the same order of magnitude, which indicates a total mass balanced in the S2S system, while the upper-range estimate of sediment delivered into the sink is up to 3 times the measured sediment volume, which is expected as the effects of sediment transient storage along sediment routing system, as well as a sediment post-deposition escape.

2.4 Discussion

2.4.1 The Mass Balance

The upper-range estimate of sediment delivered from the source is 2.5 times the measured sediment volume in the sink area, which, if accurate, would suggest significant sediment escape (Bhattacharya et al. 2016). Because the Cretaceous Western Interior Seaway was a ramp margin during the Cenomanian, and no shelf-slope break existed, there are no submarine fan deposits. Hyperpycnal flows have been documented in the proximal part of the shelf (Bhattacharya and Maceachern 2009), but owing to the low gradient, it would be difficult for sediment to accelerate or to be transported far from the shoreline to deep water (Varban and Plint 2008). The alternative sediment transport mechanism is wave reworking, but Allomember E is one of the most river-dominated systems in the Dunvegan (Bhattacharya 1993). The greater sediment input versus the accumulation supports the hypothesis that in Dunvegan time, mud was widely dispersed southward along the Alberta Foreland Basin by geostrophic currents associated with storm processes and counterclockwise oceanic gyres (see Plint et al. 2009). Along-shelf geostrophic flows towards the southwest would result from Coriolis deflection of the water mass in the northern hemisphere (Slingerland et al. 1996).

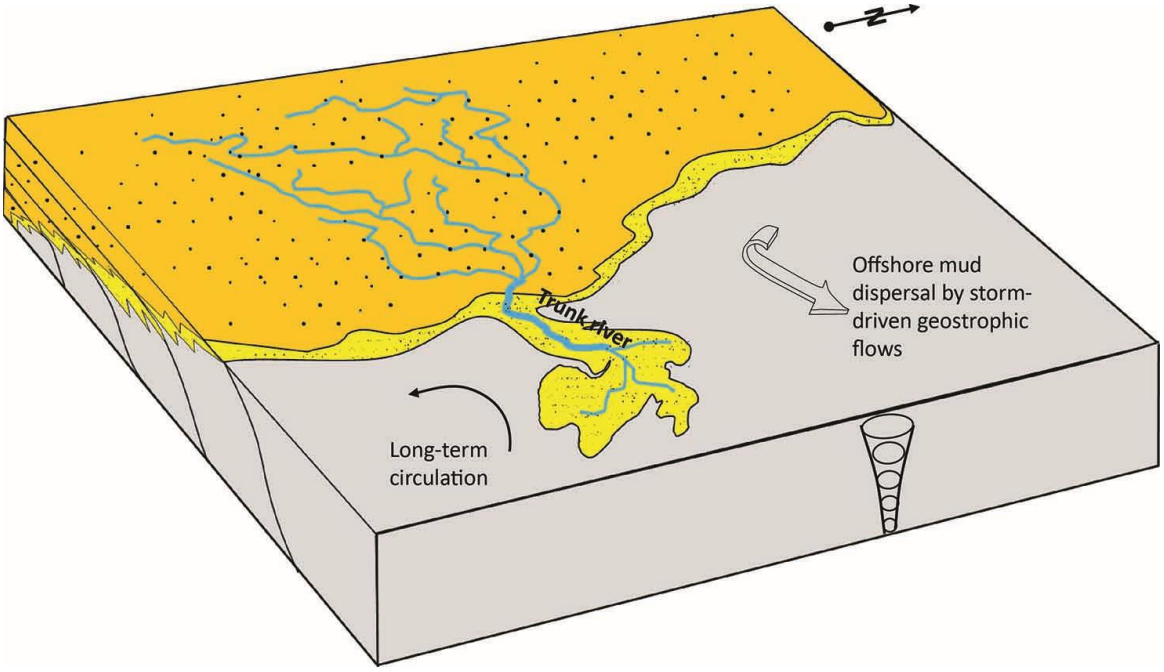

Fig. 2.17.–Block diagram of paleogeographic map of Parasequence E1 in Allomember E, Dunvegan Formation with oceanic circulation initiated gyre flows and storm-driven geostrophic flows illustrates the mud dispersal mechanisms along the shelf, which interpreted the potential sediment escape and a larger sediment volume from source area than the measured sediment volume preserved in the sink. The block diagram is based on the paleogeographic map in Bhattacharya and MacEachern (2009).

Plint et al. (2009) state that the younger Allomembers (F – D) of the Dunvegan Formation are low-gradient systems, and formed laterally extensive muddy clinothems, suggesting relatively shallow water (< 40 m). The shallow water would allow storm-driven geostrophic flows reaching the sea floor and resuspending mud for further transport. Flocculated and pelleted muds are likely to be repeatedly resuspended by concomitant storm waves and advected obliquely across and along the shelf. The long-term large-scale counterclockwise oceanic circulation in the Western Interior Seaway initiated a south-directed oceanic gyre flow that also exerted a force for mud transport

along the shelf. Combined and geostrophic flows have been emphasized as the principal mechanisms likely responsible for the offshore dispersal of both sand and mud across storm-influenced shelves (Fig. 2.17). Mud dispersal mechanisms are also reviewed and discussed by Blum and Hattier-Womack (2009), showing that mud transported by hyperpycnal plumes can be merged with alongshore current and resuspended for transport basinward. Mud therefore can be transported over hundreds of kilometers along the shelf. The study of the Kaskapau Formation shales, which lie directly above the Dunvegan Alloformation, suggests that mud was resuspended by storm waves and transported as much as 250 km offshore by wind-driven currents (Varban and Plint 2008).

The modern Amazon S2S system shows that < 50% of the sediment delivered by the Amazon River is deposited on the adjacent inner-shelf subaqueous delta, whereas the remaining sediment is transported northwards by the Guyana Current towards the Orinoco Delta (Warne et al. 2002; Sømme et al. 2009b). Romans et al. (2015) also revealed that more than 50% of the sediment delivered through the Eel River to the sea was transported beyond the shelf. Also the Po Delta, Mississippi, and Atchafalaya show significant along-shelf export, even though the latter two are river-dominated (Allison et al. 2000; Draut et al. 2005; Cattaneo et al. 2007). Similar mud transport mechanisms may be invoked to explain the difference between the volumes of estimated sediment supplied and accumulated in the proximal part of the Dunvegan shelf. In addition, the isopach maps represent the volumes of sediment accumulated proximal to river mouth and do not incorporate along-shelf or across-shelf mud belts.

In addition to sediment escape on the shelf, sediment sequestration and partitioning inside the transfer systems (e.g., deposited in the floodplain) may be a secondary mechanism attributed to the volume difference between the source and sink (Allen 2008a; Romans et al. 2015). In sediment routing systems, although fluvial systems serve as the transfer zones, where sediment is considered not purely eroded, nor accumulated, there is still erosion and storage, thus a proportion of sediment can be sequestered or permanently stored within a river and its floodplain (Walling and Collins 2008; Holbrook and Bhattacharya 2012; Romans et al. 2015); unfortunately, the sequestration ratio remains equivocal in ancient systems.

In the Dunvegan Alloformation, the tectonically active drainage basin is estimated to have been on the order of 10^5 km^2 in area, which is considered to be a moderate drainage system and suggests a relatively long sediment routing system. As a consequence, sediment sequestration could be considerable in the transfer systems (Milliman and Syvitski 1992; Covault et al. 2010; Romans et al. 2015). Moreover, landward tectonic flexural subsidence has been demonstrated to be important in Allomember E, as indicated by landward thickening of the nonmarine strata updip (Plint and Wadsworth 2003). Landward sequestration may be important, but it remains equivocal as to when this occurred (i.e., which parasequence of Allomember E). Timing of flexural subsidence is critical to unravel this issue and may have been more important in the deposition of the older parasequences in Allomember E, which do not show signs of degradational stacking that would indicate falling sea level. Rather, interfluve paleosols, described by Plint and Wadsworth (2003) suggest degradation during the falling stage of the valley that occurs

in the latter stage of deposition of Allomember E, and this limits the possibility of mud sequestration in floodplains during the falling stage associated with valley erosion.

2.4.2 Estimates of Paleodischarge and Sediment Volumes

Paleodischarge of the ancient trunk river was estimated to be in the range of 1.6 – 3.7 × 10^3 m^3/s, which is in agreement with the paleodischarge estimated by Bhattacharya and MacEachern (2009). The discharge of the Rhine River is approximately 3.5 × 10^3 m^3/s, which represents a likely modern analogue for the Dunvegan trunk river, as was also suggested by Davidson and North (2009).

Based on the estimates of sediment transport in the trunk river of Allomember E, the bedload is calculated to be about 4% of the total sediment load, compared with a more common value of 10% reported in the literature on modern rivers (Turowski et al. 2010). The low percentage calculated here for the Dunvegan can be attributed to low shear stress due to the low-gradient in contrast to smaller-scale and steeper-gradient mountainous rivers, the bedload ratio of which can be up to 40% (Turowski et al. 2010). On the other hand, the estimated bedload sediment volume is about 5 - 7 km^3, whereas the sand volume estimated from the isolith map is about 26 km^3. This indicates that a significant amount of very-fine-grained sandy sediments (i.e., < 62-125 microns) were transported as suspended load. Core data (Bhattacharya 1992) shows that much of the sand in the lowstand delta is in the very fine upper range (88-125 microns), supporting the idea of significant transport in suspension.

The average thickness of Parasequence E1 downstream is about 6 - 8 m (Fig. 2.15), which represents an approximate sedimentation rate of 0.3 m/kyr, given the depositional

duration of 25,000 years. The Dunvegan corresponds to the Unit 8 on the "Sedimentation Rate Scale" (SRS) of Miall (2014), characterized as channel belts or delta deposits (his Fig. 1). The sedimentation rate reflects that each parasequence of Allomember E was deposited under the control of short-term Milankovitch cycles (Miall 2014) and supports the hypothesis that allogenic Milankovitch cyclicity produced the high-frequency sequences in the Dunvegan Formation.

According to Davidson and North (2009), assuming a Northern mid-latitude warm humid climate, the drainage basin area of Allomember E can be estimated with the regional curve parameters:

$d_m = 1.11(DA)^{0.31}$

$Q_w = 100.6(DA)^{0.76}$

where d_m is bankfull flow depth, Q_w is water discharge, and DA is drainage-basin area. The estimated drainage-basin area is on the order of $1.4 – 1.8 \times 10^5$ km^2, which is consistent with the drainage-basin area estimated by both Plint and Wadsworth (2003) and Bhattacharya et al. (2016) based on paleotectonic and paleogeographic reconstructions.

The modern Cfb climate zone is located between 40o N and 55o N. Similarly, the latitude of the Maritime Temperate climate zone, which represents the climate thought to be the most characteristic of the Dunvegan Formation, is between 45^o N and 55^o N (Davidson and North 2009). Nonetheless, McCarthy et al. (1999) suggested that the Dunvegan Formation was deposited at a paelolatitude of 65^o N, which is higher than its modern climate analog. This is explained by the idea that the Cenomanian represented a

"greenhouse" time in earth history with a correspondingly warmer climate (Glancy et al. 1993).

The Rhine River, which is considered as a modern analog to the Dunvegan system, based on the regional climate classification, has a basin area of 1.6×10^5 km^2 and a discharge of 3.5×10^3 m^3/s. The drainage-basin area is quite similar to the estimated drainage-basin area of the Dunvegan, but the estimated discharge of the Dunvegan trunk river, using the regional curve equation listed above, is significantly larger than the Rhine River, by a factor of 5 (Davidson and North 2009). River discharge is substantially related to drainage area, relief, and climate. The discharge of the Dunvegan trunk river seems to be rather overestimated by the regional curve method. Davidson and North (2009) admitted that the regional-curve method is less reliable in predicting discharge than estimating drainage-basin area.

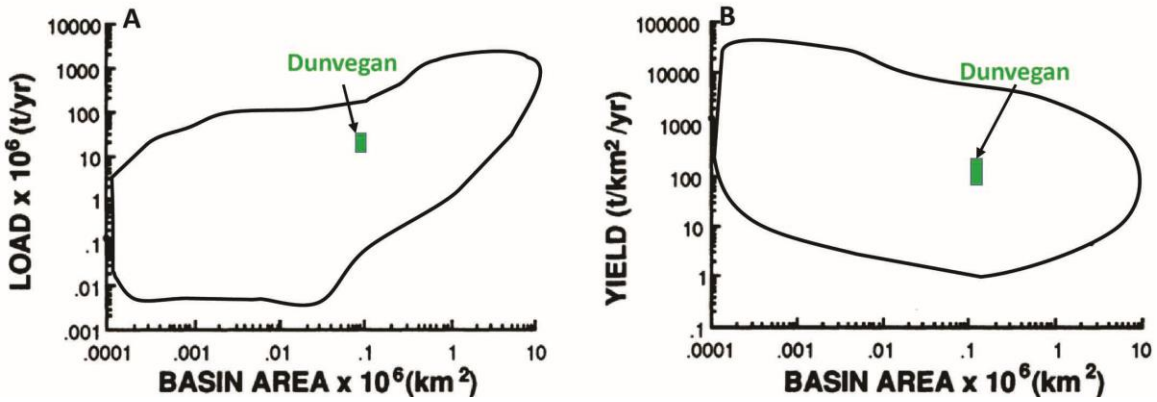

Fig. 2.18.–A) Sediment load vs. basin area; B) Sediment yield vs. basin area of the global river database. Note the strongly normal trend between sediment load and basin area, whereas the generally inverse relationship between yield and basin area (modified Milliman and Syvitski, 1992).

The estimated sediment load of the Dunvegan trunk river ranges from 12.5 to 28.6 MT/yr, given a bulk density of 2.4 g/cm^3 (Beaumont 1981), and sediment-yield estimates range from 89.3 to 158.9 t/km^2/yr (Table 2). The correlations between estimated drainage-basin area and sediment load and sediment yield of the Dunvegan trunk fluvial system are plotted on a global modern-river dataset (Fig. 2.18A, B). The Dunvegan E1 trunk fluvial system can be categorized as a moderate-size mountain-river drainage system, according to modern-river analogs (Milliman and Syvitski 1992). Appropriate modern-analog selection, based on an accurate quantitative approach, allows better prediction of the size and geometry of an ancient system. Linking modern-analog systems to outcrops and subsurface data helps to reconstruct paleogeography and scaling of depositional environments, as well as estimating the scales and dimensions of paleodrainage networks. With the knowledge of the geometry and paleohydrological elements of the paleodrainage system, paleoclimate can also be reconstructed.

Table 2.2 Estimated drainage-basin areas, sediment loads, and sediment yields for the trunk river of Allomember E

Channel	Drainage Basin Area (×106 km2)	Sediment discharge (×106 m3/s)	Sediment Load (Mt/yr)	Sediment Yield (t/km2/yr)	Remark
E1	0.14 – 0.18	5.2 – 11.9	12.5 – 28.6	89.3 – 158.9	Moderate-size mountain river

2.4.3 Comparison to BQART Method

Syvitski and Milliman (2007) introduced the “BQART" method of sediment-discharge estimation based upon discharge (*Q*), drainage area (*A*), relief (*R*), temperature (*T*), and *B*, which is a factor determined by multiple geological elements that are discussed below. We also applied this method to estimate sediment discharge independently of the fulcrum

approach. Paleoclimate analogized by the Köppen-Geiger climate classification and associated with the regional curves of Davidson and North (2009) indicates that the average temperature of the Dunvegan area was between -3 ^{o}C and 18 ^{o}C. Fossil flora described by Bell (1963) show a dominance of tropical plants, such as *Ficus* and *Magnolia,* characterized by broad, smooth-edged leaves. This suggests that, despite being at a temperate latitude, the Cretaceous Dunvegan system was actually a tropical – subtropical paleoclimate zone, the average temperature of which would have been around 18 ^{o}C, according to the Köppen-Geiger climate classification. Dennis et al. (2013) estimated that mean annual temperature of the Late Cretaceous Western Interior Seaway of 20 ^{o}C using a carbonate-isotope thermometer. We used 20 ^{o}C as the mean temperature in our estimation. Therefore a more applicable equation is

$Q_s = 0.02BQ^{0.31}A^{0.5}RT$, and

$B = IL(1\text{-}T_E)E_h$,

where I is the glacier erosion factor ($I \geq 1$), L is an average basin-wide lithology factor, T_E is the trapping efficiency of lakes and man-made reservoirs, such that $(1\text{-}T_E) \leq 1$, and E_h is a human-influenced soil erosion factor.

The Late Cretaceous is well accepted as a "greenhouse" world without significant ice cover; therefore, I equals 1. L is set at 2, as suggested by Syvitski and Milliman (2007) for a clastic soft sedimentary basin. T_E and E_h are set at 1 as there could not have been any anthropogenic effects in the Cretaceous. The current height of the Laramide-age Rocky Mountains is about 4,400 m after erosion, and the peak is less than 3000 m in Canada, but Laramide orogenic activity occurred after the Dunvegan (Dickinson and Snyder 1978).

Hence the continental relief during the Dunvegan time would likely be less than today. Beaumont (1981) modelled the formative mechanisms of the Alberta Foreland Basin of Western Canada and implied that the Rocky Mountains were about 2000 m above sea level during the Late Cretaceous, and we thus assume a relief of 2,000 m for the "BQART" analysis. As the discharge estimated from trunk-river dimensions is the bankfull discharge, and likely only occurs 2% of a year, the annual sediment load is used for comparison. Therefore, the estimated sediment discharge using the BQART formula ranges from 5.2 to 7.6 $\times 10^6$ m^3/s, the lower end of which is the same as the lower range of the annual sediment discharge estimated by the fulcrum method. The upper limit of the BQART estimate is about 60% of the upper-range estimate using the fulcrum method (Fig. 2.19; Table 2). The BQART calculation is sensitive to estimates of relief, temperature, glacial cover, and anthropogenic effects. Anthropogenic effects and glaciers are almost certainly not relevant factors for the Dunvegan, and we believe that the hinterland relief was not likely much higher than our estimate. However, the average temperature may have been higher than 20 ^oC. Slingerland et al. (1996) discussed that the temperature of the Western Interior Seaway during the Late Cretaceous could have been higher than 20 ^oC. Using a higher temperature value would increase the BQART estimate, which results in an upper-range value more similar to the upper-end estimate using the fulcrum approach detailed above.

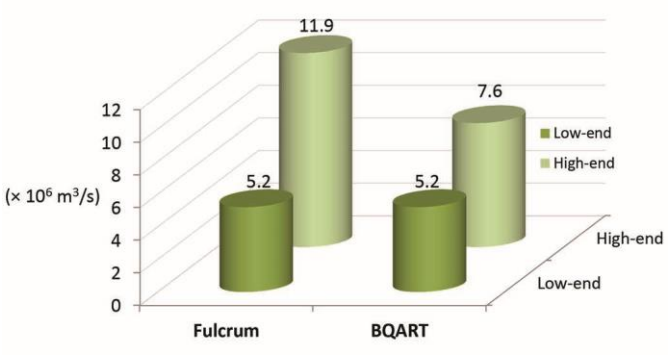

Fig. 2.19.–A comparison of estimated sediment discharge using the fulcrum approach and the BQART method. The lower-end values are identical, and the higher-end value of the sediment discharge estimated using the fulcrum approach is greater than that of the BQART method. The difference could be caused by the conservatively lower temperature used in the BQART.

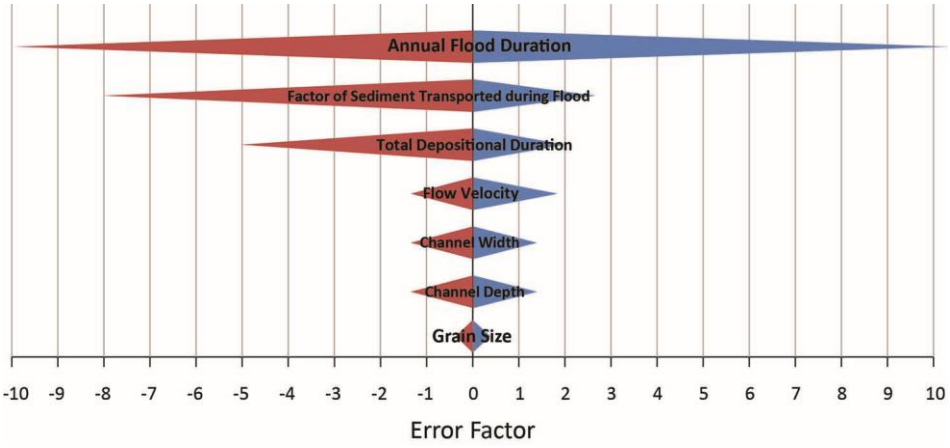

Fig. 2.20.–Tornado chart indicates magnitude of errors and uncertainties in the fulcrum approach. The error factor of each parameter is a factor of the extreme values to the mean value. The most sensitive error is the annual discharge estimate related to annual flood duration, and can show an error of an order of magnitude.

2.4.4 Errors and Uncertainties

The fulcrum approach involves a number of uncertainties, including field measurements, numerical assessments used to estimate paleohydrologic parameters, paleomorphodynamics derived from stratigraphic records, applicability of empirical

equations, chronologic estimates, and selection of modern-analogue data. The integration of these variables constrains the accuracy of sediment-volume estimation to at worst one order of magnitude (see discussion in Hajek and Wolinski 2012; Holbrook and Wanas 2014; Bhattacharya et al. 2016) (Fig. 2.20).

An analysis of error and uncertainty shows that the most sensitive error is the annual-discharge estimate related to annual flood duration, and can show an error of an order of magnitude (Fig. 2.20). This agrees with the most uncertain element in the study of Holbrook and Wanas (2014). The annual discharge estimated is a function of estimates of bankfull event duration, recurrence, and sediment transport capacity, which remain difficult to constrain in deep-time systems. For example, bankfull floods are easily masked or overprinted in S2S systems (Wang et al. 2011; Cramer et al. 2015; Romans et al. 2015). The bankfull flood is defined as the moment when the channel is fully filled with water. Durations and return periods of bankfull flood vary from river to river, and they are still controversial in the hydrologic community. Bankfull floods are highly dependent on climate regime and tectonic topography, associated with seasonality and annual cyclicity (Arora and Boer 2001). Durations of bankfull events in modern rivers are also highly variable, ranging from a couple of days up to 80 days per year (Andrews 1984; Holbrook and Wanas 2014). The proportion of sediment load carried and transported during bankfull flood events is also highly variable, as it is controlled by bankfull-event duration, sediment supply, drainage-basin scale, fluvial diffusivity, annual flood frequency, river normal flow condition, and high flow frequency and magnitude, and may range from 25 to 90% (Nolan et al. 1987; Andrews and Nankervis 1995; Moog and

Whiting 1998; Sichomgabula 1999; Davide et al. 2003; Meybeck et al. 2003; Powell et al. 2006). Flood events of the Dunvegan trunk river may transport a low proportion of annual sediment due to a long sediment route and low gradient, compared to more vigorous smaller river systems (Meybeck et al. 2003).

It may not be feasible to estimate long-term sediment volumes based on simply summing short-term estimates. Miall (2014) emphasizes the fragmentary nature of sedimentary systems and the difficulty of assigning time to rocks. This argument leads to a question as to whether the 25,000 years assumed for parasequence E1 represents the effective sedimentation time, or whether there are significant time gaps at the top flooding surface or associated with the valley sequence boundary. If the time scale is shorter, the annual sediment discharge may not represent an average value, especially when flood magnitudes with different return periods are considered (Sadler 1999; Holbrook and Wanas 2014; Miall 2014; Sadler and Jerolmack 2015). Nonetheless, when we estimated annual sediment discharge, we considered both short-term peaks of concentrated sediment transport and the percentage of the concentration of total annual discharge. In other words, we have assumed a constant averaged annual sediment discharge of the system by applying the concept of peak-flood-duration sediment concentration and related proportion of total annual discharge. Therefore, the annual discharge can be used to estimate total sediment volumes.

The fulcrum approach does not take sediment stored landward of the fulcrum into consideration, but only accounts for sediment passing the fulcrum, which therefore inevitably introduces uncertainties. Multiple fulcrum assessments along longitudinal

profiles of trunk valleys could account for variable storage of sediment in a valley system (Holbrook and Wanas 2014). Multiple drainage systems may coexist in the Dunvegan deltaic complex of Allomember E (Fig. 2.3), which can be analyzed by dividing different drainage systems, estimating and combining multiple feeding rivers, and comparing them to the documented sediment accumulation volumes in the sink. If the estimated sediment volume delivered by a single fulcrum trunk channel was less than the sediment accumulated, then multiple trunk channels can be inferred (Holbrook and Wanas 2014).

Alternatively, Sadler (1999) suggested that over time scales of Milankovitch cycles, the average effective sediment accumulation rates (the rate of sediment preserved in the basin over total source sediment) are in the range of 10 – 20%. Given the instantaneous sediment discharge of 2.1 – 4.8 m^3/s, including both bedload and suspended load, and the total chronometric duration of 25,000 years, sediment accumulations in 10% of total depositional duration are estimated to be in the range of 1.7 – 3.7 $\times 10^{11}$ m^3 (166 – 370 km^3), which is consistent with the results of 1.4 – 3.1 $\times 10^{11}$ m^3 (135 – 307 km^3). If we use 20% as effective sedimentation rate, the results are still on the same order of magnitude.

2.4.5 Hyperpycnal Flows

The estimated bankfull flood discharge of the Dunvegan trunk river is in the range of 1.6 – 3.7 $\times 10^3$ m^3/s. Milliman and Syvitsky (1995) suggest that rivers with *average* discharge lower than 6000 m^3/s routinely generate hyperpycnal flows during floods (Bhattacharya and MacEachern 2009). The Dunvegan drainage system is adjacent to a tectonically active mountain belt in a warm humid climate and drained into a shallow

ocean (less than a few hundred meters deep), albeit it has a relatively low slope. In addition, examination of cores through delta-front and prodeltaic facies, especially in Allomember E, shows abundant hyperpycnites, turbidities, and wave-enhanced sediment-gravity-flow deposits (Bhattacharya and MacEachern 2009). This suggests that the Dunvegan rivers routinely generated hyperpycnal flows. However, it is unlikely that direct river-driven hyperpycnal flows were able to flow very far on such low slopes of the Dunvegan shelf. Longer-scale mud transport and dispersal on the shelf in the form of fluid mud was likely enhanced by storm waves. Abundant and ubiquitous hummocky cross-stratification and wave ripples observed in shoreface and deltaic successions indicate a storm-dominated seaway (Pattison and Walker 1992). This further confirms the hypothesis of postdepositional mud dispersal accounting for the volume difference between sediment influx and sediment accumulation. It is plausible that hyperpycnal flows contributed to the mud dispersal along the shelf, combined with other oceanic currents.

2.5 Conclusions

The fulcrum approach assumes that the total mass balance in a closed S2S system should match the sediment volume delivered from the source area through a fulcrum point (i.e., trunk river) to that deposited in the sink. Ancient trunk rivers are prominent fulcrum candidates, paleohydrologic parameters of which can be used to estimate paleodischarge and instantaneous sediment volumes passing through them. Consequently, the total sediment volumes can be estimated with a deep-time depositional duration. The workflow comprises trunk-river dimension and paleoslope reconstruction, grain-size evaluation,

instantaneous and annual discharge estimates, analysis of long-term depositional duration, and measurements of sink-area sediment accumulation.

The fulcrum approach was tested in the Upper Cretaceous Dunvegan Alloformation by comparing the total mass balance between source sediment production and sink accumulation through paleohydrologic assessment of the trunk river. The results indicate that the trunk river of Allomember E was 10-15 m deep and 150-230 m wide, flowed over a low-gradient paleoslope of about 4.1 - 6.1 $\times 10^{-5}$, and carried fine- to medium-grained sand. The river is estimated to have transported 1.4 $\times 10^{11}$ m^3 – 3.1 $\times 10^{11}$ m^3 (135-307 km^3) of sediment into the basin within 25,000 years, which is consistent with the 1.3 $\times 10^{11}$ m^3 (130 km^3) of sediment documented in the sink area. The upper-range estimate of sediment delivered to the sink is 2.5 times the measured sediment-sink volume and suggest sediment escape on the shelf or sediment sequestration inland. This supports the hypothesis of mud dispersal in Dunvegan time and accommodation increase landward due to tectonic subsidence. The concomitant storm-initiated hyperpycnal flows could also help to explain the mud dispersal. These estimates also allow more robust comparison of ancient and modern analogs and their scaling relationships.

Acknowledgements

We thank Dr. Philip Allen, an anonymous reviewer, and Associate Editor Dr. Peter Burgess for their valuable and thoughtful comments and suggestions that greatly improved the manuscript. We appreciate the valuable discussion with Dr. John Holbrook and the thoughtful review of Dr. Andrew Miall during the research. Funding for this project was generously supplied by NSERC Discovery Grant RPG IN05780-14 to Dr.

Bhattacharya and sponsors of the McMaster University Quantitative Sedimentology Laboratories (QSL) including BP and Inpex. We also thank Editor Dr. James MacEachern and Technical Editor Dr. John Southard for their constructive communication and reviews.

References

Adams, M.M., and Bhattacharya, J.P., 2005, No change in fluvial style across a sequence boundary, Cretaceous Blackhawk and Castlegate Formations of Central Utah, U.S.A: Journal of Sedimentary Research, v. 75, p. 1038–1051.

Alexander, J., Fielding, C.R., Wakefield, S.J., George, M.T., and Cottnam, C.F., 2001, Fluvial geochemistry through a short-duration, tropical-cyclone induced discharge event in the Burdekin River and Hann Creek, North Queensland, Australia: Aquatic Geochemistry, v. 7, p. 275–293.

Allen, P.A., 2008a, From landscapes into geological history: Nature, v. 451, p. 274–276.

Allen, P.A., 2008b, Time scales of tectonic landscapes and their sediment routing systems: Geological Society, London. Special Publications, 296, p. 7–28.

Allen, P.A., Armitage, J.J., Carter, A., Duller, R.A., Michael, N.A., Sinclair, H.D., and Whittaker, A.C., 2013, The Qs problem: Sediment volumetric balance of proximal foreland basin systems: Sedimentology, v. 60, p. 102–130.

Allison, M.A., Kineke, G.C., Gordon, E.S., and Goñi, M.A., 2000, Development and reworking of a seasonal flood deposit on the inner continental shelf off the Atchafalaya River: Continental Shelf Research, v. 20, p. 2267-2294.

Andrews, E.D., 1980, Effective and bankfull discharge of streams in the Yampa River Basin, Colorado and Wyoming: Journal of Hydrology, v. 46, p. 311–330.

Andrews, E.D., 1984, Bed-material entrainment and hydraulic geometry of gravel-bed rivers in Colorado: Geological Society of America, Bulletin, v.95, p. 371-378.

Andrews, E.D., and Nankervis, J.M., 1995, Effective discharge and the design of channel maintenance flows for gravel-bed rivers: natural and anthropogenic influence in fluvial geomorphology: American Geophysical Union, Geophysical Monograph, v. 89, p. 151–164.

Arora, V.K., and Boer, G.J., 2001, Effects of simulated climate change on the hydrology of major river basins: Journal of Geophysical Research, v. 106, p. 3335-3348.

Asselman, N.E.M., 1999, Suspended sediment dynamics in a large drainage basin: the River Rhine: Hydrological Processes, v. 13, p. 1437–1450.

Beaumont, C., 1981, Foreland basins: Geophysical Journal International, v. 65, p. 291-329.

Bell, W.A., 1963, Upper Cretaceous floras of the Dunvegan, Bad Heart, and Milk River Formations of Western Canada: Geological Survey of Canada, Bulletin 94, p. 1–178.

Bhattacharya, J.P., 1992, Regional to subregional facies architecture of river-dominated deltas in the Alberta subsurface, Upper Cretaceous Dunvegan Formation, *in* Miall, A.D., and Tyler, N., eds., The Three-Dimensional Facies Architecture of Terrigenous Clastic Sediments and Its Implications for Hydrocarbon Discovery and Recovery: Concepts in Sedimentology and Paleontology 3: p. 189-206.

Bhattacharya, J.P., 1993. The expression and interpretation of marine flooding surfaces and erosional surfaces in core; examples from the Upper Cretaceous Dunvegan

Formation, Alberta foreland basin, Canada, *in* Posamentier, H.W., Summerhayes, P.C., Haq, B.U., and P. Allen, G.P., eds., Sequence Stratigraphy and Facies Associations: p. 125–160.

Bhattacharya, J.P., 2006., Deltas, *in* Posamentier, H.W., and Walker, R.G., eds., SEPM Special Publication 84, p. 231–262.

Bhattacharya, J.P., Copeland, P., Lawton, T. E., and Holbrook, J., 2016, Estimation of source area, river paleo-discharge, paleoslope, and sediment budgets of linked deep-time depositional systems and implications for hydrocarbon potential: Earth-Science Reviews, v.153. p. 77–110.

Bhattacharya, J.P., and Maceachern, J.A., 2009, Hyperpycnal rivers and prodeltaic shelves in the Cretaceous Seaway of North America: Journal of Sedimentary Research, v. 79, p. 184–209.

Bhattacharya, J.P., and Tye, R.S., 2004, Searching for modern Ferron analogs and applications to subsurface interpretation, *in* Chidsey, T.C., Jr., Adams, R.D., and Morris, T.H., eds., Regional to Wellbore Analog for Fluvial–Deltaic Reservoir Modeling: the Ferron Sandstone of Utah: American Association of Petroleum Geologists, Studies in Geology, v. 50, p. 39–57.

Bhattacharya, J.P., and Walker, R.G., 1991a, Allostratigraphic subdivision of the Upper Cretaceous Dunvegan, Shaftesbury, and Kaskapau formations in the northwestern Alberta subsurface: Bulletin of Canadian Petroleum Geology, v. 39, p. 145–164.

Bhattacharya, J.P., and Walker, R.G., 1991b, River-and wave-dominated depositional systems of the Upper Cretaceous Dunvegan Formation, northwestern Alberta: Bulletin of Canadian Petroleum Geology, v. 39, p. 165–191.

Blum, M.D., and Törnqvist, T.E., 2000, Fluvial responses to climate and sea-level change: a review and look forward: Sedimentology, v. 47, p. 2–48.

Blum, M.D., and Hattier-Womack, J., 2009, Climate change, sea-level change, and fluvial sediment supply to deepwater depositional systems, *in* Ben Kneller, B., Martinsen, O.J., and McCaffrey, B., eds., External Controls on Deep-Water Depositional Systems, SEPM Special Publication 92, p. 15–39.

Blum, M., Martin, J., Milliken, K., and Garvin, M., 2013, Paleovalley systems: insights from Quaternary analogs and experiments: Earth-Science Reviews, v. 116, p. 128–169.

Bridge, J.S., and Mackey, S.D., 1993, A revised alluvial stratigraphy model, *in* Marzo, M., and Puigdefabregas, C., eds., Alluvial Sedimentation: International Association of Sedimentologists, Special Publication 17, p. 319–336.

Bridge, J.S., and Tye, R.S., 2000, Interpreting the dimensions of ancient fluvial channel bars, channels, and channel belts from wireline-logs and cores: American Association of Petroleum Geologists, Bulletin, v. 84, p. 1205–1228.

Carroll, A.R., Chetel, L.M., and Smith, M.E., 2006, Feast to famine: Sediment supply control on Laramide basin fill: Geology, v. 34, p. 197–200.

Carvajal, C., and Steel, R., 2012, Source-to-sink sediment volumes within a tectono-stratigraphic model for a Laramide shelf-to-deep-water basin: methods and results,

in Busby, C., and Azor, A., eds., First edition, Tectonics of Sedimentary Basins: Recent Advances, Blackwell Pubishing Ltd., p. 131–151.

Castelltort, S., and Van Den Driessche, J., 2003, How plausible are high-frequency sediment supply-driven cycles in the stratigraphic record: Sedimentary Geology, v. 157, p. 3–13.

Cattaneo, A., Trincardi, F., Asioli, A., and Correggiari, A., 2007, The Western Adriatic shelf clinoform: energy-limited bottomset: Continental Shelf Research, v. 27, p. 506-525.

Clark, M.J., 1988, Periglacial hydrology, *in* Clark, M.J., Advances in Periglacial Geomorphology: Chichester, John Wiley and Sons, p. 415–462.

Covault, J.A., Romans, B.W., Fildani, A., McGann, M., and Graham, S A., 2010, Rapid climatic signal propagation from source to sink in a southern California sediment-routing system: The Journal of Geology, v. 118, p. 247–259.

Covault, J.A., Romans, B.W., Graham, S.A., Fildani, A., and Hilley, G.E., 2011, Terrestrial source to deep-sea sink sediment budgets at high and low sea levels: Insights from tectonically active Southern California: Geology, v. 39, p. 619–622.

Cramer, B.D., Vandenbroucke, T.R.A., and Ludvigson, G.A., 2015, High-Resolution Event Stratigraphy (HiRES) and the quantification of stratigraphic uncertainty: Silurian examples of the quest for precision in stratigraphy: Earth-Science Reviews, v. 141, p. 136–153.

Dade, W.B., and Friend, P. F., 1998, Grain-size, sediment transport regime, and channel slope in alluvial rivers: Journal of Geology, v. 106, p. 661–675.

Davide, V., Pardos, M., Diserens, J., Ugazio, G., Thomas, R., and Dominik, J., 2003, Characterisation of bed sediments and suspension of the river Po (Italy) during normal and high flow conditions: Water Research, v. 37, p. 2847–2864.

Davidson, S.K., and North, C.P., 2009, Geomorphological regional curves for prediction of drainage area and screening modern analogues for rivers in the rock record: Journal of Sedimentary Research, v. 79, p. 773–779.

Davidson, S.K., and Hartley, A.J., 2010, Towards a quantitative method for estimating paleohydrology from clast size and comparison with modern rivers: Journal of Sedimentary Research, v. 80, p. 688–702.

Davidson, S.K., and Hartley, A.J., 2014, A Quantitative Approach To Linking Drainage Area and Distributive-Fluvial-System Area In Modern and Ancient Endorheic Basins: Journal of Sedimentary Research, v. 84, p. 1005–1020.

Dennis, K.J., Cochran, J.K., Landman, N.H., and Schrag, D.P., 2013, The climate of the Late Cretaceous: New insights from the application of the carbonate clumped isotope thermometer to Western Interior Seaway macrofossil: Earth and Planetary Science Letters, v. 362, p. 51–65.

Dickinson, W.R., and Snyder, W.S., 1978, Plate tectonics of the Laramide orogeny, *in* Matthews III, V., eds., Geological Society of America, Memoirs 151, p. 355–366.

Dott, R.H., Jr., 1996, Episodic event deposits versus stratigraphic sequences - shall the twain never meet: Sedimentary Geology, v. 104, p. 243–247.

Draut, A.E., Kineke, G.C., Velasco, D.W., Allison, M.A., and Prime, R.J., 2005, Influence of the Atchafalaya River on recent evolution of the chenier-plain inner

continental shelf, northern Gulf of Mexico: Continental Shelf Research, v. 25, p. 91–112.

Duller, R.A., Whittaker, A.C., Fedele, J.J., Whitchurch, A., Springett, J., Allen, P.A., Smithells, R.L., and Fordyce, S., 2010, From grain size to tectonics: Journal of Geophysical Research, Earth Surface, v. 115, p. 1–19.

Fatorić, S., and Chelleri, L., 2012. Vulnerability to the effects of climate change and adaptation: the case of the Spanish Ebro delta: Ocean and Coastal Management, v. 60, p. 1–10.

Fedele, J., and Paola, C., 2007, Similarity solutions for fluvial sediment fining by selective deposition: Journal of Geophysical Research, v. 112, No. F02038, 13 p.

Foreman, B.Z., Heller, P.L., and Clementz, M.T., 2012, Fluvial response to abrupt global warming at the Palaeocene/Eocene boundary: Nature, v. 491, p. 92–95.

Galloway, W.E., 1975. Process framework for describing the morphologic and stratigraphic evolution of deltaic depositional systems, *in* Broussard, M.L. eds., Deltas: Models for Exploration, Houston Geological Society, p. 87–958.

Galloway, W.E., 1989, Genetic stratigraphic sequences in basin analysis I: architecture and genesis of flooding-surface bounded depositional units: American Association of Petroleum Geologists, Bulletin, v. 73, p. 125–142.

Garcia, M., and Parker, G., 1991, Entrainment of bed sediment into suspension: Journal of Hydraulic Engineering, v. 117, p. 414–435.

Gibling, M.R., 2006, Width and thickness of fluvial channel bodies and valley fills in the geological record: A literature compilation and classification: Journal of Sedimentary Research, v. 76, p. 731–770.

Gingras, M.K., MacEachern, J.A., and Pemberton, S.G., 1998, A comparative analysis of the ichnology of wave- and river-dominated allomembers of the Upper Cretaceous Dunvegan Formation: Bulletin of Canadian Petroleum Geology, v. 46, p. 51–73.

Glancy, T.J. Jr., Arthur, M.A., Barron, E.J., and Kauffman, E.G., 1993, A paleoclimate model for the North American Cretaceous (Cenomanian-Turonian) epicontinental sea, *in* Caldwell, W.G.E., and Kauffman, E.G., eds., Evolution of the Western Interior Basin: Geological Association of Canada, Special Paper 39, p. 219–241.

Hajek, E.A., and Heller, P.L., 2012, Flow-depth scaling in alluvial architecture and nonmarine sequence stratigraphy: example from the Castlegate Sandstone, central Utah, USA: Journal of Sedimentary Research, v. 82, p. 121–130.

Hajek, E.A., and Wolinsky, M.A., 2012, Simplified process modeling of river avulsion and alluvial architecture: connecting models and field data: Sedimentary Geology, v. 257–260, p. 1–30.

Hampson, G.J., Jewell, T.O., Irfan, N., Gani, M.R., and Bracken, B., 2013, Modest change in fluvial style with varying accommodation in regressive alluvial-to-coastal-plain wedge: Upper Cretaceous Blackhawk Formation, Wasatch Plateau, central Utah, U.S.A.: Journal of Sedimentary Research, v. 83, p. 145–169.

Hay, W.W., and Floegel, S., 2012, New thoughts about the Cretaceous climate and oceans: Earth-Science Reviews, v. 115, p. 262–272.

Holbrook, J., Scott, R.W., and Oboh-Ikuenobe, F.E., 2006, Base-level buffers and buttresses: a model for upstream versus downstream control on fluvial geometry and architecture within sequences: Journal of Sedimentary Research, v. 76, p. 162–174.

Holbrook, J.M., and Bhattacharya, J.P., 2012, Reappraisal of the sequence boundary in time and space: Case and considerations for an SU (subaerial unconformity) that is not a sediment bypass surface, a time barrier, or an unconformity: Earth-Science Reviews, v. 113, p.271–302.

Holbrook, J., and Wanas, H., 2014, A fulcrum approach to assessing source-to-sink mass balance using channel paleohydrologic paramaters derivable from common fluvial data sets with an example from the cretaceous of egypt: Journal of Sedimentary Research, v.84, p. 349–372.

Hutton, E.W.H., and Syvitski, J.P.M., 2008, Sedflux 2.0: an advanced process–response model that generates three-dimensional stratigraphy: Computers & Geosciences, v. 34, p. 1319–1337.

Jaeger, J.M., and Koppes, M., 2015, The role of the cryosphere in source-to-sink systems: Earth-Science Reviews, v. 153. p. 43–76.

Jerolmack, D., and Sadler, P., 2007, Transience and persistence in the depositional record of continental margins: Journal of Geophysical Research, v. 112, p. 1–14.

Kettner, A.J., and Syvitski, J.P.M., 2008, HydroTrend v. 3.0: a climate-driven hydrological transport model that simulates discharge and sediment load leaving a river system: Computers & Geosciences, v. 34, p. 1170–1183.

Kottek, M., Grieser, J., Beck, C., Rudolf, B., and Rubel, F., 2006, World map of the Köppen-Geiger climate classification updated: Meteorologische Zeitschrift, v. 15, p. 259–263.

Kraus, M.J., 1999, Paleosols in clastic sedimentary rocks: their geologic applications: Earth-Science Reviews, v. 47, p. 41–70.

Leclair, S.F., and Bridge, J.S., 2001, Quantitative interpretation of sedimentary structures formed by river dunes: Journal of Sedimentary Research, v. 71, p. 713–716.

Lee, H.J., Syvitski, J.P., Parker, G., Orange, D., Locat, J., Hutton, E.W., and Imran, J., 2002, Distinguishing sediment waves from slope failure deposits: field examples, including the 'Humboldt slide', and modelling results: Marine Geology, v. 192, p. 79–104.

Leithold, E.L., Blair, N.E., and Wegmann, K.W., 2015, Source-to-sink sedimentary systems and global carbon burial: A river runs through it: Earth-Science Reviews, v. 153. P. 30–42.

Leopold, L.B., and Maddock, T., Jr., 1953, The Hydraulic Geometry of Stream Channels and Some Physiographic Implications: U.S. Geological Survey, Professional Paper 252, 57 p.

Liang, M., Voller, V.R., and Paola, C., 2014, A reduced-complexity model for river delta formation—part 1: modeling deltas with channel dynamics: Earth Surface Dynamics. Discuss 2, p. 823–869.

Matenco, L., Andriessen, P., Andriessen, P.A.M., Avram, C., Bada, G., Beekman, F., and Wong, H., 2013, Quantifying the mass transfer from mountain ranges to deposition

in sedimentary basins: Source to sink studies in the danube basin-black sea system: Global and Planetary Change, v. 103, p. 1–18.

McCarthy, P.J., Faccini, U.F., and Plint, A.G., 1999, Evolution of an ancient coastal plain: palaeosols, interfluves and alluvial architecture in a sequence stratigraphic framework, Cenomanian Dunvegan Formation, NE British Columbia, Canada: Sedimentology, v. 46, p. 861–891.

McCarthy, P.J., and Plint, A.G., 2003, Spatial variability of palaeosols across Cretaceous interfluves in the Dunvegan Formation, NE British Columbia, Canada: palaeohydrological, palaeogeomorphological and stratigraphic implications: Sedimentology, v. 50, p. 1187–1220.

Meybeck, M., Larochea, L., Dürra, H.H., and Syvitski, J.P.M. 2003, Global variability of daily total suspended solids and their fluxes in rivers: Global and Planetary Change, v. 39, p. 65–93.

Miall, A.D., 2006, Reconstructing the architecture and sequence stratigraphy of the preserved fluvial record as a tool for reservoir development: A reality check: American Association of Petroleum Geologists, Bulletin, v. 90, p. 989–1002.

Miall, A.D., 2014, The emptiness of the stratigraphic record: A preliminary evaluation of missing time in the Mesaverde Group, Book Cliffs, Utah: Journal of Sedimentary Research, v. 84, p. 457–469.

Michael, N.A., Whittaker, A.C., and Allen, P.A., 2013, The functioning of sediment routing systems using a mass balance approach: example from the Eocene of the southern Pyrenees: The Journal of Geology, v. 121, p. 581–606.

Michael, N.A., Carter, A., Whittaker, A.C., and Allen, P.A., 2014, Erosion rates in the source region of an ancient sediment routing system: comparison of depositional volumes with thermochronometric estimates: Geological Society of London, Journal, v. 171, p. 401–412.

Milliman, J.D., and Syvitski, J.P.M., 1992, Geomorphic/tectonic control of sediment discharge to the ocean: The importance of small mountainous rivers: The Journal of Geology, v. 100, p. 525–544.

Moog, D.B., and Whiting, P.J., 1998, Annual hysteresis in bed load rating curves: Water Resources Research, v. 34, p. 2393–2399.

Mulder, T., and Syvitski, J.P., 1995, Turbidity currents generated at river mouths during exceptional discharges to the world oceans: The Journal of Geology, v. 103, p. 285–299.

Nolan, K.M., Lisle, T.E., and Kelsey, H.M., 1987, Bankfull discharge and sediment transport in northwestern California, *in* Beschta, R.L., Blinn, T., Grant, G.E., Ice, G.G., and Swanson, F., eds., Erosion and Sedimentation in the Pacific Rim: Wallingford, U.K., International Association of Hydrological Sciences, Publication 165, p. 439–450.

Olariu, C., and Bhattacharya, J.P., 2006, Terminal distributary channels and delta front architecture of river-dominated delta systems: Journal of sedimentary research, v. 76, p. 212–233.

Paola, C., and Mohrig, D., 1996, Palaeohydraulics revisited: palaeoslope estimation in coarse-grained braided rivers: Basin Research, v. 8, p. 243–254.

Paola, C., 2000, Quantitative models of sedimentary basin filling: Sedimentology, v. 47, p. 121–178.

Paola, C., and Martin, J.M., 2012, Mass-balance effects in depositional systems: Journal of Sedimentary Research, v. 82, p. 435–450.

Parker, G., 1978, Self-formed rivers with stable banks and mobile bed: Part I, the sand–silt river: Journal of Fluid Mechanics, v. 89, p. 109–126.

Parker, G., Paola, C.,Whipple, K.X., and and Mohrig, D., 1998, Alluvial fans formed by channelized fluvial and sheet flow. I: Theory: Journal of Hydraulic Engineering, v. 24, p. 985–995.

Parker, G., Muto, T., Akamatsu, Y., Dietrich, W.S., and Lauer, J.W., 2008, Unraveling the conundrum of river response to rising sea-level from laboratory to field. Part I: laboratory experiments: Sedimentology, v. 55, p. 1643–1655.

Pattison, S.A., and Walker, R.G., 1992, Deposition and interpretation of long, narrow sandbodies underlain by a basinwide erosion surface: Cardium Formation, Cretaceous Western Interior Seaway, Alberta, Canada: Journal of Sedimentary Petrology, v. 62, p. 292–309.

Petter, A.L., Steel, R.J., Mohrig, D., Kim, W., and Carvajal, C., 2013, Estimation of the paleoflux of terrestrial-derived solids across ancient basin margins using the stratigraphic record: Geological Society of America, Bulletin, v. 125, p. 578–593.

Plint, A.G., 2000, Sequence stratigraphy and paleogeography of a Cenomanian deltaic complex: The Dunvegan and Lower Kaskapau formations in subsurface and

outcrop, Alberta and British Columbia, Canada: Bulletin of Canadian Petroleum Geology, v. 48, p. 43–79.

Plint, A.G., McCarthy, P.J. and Faccini, U.F., 2001, Nonmarine sequence stratigraphy: Updip expression of sequence boundaries and systems tracts in a highresolution framework, Cenomanian Dunvegan Formation, Alberta foreland basin, Canada: American Association of Petroleum Geologists, Bulletin, v. 85, p. 1967–2001.

Plint, A.G., 2002, Paleovalley systems in the Upper Cretaceous Dunvegan Formation, Alberta and British Columbia: Bulletin of Canadian Petroleum Geology, v. 50, p. 277–296.

Plint, A., and Wadsworth, J., 2003, Sedimentology and palaeogeomorphology of four large valley systems incising delta plains, western Canada Foreland Basin: implications for mid-Cretaceous sea-level changes: Sedimentology, v. 50, p. 1147–1186.

Plint, A.G., and Wadsworth, J.A., 2006, Delta-plain paleodrainage patterns reflect small-scale fault movement and subtle forebulge uplift, *in* Dalrymple, R.W., Leckie, D.A., and Tillman, R.W., eds., Upper Cretaceous Dunvegan Formation, Western Canada Foreland Basin, SEPM, Special Publication 85, p. 219–237.

Plint, A.G., and Kreitner, A.M., 2007, Extensive thin sequences spanning cretaceous foredeep suggest high-frequency eustatic control: Late Cenomanian, Western Canada foreland basin: Geology, v. 35, p. 735–738.

Plint, A.G., Tyagi, A., Hay, M.J., Varban, B.L., Zhang, H., and Roca, X., 2009, Clinoforms, paleobathymetry, and mud dispersal across the western Canada

Cretaceous Foreland Basin: evidence from the Cenomanian Dunvegan Formation and Contiguous Strata: Journal of Sedimentary Research, v. 79, p. 144–161.

Powell, G.E., Mecklenburg, D., and Ward, A., 2006, Evaluating channel-forming discharges: a study of large rivers in Ohio: American Society of Agricultural and Biological Engineers, Transactions, v. 49, p. 35–46.

Posamentier, H.W., and Vail, P.R., 1988, Eustatic controls on clastic deposition II - sequence and systems tract models, *in* Wilgus, C.K., Hastings, B.S., Posamentier, H.W., Van Wagoner, J., Ross, C.A., and Kendall, C.G.St.C., eds., Sea-Level Changes—An Integrated Approach, SEPM, Special Publication 42, p. 125–154.

Reesink, A.J.H., Van den Berg, J.H., Parsons, D.R., Amsler, M.L., Best, J.L., Hardy, R.J., and Szupiany, R.N., 2015, Extremes in dune preservation: Controls on the completeness of fluvial deposits: Earth-Science Reviews, v. 150, p. 652–665.

Romans, B.W., and Graham, S.A., 2013, A deep-time perspective of land-ocean linkages in the sedimentary record: Annual Review of Marine Science, v. 5, p. 69–94.

Romans, B.W., Castelltort, S., Covault, J.A., Fildani, A., and Walsh, J.P., 2015, Environmental signal propagation in sedimentary systems across timescales: Earth-Science Reviews, v. 153. P. 7–29.

Rosgen, D., 1997, A geomorphological approach to restoration of incised rivers: *in* Wang, S.S.Y., Langendoen, E.J. and Shields, F.D. Jr., eds., Proceedings of the Conference on Management of Landscapes Disturbed by Channel Incision, The Center for Computational Hydroscience and Engineering, The University of Mississippi, p. 1–11.

Rubin, D.M., and McCulloch, D.S., 1980, Single and superimposed bedforms: a synthesis of San Francisco Bay and flume observations: Sedimentary Geology, v. 26, p. 207–231.

Sadler, P.M., 1981, Sediment accumulation rate and the completeness of stratigraphic sections: Journal of Geology, v. 89, p. 569–584.

Sadler, P.M., 1999, The influence of hiatuses on sediment accumulation rates: GeoResearch Forum, v. 5, p. 15–40.

Sadler, P.M., and Jerolmack, D.J., 2015, Scaling laws for aggradation, denudation and progradation rates: the case for time-scale invariance at sediment sources and sinks, *in* Smith, D.G., Bailey, R.J., Burgess, P.M., and Fraser, A.J., eds., Geological Society of London, Special Publications 404, p. 69–88.

Sichomgabula, H.M., 1999, Magnitude-frequency characteristics of effective discharge for suspended sediment transport, Fraser River, British Columbia, Canada: Hydrological Processes, v. 13, p. 1361–1380.

Simon, A., Dickerson, W., and Heins, A., 2004, Suspended-sediment transport rates at the 1.5-year recurrence interval for ecoregions of the United States: Transport conditions at the bankfull and effective discharge: Geomorphology, v. 58, p. 243–262.

Slingerland, R., Kump, L.R., Arthur, M.A., Fawcett, P.J., Sageman, B.B., and Barron, E.J., 1996, Estuarine circulation in the Turonian western interior seaway of North America: Geological Society of America, Bulletin, v. 108, p. 941–952.

Sømme, T.O., Helland-hansen, W., Martinsen, O.J., and Thurmond, J.B., 2009, Relationships between morphological and sedimentological parameters in source-to-sink systems: A basis for predicting semi-quantitative characteristics in subsurface systems: Basin Research, v. 21, p. 361–387.

Sømme, T.O., Martinsen, O.J., and Thurmond, J.B., 2009, Reconstructing morphological and depositional characteristics in subsurface sedimentary systems: An example from the Maastrichtian-Danian Ormen Lange system, Møre Basin, Norwegian Sea: American Association of Petroleum Geologists, Bulletin, v. 93, p. 1347–1377.

Sømme, T.O., Piper, D.J.W., Deptuck, M.E., and Helland-Hansen, W., 2011, Linking onshore-offshore sediment dispersal in the Golo source-to-sink system (Corsica, France) during the late Quaternary: Journal of Sedimentary Research, v. 81, p. 118–137.

Sømme, T.O., and Jackson, C.A.L., 2013, Source-to-sink analysis of ancient sedimentary systems using a subsurface case study from the Møre-Trøndelag area of southern Norway: Part 2 - sediment dispersal and forcing mechanisms: Basin Research, v. 25, p. 512–531.

Stott, D.F., 1982, Lower Cretaceous Fort St. John Group and Upper Cretaceous Dunvegan Formation of the Foothills and Plains of Alberta, British Columbia, District of Mackenzie and Yukon Territory: Geological Survey of Canada, Bulletin 328, v. 328, p. 124.

Strong, N., Sheets, B., Hickson, T., and Paola, C., 2005, A mass-balance framework for quantifying downstream changes in fluvial architecture, *in* Blum, M.D., Marriott,

S.B., and Leclair, S.F., eds., Fluvial Sedimentology VII, International Association of Sedimentologists, Special Publication 35, p. 243–253.

Syvitski, J.P.M., and Milliman, J.D., 2007, Geology, geography, and humans battle for dominance over the delivery of fluvial sediment to the coastal ocean: Journal of Geology, v. 115, p. 1–19.

Turowski, J.M., Rickenmann, D., and Dadson, S.J., 2010, The partitioning of the total sediment load of a river into suspended load and bedload: a review of empirical data: Sedimentology, v. 57, p. 1126–1146.

Vandenberghe, J., 2003, Climate forcing of fluvial system development: an evolution of ideas: Quaternary Science Reviews, v. 22, p. 2053–2060.

Van Rijn, L.C., 1984, Sediment transport. II: Suspended load transport: Journal of Hydraulic Engineering, v. 110, p. 1431–1456.

Van Wagoner, J.C., Mitchum, R.M., Campion, K.M., and Rahmanian, V.D., 1990, Siliciclastic Sequence Stratigraphy in Well Logs, Cores, and Outcrops: American Association of Petroleum Geologists, Methods in Exploration Series 7, 55 p.

Varban, B.L., and Plint, A.G., 2008, Palaeoenvironments, palaeogeography, and physiography of a large, shallow, muddy ramp: Late Cenomanian–Turonian Kaskapau Formation, Western Canada foreland basin: Sedimentology, v. 55, p. 201–233.

Walling, D.E., and Collins, A.L., 2008, The catchment sediment budget as a management tool: Environmental Science and Policy, v. 11, p. 136–143.

Wang, Y., Straub, K.M., and Hajek, E.A., 2011, Scale-dependent compensational stacking: An estimate of autogenic time scales in channelized sedimentary deposits: Geology, v. 39, p. 811–814.

Warne, A.G., Meade, R.H., White, W.A., Guevara, E.H., Gibeaut, J., Smyth, R.C., Aslan, A., and Tremblay, T., 2002, Regional controls on geomorphology, hydrology, and ecosystem integrity in the Orinoco Delta, Venezuela: Geomorphology, v. 44, p. 273–307.

Whittaker, A.C., Attal, M., and Allen, P.A., 2010, Characterizing the origin, nature, and fate of sediment exported from catchments perturbed by active tectonics: Basin Research, v. 22, p. 809–828.

Whittaker, A.C., Duller, R.A., Springett, J., Smithells, R.A., Whitchurch, A.L., and Allen, P.A., 2011, Decoding downstream trends in stratigraphic grain size as a function of tectonic subsidence and sediment supply: Geological Society of America, Bulletin, v. 123, p. 1363–1382.

Wolman, M.G., and Miller, J.P., 1960, Magnitude and frequency of forces in geomorphic processes: The Journal of Geology, v.68, p. 54–74.

Wright, S., and Parker, G., 2004, Flow resistance and suspended load in sand-bed rivers: simplified stratification model: Journal of Hydraulic Engineering, v. 130, p. 796–805.

CHAPTER 3

HIGH-RESOLUTION SEQUENCE STRATIGRAPHY OF THE LATE CRETACEOUS GALLUP SYSTEM, NEW MEXICO, U.S.A.

Abstract

Deciphering the relationships between traditional lithostratigraphy and sequence stratigraphy is the key to correctly understanding time-stratigraphic relationships and basin evolution. Insufficient sample spacing, which induces "aliasing", and lack of datums are both problematic issues for sequence stratigraphic correlation. High-resolution sequence stratigraphic analysis of the Cretaceous Gallup system, deposited during the Late Turonian to Early Coniacian, documents the high-frequency depositional cyclicity using detailed facies analysis in extensively exposed outcrops in northwestern New Mexico, US. Seventy-one sedimentological sections were measured along the depositional-dip-oriented outcrop belt, with less than 1 km average distance between measured sections. Laterally extensive bentonite layers, deposited on nearly horizontal seabed, provide chronological control and are used as rigorous datums for accurate correlations with minimal stratigraphic distortion. Based on the integration of key bounding surfaces with detailed facies analysis, we identified twelve stratigraphic sequences, consisting of twenty-six parasequence sets composed of sixty-one parasequences. Four classes of shoreline trajectory are quantified: ascending regressive with accelerating and decelerating rates, descending regressive, and transgressive. The shoreline transgressed up to 60 km and regressed up to 48 km, associated with estimated changes of sea level ranging from -34 m to 38 m. Parasequence sets show aggradational–

progradational, retrogradational, progradational–aggradational, and degradational stacking patterns. These accommodation successions help to define systems tracts. The results show that the previously mapped sandstone tongues are equivalent to high-frequency sequence sets. Chronostratigraphic analysis shows that the Dilco Member is diachronous and correlated to different sequences. The Torrivio Member fluvial sandstone was probably deposited diachronously, and part of it may be Gallup age. The matching magnitudes of relative sea level falls and rises, and an absence of evidence of tectonism (e.g., angular unconformities), suggest a eustatic control. Autogenic processes may have operated during deposition but were not the dominant controls. The estimated depositional durations of sequence, parasequence set, and parasequence are 100 kyr, 46.2 kyr, and 19.7 kyr, respectively, implying that Milankovitch-cycle-dominated glacio-eustasy may be the key control on the high-frequency sequence stratigraphy of the Gallup system in greenhouse age.

3.1 Introduction

3.1.1 Lithostratigraphy versus Sequence Stratigraphy

Deciphering the relationships between traditional lithostratigraphy and newer sequence stratigraphy is the key to correctly understanding the time-stratigraphic relationships and evolution of any depositional system (Mitchum et al. 1977). Lithostratigraphy defines stratigraphic units based on arbitrary vertical and horizontal lithofacies boundaries, obscuring the genetic stratal relationships: this is more severe where lithological sandstone “tongues” inter-finger with shales (Wheeler and Mallory 1956; Bhattacharya 1993, 2011; Nummedal and Molenaar 1995; Van Wagoner 1995; Plink-Bjorklund 2008).

Sequence stratigraphy allows subdivision of a lithostratigraphic body into genetic units defined by correlation of varying lithofacies on the basis of bounding discontinuities (Posamentier et al. 1988; Van Wagoner et al. 1988; Bhattacharya 1993, 2011; Pattison 1995; Hampson 2000). As a result, previously defined lithostratigraphic members and tongues in clastic wedges are recognized to comprise multiple parasequences, parasequence sets, and in some cases, high-frequency sequences (Pattison 1995, 2010; Taylor and Lovell 1995; MacEachern et al. 1998; McLaurin and Steel 2000; Garrison and van den Bergh 2004; Hampson et al. 2008).

Although high-resolution sequence stratigraphy has been recently applied to many outcrops of ancient systems, insufficient sample spacing of measured sections may result in misinterpretation and "aliasing" (Van Wagoner et al. 1990; Nummedal and Molenaar 1995; Taylor and Lovell 1995; Hampson 2000; Hampson and Storms 2003; Li et al. 2012), where stratigraphic units may pinch out over shorter distances than correlated owing to the limited extent of stratal clinoforms (Rich 1951). Complications of stratal stacking patterns may also be difficult to observe in sparse sample areas. The aliasing issue hampers decoding of high-frequency sequence stratigraphy and its associated controlling mechanisms.

The modern practice of sequence stratigraphy has been improved with the integration of advanced analytical techniques, such as shoreline trajectory analysis (Helland-Hansen and Martinsen 1996) and recognition of accommodation successions (Neal and Abreu 2009). However, such geometrical description has been largely anchored to seismic data; the applicability to outcrops or well logs requires further testing in various geological

settings with robust datasets. These geometric tools require reliable isochronous datums. The lack of datums that are geologically instantaneous and flat in many previous studies results in distorted geometries and miscorrelation of strata (Bhattacharya 2011). Such miscorrelation fails to establish an accurate sequence stratigraphic framework that allows quantifying changes in base level and accommodation. The lack of high-precision age control also makes it difficult to estimate stratal cyclicity, which is a key to determining the dominant controls (external and internal) on sequence development.

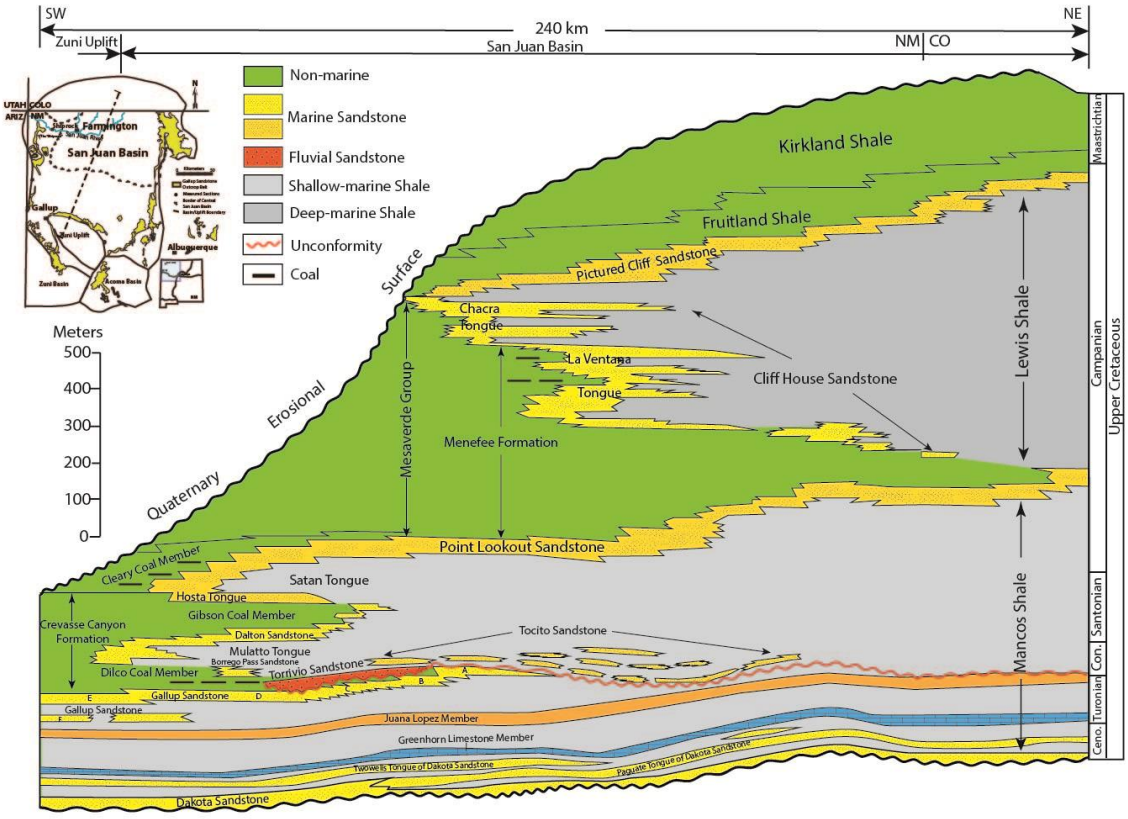

Fig. 3.1.–Lithostratigraphy of the Late Cretaceous in the San Juan Basin, NM (modified after Fassett, 2013; Dubiel, 2013; Nummedal and Molenaar, 1995). The present study focuses on the Turonian-Coniacian Gallup Formation, the Torrivio Member and the Dilco Member of the Crevasse Canyon Formation, and the Tocito Sandstone.

The Cretaceous Turonian–Coniacian Gallup depositional system of the San Juan Basin has been well studied owing to its richness of fuel fossil resources. However, like other clastic depositional wedges along the Western Interior Seaway, the lithostratigraphic terminology obscures the sequence stratigraphic relationships (Campbell 1971; Molenaar 1973; Nummedal and Riley 1991; Nummedal and Molenaar 1995). The Gallup Formation (also known as the Gallup Sandstone), previously interpreted as entirely shallow marine deposits, interfingers with the Lower Mancos Shale (Campbell 1971, 1973, 1979; Molenaar 1973, 1974; McCubbin 1982; Nummedal and Molenaar 1995; Fig. 3.1). The overlying nonmarine Dilco Coal Member of the Crevasse Canyon Formation is characterized by coal-bearing coastal and floodplain facies. The Torrivio Member is distinguished by coarse-grained fluvial sandstone deposits. Despite gradational contacts (i.e., shazam lines) between the Gallup and related strata (Fig. 3.1), previous sequence stratigraphic interpretations of the lithostratigraphic units were based on correlation of widely-spaced regional measured sections that lacked a consistent stratigraphic datum (Nummedal and Molenaar 1995).

3.1.2 Controls on High-Frequency Sequence Stratigraphy

Controlling mechanisms of high-frequency sequence stratigraphic cycles in the Cretaceous "*Greenhouse*" remain debatable, especially regarding glacio-eustatic origin (e.g., Miller et al. 2005; Zhu et al. 2012) versus high-frequency tectonics in foreland basins (e.g., Vakarelov et al. 2006; Fielding 2011). Various autogenic processes also can control high-frequency sequences and mask allogenic signals (Muto and Steel 1992, 2001; Hajek and Straub 2017). Geometrical analysis and quantification of shoreline trajectory

and relative sea level change can help to decipher dominant controls (Bhattacharya 2011; Holbrook and Bhattacharya 2012), and results can be used to test the hypothesis that growth and decay of ephemeral Antarctic ice sheets account for tens-of-meters scale sea level changes in the Cretaceous greenhouse (Miller et al. 2005).

In this paper, we analyze the sequence stratigraphy of the Gallup system, applying facies and geometric analyses to the extensive outcrops of fluvial and shallow marine deposits. The aims of this paper are three-fold: (i) to document the high-frequency sequence stratigraphy of the Gallup system; (ii) to decipher the relationships among the lithostratigraphic units in the context of sequence stratigraphy and chronostratigraphy—including the stratigraphic distinction between parasequences and parasequence-equivalent sandstone tongues (*sensu* Van Wagoner et al. 1990); and (iii) to investigate the major controls on the high-frequency stratal cyclicity.

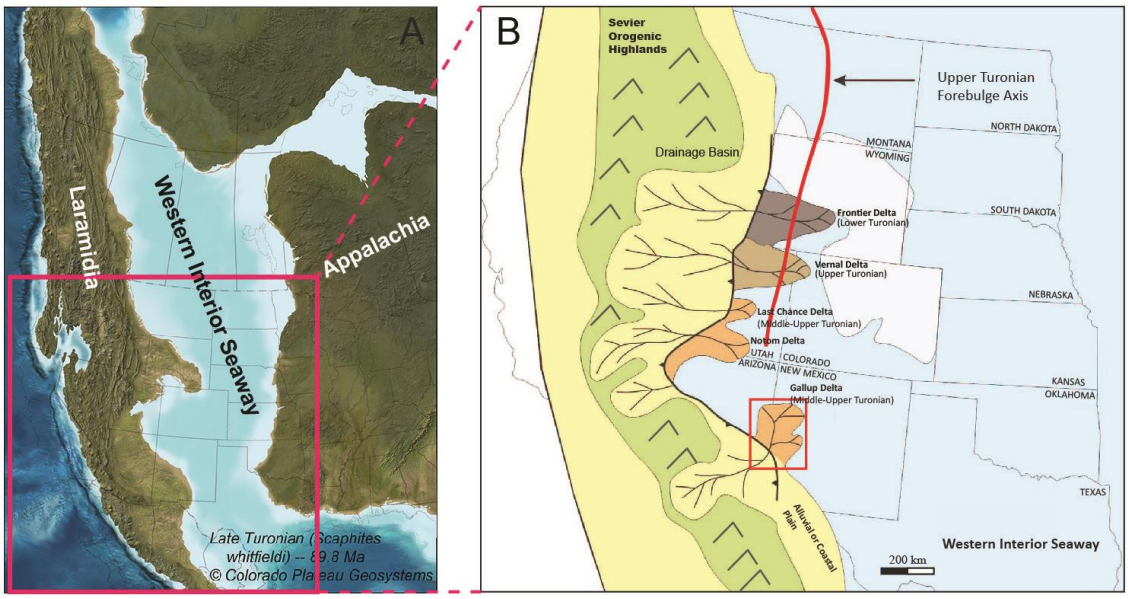

Fig. 3.2.–(A) The Late Cretaceous Turonian (89.9 Ma) Western Interior Seaway of North America (modified from the paleogeographic map of deeptimemaps.com). (B) Paleogeographic

reconstruction showing the Cretaceous Western Interior Seaway and relative positions of Ferron Formation and Gallup Sandstone deltas in the upper Cretaceous (modified after Hutsky and Fielding, 2016).

3.2 Geological Setting and Previous Work

During the Late Mesozoic, the collision between the North American and Farallon Plates formed a north-south-oriented orogenic belt on the western margin of the North American Craton. Eastward thrusting and folding of the associated Sevier thrust belt created crustal shortening and static tectonic subsidence from the Late Jurassic to Early Tertiary time, forming the elongate North American Western Interior Foreland Basin (Pang and Nummedal 1995; Liu and Nummedal 2004). During Cretaceous time, North America was progressively flooded by the Tethys Sea from the south and the Boreal Ocean from the north to form the Western Interior Seaway (Kauffman and Caldwell 1993; Fig. 3.2).

The Cretaceous Gallup Sandstone, located along the western and southern edges of the San Juan Basin, New Mexico, represents the southernmost major progradational deltaic complex along the western U.S.A. margin of the seaway (Gardner 1995) (Fig. 2B). The integration of radiometric data calibrated with ^{39}Ar – ^{40}Ar dating (Obradovich 1993) and biozone data (*Inocerumus dimidius – Inocerumus perplexus*; *Scaphites whitfieldi*; Cobban 1951; Cobban et al. 2006) suggests that the Gallup Formation was deposited during the late Turonian to early Coniacian over approximately 1.2 million years (89.6–88.4 Ma). In the Late Cretaceous, the paleolatitude of the Gallup system was between 30 °–40 °north, where the paleoclimate was warmer and more humid than present (Glancy et al. 1993; Kauffman and Caldwell 1993; Hay and Floegel 2012). Previous studies interpreted the Gallup as marine sandstones intertonguing with the marine Mancos Shale

and eventually pinching out eastward. The Gallup Sandstone downlaps onto the marine Juana Lopez Member of the Mancos Shale Formation and is unconformably overlain by the marine Tocito Sandstone seaward; it grades landward into the nonmarine Dilco Member of the Crevasse Canyon Formation, which is locally truncated by the coarse-grained fluvial Torrivio Member (Fig. 3.1).

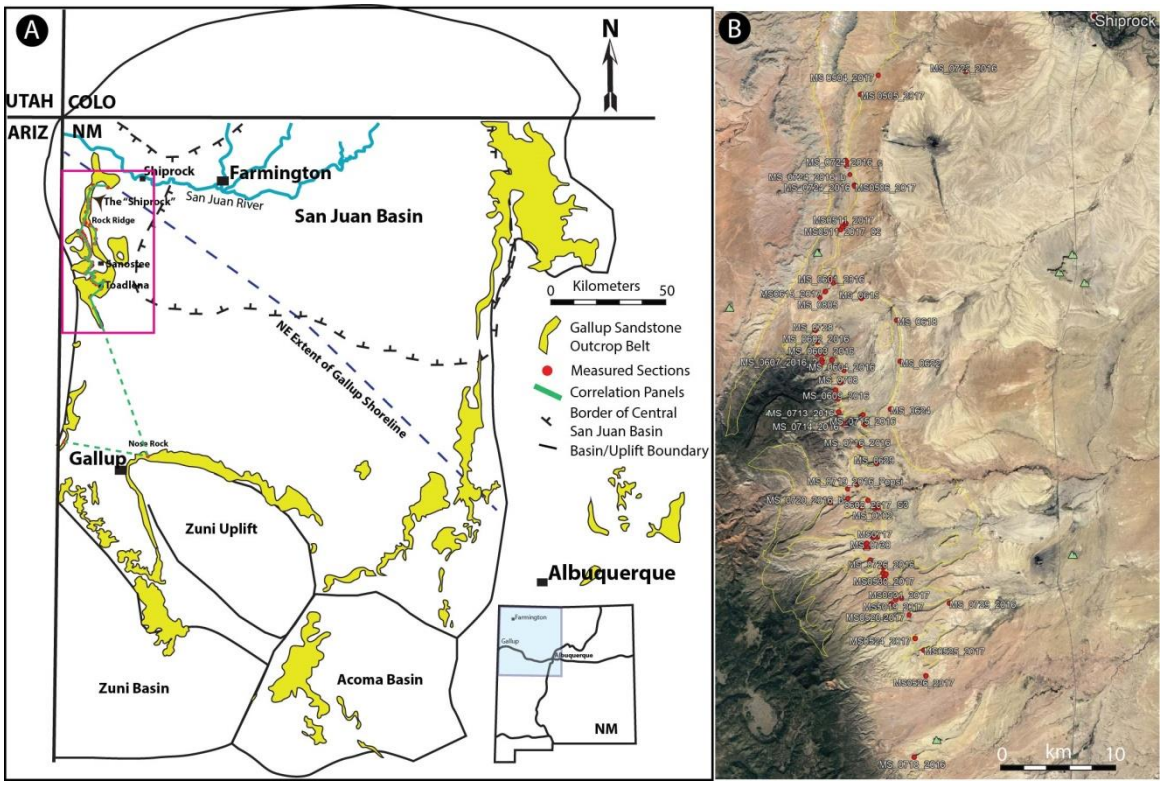

Fig. 3.3.–Maps of Gallup outcrop exposures at the western and southern margins of the San Juan Basin. (A) Regional outcrop distribution of the Gallup Fm. Paleoshoreline and tectonic outlines are superimposed on the map (modified after Campbell, 1979 and Loparco, 2010). The pink box shows the zoomed-in map in (B). (B) Google Earth map shows measured section locations.

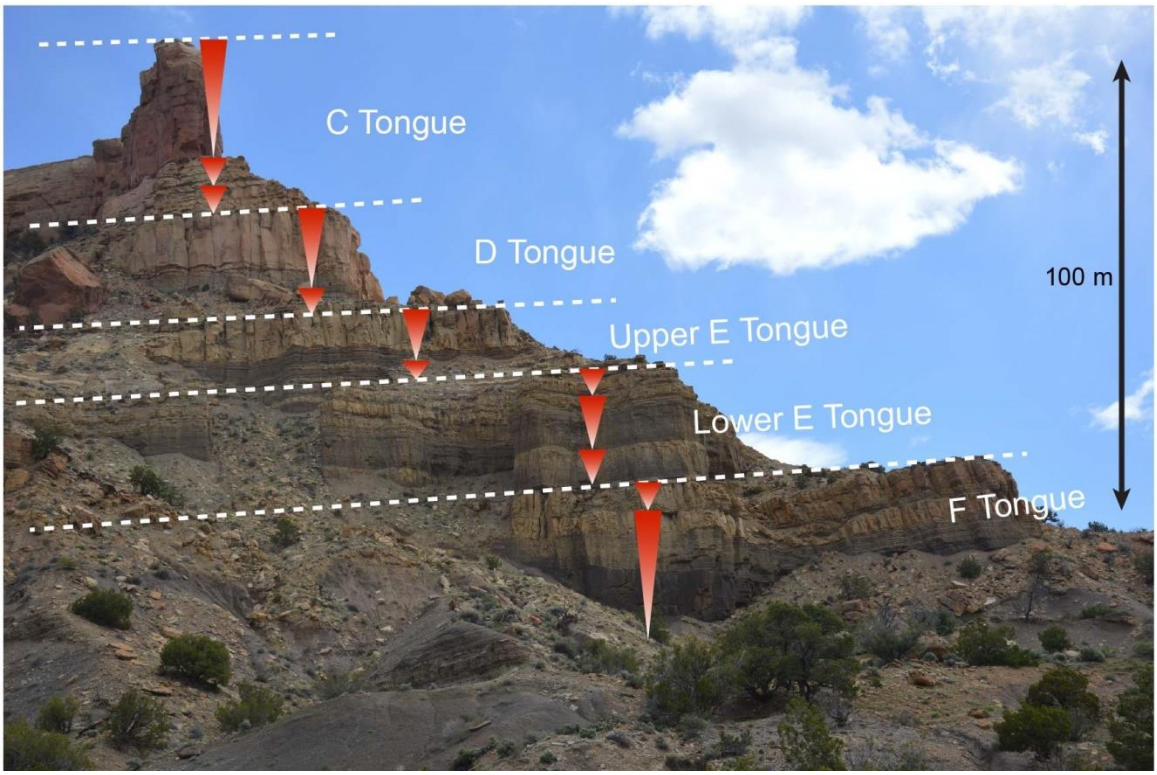

Fig. 3.4.–Outcrops of the Gallup at the "Nose Rock" Cliff close to the Town of Gallup showing the Gallup Sandstone tongues interbedded with the Mancos Shale. See Figure 3.3 for the location. Triangles indicate stratal progradation and relative sea level trend. The remarkably 1-D stratigraphic vertical variability also suggests a high-frequency stratigraphic cyclicity.

The Gallup Sandstone was previously divided into six sandstone tongues, labeled A to F from the youngest to the oldest: they show an aggradational to progradational stacking pattern. Paleogeographic maps show northwest-southeast-trending paleoshorelines primarily prograding towards the northeast (Campbell 1979; Molenaar 1983; Nummedal 1990; Figs. 3.1 - 3.4). The uplifted highlands in the west and southwest produced a large volume of sediment that was transported through various sediment routing systems and ultimately deposited in the seaway (Molenaar 1983). The Gallup system comprises fluvial to shallow marine shelf facies (Fig. 3.5). The complicated transitions between marine and

nonmarine deposits suggests continual shoreline shifts and high-frequency relative sea level fluctuations. The absence of deepwater submarine deposits indicates a low-gradient basinal ramp margin setting with shallow water (< 200m water depth; Nummedal 1990).

The study of the Gallup Sandstone was initiated by Sears in 1925. Significant studies were published in the 1970s and 1980s with discoveries of coal and petroleum resources. The Gallup Sandstone and related strata have been studied from a wide range of perspectives including, the lithostratigraphy (Molenaar 1983), genetic depositional systems and facies analyses (Campbell 1971, 1973, 1979; Molenaar 1973; McCubbin 1982; Molenaar 1983; Tillman 1985; Nummedal and Swift 1987; Nummedal 1990), and sequence stratigraphic interpretations (Weimer 1984; Nummedal 1990; Nummedal and Riley 1991; Jennette and Jones 1995; Nummedal and Molenaar 1995; Valasek 1995). The earlier attempt at sequence stratigraphic analysis interpreted two sequences based on correlation of two regional erosional surfaces (Fig. 18 of Nummedal and Molenaar 1995). However, those sequence stratigraphic attempts were problematic: the resolution is significantly low as a result of widely-spaced data controls; correlations lack datums; and analyses only focused on sandstone cliffs with limited interpretation of mudstone sections.

3.3 Data and Methodology

Extensive and continuous cliff exposures of the Gallup system surrounding the west, east, and south of the San Juan Basin in northwestern New Mexico allows for detailed analyses of sedimentological facies and high-resolution sequence stratigraphy (Fig. 3.3 and 3.4). The nearly continuous 60 km long, north -south-trending outcrop belt—extends from the south of Toadlena to the north of Shiprock. It obliquely intersects previously-mapped

paleoshorelines, and enables high-resolution sequence stratigraphic correlation along depositional dip (Fig. 3.3). In our study area, the outcrops mostly constitute strata that are equivalent to the A and B tongues of Nummedal and Molenaar (1995). Strata equivalent to the C tongue only crop out in the south (Sanostee and Toadlena area; Fig. 3.3). The Gallup Formation pinches out about 10 km north of the Ship Rock monument and allows observation of the stratigraphic relationships between the Gallup, Tocito, and Juana Lopez.

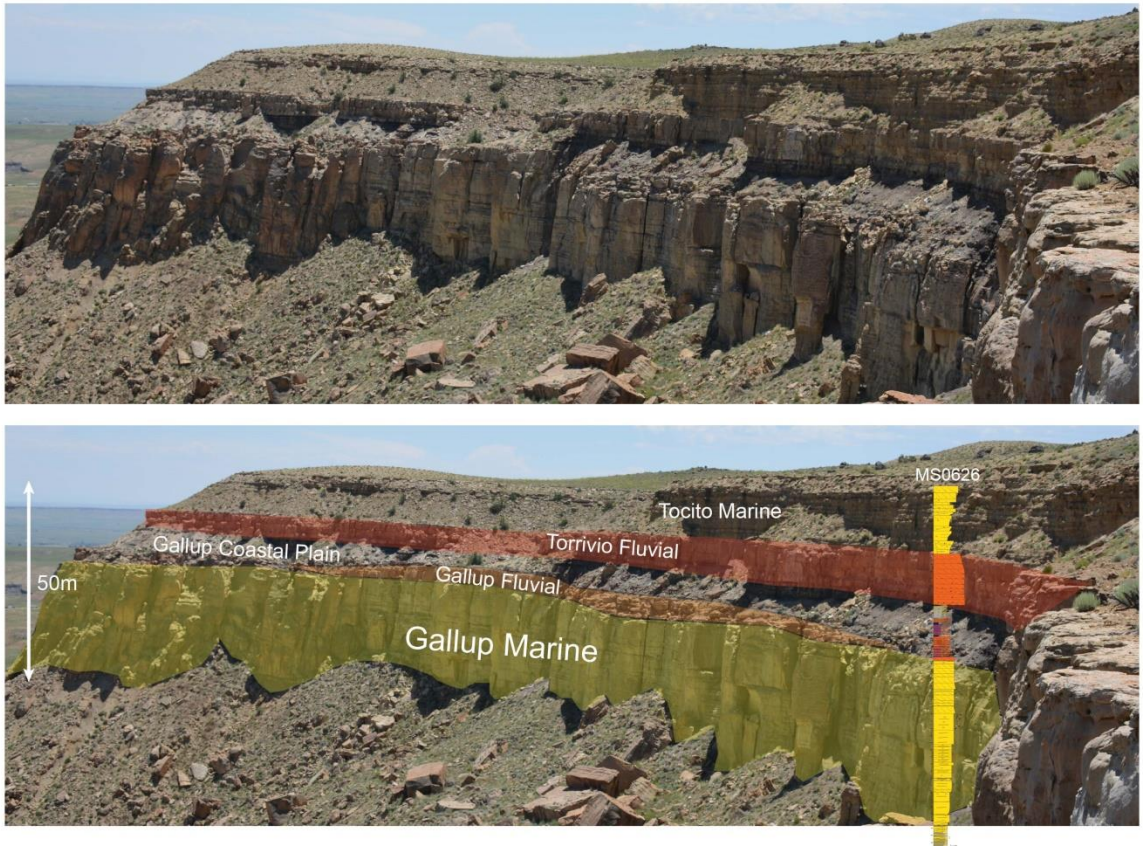

Fig. 3.5.–Superbly exposed Gallup outcrops along the "Amphitheatre" Cliff show different stratigraphic units. The dominant marine facies of the Gallup Formation was incised by the overlying fluvial channels, which transits to coastal plain facies. The Torrivio fluvial channels

truncate the underlying Gallup Formation and then was onlapped and overlain by the marine Tocito sandstone.

With the help of measuring devices such as Jacob staff, laser rangefinder, and GPS, seventy-one sedimentological sections were measured from both cliff exposure and trenched slopes. The measured sections document lithofacies, grain size, sedimentary structures, trace fossils, body fossils, and paleocurrents. Trenching reveals a rather greater proportion of sandstone facies than previously shown, buried in the covered slopes. The slopes also contain newly identified bentonites, which are vital to the present study. Several sections are near the sections previously measured by Nummedal and Molenaar (1995). Comparison of these sections shows consistency in overall stratigraphic thickness, lithofacies, sedimentary structures, and depositional trends. Our study focuses on a relatively small area (the Shiprock area), thus allowing for a more intensive and detailed investigation of high-frequency sequence stratigraphy than the previous basin-wide studies.

Sixty-eight sections are around the Shiprock area with an average spacing of 880 m. Such close-spaced sampling ensures an accurate correlation and enables us to “walk-out” or trace key surfaces. It also avoids “aliasing” and ensures individual high-frequency sequence stratigraphic units are identified and documented without missing high-frequency variation. There is a 25 km gap with no outcrop between Toadlena and Window Rock (Fig. 3.3); scouting around the area north of Window Rock also shows the outcrop is heavily covered by vegetation and falling rocks and is hard to measure. Therefore, two sections were measured further updip around Window Rock near the AZ–

NM border line and one section at “Nose Rock” point (close to the town of Gallup), and tied to our main sequence stratigraphic correlation to document the updip stratigraphic variability (Fig. 3.3).

Marine bentonites, the deposits of volcanic ash falls draping the sea floor, are considered to be synchronous and extensive and are thus used as regional datums (Bhattacharya 2011; Miall 2013). Bentonites can be found by trenching in slope sections (Fig. 3.6). Hanging the cross-section onto bottom datums, particularly those that represent deep marine floors that have minimal gradient, can reflect the true stratigraphic geometry (i.e., clinoform) and avoid geometric distortion due to top hung or lack of datum (Bhattacharya 2011).

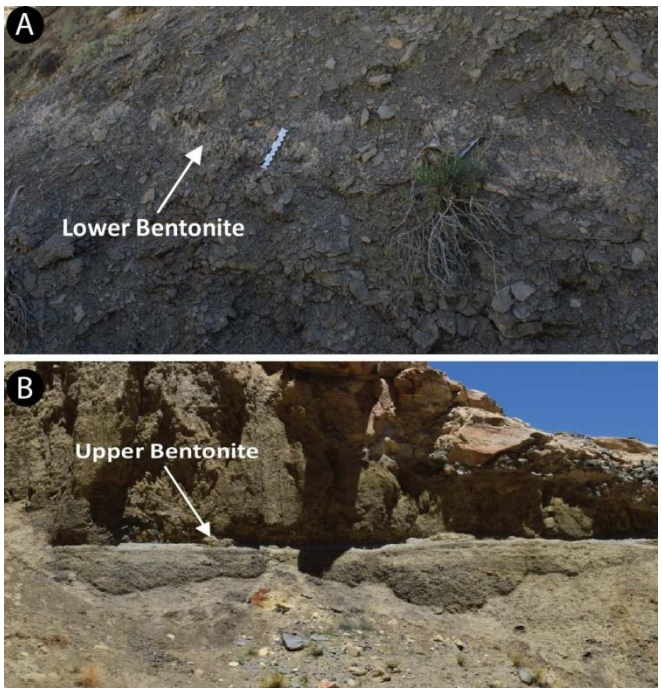

Fig. 3.6.–“Lower” and “Upper” bentonite layers are found continuously on outcrops and used as regional datums. (A) “Lower Bentonite” in muddy slope (Measured section 0711). (B) “Upper Bentonite” in outcrop exposure (Measured section 0711).

This paper presents the sequence stratigraphic analysis based on the classic conceptual sequence stratigraphic models (*sensu* Van Wagoner et al. 1988) with the integration of geometric analyses of stratal stacking patterns, incorporating shoreline trajectory (Helland-Hansen and Martinsen 1996) and accommodation successions (Neal and Abreu 2009). The sequence stratigraphic units employed in the study consist of parasequences, parasequence sets, four-fold systems tracts (i.e., FSST, LST, TST, and HST; Plint and Nummedal 2000), depositional sequences, sequence sets, and composite sequences (Neal and Abreu 2009). Walther's Law, stratal termination and lapout relationships are applied to identify key bounding surfaces (Mitchum et al. 1977). Sequence boundaries are placed at the bases of FSST in this study to respect the fact that the onset of a new sequence is defined by an unconformity resulting from a relative sea level fall and an abrupt basinward shift of facies.

Facies-based analysis allows distinction of key surfaces with the observation of changes in facies that break Walther's Law. For example, distal facies abruptly overlying proximal facies marks a flooding surface; proximal facies erosively overlying distal facies suggest a sequence boundary. Ichnology can also help to identify surfaces (Miller et al. 2018), for instance, the *Glossifungites* ichnofacies may indicates a transgressive surface of erosion or more rarely, a sequence boundary (Maceachern et al. 1992). The outcrop data also allows detailed interpretation of key stratigraphic surfaces with the observation of subtle facies changes. For example, a grain-size-decrease or bioturbation-intensity-increase can be used to identify flooding surfaces (Sadeque et al. 2007). The lateral variability of facies can be observed by tracing key surfaces and stratigraphic units

between measured sections, and this was accomplished by walking along cliffs and/or correlating on photomosaics.

Shoreline trajectory analysis requires the recognition of actual shoreline position, where coastal plain facies meet shallow marine facies (i.e. foreshore or beach boundary). In the Gallup sequences, there are a number of parasequences with only lower shoreface or distal delta front preserved; therefore, tracking the boundary between marine sand and offshore mud facies is more practical for the purpose of quantitative shoreline trajectory analysis, although the position of this boundary can be sensitive to local or short-term changes of sediment supply. In ramp settings, it is assumed that the depositional profiles of individual parasequences remain similar through deposition; thus the magnitudes of dislocation of different facies boundaries are assumed to be consistent. Therefore, the horizontal distances between the facies boundaries of marine sandstone and mudstone are interpreted to reflect the relative magnitudes of shoreline translation (Hampson et al. 2001; Zhu et al. 2012). Similarly, relative sea level change can be estimated from projected vertical distances between paleoshorelines, or other key facies boundaries, recorded in successive parasequences. Relative sea level change can also be estimated using parasequence thickness, which is considered to reflect the accommodation linked to relative sea level position (Ainsworth et al. 2018). These estimates may not be exceedingly accurate, given compaction of strata during deposition and subsequent deformation or tilting of datums, but are considered sufficient to quantitatively examine the shoreline migration and the relative sea level change through the development of stratigraphic sequences over the relatively local area of our study.

Accommodation successions are used to evaluate stratal geometries and lapout patterns and can be genetically linked to systems tracts, independent of conceptual sequence stratigraphic models or relative sea level positions (Neal and Abreu 2009). In the Gallup study, after mapping out individual parasequences, we group them into parasequence sets based on their stacking patterns and link the parasequence sets to relevant systems tracts. An individual parasequence may also represent a systems tract, especially FSST, LST, and TST, in response to limited accommodation or sediment supply. We also identify sequence sets on the basis of the geometric relationships of successive accommodation successions of individual sequences (Neal and Abreu 2009).

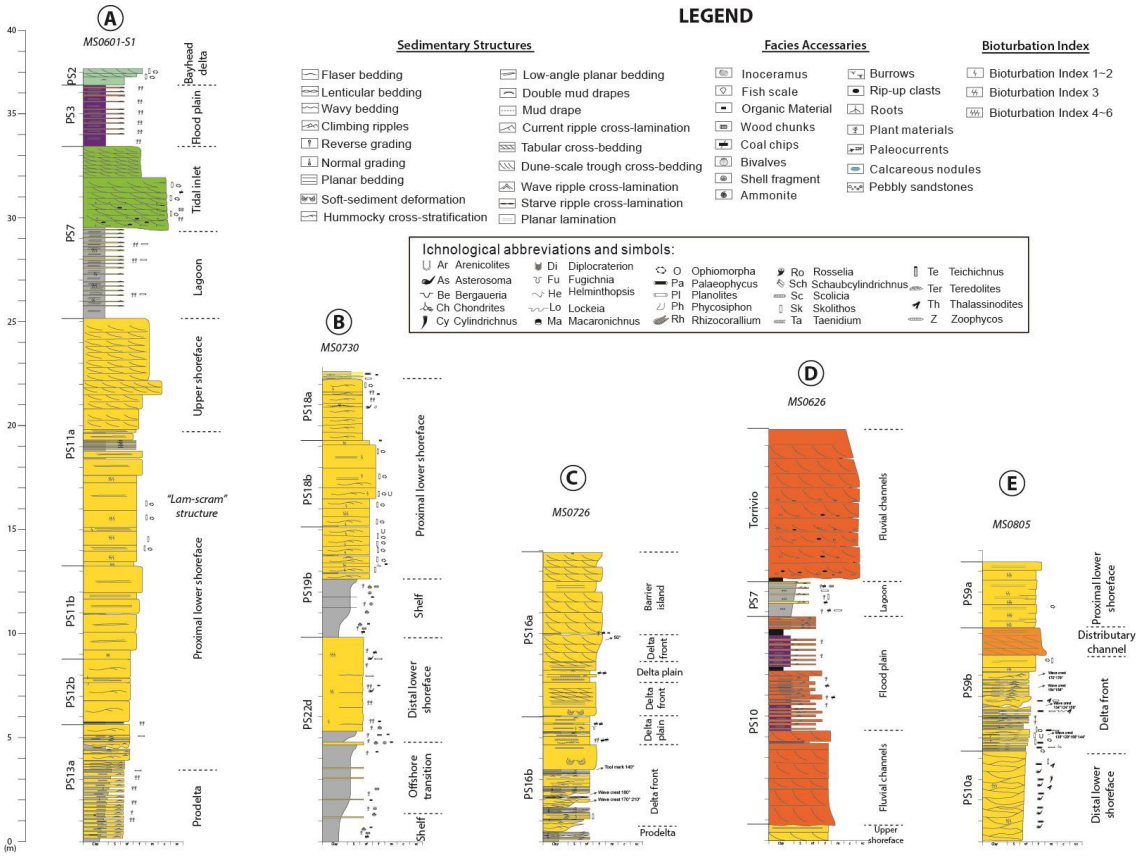

Fig. 3.7.–Measured sections showing key depositional facies associations. (A) Prodelta – proximal lower shoreface – upper shoreface – lagoon – tidal inlets – flood plain – bayhead delta

facies succession. A key facies of proximal lower shoreface is known as “lam-scram”, representing the interbedding of laminated and bioturbated sandstones. (B) Shelf – offshore transition – distal lower shoreface and shelf – proximal lower shoreface facies succession showing lower very fine-grained bioturbated distal lower shoreface sandstones and very fine- to fine-grained hummocky cross stratified proximal lower shoreface sandstones. (C) Prodelta – delta front – delta plain – barrier island facies succession. Note the “ball-and-pillow” structure showing the soft sediment deformation due to the unstable delta front environments. (D) Fluvial channel – flood plain – lagoon – fluvial channel facies succession. The flood plain to lagoon facies transition represents marine transgression. (E) Distal lower shoreface – delta front – distributary channel – proximal lower shoreface succession.

3.4 Facies Associations

We identify sixteen environmental facies associations: shelf (Fig. 3.7B), offshore transition (Fig. 3.7B), prodelta (Fig. 3.7A), delta front (Fig. 3.7C and E), delta plain (Fig. 3.7C), distal lower shoreface (Fig. 3.7B and E), proximal lower shoreface (Fig. 3.7A, B, E), upper shoreface (Fig. 3.7A), foreshore, distributary channel (Fig. 3.7E), barrier island (Fig. 3.7C), lagoon–bay fill (Fig. 3.7A and D), bayhead delta (Fig. 3.7A), fluvial channel (Fig. 3.7D), floodplain (Fig. 3.7A and D), and tidal inlet–delta (Fig. 3.7A). Table 3.1 and Figure 3.7 summarize and illustrate the interpreted facies and facies associations. We do not classify middle shoreface as an individual facies association in that we realize it is difficult to distinguish it from lower shoreface (i.e. hummocky vs. swaley cross-stratification; Plint 2010). The lower shoreface association is further divided into proximal and distal lower shoreface (i.e. proximal lower shoreface is storm-dominated deposits above storm wave base; distal lower shoreface is occasionally below storm wave base to allow bioturbation; MacEachern et al. 2010; Plint 2010). Paleocurrent

measurements indicate a predominantly northeast-oriented progradational system with the influence of southeast-dominated longshore drift (Fig. 3.8).

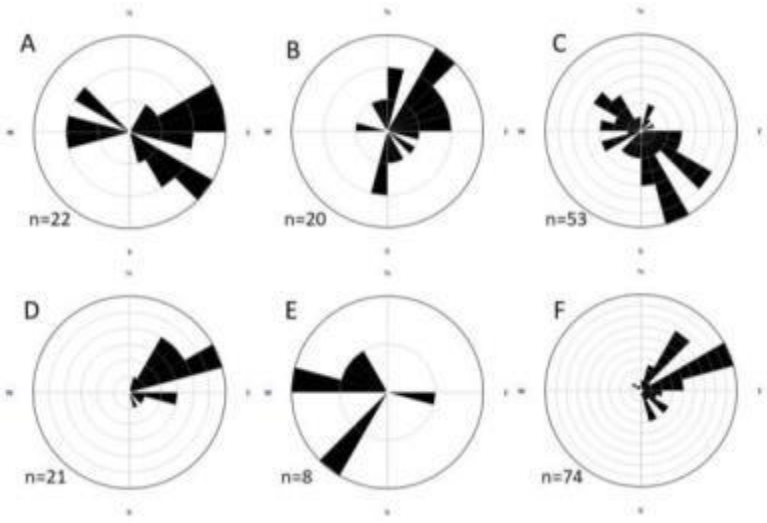

Fig. 3.8.–Paleocurrent measurements from key depositional facies associations. Paleocurrent measurements from (A) delta front showing the general east-trend deltaic progradation, (B) lower shoreface showing a northeast to north-south oriented deposition, which can be related to strong river influence and shore normal storm influence and along-shore wave reworking, (C) upper shoreface indicating southeast dominated southeast-northwest oriented bi-directional longshore drifts, (D) distributary channels showing a mostly northeast oriented channel system that perpendicular to the shoreline, (E) tidal facies indicating west to southwest tidal let direction, and (F) fluvial channels suggesting mostly northeast and occasionally southeast river flowing direction that indicates the system prograded northeastward.

Table 3.1 Summary of facies successions in the Gallup Sandstone. Bioturbation index (BI) scheme by Taylor and Goldring (1993).

Depo. facies associations	Proportion of total facies	Lithology, sedimentary structures, and characteristics	Ichnology
Shelf	21.3%	High clay content dark mudstones and shale with silty mudstones to muddy siltstones. Clay content can be up to 90%. Centimeter-scale thin-bed very fine-grained ripple cross laminated sandstones are commonly imbedded. Mudstones and siltstones show massive, laminated or graded beds. Bouma sequences are occasionally seen. Body fossils of ammonites, inoceramids, and bivalves and fish scales are common. Abundant organic materials and shell fragments. Plant and carbonaceous materials are locally seen.	Absent to thorough bioturbation. BI: 0-6. Zoophycos to *Cruziana* Ichnofacies. Ichnofauna: *Ch, Pl, Pa, Ph, As, Tei, Z. Ro, Cy, Rh,* and *Di.*
Offshore transition	9.8%	Silty to sandy mudstones and sandy siltstones interbedded with centimeter-scale thin-bed very fine-grained sandstones. Wave, combined-flow, or starved ripple cross laminations are in sandstones. Hummocky cross stratification (HCS) or planar bedding are local. Sole marks are common. Commonly coarsening upward. Mudstones contain graded beds and horizontal lamination; otherwise are intensely bioturbated. Bouma sequences are common. Body fossils of ammonites, inoceramids, and bivalves are common. Abundant organic materials, shell fragments, and plant materials. Wood debris is seen locally.	Absent to thorough bioturbation. BI: 0-6. *Cruziana* Ichnofacies. Ichnofauna: *Ch, Pl, Pa, Ph, As, Ro, Cy, Rh,* and *Di.*
Prodelta	7.5%	Mudstones dominated heterolithic interval with very fine-grained sandstones. Normal grading beds and horizontal lamination are dominant in mudstones. Thin bed (1-10cm) sandstones show current and combined-flow ripple cross lamination, and occasionally HCS and planar lamination. Typically coarsening upward. Bouma sequence, soft sediment deformation, loading structures, and microfaults are commonly seen. Abundant plant and organic materials. Wood chips are also commonly seen. Body fossils are often seen.	Absent to sparse, locally low bioturbation. BI: 0-2. *Cruziana* Ichnofacies. Ichnofauna: *Ch, Pl,* and *Pa.*
Delta front	5.3%	Upper very fine- to medium-grained sandstones locally interbedded with thin bed mudstones or siltstones. Soft sediment deformation structures are prevalent (e.g. "ball and pillow" structure), varying from decimeter- to meter-scale. Individual sandstone beds are less than 1 meter thick. HCS, planar bedding, wave, combined-flow, and current ripple cross-lamination present in fine-grained sandstones; cross beddings are seen in coarser-grained sandstones. Abundant plant materials, coaly chips, and wood chunks. Sole marks are commonly seen. The facies successions typically show coarsening-upward trend.	Absent to sparse bioturbation. BI: 0-1. Mixed *Cruziana* and *Skolithos* Ichnofacies. Ichnofauna: *Pl, Pa, Sk, O, Th, Ar,* and *Ro.*
Delta plain	0.2%	Very fine- to fine-grained sandstones interbedded with carbonaceous mudstones. Planar bedding and ripple cross lamination are common in sandstones. Cross beddings and HCS are locally seen. Mud drapes are commonly seen. Abundant plant materials, coaly chips, and wood chunks along laminated sandstones.	Absent to sparse bioturbation. BI: 0-1. *Cruziana* Ichnofacies. Common ichnofauna: *As* and *Pa*
Distal Lower shoreface	12.5%	Muddy to silty lower to upper very fine-grained intensely bioturbated sandstones. It is difficult to identify any sediment structure due to intense bioturbation, and only remnant forms of ripple cross lamination, low-angle cross lamination, and HCS are seen very locally. Inoceramids and bivalves fossils and shell fragment are common. Plant and organic materials are very often seen and can be abundant locally.	Moderate to thorough bioturbation. BI: 3-6. Often thoroughly bioturbated and hard to identify individual ichnofaunas. *Cruziana*

			Ichnofacies. chnofauna: *As, Di, Ch, Rh, Pa, Pl, Ph, Ro, Tei. O, Gy,* and *Fu.*
Proximal Lower shoreface	18.4%	Lower very fine- to lower fine-grained sandstones with HCS, planar to low-angle cross bedding, and wave or combined-flow ripple cross-lamination. It typically upgrades to laminated sandstones interbedded with bioturbated sandstones, showing the "lam-scram" structure. The HCS or planar bedsets vary from 10 cm to 1 m thick (mega HCS), and the bioturbated sandstone beds are 10 cm to 1 m thick. Abundant gutter casts developed at the bottom, and wave ripple cross-lamination typically capped the HCS beds. Abundant plant materials and sporadic wood chunks are associated with HCS. Mud drapes along HCS or planar bedding are seen locally.	Absent to thorough bioturbation. BI: 0-6. Mixed *Cruziana* and *Skolithos* Ichnofacies. Ichnofauna: *Ch, Pa, Pl, As, O, Sk, Th, Ar, Ph. Ro, Cy, Di, Tei, Rh,* and *Lo.*
Upper shoreface	7.1%	Lower fine- to lower coarse-grained dune-scale trough and tabular cross-bedded and planar bedded sandstones. The majority is upper fine- to medium-grained trough cross-bedded sandstones. Generally coarsening and thickening upward. Bi-directional or multi-directional cross-beddings with cross-sets of 20 - 40 cm thick. Bed sets are from 50 cm to 3 meters thick. Contacts between the upper shoreface and lower shoreface are concordant and sharp, marked by an obvious increase of grain size.	Absent to sparse bioturbation. High bioturbation is local and due to transgression. BI: 0-5. *Skolithos* Ichnofacies. Ichnofauna: *O, Sk, Ar,* and *Th.*
Foreshore	0.01%	Fine-grained planar to sub-planar bedded sandstones, gently dipping seaward.	Absent to sparse bioturbation. BI: 0-1. *Skolithos* Ichnofacies. *O and Sk* are occasionally seen.
Distributary channel	0.8%	Mostly granulely upper fine- to lower coarse-grained dune-scale trough or tabular cross bedded and locally planar bedded sandstones. Lower very coarse-grained sandstones are seen locally. Thin bed (2-10cm) mudstones draping on sandstones are occasionally seen. Erosive base and fining upward. Sandstones present bar shape with limited lateral extension. Abundant mud rip-up clasts, plant materials, coaly chips, and wood chunks. Paleocurrents are perpendicular to the paleoshorlines.	Absent to sparse bioturbation. BI: 0-1. *Skolithos.* Ichnofacies. Ichnofauna: *Sk* and *O.*
Barrier island	1.1%	Lower fine- to upper medium-grained dune-scale cross-bedded with locally planar bedded sandstones and bioturbated sandstones. HCS are seen locally.	Absent to intense bioturbation. BI: 0-4. *Skolithos* Ichnofacies. Ichnofauna: *O, Sk, Pa,* and *Th.*
Lagoon and bay fill	3.3%	Mudstones dominated heterolithic sections with thin-bed very fine lower- to fine lower-grained sandstones. Ripple cross laminations are common. Graded beds and horizontal laminations are seen in mudstones. Abundant plant materials, wood chips, coaly chips, and carbonaceous materials. Coal seams are seen locally. Roots are rare.	Low to intense bioturbation. BI: 0-5. *Cruziana* Ichnofacies. Ichnofauna: *Pl, Pa,* and *Tei.*
Bayhead delta	1.0%	Relatively thin-bed (up to 30 cm) lower very fine- to upper fine-grained ripple cross laminated to dune-scale cross bedded sandstones. Thin-bed mudstones are locally embedded. Bioturbation is often seen. The successions show coarsening upward trend. Abundant plant and organic materials, wood chips, coaly chips, and carbonaceous materials.	Low to intense bioturbation. BI: 0-5. *Skolithos* Ichnofacies. Ichnofauna: *O, Sk, Th, Tei. Cy* and *Di.*
Tidal inlet	1.4%	Lower fine- to lower coarse-grained cross-bedded sandstones. Granules are seen locally. Ripple cross	Low to intense bioturbation.

and delta		laminations, planar beddings, herringbone, and double mud drapes are seen locally. The successions are fining upward. Abundant plant material. Wood and coal chips are often seen.	BI: 0-4. *Skolithos* Ichnofacies. Common ichnofauna: *O, Sk,* and *Tei.*
Floodplain	1.5%	Carbonaceous and coaly mudstones with abundant plant material, roots, wood chips, and coal chips. Centimeter-scaled thin-bed very fine-grained current ripple cross laminated sandstones are interbedded with mudstones. Slickenside structure is seen locally. Coal beds are common, from a few centimeters to 50 centimeters thick.	Absent to sparse bioturbation. BI: 0-1.
Fluvial channel and bar	8.6%	Pebbly coarse-grained sandstones are above the sharp and erosive base surfaces, and often mixed with mud rip-up clasts, coal chips, and wood trunks. The successions are fining upward and typically upgrade to medium-grained dune-scale trough or tabular cross-bedded sandstones.	Absent to sparse bioturbation. BI: 0-1.

In the shallow marine facies associations, we interpret the depositional profile to represent coastal, shoreface, deltaic, and shelf environments. Shoreface associations, consisting of upper shoreface and lower shoreface facies, are generated by storm and fair-weather wave processes (Plint 2010). Deltaic systems, constituting prodelta, delta front (subaqueous), and delta plain facies, are genetically related to fluvial influence (Bhattacharya 2010). The Gallup clastic wedge, deposited in an epicontinental ramp setting, manifests a mixed-process influenced deltaic system: the deposition is influenced by river input, storm processes, and fair-weather wave reworking. Tides are also observed but primarily related to coastal environments, associated with marine transgression (Boyd et al. 1992; Boyd 2010; Lin and Bhattacharya 2018).

Facies analysis, on the basis of one-dimensional measured sections, is the foundation of high-resolution sequence stratigraphic evaluation. Depositional facies associations are affected by the combination of sediment supply and accommodation (Jervey 1988): deltaic deposits can reflect a rapid seaward progradation dominated by low accommodation versus sediment supply (A/S) ratio; in contrast, distal lower shoreface facies suggest a high or increasing A/S ratio, given the highly bioturbated nature of the fine-grained sediment.

3.5 High-Resolution Sequence Stratigraphy

Our high-frequency sequence stratigraphic analysis of the Gallup system is shown in Figure 3.9. The cross-section shows the bounding surfaces, sequence stratigraphic units (e.g., parasequences, parasequence sets, and sequences), and facies associations.

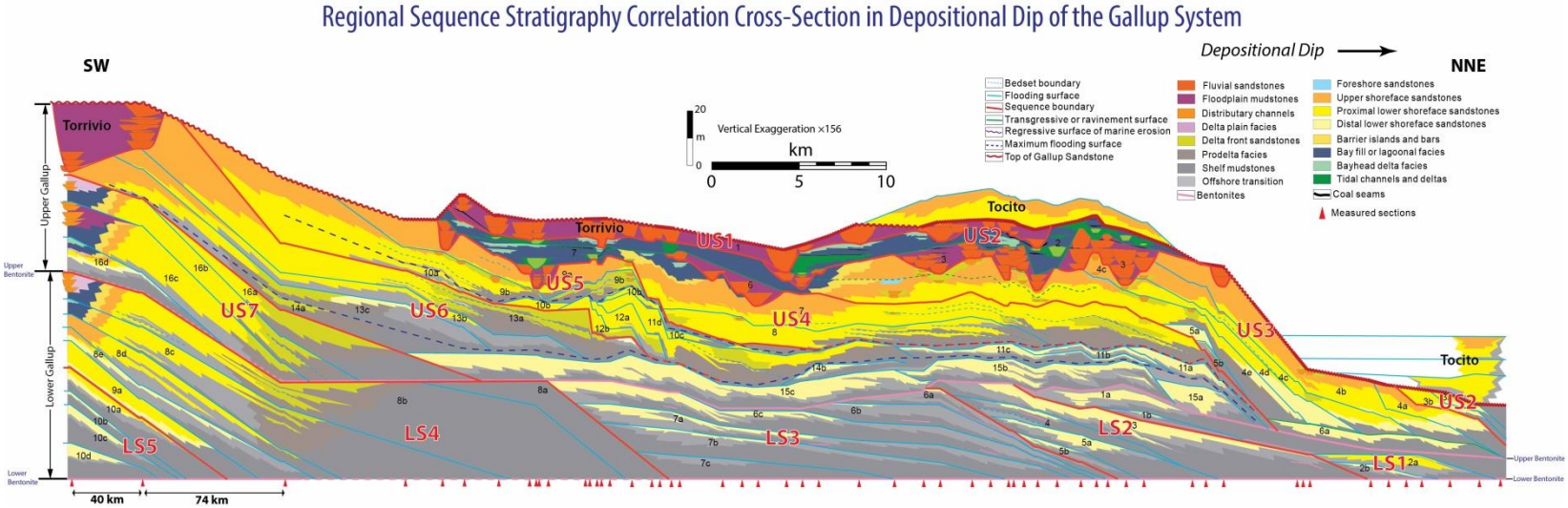

Fig. 3.9.–High-resolution dip-direction sequence stratigraphy of the Gallup system. The upper Gallup system is constituted of six sequences, subdividing into sixteen parasequence sets and thirty-six parasequences. The lower Gallup consists of six sequences, ten parasequence sets, and twenty-four parasequences. A regional unconformity lies between the overlain Tocitio Sandstone and the Gallup system.

Trenching reveals two continuous bentonite layers that range from 10 to 50 cm thick and are named the “Upper Bentonite” and “Lower Bentonite” respectively. XRF scans of samples of each bentonite layer from the south, middle, and north shows very similar mineral characteristics and thus suggests the bentonites can be correlated throughout the study area. These two bentonite layers can most probably be correlated to the subsurface M-1 and M-3 bentonite markers of McCubbin (1982). The “Lower Bentonite” marks the boundary between the Gallup Formation and the underlying Juana Lopez Member; it is assumed to be deposited synchronously on a nearly flat ocean bottom, and therefore, is used as the bottom datum for the sequence stratigraphic correlation. The overlying parasequences in the Gallup downlap onto the top of the Juana Lopez Member (Fig. 9), suggesting that the bentonite lies within a condensed section and drapes a maximum flooding surface.

Fig. 3.10.–The photo of the “Rock Ridge”, which is also known as the parasequence point, shows two coarsening upward facies successions that are interpreted as two parasequence sets capped by major flooding surfaces (FS). The FS mark facies changes and distinguish distal facies from proximal facies.

3.5.1 Major Bounding Surfaces

We establish the high-resolution sequence stratigraphic framework of the Gallup system based on identification of fundamental sequence stratigraphic surfaces, including flooding surfaces (FS), sequence boundaries (SB), maximum flooding surfaces (MFS), and ravinement surfaces (RS) or transgressive surfaces of erosion (TSE; Pattison 1995; Fig. 3.10 to 3.13). We choose to use RS for this paper.

Flooding surfaces, which define parasequences, are used as the most fundamental surfaces with the lowest hierarchy in the study (Van Wagoner et al. 1988; Bhattacharya 1993; Korus and Fielding 2017). Flooding surfaces are typically manifested by a "shale-on-sand" contact (*sensu* Van Wagoner et al. 1988; Fig. 3.10), such as the FS of Parasequence 15c. Alternatively, FS may be expressed as "sand-on-sand" contacts in proximal areas (Fig. 3.11) and "shale-on-shale" contacts in distal areas, represented by the FS of Parasequence 8 of the upper Gallup and the FS of Parasequence 11a, respectively. Flooding surfaces generally define clinoforms that dip seaward (Fig. 3.9).

Two types of SB are distinguished including: subaerial and subaqueous erosional surfaces. Fluvial channels incising into underlying marine strata mark a subaerial erosional SB, also known as the subaerial unconformity (SU; Fig. 3.12A). The surface is often associated with the woodground trace fossil—*Teredolites*, which indicates erosional discontinuities, such as log ground facies erosionally overlies marine–marginal marine facies, representing an abrupt change in depositional environments (Bromley et al. 1984; Savrda et al. 1993; Fig. 3.13A). The subaqueous SB is often characterized by sharp- or erosional-based shoreface or deltaic sandstones, associated with abundant gutter casts

(Fig. 3.12B), overlain and downlapped by a FSST, such as the SBs below Parasequences 12b and 8 of the upper Gallup (Fig. 3.9). The *Glossifungites* ichnofacies commonly exists along these subaqueous erosional surfaces (Pemberton and MacEachern 1995). Sequence boundaries are also defined by onlap of younger parasequences (Fig. 3.14), such onlap is observed along the top boundaries of Sequence 4-1 of the lower Gallup and Sequence 6-4 of the upper Gallup (Fig. 3.9). Sequence boundaries become more complicated landward—truncated by younger sequence boundaries or coalesced with TS or RS (Bhattacharya 1993). The top boundary of Sequence 3 of the upper Gallup is truncated by the top boundary of Sequence 2 landward. The top boundary of Sequence 4 of the upper Gallup is concordant with the transgressive surface in the coastal section (Fig. 3.9).

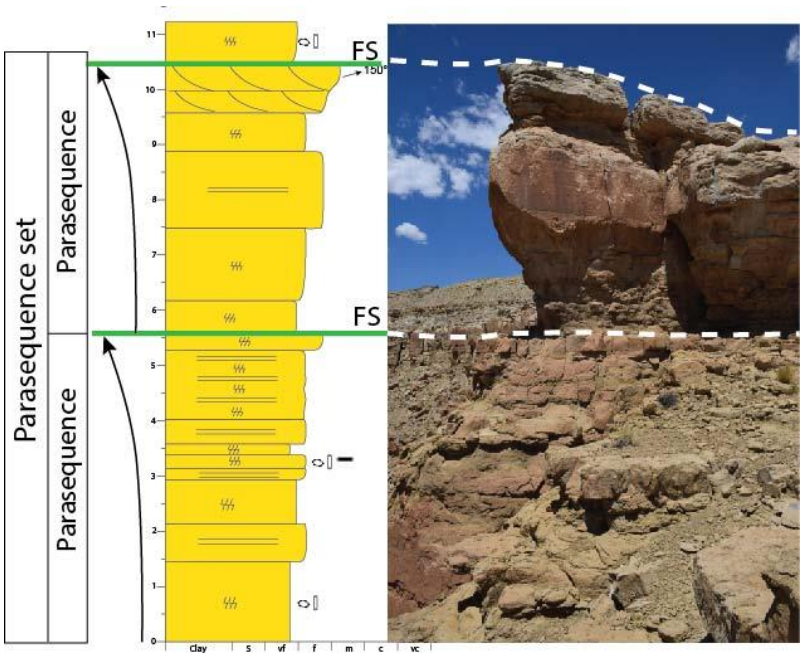

Fig. 3.9.–An outcrop example of FS crossing through “sand-on-sand” stacking model (MS 0715-2016). Subtle facies changes across FS include grain size decrease and laminated sandstones grading into intensively bioturbated sandstones.

Fig. 3.10.– Sequence boundaries (SB) in outcrops. (A) S SB at the base of fluvial channel incision. Fluvial channels incised into underlying marine strata indicate subaerial erosion that suggests a SB. The photo is taken at MS 0711. Channels incise into parasequence 4e of the upper Gallup. (B) Sharp-based shoreface sandstones mark an erosional surface resulted from forced regression, which suggests a SB. The photo is taken at MS 0607-S1. The sharp-based shoreface belongs to Parasequence 8, and the SB marks the onset of Sequence 4 of the upper Gallup.

Two MFS are identified in the Gallup system in the thickest shale sections and around the transition from fining to coarsening upward facies successions (Fig. 3.13E). The MFS overlies a number of parasequences, showing a large lateral extent, and are downlapped by younger progradational parasequences (see the MFS overlying Parasequence Sets 14 and 15 and Parasequence Sets 10 and 11 respectively in Figure 3.9). These MFS represent two regional-scale marine transgressions. We use coal seams (Fig. 3.13B) and surfaces with stratigraphically important ichnofacies, such as *Glossifungites* (Fig. 3.13C) or change in bioturbation index (BI) to identify TS in the coastal plain sections, where typical marine flooding surface characteristics are lacking (e.g., the TS of Parasequence 7 of the upper Gallup). In many cases, transgressive surfaces coalesce with or are

overprinted by ravinement surfaces; the latter can be associated with transgressive lags (Fig. 3.13D), as well as *Thalassinoides* or *Teredolites* (MacEachern et al. 1992; Fig. 3.13A and B).

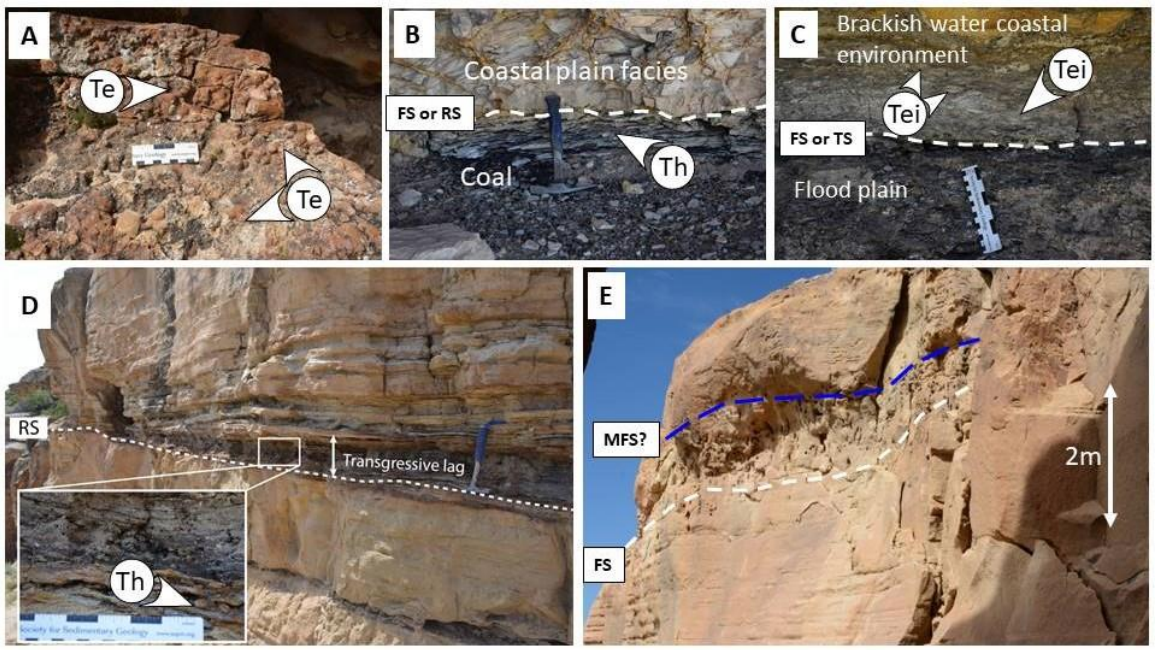

Fig. 3.11.–Facies of key surfaces. (A) Teredolites (Te) along the bottom of coarse-grained trough cross bedded fluvial sandstones indicating a subaerial erosional SB (MS 0730). (B) Firmground Thalassinoides (Th) in a coal bed, which is overlain by coastal facies, indicating a Glossifungites ichnofacies associated RS (MS 0726). FS=flooding surface, RS=ravinement surface. (C) Teichichnus (Tei) in a brackish water coastal environment overlying slickensided coaly mudstones, indicating a marine transgression. The facies boundary is interpreted as a TS/RS (MS 0713). TS=transgressive surface. (D) A transgressive lag, consisting of granules and coarse-grained sand with abundant coal chips and rip-up clasts overlying a RS. Thalassinoides (Th) are along the RS (MS 0607-S1). (E) A 30 cm thick intensely bioturbated sandstone section overlying planar bedded sandstones indicating a marine transgression, the lower boundary of which can be interpreted as a TS/RS. The bioturbated sandstones are overlain by cross bedded sandstone deposits during subsequent regression, and the facies boundary may represent a maximum flooding surface (MFS), downlapped by the overlying sandstones (MS 0706).

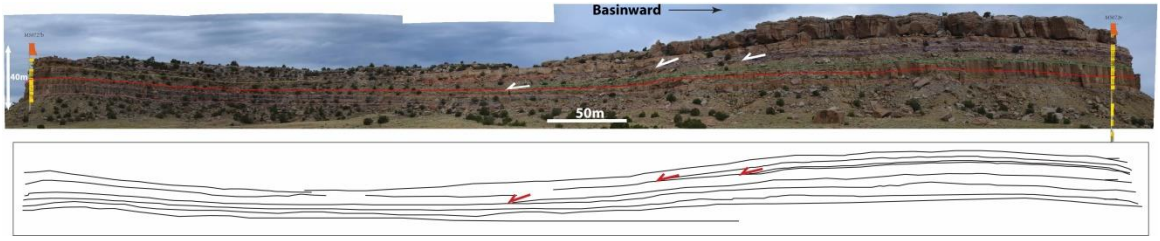

Fig. 3.12.–Outcrop photomosaic and surface interpretation showing onlap terminations (MS 0727 – MS 0726).

Table 2. Summary of sequence stratigraphy, systems tract, accommodation succession, shoreline trajectory and migration distance, and relative sea level change of the Gallup system. SS: sequence set; PS: parasequence set; APD: aggradation–progradation–degradation; R: retrogradation; PA: progradation–aggradation; D: degradation (Neal and Abreu 2009). A: accelerating; D: decelerating. Negative values of the shoreline migration distance mean landward shoreline retreat; positive values mean basinward shoreline regression. Negative values of the relative sea level change indicate relative sea level fall, whereas positive values indicate relative sea level rise.

Fm	SS	Sequence	PS	Parasequence	Systems Tract	Accommodation Succession	Shoreline Trajectory	Shoreline Migration Distance (km)	Relative sea level change (m)
T	APSS	1	1	1	LST				
		2	2	2	TST	R	Transgressive	-16	
			3	3a, 3b	LST	PA	Ascending regressive-A	0.2	6
		3	4	4a, 4b, 4c, 4d, 4e	HST	APD	Ascending regressive-D	16	-30
			5	5a, 5b	TST	R	Transgressive	-14.9	34
			6	6	LST	PA	Ascending regressive-A	15.4	-34
		4	7	7	TST+HST	APD	Ascending regressive-D	10.9	-10
			8	8	FSST	D	Descending regressive	21.1	-13
Upper Gallup	APDSS	5	9	9a, 9b	HST	AP	Ascending regressive-D	10.8	-2
			10	10a, 10b, 10c	TST	R	Transgressive	-44.3	38
			11	11a, 11b, 11c, 11d	FSST+LST	D	Ascending regressive	32.3	-13
			12	12a, 12b	FSST	D	Descending regressive	1.6	-6
		6	13	13a, 13b, 13c	HST	APD	Ascending regressive-D	17.3	-10
			14	14a, 14b	TST	R	Transgressive	-51.3	33
			15	15a, 15b, 15c	FSST	D	Descending regressive	47.9	-18
		7	16	16a, 16b, 16c, 16d	HST	APD	Ascending regressive-D	12.6	26
								-60	
	ADPSS	1	1	1a, 1b	TST	PA	Transgressive	1.1	8
								-16.1	17
			2	2a, 2b	LST	PA	Ascending regressive-A	1	3
								6.2	-28
		2	3	3	HST	APD	Ascending regressive-D	14.5	7
			4	4	TST	R	Transgressive	-3.6	10
			5	5a, 5b	LST	PA	Ascending regressive-A	2.2	5
								8	-15
Lower Gallup		3	6	6a, 6b, 6c	TST+HST	APD	Ascending regressive-D	7.5	20
			7	7a, 7b, 7c	LST	PA	Ascending regressive-A	10.5	17
								14.4	-26
			8	8a, 8b, 8c, 8d, 8e	TST+HST	APD	Ascending regressive-D	10	25
		4	9	9a	LST	AP	Ascending regressive-D	2.3	-2
		5	10	10a, 10b, 10c, 10d	HST	AP	Ascending regressive	2.8	7

3.5.2 High-Frequency Sequence Stratigraphy

Sixty-one individual parasequences are identified, composing twenty-six parasequence sets and thirteen sequences. The "Upper Bentonite" divides the Gallup system into upper and lower units. The upper Gallup comprises seven sequences, including the Torrivio Member as an individual sequence, constituting sixteen parasequence sets and thirty-seven parasequences. The lower Gallup consists of five sequences, ten parasequence sets, and twenty-four parasequences (Table 3.2).

The lower and upper Gallup are described and named separately. This allows more sequences and parasequences (older) to be identified in the more proximal areas (south) in future studies and incorporated into the regional sequence stratigraphic framework without having a naming conflict. Parasequence sets and sequences are named in ascending numerical order from top to bottom: smaller numbers represent younger units; parasequences are named in ascending alphabetic order within each parasequence set—"a" is the youngest parasequence (Table 3.2). The ascending order also allows yet-to-be identified older units to be integrated into the regional work building on our nomenclature. The youngest Gallup unit has been well documented below the Tocito unconformity, and therefore no younger Gallup units are anticipated to be identified in future studies.

The Lower Gallup.--- In the lower Gallup, Sequence 5 is the oldest and is only exposed in the southernmost area. This sequence contains four well-defined parasequences comprising upward coarsening successions with shelfal mudstones grading into distal lower shoreface sandstones. They are likely the distal sections of the HST. Parasequence 9a shows a basinward shift of facies, expressed by an increase in sandstone content and

parasequence thickness. Therefore, Parasequence 9a is interpreted to represent the LST of a younger sequence (Sequence 4) and its bottom boundary represents a SB. Parasequence Set 8 shows an overall aggradational-progradational stacking pattern and overlies the previous LST, thus representing a HST, although Parasequence 8e may represent a TST. The shoreline aggradation and progradation allowed coastal facies to be deposited at the top of Parasequences 8c and 8b. The top of Parasequences 8b and 8a are truncated by a regional ravinement surface draped by the bentonite layer downdip, demonstrating toplap termination and indicating sediment bypass, which defines the top SB of Sequence 4 (Fig. 3.9).

Sediment of the more distal Parasequence Set 7 is coarser than that of Parasequence 8a, suggesting a violation of Walther's Law and thereby a basinward shift of the depositional system, attributed to the onset of a new sequence (Sequence 3). Parasequences 7a – 7c show an aggradational stacking pattern that suggests a base level rise following a base level fall. They also onlap onto the previous sequence boundary. Therefore, Parasequence Set 7 is interpreted as the LST of Sequence 3; the onlapping stratal terminations are also used to interpret the underlying sequence boundary (Neal et al. 2016). The top of Parasequence Set 6 is concordant with and truncated by the bentonite-draping ravinement surface (the "Upper Bentonite"). The toplapping to offlapping terminations, associated with a decrease of sand content from Parasequences 6c to 6a, are interpreted to represent a progradational HST (Martin et al. 2009). The bottom part of Parasequence 6c may also encompass part of the TST, but a clear

boundary to differentiate the TST and HST is lacking. The top truncation is interpreted to be formed in part by erosion of a later, basin-wide marine transgression.

Similar basinward shift of facies and onlapping terminations are observed distally (NNE) and used to distinguish Sequence 2 and Sequence 1 and their associated sequence boundaries. In Sequence 2, Parasequences 5a and 5b represent a LST with the stratal onlap and an aggradational stacking pattern, whereas Parasequence 4 is interpreted as a TST showing a retrogradational stacking pattern. The top of Parasequence 3 is concordant with the bentonite proximally and diverges seaward as it dips towards the distal locality. The foreset shows toplap to offlap; and the paraseqwuence is also onlapped by Parasequence Sets 2 and 1. As a result, Parasequence 3 is interpreted to represent a HST, and its top surface is interpreted as the bounding SB. Parasequence Set 2 is interpreted as the LST of Sequence 1 on the basis of its aggradational stacking pattern, and onlaps onto the underlying SB. Parasequence Set 1 shows a back-stepping stacking pattern with a stratigraphic rise interpreted to represent a TST (Fig. 3.9).

The entire lower Gallup interval represents a sequence set containing a series of sequences with an aggradational-progradational-degradational (APD) stacking pattern. The lower Gallup downlaps onto the “Lower Bentonite”-draped MFS (Table 3.2; Neal and Abreu 2009). The sequence set can be interpreted to represent a transition from a HST to a following FSST sequence set. From Sequence 4 to 1, the sequence sets show a vigorous horizontal basinward shift with nearly no vertical stratigraphic rise. This geometry most likely indicates a forced regression that is likely linked to relative sea level fall (Posamentier et al. 1992; Korus and Fielding 2017). The top SB of Sequence 4 may

be interpreted as a composite sequence boundary. The “Upper Bentonite” layer may reflect a significant regional marine transgression and mark the MFS of the entire composite sequence set of the Gallup system (Fig. 3.9).

The Upper Gallup.--- In the upper Gallup, Parasequence Set 16 defines the HST of Sequence 7, based on the aggradational-progradational stacking pattern and the preserved coastal facies. From Sequence 7 to 6, the depositional system shows significant basinward advance: the parasequences of Parasequence Set 15 prograded over 47 km with minimal vertical stratigraphic rise. There is a marked down-shift between Parasequences 15b and 15a, which juxtaposes sandstones over distal mudstones of Parasequence 16a. Also, the parasequences of Parasequence Set 15 show very similar thickness, contain only distal lower shoreface sandstones and shelf mudstones, and prograde at a nearly flat trajectory. The characteristics described above define Parasequence Set 15 as the FSST of Sequence 6, attributed to forced regression. The thin nature also characterizes parasequences in the FSST due to foreshortening reflecting limited and decreasing accommodation (Posamentier et al 1992). The lack of coarse-grained transgressive lags, a key characteristic of forced regression, may be attributed to distality (MacEachern et al. 1999).

Parasequence Set 14 consists of two isolated parasequences that step back with respect to Parasequence Set 15 are capped by a regionally extensive mudstone that suggests a MFS. The stacking pattern suggests a notably high A/S ratio, and PS 14 is interpreted as a TST. Parasequence Set 13 aggrades and then progrades, and downlaps onto the underlying MFS; hence it is interpreted as a HST. The contact between Parasequences 13a and 12b is characterized by the sharp base of the shoreface and delta

deposits of Parasequence 12b, associated with abundant gutter casts. The surface above Parasequence 13a also shows a decline in stratigraphic level and is onlapped by the younger parasequences (Parasequences 12b and 10b). Thus, the surface above Parasequence 13a marks a SB, coincident with a RSME at the base of Parasequence 12b; the SB grades distally into a correlative conformity that coalesces with the underlying MFS (Fig. 3.9).

Parasequence Sets 12 and 11 represent the FSST of Sequence 5, characterized by a stepped degradational stacking pattern, with over 33 km of basinward translation and 19 m of shoreline descent. Such stratigraphic architecture is interpreted to likely result from forced regression (Posamentier and Morris 2000). Parasequences thin from Parasequences 11d to 11b, and then thicken in Parasequence 11a; an increase in accommodation from FSST to LST may explain the variation in thickness. Parasequence Set 10 back-steps, interpreted to result from an increase in accommodation outpacing sediment supply during marine transgression. This parasequence set thus represents the TST of Sequence 5. A widespread mudstone layer overlies Parasequence Sets 10 and 11 across almost the entire depositional section and may represent a maximum flooding zone (*sensu* Korus and Fielding 2017; Siggerud and Steel 1999), thus a MFS is interpreted. The aggradational-progradational stacking pattern, associated with the progradation of proximal depositional facies in Parasequence Set 9 is interpreted as the HST of Sequence 5, downlapping onto the MFS.

Sequence 5 is incised by overlying fluvial channel belts updip, suggesting a new sequence defined by a subaerial sequence boundary. This SB descends abruptly and

merges with a RSME, characterized by the sharp basal boundary of shorefaces in Parasequence 8. Such SB links the subaerial unconformity and its correlative subaqueous unconformity. It is also onlapped by Parasequence 8. The sharp-based proximal lower shoreface deposits of Parasequence 8 abruptly overlie shelf mudstones at the proximal part; and such contact suggests the onset of a FSST (Fig. 3.12B). The internal discontinuous bounding surfaces of Parasequence 8 may represent the flooding surfaces between episodic forced regressions. Hence, parasequence 8 may be further subdivided into multiple parasequences; however, the discontinuous surfaces can be traced only in the distal area and become untraceable in the proximal section due to the amalgamation of forced regressive sandstones (Plint and Nummedal 2000). A transgressive lag, consisting of coarse-grained materials and terrestrial debris, locally caps Parasequence 8, marking the surface as a transgressive ravinement surface.

Parasequence 7 extends over 50 km with facies varying from coastal lagoonal and bayfill to shelf deposits. The parasequence locally preserves a complete facies succession from marine mudstones to nonmarine deposits. The coastal plain facies overlying marine shorefaces suggests shoreline progradation and aggradation, interpreted as a HST. Tidal channel facies, transit laterally into lagoonal facies and are interpreted to represent a partially preserved TST. Parasequence 7 is locally incised by fluvial channels that erode through the TST into the underlying shorefaces, suggesting a subaerial erosional sequence boundary. Further updip in the coastal succession, the subaerial unconformity becomes cryptic. Nonetheless, a coal bed is correlated to the transgressive surface and the base of the coal bed is considered to correlate to the subaerial SB; the top, overlain by coastal

deposits, represents a transgressive surface and suggests a marine incursion (Kamola and Van Wagoner 1995). Subaerial erosion is lacking in the distal portion, and the SB coalesces with the FS; however, at the distal locality the surface is onlapped by younger parasequence sets, supporting the interpretation of a SB (Fig. 3.9).

Parasequence 6 is a gently-dipping basinally isolated succession comprising only distal lower shoreface and shelf deposits. The geometry and position, and its onlapping relationship with the previous SB, suggests that this parasequence is most likely the LST of the younger sequence (Sequence 3). Parasequence Set 5 shows onlapping terminations, retrogradational stacking, and intensively bioturbated distal lower shoreface facies. These observations indicate a TST. Parasequence Set 4 laterally extends a distance of ~60 km and demonstrates an aggradational-progradational-degradational stacking pattern. The geometry clearly defines the topset, foreset, and bottomset of a clinoform set with varying dip angles. The preservation of coastal facies indicates progradation and topset aggradation, reflecting positive accommodation, and suggests that Parasequence Set 4 is a HST.

Channels incising deep into shorefaces of Sequence 3 suggests a basinward shift of the system and in turn a new sequence (Sequence 2). The erosional basal surface, spanning a distance of 15 km, is interpreted as a subaerial unconformity. However, the SB is nearly impossible to trace downdip, as it is truncated by the regional unconformity between the Gallup Formation and the overlying Tocito Sandstone. Nevertheless, the stacking pattern changes from progradation-degradation to aggradation, as observed between Parasequences 4a to 3b, and allows for a SB interpretation above Parasequence

Set 4. PS 4 is interpreted to represent a late HST. On the other hand, the more distal facies associations show a slight landward shift of the depositional system, and the aggradational Parasequence Set 3 may represent the LST of Sequence 2. Landward, Parasequence 2 comprises only coastal plain deposits and likely represents a transgressive coastal environment in a widespread TST (Boyd 2010).

Sequence 1 is designated as the entire coarse-grained fluvial dominated succession, equivalent to the Torrivio Sandstone. The sequence boundary is continuous and distinct throughout the outcrops expressed by basal surfaces of fluvial channels truncating underlying coastal deposit sections (Figs. 3.5 and 3.9). Coals and the *Glossifungites* ichnofacies are associated at the SB locally. This fluvial succession is persistent in most of the outcrops, with floodplain facies and other fine-grained deposits present locally; it disappears around the north of the Beautiful Mountain area. The top of Sequence 1 is either covered by modern alluvial deposits or is the top of cliff in the southern area (i.e., Sanostee and Toadlena). In the Beautiful Mountain area, the fluvial sandstone is capped by the fine-grained deposits (often in the form of a covered slope), and may be either the nonmarine facies of the Dilco Member or the marine mudstones of the overlying Tocitio interval.

The upper Gallup, consisting of aggradational-progradational-degradational (APD) and aggradational-progradational (AP) sequence sets, indicates a composite sequence. Sequences 7 - 5 represent an APD sequence set, and Sequence 4 to 1 constitute an AP sequence set (Table 2). The robust progradation of the sequence sets probably resulted from an overall low A/S ratio that is attributed to high sediment supply from the orogenic

belt with low accommodation. The top of the composite sequence is bounded by the regional unconformity between the Gallup system and the Tocito Sandstone and is onlapped by the Tocito parasequences.

3.5.3 Shoreline Trajectories and Accommodation Successions

Four classes of shoreline trajectory are identified in the Gallup system: ascending regressive with decelerating rate (the trajectory is convex upward), ascending regressive with accelerating rate (the trajectory is concave upward), descending regressive, and transgressive (Helland-Hansen and Martinsen 1996; Helland-Hansen and Hampson 2009; Fig. 3.15). Each class of shoreline trajectory is formed as a result of the successive stacking of genetically related parasequences. The shoreline migration displays exceedingly-low-angle trajectories, either regressive or transgressive. The low angles range from 0.02° - 0.6°, and are interpreted to reflect the imbalance between accommodation and sediment supply (Helland-Hansen and Gjelberg 1994). These low-angle trajectories also reflect the ramp setting with limited accommodation.

In the lower Gallup, shoreline trajectory is predominantly ascending regressive, punctuated by three descending regressions. The descending shoreline migrations correspond to relative sea level falls and basinward shifts of the depositional system, marking the onsets of the subsequent sequence. Those three shoreline descending regressions are associated with estimated relative sea level falls of 26 m, 15 m, and 28 m, respectively (Table 3.2). The shoreline of the lower Gallup advanced ~60 km in total, indicating the progradational nature of the composite sequence. The maximum shoreline

regression in the lower Gallup is estimated to be ~15 km, associated with a 26 m fall in relative sea level, during the degradation from Sequences 4 to 3.

The upper Gallup shows more prominent transgressive-regressive cycles of shoreline migration, manifested by the frequent alternation of descending regressive and transgressive shoreline translation (Fig. 3.15). The low-angle descending regressive shoreline trajectories extend distances of 21 - 48 km and are most likely the result of vigorous and rapid forced regressions with a constantly negative A/S ratio (e.g., Parasequence Sets 15, 12-11, and Parasequence 8). They are interpreted to be associated with low-amplitude high-frequency relative sea level falls. Parasequence 15 and Parasequence Sets 12-11 show 18 m and 19 m of relative sea level fall respectively. Parasequence Set 6 records the largest relative sea level fall of 34 m (Table 3.2). Moreover, the long-distance forced regression may result from a high sedimentation rate—related to the proximity to the orogenic belt, in a low accommodation setting. The descending shorelines characterize FSST and mark the onset of new depositional sequences. On the other hand, two significant transgressive shoreline trajectories occurred during Parasequence Sets 14 and 10, recording two major marine incursions, with 51 km and 44 km of shoreline retreat respectively; these two transgressions are associated with 33 m and 38 m rises in relative sea level (Table 3.2).

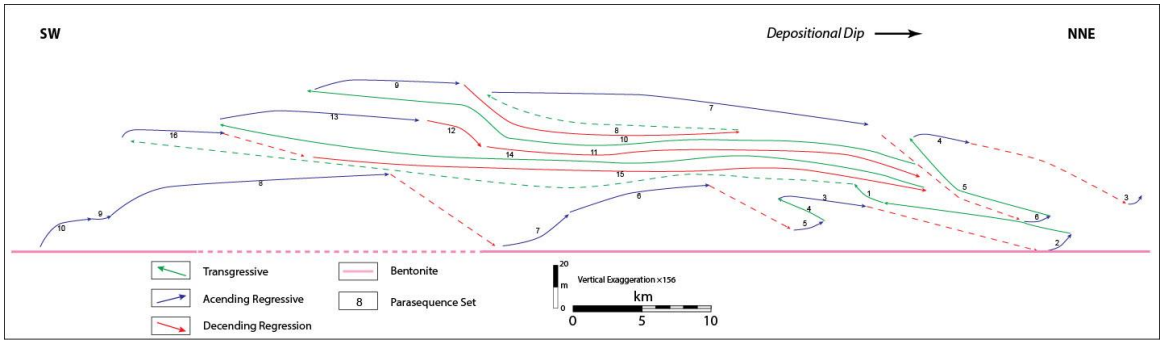

Fig. 3.13.–Shoreline trajectories of the Gallup system. Four classes of trajectory have been identified, consisting of ascending regression with decelerating rate (convex upward), ascending regression with accelerating rate (concave upward), descending regression, and transgression.

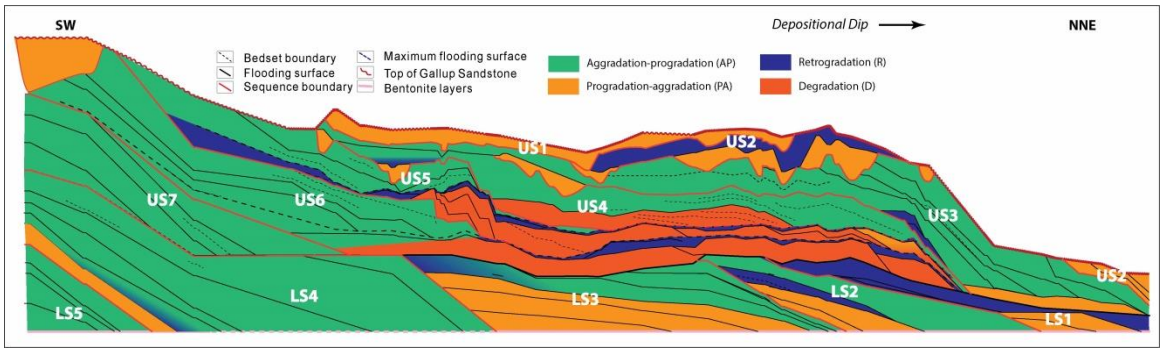

Fig. 3.14.–Cross-section showing accommodation successions of the Gallup system. Progradational–aggradational (PA) stacking of parasequence sets correlate to the conventional LST; retrogradational parasequence sets correlates to TST; aggradational–progradational (AP) stacking represents HST; degradation (D) is characterized by downstepping parasequences and correlates to FSST, associated with subaqueous SB.

We observed four classes of distinct stacking patterns of parasequence sets: progradational–aggradational (PA), aggradational–progradational (AP), retrogradational (R), and degradational (D) (Fig. 3.16). The geometric patterns also correlate to systems tracts, interpreted to be related to specific changes in the interaction of accommodation and sediment supply as also reflected by the shoreline trajectory. The progradational–aggradational (PA) parasequence sets indicate an increasing ratio of accommodation over

sedimentation rate and correlate to the conventional LST of a sequence with an accelerating ascending shoreline regression. The retrogradational (R) parasequence stacking represents a classic TST with shoreline transgression. The aggradational–progradational (AP) stacking pattern implies a decreasing ratio of accommodation over sediment supply and represents a HST with a decelerating shoreline regression. We discern degradation (D) as an individual stacking pattern, indicating negative accommodation due to sea level falls and interpreted as a FSST. Degradational stacking is also associated with sequence boundaries in marine sections—where the SB cannot be characterized by, but correlated to the subaerial unconformity (Plint 1988).

3.6 Discussion

3.6.1 The Basic Stratigraphic Unit and Key Surfaces

The classification of hierarchical components is the key element of sequence stratigraphy. Early researchers, represented by the Exxon group, used a nomenclature consisting of laminae to composite sequence set and numerical orders to describe the hierarchical rock units corresponding to various depositional durations (Mitchum et al. 1991; Neal and Abreu 2009). Parasequences, equivalent to 5^{th} - order sequences, are widely applied as the basic building blocks of sequence stratigraphy (Posamentier et al. 1988; Van Wagoner et al. 1988; Hunt and Tucker 1992; Hampson et al. 2008; Charvin et al. 2010; Miller et al. 2018). More recently, a number of researchers prefer using the term “clinothem” to define an offlapping depositional succession bounded by clinoform surfaces and to represent the basic stratigraphic unit (Rich 1951; Deibert et al. 2002; Plink-Björklund and Steel 2004; Johannessen and Steel 2005; Plint et al. 2009; Romans et al. 2009; Enge et al. 2010;

Burgess and Steel 2017; Miller et al. 2018). Others tend to interpret an upward-coarsening depositional succession as a high-frequency sequence (*sensu* Mitchum et al. 1991; Korus and Fielding 2017).

In the present study, we identify the parasequence as the fundamental component of sequence stratigraphy. By contrast, clinothems would be better defined in a passive continental margin with clearly present topset, foreset, and bottomset geometries (Johannessen and Steel 2005). Another problem of using the term clinothem appears to be their obscurely defined hierarchical scales (i.e., bedset equivalent clinothem versus sequence equivalent clinothem; Enge et al. 2010; Fielding 2015). We argue that a clinothem should be defined as an allogenic-dominated stratigraphic succession of genetically related strata, bounded by clinoforms, in which case, a clinothem equals a parasequence (Plink-björklund 2008; Cavajal and Steel 2012).

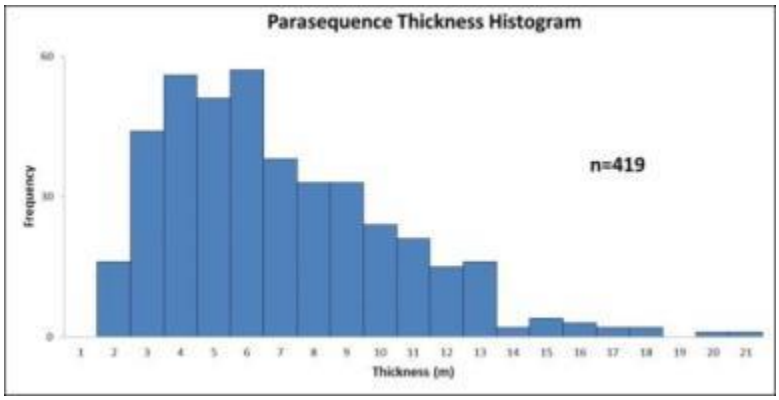

Fig. 3.15.–Histogram showing thicknesses of parasequence frequency distribution of the Gallup sequences. The thicknesses of parasequence vary from 1 to 20m, with an average thickness of 6.2m. Most parasequences are 3-9m thick. Note that thickness of parasequence is determined by accommodation, sediment supply, and position along depositional profile.

The thickness of a parasequence is dependent on accommodation and sediment supply (Ainsworth et al. 2018). The thicknesses of parasequences in the Gallup system vary from 1 to 20 m, with an average of 6.2 m. Most parasequences are about 3 to 9 m thick (Fig. 3.17). The parasequences identified in this study are generically thinner than those defined in previous studies (Van Wagoner et al. 1990; Kamola and Van Wagoner 1995; Pattison 1995; Taylor and Lovell 1995; McLaurin and Steel 2000; Plint et al. 2009; Ainsworth et al. 2017). This may in part reflect the fact that our high-frequency sequence stratigraphic analysis allows identification of more parasequence cycles, especially in the parasequence-amalgamated sections (Plint and Kreitner 2007); the thinner parasequences may also result from post-deposition erosion in the context of an overall regressive ramp setting.

Bhattacharya (1993) defined a hierarchy of flooding surfaces, including minor and major flooding surfaces. He also pointed out that the main difference between these two types of flooding surfaces is areal extent. Van Wagoner et al. (1990) suggested that minor and major flooding surfaces bound parasequences and parasequence sets respectively. In the present study, although we do not distinguish the hierarchy, we concur that the flooding surfaces of parasequences are equivalent to minor flooding surfaces and those of parasequence sets represent major flooding surfaces.

The repeated, asymmetric upward-coarsening successions diagnostic of FS-capped parasequences in shallow marine and distal areas, is often absent in coastal plain sections. In the present study, we use the tops of coal seams overlain by brackish water deposits, as the correlative Transgressive Surfaces (TS), as they indicate marine incursion (Fig.

3.13B). A similar practice was used by Kamola and Van Wagoner (1995) to interpret flooding surfaces in coastal plain successions of the Spring Canyon Member, in the Blackhawk Formation in the Book Cliffs.

Besides flooding surfaces, we also identified several discontinuity surfaces, most likely equivalent to bedset boundaries, that could be also defined as intra-parasequence clinoforms (Charvin et al. 2010). These bounding surfaces may be prominent in some sections but were not extensive enough to be interpreted as a parasequence-bounding FS. A likely confusion between FS and bedset boundaries may result in misinterpretation of the high-frequency cyclicity of deposition. By reviewing the sequence stratigraphic work of the Upper Cretaceous Kenilworth Member, Blackhawk Formation in the Book Cliff done by Pattison (1995) and Taylor and Lovell (1995), Hampson (2000) argued that parasequences may be over-interpreted as a result of misidentifying minor discontinuity surfaces as flooding surfaces. In this Gallup study, after identifying the possible FS candidates in each measured section, we correlate these surfaces away from the initial control points. We only interpret a bounding surface as a FS when we observe lapout terminations at both ends. It is rather more difficult to identify significant surfaces in either sand-prone proximal intervals due to the amalgamation of sandstones (Fig. 3.11), or in distal muddy successions, as the surfaces may have become conformable and may be too subtle to recognize. In this case, a detailed facies analysis is required to discern those surfaces; for example, a slight decrease in grain size or in sand content, or an increase in bioturbation intensity, may indicate changes in deposition, and in turn help to interpret the surfaces.

The subaqueous SB often correlates updip to the erosional bases of channel—subaerial SB, and becomes cryptic and eventually conformable seaward where storm wave erosion is less intense in response to increased water depth. Such correlation between the subaerial and subaqueous unconformities and the correlative conformities was also shown by Korus and Fielding (2017) in the sequence stratigraphic analysis of the Ferron Sandstone in Utah. The proximal part of the subaqueous SB often coalesces with a regressive surface of marine erosion (RSME; Posamentier et al. 1992). RSME, characterized by sharp-based shorefaces and gutter casts, are formed by vigorous storm waves during forced regression (Plint and Nummedal 2000). RSME, the basal surface of FSST, can be a good candidate for a SB. However, as shown at the base of Parasequence 8 of the upper Gallup, the RSME constitutes a series of forced regressive erosional basal surfaces, representing a composite surface (Fig. 3.18).

High-resolution sequence stratigraphic analysis ensures the identification of key surfaces, especially in lithostratigraphic units (Nummedal 1990; Nummedal and Molenaar 1995; Taylor and Lovell 1995). Subtle high-frequency stratigraphic bounding surfaces require detailed facies analysis and correlation for identification. The identification of flooding surfaces expressed by detailed facies analysis of “sand-on-sand” contacts in shoreface successions or “shale-on-shale” contacts in heterolithic intervals and coastal facies sections shows a considerably greater number of high-frequency parasequences and indeed sequences than previously identified. Therefore, the notion that the previously identified sandstone tongues are simple parasequences has been proved to be incorrect. In

this case, many of the previously interpreted sandstone-tongues are now interpreted to be parasequence sets or even full-fledged sequences.

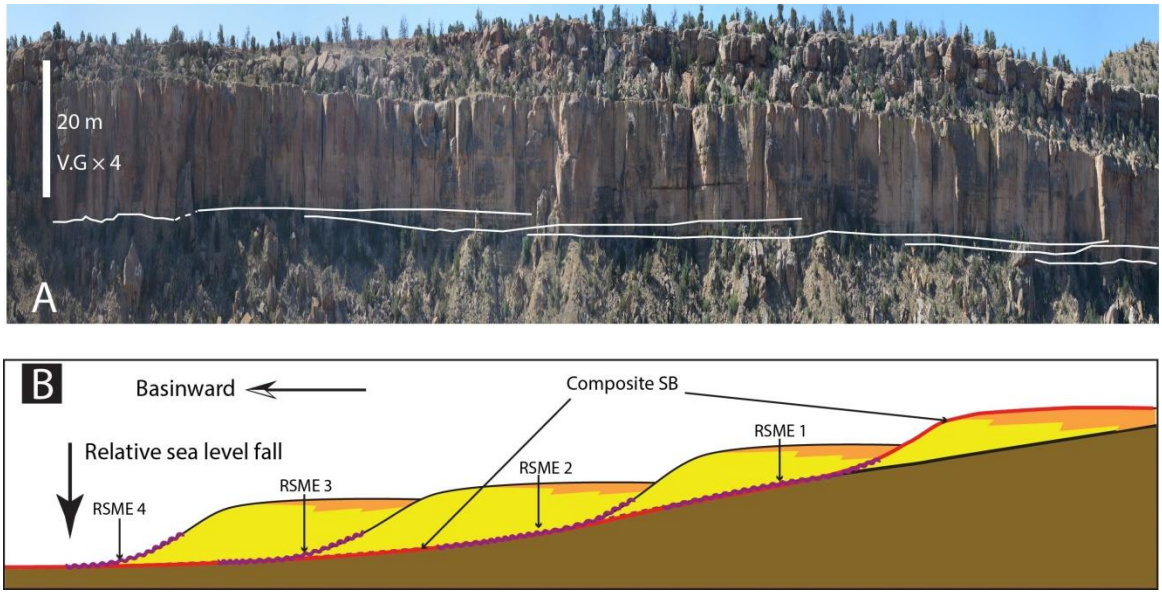

Fig. 3.16.–(A) An outcrop photomosaic showing sharp-based shorefaces and associated RSME. Note that the RSME comprises multiple erosional surfaces dipping seaward and extending locally. The photo is taken at the location of MS 0720b. (B) A sketch model showing a composite SB is constituted of multiple RSMEs during FSST.

3.6.2 The Relation between Lithostratigraphy and Sequence Stratigraphy

The sequence stratigraphic correlation of the Gallup system shows high-frequency stratigraphic cycles (Fig. 3.9), which were not identified using the traditional lithostratigraphy and indicate large diachroneity in the correlation of lithostratigraphic units. Figure 3.19 displays the lithostratigraphic correlation of Nummedal and Molenaar (1995) superimposed on our newly developed sequence stratigraphic cross-section. The earlier correlation shows only two sequence boundaries, including the basal surface of the Torrivio fluvial sandstone (Fig. 3.19). In contrast, we have identified thirteen sequences with twelve associated sequence boundaries. Our correlation suggests that the previously

defined sandstone tongues encompass two depositional sequences on average. This also argues that the practice of defining sandstone tongues as parasequences is inappropriate (Kamola and Van Wagoner 1995; Plink-Björklund 2008).

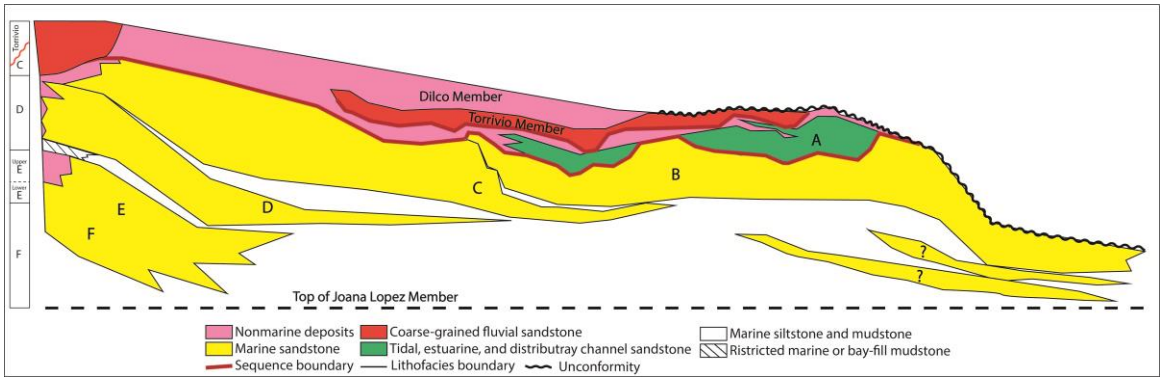

Fig. 3.17.–Cross-section showing the previously defined lithostratigraphy of the Gallup system. The Gallup Sandstone was defined to comprise six marine sandstone tongues (A to F). The Dilco Member represents the nonmarine facies, overlying the Gallup Sandstone. The Torrivio Sandstone Member contains coarse-grained fluvial sandstones and ersosively overlies the Dilco Member and Gallup Sandstone. This cross-section is modified based on the regional cross-section (Fig. 4) of Nummedal and Molenaar (1995). Compared with Figure 3.9, this cross-section illustrates the diachronous correlation of the lithostratigraphic sandstone tongues with little sequence stratigraphic detail.

The sequence stratigraphic relationship between the Gallup Sandstone, the Torrivio Sandstone, and the Dilco Member remains equivocal. Whether the Torrivio Sandstone is the Gallup age equivalent or younger has long been debated (Molenaar 1973; Nummedal and Swift 1987; Nummedal et al. 1989; Jones et al. 1991; Riley 1993; Nummedal and Molenaar 1995). Although the majority of previous work agrees that the basal surface of the Torrivio is erosional and thus represents a sequence boundary, some have argued that the Torrivio Sandstone may be diachronous, wherein the older section was deposited during Gallup time and fed more distal Gallup shorefaces. Our correlation shows that the

Torrivio coarse-grained fluvial deposits appear to be synchronous and younger than the Gallup deposits in the Ship Rock area (Fig. 3.20). The Torrivio erosionally overlies the coastal plain succession of the Dilco Member, bounded by the SB at the base (Fig. 3.9). In the most updip area (Window Rock and Rock Nose point), the Torrivio fluvial channels incise into Gallup shoreface deposits. One interpretation would be that this Torrivio Sandstone is the same age as the other Torrivio fluvial succession—younger than the Gallup; alternatively, the Torrivio fluvial at the most proximal area may be "Gallup" age and fed the FSST (Parasequence Sets 12 and 11) of Sequence 5, in which case the Torrivio Member would be diachronous (Fig. 3.20). It may be possible to use provenance analysis, such as Detrital Zircons, to resolve this equivocality.

The Dilco Member is unequivocally diachronous (Figs. 3.9; 3.20). The coastal facies are allocated into different parasequence sets (e.g., Parasequence Sets 7, 4, and 2), deposited at different times, and separated by flooding surfaces or transgressive surfaces. Therefore, the Dilco Member represents a lithostratigraphic facies unit that genetically correlates to different Gallup marine sandstones in multiple depositional cycles (Fig. 3.20). As a consequence, the age of the Dilco Member should be equivalent to Gallup time; it is older than and truncated by the Torrivio Member at least around the study area.

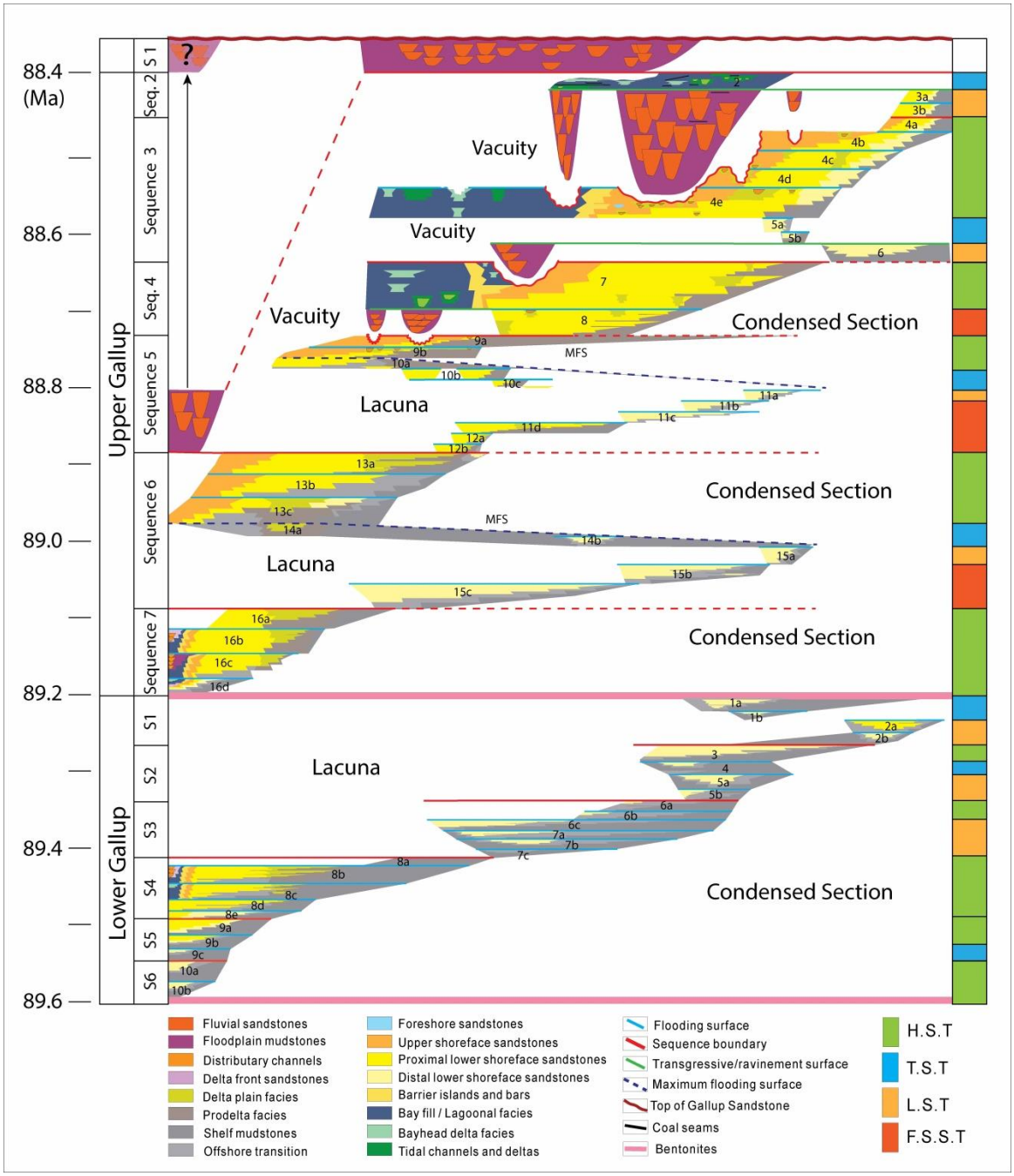

Fig. 3.18.–Wheeler diagram of the Gallup system showing chronostratigraphic relationships among all identified parasequences. The geological time on the left was estimated from biostratigraphic and radiometric analyses (Cobban 1951; Obradovich 1993). Colored bar on the right indicating systems tracts estimated on the basis of geometric stacking patterns.

3.6.3 Controlling Mechanisms of High-Frequency Sequence Stratigraphy

The number of parasequence identified in the Gallup system explicitly demonstrates the high-frequency sequence stratigraphy (Fig. 3.9; Table 3.2). Such high-frequency stratal cyclicity may be either allogenic- or autogenic- controlled, and the various controlling factors may have operated simultaneously (Heller *et al.* 1993; Gardner, 1995; Sageman et al. 1997; Muto and Steel, 2002; Holbrook et al. 2006). Although sub-million-year tectonic pulses have been documented to occur in the Cretaceous Western Interior of the North America (Vakarelov et al. 2006), the frequency of these sequences appears to be at a half-million-year scale, which is too slow to account for the cyclicity identified in the Gallup system—given the number of depositional cycles (12 sequences) in the depositional duration (1.2 Ma).

However, we have observed some tectonic signature based on detailed geometric analysis: angular discordance between the Gallup Formation and the Tocito Sandstone is interpreted as a tectonically-driven regional unconformity, manifested by an angular unconformity around the top of Parasequence Sets 4 and 3 (Fig. 3.9). Using the flattened "Upper Bentonite" as the datum, the correlation shows a local angular unconformity below the "Upper Bentonite," implying tectonic influence (Fig. 3.21). The correlation also shows an undulating topography of the "Lower Bentonite." Jennette et al. (1991) showed a similar tectonic feature, which may be explained by the flexural subsidence of the foreland basin (Pang and Nummedal 1995), or by tectonic uplift along a peripheral bulge (Flemings and Jordan 1990; Fielding 2011; Fig. 3.21). Moreover, an overall 109 m cumulative relative sea level rise (Table 3.2) most likely reflects a combination of

compactional and longer-term tectonic subsidence, however, the higher-frequency of variations of relative sea level significantly exceeds the tectonic foreland-basin processes. High-frequency tectonism may be important at the composite sequence scale, but is unlikely to have formed all 12 sequences.

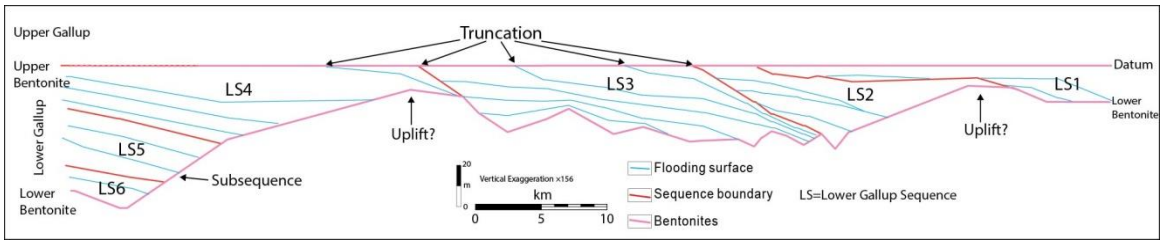

Fig. 3.19.–Stratigraphic correlation of the lower Gallup using the "Upper Bentonite" as the top datum. The topography of the "Lower Bentonite" may imply tectonic influence to sequence stratigraphic evolution.

Although autogenic processes have been proven to be able to regulate depositional and stratigraphic records and to mask allogenic sequence stratigraphic architectures (Jerolmack and Paola 2010; Mikes et al. 2015; Trampush et al. 2016; Li et al. 2016; Hajek and Straub 2017), the autogenic influence in the formation of the high-frequency sequence stratigraphy of the Gallup system seems limited. In shallow marine and deltaic environments, autoretreat, autostepping, and deltaic compensation are the major autogenic processes that can affect shoreline trajectories (Muto and Steel 1992, 2001; Trampush et al. 2016). Although some may have operated simultaneously with external forcing, lack of clear evidence hampers interpreting such autogenic processes as the predominant controlling factors. The geometries of the shoreline trajectories of the Gallup (Fig. 3.15) do not match the convex basinward migration curve of autoretreat described by Muto and Steel (1992); the shoreline retreats observed show low-angle non-

accretionary trajectories, instead of thick retrogradational succession resulting from long-term slow autoretreat process. In addition, the shoreline retreats in the present study typically take place after forced regression—differentiated from the "precursory regression" before autoretreat (Muto and Steel 1997), and therefore, most likely represent true marine transgressions. In the absence of outcrops along depositional strike, we are unable to identify delta compensation cycles in the Gallup deposits. However, a special class of delta—the "storm-flood-dominated delta", characterized by strong storm signature in conjunction with river influence, may show evidence of delta lobe switching.

Eustasy plays a critical role in sequence stratigraphy by determining the rate and sense of accommodation change (Posamentier et al. 1988; Mitchum and Van Wagoner 1991; Plint and Kreitner 2007). Although tectonic and autogenic controls may be invoked to discredit eustatic control, the change in eustatic sea level position still dominates high-frequency variations in base level and accommodation (Blum and Tornqvist 2000; Gale et al. 2002; Muto and Steel 2002; Haq 2014; Hampson 2016; Vakarelov et al. 2006; Hajek and Straub 2017). In the entire Gallup time, we have documented three major shoreline transgressions, including the one along the boundary between the lower and upper Gallup, with distances of 44 km, 51 km, and 60 km respectively (Table 3.2; Fig. 3.15). Such high-frequency, rapid, and large magnitude transgressions are likely eustatically controlled. The relatively thin transgressive parasequences also suggest a eustatic origin, based on the model discussed by Jones et al. (2018a). The sandstones-shale intertonguing represents high-frequency depositional environmental shifts, which may indicate small-scale regressive-transgressive cycles of global eustatic sea level proposed by Haq (2014),

in which case, the regional ravinement surface draped by the "Upper Bentonite" may indicate a regional marine transgression that coincides with a eustatic sea level rise during the early Coniacian age (Haq 2014; Jones et al. 2018b). The estimated maximum relative sea level changes are -38 m and 34 m respectively—the matching magnitudes of relative sea level fall and rise are more compatible with eustatic cycles. Tectonic movements typically do not have the matching magnitudes of uplift and subsidence, especially at the frequencies observed here.

Three FSSTs are identified in the upper Gallup (Parasequence Sets 15, 12-11, and Parasequence 8; Table 3.2), comprising long-distance (up to 48 km; Table 3.2) progradational to degradational parasequences with extremely low-angle trajectories (Fig. 3.9 and 3.15). The associated relative sea level falls are estimated to be 18 m, 19 m, and 13 m (Table 3.2). The FSST of Sequence 4 (Parasequence 8) appears to link to the incised channels updip. The forced regressions that are associated with a few tens of meters base level falls and linked to channel incision are most likely controlled by eustasy. In addition, the shorelines of the sequence sets in the lower Gallup (particular Sequences 4 to 1) advanced more than 50 km horizontally but show minimum vertical stratigraphic dislocation—this progradational-degradational stacking of the sequence sets implies a eustatic control with little, if any, evidence of vertical tectonism, such as stationarily stacked strata and angular unconformities (Fig. 3.9).

A correlation using the "Upper Bentonite" as the datum shows similar sequence stratigraphic geometries and shoreline trajectory (Fig. 3.21) to the "Lower Bentonite"-based correlation (Fig. 3.9), especially in the distal part (the Toadlena to Shiprock area).

The relative sea level estimates based on the "Upper Bentonite"-based correlation suggest that the maximum sea level fall and rise are -37 m and 34 m respectively. These estimates are close to the estimates described above and also indicate eustatic sea level fluctuations.

Ice sheet growth can gradually lock sea water to result in sea level fall with stepped forced regression downdip and fluvial incision updip (Bhattacharya 2011). Miller et al. (2005) argued that the Cretaceous time was never ice free and the growth and decay of small- to medium-sized ephemeral Antarctic ice sheets account for about 15-30 m sea level change. Climate-induced changes in ocean temperature and groundwater storage can also change sea level position up to 15 m (Jacobs and Sahagian 1993; Miller et al. 2005). The magnitudes of sea level fall and rise that we document in the Gallup system match reasonably well to the magnitudes of eustatic-dominated sea level changes hypothesized for the Late Cretaceous (Jacobs and Sahagian 1993; Miller et al. 2005). We conclude that the high-frequency sequence stratigraphic nature of the Gallup system is entirely consistent with a glacio-eustatic origin. Such controlling mechanisms in the Cretaceous greenhouse age have been interpreted in other deltaic systems in the Western Interior Seaway (Plint and Kreitner 2007; Gale et al. 2008; Zhu et al. 2012; Horner et al. 2018) and elsewhere (Chen et al. 2015). Frakes (1979) also inferred that extensive polar land areas were snow-covered in the winter during at least parts of the Mesozoic.

Milankovitch-cycle-driven climate changes may dominate such glacio-eustatic controls (Glancy et al. 1993; Sageman et al. 1997; Gale et al. 2008; Zhu et al. 2012; Chen et al. 2015). Although the estimated depositional duration (~1.2 Ma) may be refined by high-resolution bentonite dating (Zhu et al. 2012), we would tend to assume it is within

the error range of presently available dates. Within the 1.2 Ma, we identified twelve sequences, twenty-six parasequence sets, and sixty-one parasequences: the average depositional duration of a sequence, parasequence set, and parasequence is about 100 kyr, 46.2 kyr, and 19.7 kyr, respectively. These estimated depositional time scales appear to be concurrent with the eccentricity (100 kyr), obliquity (41 kyr), and precession (19 kyr or 23 kyr) cycles defined by Milankovitch, implying that the high-frequency sequence stratigraphy of the Gallup system is most likely dominated by high-frequency astronomically forced glacio-eustasy. Our interpretation, therefore, supports glacio-eustasy as the ubiquitous control of the sequence stratigraphic evolution in Cretaceous sequences (Sageman et al. 1997; Gale et al. 2008; Locklair and Sageman 2008; Zhu et al. 2012; Chen et al. 2015). We would certainly map out more parasequences in the southern area (between Toadlena and Window Rock) if data permitted. However, the total number of the identified stratigraphic unit would probably not change significantly, and the estimated depositional durations would remain in the range of Milankovitch cycles.

3.7 Conclusions

High-resolution sequence stratigraphy is applied for the first time to the Late Cretaceous Gallup system in northwestern New Mexico. With detailed depositional facies analysis, using bentonite layers as the most favorable chronostratigraphic datums, this study has established a high-frequency sequence stratigraphic framework with fundamental sequence stratigraphic units and bounding surfaces.

Five depositional sequences, comprising ten parasequence sets and twenty-four parasequences are identified in the lower Gallup; seven sequences, consisting of sixteen

parasequence sets and thirty-seven parasequences, constitute the upper Gallup. FSST, LST, TST, and HST are recognized. The FSST is separated as an independent systems tract to represent specific deposition during relative sea level fall. Systems tracts of ramp margin settings can be explicitly linked to systematic stacking patterns of parasequences, independent of relative sea level position to a shelf margin, as originally defined.

Quantified shoreline trajectory and accommodation successions, associated with chronostratigraphic analysis, help to elucidate the sequence stratigraphic evolution, to decipher the relationship between lithostratigraphy and sequence stratigraphy, and to evaluate the dominant controls of the high-frequency stratal cyclicity. The shoreline trajectory of the Gallup system shows maximum relative sea level fall and rise are -34 m and 38 m respectively. The matching values suggest a eustatic origin.

The study successfully deciphers the relationship between the previously defined lithostratigraphic units and sequence stratigraphy, showing large time translation of the lithostratigraphic correlation. The traditionally mapped lithostratigraphic sandstone tongues are interpreted as high-frequency sequence sets rather than conventional parasequences.

Greenhouse glacio-eustatic variation most likely controls the high-frequency sequence stratigraphic cycles of the Gallup system. The estimated depositional durations of individual parasequence, parasequence set, and sequence coincide with the eccentricity, obliquity, and precession cycles of Milankovitch bands. Tectonics may control development of composite sequence of the Gallup.

Acknowledgements

Funding for this project was generously supplied by NSERC Discovery Grant RPG IN05780-14 to Dr. Bhattacharya, by sponsors of the McMaster University Quantitative Sedimentology Laboratories (QSL) including BP and Inpex, and by the Susan Cunningham Research Chair in Geology. We also appreciate the AAPG "Martin D. Hewitt" Named Grant and GSA Research Grants for their support. Thanks are given to Monica Wiercigroch and Sean Karner for their tremendous assistance in the field. We are grateful to reviewers Prof. Guy Plint, Dr. Jack Neal, and the Associated Editor Prof. Ernesto Schwarz for thoughtful and constructive comments and suggestions that greatly improved the manuscript.

We also would like to thank the Navajo Nation for permitting the field work and the Navajo people for allowing us to work on their lands. Field work on the Navajo Nation was conducted under a permit from the Navajo Nation Minerals Department. Any persons wishing to conduct geologic investigations on the Navajo Nation must first apply for, and receive, a permit from the Navajo Nation Minerals Department, P.O. Box 1910, Window Rock, Arizona 86515, and telephone number (928) 871-6587.

References

Ainsworth, R.B., Vakarelov, B.K., MacEachern, J.A., Rarity, F., Lane, T.I., and Nanson, R.A., 2017, Anatomy of a shoreline regression: implications for the high-resolution stratigraphic architecture of deltas: Journal of Sedimentary Research, v. 87, p. 425–459.

Ainsworth, R.B., McArthur, J.B., Lang, S.C., and Vonk, A.J., 2018, Quantitative sequence stratigraphy: AAPG Bulletin, v. 102, p. 1913–1939.

Bhattacharya, J.P., 1993, The expression and interpretation of marine flooding surfaces and erosional surfaces in core; examples from the Upper Cretaceous Dunvegan Formation in the Alberta foreland basin, in Posamentier, H.W., Summerhayes, C.P., Haq, B.U., and Allen, G.P., eds., Sequence Stratigraphy and Facies Associations: IAS, Special Publication 18, p. 125–160.

Bhattacharya, J.P., 2010, Deltas, in James, N.P., and Dalrymple, R.W., eds., Facies Models 4: Geological Association of Canada, p. 233–264.

Bhattacharya, J.P., 2011, Practical problems in the application of the sequence stratigraphic method and key surfaces: integrating observations from ancient fluvial-deltaic wedges with Quaternary and modelling studies: Sedimentology, v. 58, p. 120–169.

Bhattacharya, J.P., Copeland, P., Lawton, T.F., and Holbrook, J., 2016, Estimation of source area, river paleo-discharge, paleoslope, and sediment budgets of linked deep-time depositional systems and implications for hydrocarbon potential: Earth-Science Reviews, v. 153, p. 77–110.

Blum, M.D., and Aslan, A., 2006, Signatures of climate vs. sea-level change within incised valley-fill successions: Quaternary examples from the Texas gulf coast: Sedimentary Geology, v. 190, p. 177–211.

Blum, M.D, and Tornqvist, T.E., 2000, Fluvial responses to climate and sea-level change: a review and look forward: Sedimentology, v. 47, p. 2–48.

Boyd, R., 2010, Transgressive wave-dominated coasts, in James, N.P., and Dalrymple, R.W., eds., Facies Models 4: Geological Association of Canada, p. 265–294.

Boyd, R., Dalrymple, R.W., and Zaitlin, B.A., 1992, Classification of clastic coastal depositional environments: Sedimentary Geology, v. 80, p. 139–150.

Burgess, P.M., and Steel, R.J., 2017, How to interpret, understand, and predict stratal geometries using stratal-control spaces and stratal-control-space trajectories: Journal of Sedimentary Research, v. 87, p. 325–337.

Campbell, C.V., 1971, Depositional model; upper Cretaceous Gallup beach shoreline, Ship Rock area, northwestern New Mexico: Journal of Sedimentary Research, v. 41, p. 395–409.

Campbell, C.V., 1973, Offshore equivalents of Upper Cretaceous Gallup beach sandstones, northwestern New Mexico, in Fassett, J.E., eds., Cretaceous and Tertiary Rocks of the Southern Colorado Plateau: Four Corners Geological Society, p. 78–84.

Campbell, C.V., 1979, Model for beach shoreline in Gallup Sandstone (Upper Cretaceous) of northwestern New Mexico: New Mexico Bureau of Mines & Mineral Resources, Circular 164, p. 1–32.

Carvajal, C., and Steel, R., 2012, Source-to-sink sediment volumes within a tectono-stratigraphic model for a Laramide shelf-to-deep-water basin: methods and results, in Busby, C., and Azor, A., eds., Tectonics of Sedimentary Basins: Recent Advances: Chicester, Blackwell Publishing, p. 131–151.

Charvin, K., Hampson, G.J., Gallagher, K.L., and Labourdette, R., 2010, Intra-parasequence architecture of an interpreted asymmetrical wave-dominated delta: Sedimentology, v. 57, p. 760–785.

Chen, X., Wang, C., Wu, H., Kuhnt, W., Jia, J., Holbourn, A., Zhang, L., and Ma, C., 2015, Orbitally forced sea-level changes in the Upper Turonian-Lower Coniacian of the Tethyan Himalaya, Southern Tibet: Cretaceous Research, v. 56. p. 691–701.

Cobban, W.A., 1951, Scaphitoid cephalopods of the Colorado group: US Government Printing Office, Geological Survey Professional Paper 239, p. 1–42.

Cobban, W.A, Walaszczyk, I., Obradovich, J.D., and McKinney, K.C., 2006, A USGS zonal table for the Upper Cretaceous Middle Cenomanian−Maastrichtian of the Western Interior of the United States based on ammonites, inoceramids, and radiometric ages: U. S. Geological Survey, Open-File Report, v. 1240, p.1–50.

Deibert, J.E., Benda, T., Løseth, T., Schellpeper, M., and Steel, R.J., 2003. Eocene clinoform growth in front of a storm-wave-dominated shelf, Central Basin, Spitsbergen: no significant sand delivery to deepwater areas: Journal of Sedimentary Research, v. 73, p. 546–558.

Dubiel, R.F., 2013, Geology, sequence stratigraphy, and oil and gas assessment of the Lewis Shale Total Petroleum System, San Juan Basin, New Mexico and Colorado: Chapter 5, Total petroleum systems and geologic assessment of undiscovered oil and gas resources in the San Juan Basin province, exclusive of Paleozoic rocks, New Mexico and Colorado: U.S. Geological Survey, Digital Data Series 69–F, p.1–45.

Enge, H.D., Howell, J.A., and Buckley, S.J., 2010, Quantifying clinothem geometry in a forced-regressive river- dominated delta, Panther Tongue Member, Utah, USA: Sedimentology v. 57, p. 1750–1770.

Fassett, J.E., 2013, The San Juan Basin, a complex giant gas field, New Mexico and Colorado: AAPG Rocky Mountain Section, 58th Annual Rocky Mountain Rendezvous, Durango, Colorado and AAPG Rocky Mountain Section Meeting, Salt Lake City, Utah, September 22-24, 2013.

Fielding, C.R., 2011, Foreland basin structural growth recorded in the Turonian Ferron Sandstone of the Western Interior Seaway Basin, U.S.A.: Geology, v. 39, p. 1107–1110.

Fielding, C.R., 2015, Anatomy of falling-stage deltas in the Turonian Ferron Sandstone of the western Henry Mountains Syncline, Utah: growth faults, slope failures, and mass transport complexes: Sedimentology, v. 62, p. 1–26.

Fielding, C.R., Ashworth, P.J., Best, J.L., Prokocki, E.W., and Smith, G.H.S., 2012, Tributary, distributary and other fluvial patterns: what really represents the norm in the continental rock record: Sedimentary Geology, v. 261, p. 15–32.

Flemings, P.B., and Jordan, T.E., 1990, Stratigraphic modeling of foreland basins: interpreting thrust deformation and lithosphere rheology: Geology, v. 18, p. 430–434.

Gale, A.S., Hardenbol, J., Hathaway, B., Kennedy, W.J., Young, J.R., and Phansalkar, V., 2002, Global correlation of Cenomanian (Upper Cretaceous) sequences: Evidence for Milankovitch control on sea level: Geology, v. 30, p. 291–294.

Gale, A.S., Voigt, S., Sageman, B.B., and Kennedy, W.J., 2008, Eustatic sea-level record for the Cenomanian (Late Cretaceous)-extension to the Western Interior Basin, USA: Geology, v. 36, p. 859–862.

Gardner, M.H., 1995, Tectonic and eustatic controls on the stratal architecture of Mid-Cretaceous stratigraphic sequences, central Western Interior Foreland Basin of North America, in Dorobek, S.L., and Ross, G.M., eds., Stratigraphic Evolution of Foreland Basins: SEPM, Special Publication 52, p. 243–281.

Garrison, J.R., and van den Bergh, T.C.V., 2004, High-resolution depositional chance delta: an application of upper Ferron Sandstone last sequence stratigraphy of the coal-zone stratigraphy, in Chidsey, T.C., Adams, R.D., and Morris, T.H., eds., Regional to Wellbore Analog For Fluvial-Deltaic Reservoir Modeling: The Ferron Sandstone of Utah: AAPG, Studies in Geology 50, p. 125–192.

Glancy, T.J., Arthur, M.A., Barron, E.J., and Kauffman, E.G., 1993, A paleoclimate model for the North American Cretaceous (Cenomanian-Turonian) epicontinental Sea, in Caldwell, W.G.E., and Kauffman, E.G., eds., Evolution of the Western Interior Basin: Geological Association of Canada, Special Paper 39, p. 219–241.

Hajek, E.A., and Straub, K.M., 2017, Autogenic sedimentation in clastic stratigraphy: Annual Review of Earth and Planetary Sciences, v. 45, p. 681-709.

Hampson, G.J., 2000, Discontinuity surfaces, clinoforms, and facies architecture in a wave-dominated, shoreface-shelf parasequence: Journal of Sedimentary Research, v. 70, p. 325–340.

Hampson, G.J., 2016, Towards a sequence stratigraphic solution set for autogenic processes and allogenic controls : Upper Cretaceous strata: Journal of the Geological Society, v. 173, p. 817–836.

Hampson, G.J., and Storms, J.E.A., 2003, Geomorphological and sequence stratigraphic variability in wave-dominated, shoreface-shelf parasequences: Sedimentology, v. 50 p. 667–701.

Hampson, G.J., Burgess, P.M. and Howell, J.A., 2001, Shoreface tongue geometry constrains history of relative sea-level fall: examples from Late Cretaceous strata in the Book Cliffs area, Utah: Terra Nova, v. 13 p. 188–196.

Hampson, G.J., Rodriguez, A.B., Storms, J.E.A., Johnson, H.D., and Meyer, C.T., 2008, Geomorphology and high-resolution stratigraphy of progradational wave-dominated shoreline deposits : impact on reservoir-scale facies architecture, in Hampson, G.J., Steel, R.J., Burgess, P.M., and Dalrymple, R.W., eds., Recent Advances in Models of Siliciclastic Shallow Marine Stratigraphy: SEPM, Special Publication 90, p. 117–142.

Haq, B.U., 2014, Cretaceous eustasy revisited: Global and Planetary Change, v. 113. P. 44–58.

Hay, W.W., and Floegel, S., 2012, New thoughts about the Cretaceous climate and oceans: Earth-Science Reviews, v. 115, p. 262–272.

Helland-Hansen, W., and Gjelberg, 1994, Conceptual basis and variability in sequence stratigraphy: a different perspective: Sedimentary Geology, v. 92, p. 31–52.

Helland-Hansen, W., and Hampson, G.J., 2009, Trajectory analysis: concepts and applications: Basin Research, v. 21, p. 454–483.

Helland-Hansen, W., and Martinsen, O.J., 1996, Shoreline trajectories and sequences; description of variable depositional-dip scenarios: Journal of Sedimentary Research, v. 66, p. 670-688.

Heller, P.L., Beekman, F., Angevine, C.L., and Cloetingh, S.A., 1993, Cause of tectonic reactivation and subtle uplifts in the Rocky Mountain region and its effect on the stratigraphic record: Geology, v.21, p. 1003–1006.

Holbrook, J., Scott, R.W., and Oboh-Ikuenobe, F.E., 2006, Base-level buffers and buttresses: a model for upstream versus downstream control on fluvial geometry and architecture within sequences: Journal of Sedimentary Research, v. 76, p. 162–174.

Holbrook, J.M., and Bhattacharya, J.P., 2012, Reappraisal of the sequence boundary in time and space: case and considerations for an SU (subaerial unconformity) that is not a sediment bypass surface, a time barrier, or an unconformity: Earth-Science Reviews, v. 113, p. 271–302.

Hunt, D. and Tucker, M.E., 1992, Stranded parasequences and the forced regressive wedge systems tract: deposition during base-level'fall: Sedimentary Geology, v. 81, p. 1–9.

Hutsky, A.J., and Fielding, C.R., 2016, The offshore bar revisited: a new depositional model for isolated shallow marine sandstones in the Cretaceous Frontier Formation

of the Northern Uinta Basin, Utah, U.S.A.: Journal of Sedimentary Research, v. 86, p. 38–58.

Jacobs, D.K., and Sahagian, D.L., 1993, Climate induced fluctuations in sea level during nonglacial times: Nature, v. 361, p. 710–712.

Jennette, D.C., and Jones, C.R., 1995, Sequence stratigraphy of the Upper Cretaceous Tocito Sandstone : a model for tidally influenced incised valleys, San Juan Basin, New Mexico, in Van Wagoner, J.C., and Bertram, G.T., eds., Sequences Stratigraphy of Foreland Basin Deposits: AAPG, Memoir 64, p. 311–347.

Jennette, D.C., Jones, C.R., Van Wagoner, J.C. and Larsen, J.E., 1991, High-resolution sequence stratigraphy of the Upper Cretaceous Tocito Sandstone: the relationship between incised valleys and hydrocarbon accumulation, San Juan Basin, New Mexico, in Van Wagoner, J.C., Jones, C.R., Taylor, D.R., Nummedal, D., Jennette, D.C., and Riley, G.W., eds., Sequence Stratigraphy Applications to Shelf Sandstone Reservoirs: Outcrop to Subsurface Examples: AAPG, Special Volumes 25, p. 24–62.

Jerolmack, D.J., and Paola, C., 2010, Shredding of environmental signals by sediment transport: Geophysical Research Letters, v. 37, p. 1–5.

Jervey, M.T., 1988, Quantitative geological modeling of siliciclastic rock sequences and their seismic expression, in Wilgus, C.K., Hastings, B.S., Posamentier, H., Van Wagoner, J., Ross, C.A., and Kendall, C.G.St.C., eds., Sea-Level Changes: An Integrated Approach: SEPM, Special Publications, 42, 47–69.

Johannessen, E.P., and Steel, R.J., 2005, Shelf-margin clinoforms and prediction of deepwater sands: Basin Research, v. 17, p. 521–550.

Jones, C.R., Van Wagoner, J.C., Jennette, D.C., Nummedal, D., and Riley, G.W., 1991, San Juan Basin segment, New Mexico, in Van Wagoner, J.C., Nummedal, D., Jones, C.R., Taylor, D.R., Jennette, D.C., and Riley, G.W., eds., Sequence Stratigraphy Applications to Shelf Sandstone Reservoirs-Outcrop to Subsurface Examples: AAPG Field Conference, Sept. 21–28, 1991 (not consecutively paginated).

Jones, M.T., Dashtgard, S.E., and MacEachern, J.A., 2018a, A conceptual model for the preservation of thick, transgressive shoreline successions: examples from the Forearc Nanaimo Basin, British Columbia, Canada: Journal of Sedimentary Research, v. 88, p. 811–826.

Jones, M.M., Sageman, B.B., and Meyers, S.R., 2018b, Turonian sea level and paleoclimatic events in astronomically tuned records from the tropical North Atlantic and Western Interior Seaway: Paleoceanography and Paleoclimatology, v. 33, p. 470–492.

Kamola, D.L., and Van Wagoner, J.C., 1995, Stratigraphy and facies architecture of parasequences with examples from the Spring Canyon Member, Blackhawk Formation, Utah, in Van Wagoner, J.C., and Bertram, G.T., eds., Sequences Stratigraphy of Foreland Basin Deposits: AAPG, Memoir 64, p. 27–54.

Kauffman, E.G., and Caldwell, W.G.E., 1993, The Western Interior Basin in space and time, in Caldwell W.G.E, and Kauffman, E.G., eds., Evolution of the Western Interior Basin: Geological Association of Canada, Special Paper 39, p. 1–30.

Korus, J.T., and Fielding, C.R., 2017, Hierarchical architecture of sequences and bounding surfaces in a depositional-dip transect of the fluvio-deltaic Ferron Sandstone (Turonian), southeastern Utah, USA: Journal of Sedimentary Research, v. 87, p. 897–920.

Li, Q., Yu, L., and Straub, K.M., 2016, Storage thresholds for relative sea-level signals in the stratigraphic record: Geology, v. 44, p. 179–82.

Li, W., Bhattacharya, J.P., and Zhu, Y., 2012, Stratigraphic uncertainty in sparse versus rich data sets in a fluvial-deltaic outcrop analog: Ferron Notom delta in the Henry Mountains region, southern Utah: AAPG Bulletin, v. 96, p. 415–438.

Li, Y., Bhattacharya, J.P., Ahmed, S., and Garza, D., 2018, Re-evaluating the paleogeography of the river-dominated and wave-influenced Ferron Notom Delta, southern central Utah: an integration of detailed facies-architecture and paleocurrent analysis: Journal of Sedimentary Research, v. 88, p. 214-240.

Lin, W., and Bhattacharya, J.P., 2017, Estimation of source-to-sink mass balance by a fulcrum approach using channel paleohydrologic parameters of the Cetaceous Dunvegan Formation, Canada: Journal of Sedimentary Research, v. 87, p. 97–116.

Lin, W., and Bhattacharya, J.P., 2018, Depositional facies and high-resolution sequence stratigraphic analysis of a mixed-process influenced deltaic system in a stormy ramp setting: the Cretaceous Gallup System, New Mexico, U.S.A.: AAPG Annual Convention and Exhibition, Salt Lake City, US.

Liu, S., and Nummedal, D., 2004, Late Cretaceous subsidence in Wyoming: quantifying the dynamic component: Geology, v. 325, p. 397–400.

Locklair, R.E., and Sageman, B.B., 2008, Cyclostratigraphy of the Upper Cretaceous Niobrara Formation, Western Interior, U.S.A.: a Coniacian–Santonian orbital timescale: Earth and Planetary Science Letters, v. 69, p. 540–553.

MacEachern, J.A., Raychaudhuri, I., and Pemberton, S.G., 1992, Stratigraphic applications of the Glossifungites ichnofacies: delineating discontinuities in the rock record, in Pemberton, G.S., eds., Applications of Ichnology to Petroleum Exploration: A Core Workshop: SEMP, Core Workshop 17, p. 169–198.

MacEachern, J.A., Zaitlin, B.A., and Pemberton, S.G., 1998, High-resolution sequence stratigraphy of early transgressive deposits, Viking Formation, Joffre Field, Alberta, Canada: AAPG Bulletin, v. 82, p. 729–756.

MacEachern, J.A., Pemberton, S.G., Gingras, M.K., and Bann, K.L., 2010, Ichnology and Facies Models, in James, N.P., and Dalrymple, R.W., eds., Facies Models 4: Geological Association of Canada, p. 19–58.

Martin, J., Paola, C., Abreu, V., Neal, J., and Sheets, B., 2009, Sequence stratigraphy of experimental strata under known conditions of differential subsidence and variable base level: AAPG Bulletin, v. 93, p. 503–533.

McCubbin, D.G., 1982, Barrier island and strandplain facies, in Scholle, P.A., and Spearing, D., eds., Sandstone Depositional Environments: AAPG, Memoir 31, p. 247–280.

McLaurin, B.T., and Steel, R.J., 2000, Fourth-order nonmarine to marine sequences, middle Castlegate Formation, Book Cliffs, Utah: Geology, v. 28, p. 359–362.

Miall, A.D., Sophisticated stratigraphy, in Bickford, M.E., eds., The Web of Geological Sciences: Advances, Impacts and Interactions: Geological Society of America, Special Paper 500, p. 169–190.

Mikeš, D., ten Veen, J.H., Postma, G., and Steel, R., 2015, Inferring autogenically induced depositional discontinuities from observations on experimental deltaic shoreline trajectories: Terra Nova, v. 27, p. 442–448.

Miller, K.G., Kominz, M.A., Browning, J.V., Wright, J.D., Mountain, G.S., Katz, M.E., Sugarman, P.J., Cramer, B.S., Christie-Blick, N., and Pekar, S.F., 2005, The Phanerozoic record of global sea-level change: Science, v. 310, p. 1293–1298.

Miller, K.G., Lombardi, C.J., Browning, J.V., Schmelz, W.J., Gallegos, G., Mountain, G.S. and Baldwin, K.E., 2018, Back to basics of sequence stratigraphy: early Miocene and mid-Cretaceous examples from the New Jersey paleoshelf: Journal of Sedimentary Research, v. 88, p. 148–176.

Mitchum, R.M., and Van Wagoner, J.C., 1991, High-frequency sequences and their stacking patterns : sequence-stratigraphic evidence of high-frequency eustatic cycles: Sedimentary Geology, v. 70, p. 131–160.

Mitchum, R.M, Vail, P.R, and Thompson III, S., 1977, Seismic stratigraphy and global changes of sea level, part 2 : the depositional sequence as a basic unit for stratigraphic analysis, Section 2: Application of seismic reflection configuration to stratigraphic interpretation, in Payton, C.E., eds., Seismic Stratigraphy: Applications to Hydrocarbon Exploration: AAPG Memoir 26, p. 53–62.

Molenaar, C.M., 1973, Sedimentary facies and correlation of the Gallup Sandstone and associated formations, northwestern New Mexico, in Fassett, J.E., eds., Cretaceous and Tertiary Rocks of the Southern Colorado Plateau: Four Corners Geological Society, p. 85–110.

Molenaar, C.M., 1974, Correlation of the Gallup Sandstone and associated formations, Upper Cretaceous, eastern San Juan and Acoma Basins, New Mexico, in Siemers, C.T., Woodward, L.A., and Callender, J.F., eds., 25th Annual Fall Field Conference Guidebook: New Mexico Geological Society, p. 251–258.

Molenaar, C.M., 1983, Major depositional cycles and regional correlations of Upper Cretaceous rocks, southern Colorado Plateau and adjacent areas, in Reynolds, M.W., and Dolly, E.D., eds., Mesozoic Paleogeography of the West-Central United States: Rocky Mountain Section (SEPM), Rocky Mountain Symposium 2, p. 201-224.

Muto, T., and Steel, R.J., 1992, Retreat of the front in a prograding delta: Geology, v. 20, p. 967–970.

Muto, T., and Steel, R.J., 1997, Principles of regression and transgression: the nature of the interplay between accommodation and sediment supply: Journal of Sedimentary Research, v. 67, p. 994–1000.

Muto, T., and Steel, R.J., 2001, Autostepping during the transgressive growth of deltas: results from flume experiments: Geology, v. 29, p. 771–774.

Muto, T., and Steel, R.J., 2002, Role of autoretreat and A/S changes in the understanding of deltaic shoreline trajectory: a semi-quantitative approach: Basin Research, v. 14, p. 303-318.

Neal, J., and Abreu, V., 2009, Sequence stratigraphy hierarchy and the accommodation succession method: Geology, v. 37, p. 779–782.

Neal, J.E., Abreu, V., Bohacs, K.M., Feldman, H.R., and Pederson, K.H., 2016, Accommodation succession (δA/δS) sequence stratigraphy: observational method, utility and insights into sequence boundary formation: Journal of the Geological Society, v. 173, p. 803–816.

Nummedal, D., 1990, Sequence stratigraphic analysis of upper Turonian and Coniacian strata in the San Juan Basin, New Mexico, USA: NATO Advanced Workshop on Cretaceous Resources, Events and Rhythms, Backgrounds and Plans for Research, Proceedings, p. 33–46.

Nummedal, D., and Molenaar, C.M., 1995, Sequence stratigraphy of ramp-setting strand plain successions: the Gallup Sandstone, New Mexico, in Van Wagoner, J.C., and Bertram, G.T., eds., Sequences Stratigraphy of Foreland Basin Deposits: AAPG, Memoir 64, p. 277–310.

Nummedal, D., and Swift, D.J.P., 1987, Transgressive stratigraphy at sequence-bounding unconformities: some principles derived from Holocene and Cretaceous samples, in Nummedal, D., Pilkey, O.H., and Howard, J.D., eds., Sea Level Fluctuation and Coastal Evolution: SEPM, Special Publication 41, p. 241–260.

Nummedal, D., and Riley, G.W., 1991, Origin of late Turonian and Coniacian unconformities in the San Juan basin, in Van Wagoner, J.C., Jones, C.R., Taylor, D.R., Nummedal, D., Jennette, D.C., and Riley, G.W., eds., Sequence Stratigraphy

Applications to Shelf Sandstone Reservoirs: Outcrop to Subsurface Examples: AAPG, Special Volume 25, p. 33–46.

Nummedal, D., Wright, R., Swift, D.J.P., Tillman, R.W., and Wolters, N.R., 1989, Depositional systems architecture of shallow marine sequences, in Nummedal, D., Wright, R., Cole, R., Remy, R., eds., Cretaceous Shelf Sandstones and Shelf Depositional Sequences, Western Interior Basin, Colorado and New Mexico: American Geophysical Union, Field Trip Guidebook 119, p. 35–80.

Obradovich, J.D., 1993, A Cretaceous time scale, in Caldwell, W.G.E., and Kauffman, E.G., eds., Evolution of the Western Interior Basin: Geological Association of Canada, Special Paper 39, p. 379–396.

Pang, M., and Nummedal, D., 1995, Flexural subsidence and basement tectonics of the Cretaceous Western Interior basin, United States: Geology, v. 23, p. 173–176.

Pattison, S.A.J., 1995, Sequence stratigraphic significance of sharp-based lowstand shoreface deposits, Kenilworth Member, Book Cliffs, Utah: AAPG Bulletin, v. 79, p. 444–462.

Pattison, S.A.J., 2010, Alternative sequence stratigraphic model for the Desert Member to Castlegate Sandstone interval, Book Cliffs, eastern Utah: implications for the high-resolution correlation of falling stage nonmarine, marginal-marine, and marine strata, in Morgan, L.A., and Quane, S.L., eds., Through the Generations: Geologic and Anthropogenic Field Excursions in the Rocky Mountains from Modern to Ancient: Geological Society of America, Field Guide 18, p. 163–92.

Pemberton, S. G., and MacEachern, J.A., 1995, The sequence stratigraphic significance of trace fossils: examples from the Cretaceous Foreland Basin of Alberta, Canada, in Van Wagoner, J.C., and Bertram, G.T., eds., Sequences Stratigraphy of Foreland Basin Deposits: AAPG, Memoir 64, p. 429–475.

Plink-Bjorklund, P., 2008, Wave-to-tide process change in a Campanian shoreline complex, Chimney Rock Tongue, Wyoming-Utah, in Hampson, G.J., Steel, R.J., Burgess, P.M., and Dalrymple, R.W., eds., Recent Advances in Models of Siliciclastic Shallow Marine Stratigraphy: SEPM, Special Publication 90, p. 265–291.

Plink-Björklund, P., and Steel, R.J., 2004, Initiation of turbidity currents: outcrop evidence for Eocene hyperpycnal flow turbidites: Sedimentary Geology, v. 165, p. 29–52.

Plint, A.G., 1988, Sharp-based shoreface sequences and "offshore bars" in the Cardium Formation of Alberta: their relationship to relative changes in sea-level. in Wilgus, C.K., Hastings, B.S., Ross, C.A., Posamentier, H., Van Wagoner, J., Kendall, C.G.St.C., eds., Sea-Level Changes: An Integrated Approach: SEPM, Special Publication 42, p. 357–370.

Plint, A.G., 2010, Wave-and storm-dominated shoreline and shallow-marine systems, in James, N.P., and Dalrymple, R.W., eds., Facies Models 4: Geological Association of Canada, p. 167–200.

Plint, A.G., and Kreitner, M.A., 2007, Extensive thin sequences spanning cretaceous foredeep suggest high-frequency eustatic control: Late Cenomanian, Western Canada Foreland Basin: Geology, v. 35,735–738.

Plint, A.G., and Nummedal, D., 2000, The falling stage systems tract: recognition and importance in sequence stratigraphic analysis, in Hunt, D., and Gawthorpe, R.L., eds., Sedimentary Responses to Forced Regressions: Geological Society, London, Special Publication 172, p. 1–17.

Plint, A.G., Tyagi, A., Hay, M.J., Varban, B.L., Zhang, H., and Roca, X., 2009, Clinoforms, paleobathymetry, and mud dispersal across the Western Canada Cretaceous foreland basin: evidence from the Cenomanian Dunvegan Formation and contiguous strata: Journal of Sedimentary Research, v.79, p. 144–161.

Posamentier, H.W., and Morris, W.R., 2000, Aspects of the stratal architecture of forced regressive deposits, in Hunt, D. and Gawthorpe, R.L., eds., Sedimentary responses to forced regressions: Geological Society, London, Special Publication 172, p. 19–46.

Posamentier, H.W., Jervey, M.T., and Vail, P.R., 1988, Eustatic controls on clastic deposition I-conceptual framework, in Wilgus, C.K., Hastings, B.S., Ross, C.A., Posamentier, H., Van Wagoner, J., Kendall, C.G.St.C., eds., Sea-Level Changes: An Integrated Approach: SEPM, Special Publication 42, p. 109–124.

Posamentier, H. W., Allen, G. P., James, D. P., and Tesson, M., 1992, Forced regressions in a sequence stratigraphic framework: concepts, examples, and exploration significance: AAPG Bulletin, v. 76, p. 1687–1709.

Rich, J.L., 1951, Three critical environments of deposition and criteria for recognition of rocks deposited in each of them: Geological Society of America Bulletin 62, p. 1–20.

Riley, G.W., 1993, Origin of a coarse-grained, shallow marine sandstone complex: the Coniacian Tocito Sandstone, northwestern New Mexico [Ph.D. Dissertation]: Louisiana State University, 344 p.

Romans, B.W., Hubbard, S.M., and Graham, S.A., 2009, Stratigraphic evolution of an outcropping continental slope system, Tres Pasos Formation at Cerro Divisadero, Chile: Sedimentology, v. 56, p. 737–764.

Sadeque, J., Bhattacharya, J.P., MacEachern, J.A., and Howell, C.D., 2007, Differentiating amalgamated parasequences in deltaic settings using ichnology: an example from the Upper Turonian Wall Creek Member of the Frontier Formation, Wyoming, in MacEachern, J.A., Bann, K.L., Gingras, M.K., and Pemberton, S.G., eds., Applied Ichnology: SEPM, Short Course 52, p. 1–18.

Sageman, B.B., Rich, J., Arthur, M.A., Birchfield, G.E., and Dean, W.E., 1997, Evidence for Milankovitch periodicities in Cenomanian-Turonian lithologic and geochemical cycles, Western Interior USA: Journal of Sedimentary Research, v. 67, p. 286–302.

Sears, J.D., 1925, Geology and coal resources of the Gallup-Zuni Basin, New Mexico: U.S. Geological Survey Bulletin 767, 53 p.

Taylor, A.M., and Goldring, R., 1993, Description and analysis of bioturbation and ichnofabric: Geological Society of London, Journal, v. 150, p. 141–148.

Taylor, D.R., and Lovell, R.W.W., 1995, High-frequency sequence stratigraphy and paleogeography of the Kenilworth Member, Blackhawk Formation, Book Cliffs, Utah, USA, in Van Wagoner, J.C., and Bertram, G.T., eds., Sequences Stratigraphy of Foreland Basin Deposits: AAPG, Memoir 64, p. 257–275.

Tillman, R.W., 1985, The Tocito and Gallup Sandstones, New Mexico, a comparison, in Tillman, R.W., Swift, D.J.P., and Walker, R.G., eds., Shelf Sands and Sandstone Reservoirs: SEPM, Short Course 13, p. 403–463.

Trampush, S.M., Hajek, E.A., Straub, K.M., and Chamberlin, E.P., 2016, Identifying autogenic sedimentation in fluvial- deltaic stratigraphy: evaluating the effect of outcrop-quality data on the compensation statistic: Journal of Geophysical Research, Earth Surface, v. 122, p. 91–113.

Vakarelov, B.K., Bhattacharya, J.P., and Nebrigic, D.D., 2006, Importance of high-frequency tectonic sequences during Greenhouse times of Earth history: Geology, v. 34, p. 797–800.

Valasek, D., 1995, The Tocito Sandstone in a sequence stratigraphic framework: an example of landward-stepping small-scale genetic sequences, in Van Wagoner, J.C., and Bertram, G.T., eds., Sequences Stratigraphy of Foreland Basin Deposits: AAPG, Memoir 64, p. 349–369.

Van Wagoner, J.C., 1995, Sequence stratigraphy and marine to nonmarine facies architecture of foreland basin strata, Book Cliffs, Utah, U.S.A., in Van Wagoner, J.C., and Bertram, G.T., eds., Sequences Stratigraphy of Foreland Basin Deposits: AAPG, Memoir 64, p. 137–223.

Van Wagoner, J.C., Posamentier, H.W., Mitchum, R.M., Vail, P.R., Sarg, J.F., Loutit, T.S., and Hardenbol, J., 1988, An overview of the fundamentals of sequence stratigraphy and key definitions, in Wilgus, C.K., Hastings, B.S., Ross, C.A., Posamentier, H., Van Wagoner, J., Kendall, C.G.St.C., eds., Sea-Level Changes: An Integrated Approach: SEPM, Special Publication 42, p. 39–45.

Van Wagoner, J.C., Mitchum, R.M., Campion, K.M., and Rahmanian, V.D., 1990, Siliciclastic sequence stratigraphy in well logs, cores, and outcrops: concepts for high-resolution correlation of time and facies: AAPG, Methods in Exploration Series 7, p. 1–50.

Weimer, R.J., 1984. Relation of unconformities, tectonics, and sea-level changes, Cretaceous of Western Interior, USA, in Schlee, J.S., eds., Interregional Unconformities and Hydrocarbon Accumulation: AAPG, Memoir 36, p. 7–35.

Weissmann, G.S., Hartley, A.J., Nichols, G.J., Scuderi, L.A., Olson, M., Buehler, H., and Banteah, R., 2010, Fluvial form in modern continental sedimentary basins: distributive fluvial systems: Geology, v. 38, p. 39–42.

Wheeler, H.E., and Mallory, V.S., 1956, Factors in lithostratigraphy: AAPG Bulletin, v. 40, p. 2711–2723.

Zhu, Y., Bhattacharya, J.P., Li, W., Lapen, T.J., Jicha, B.R., and Singer, B.S., 2012, Milankovitch-scale sequence stratigraphy and stepped forced regressions of the Turonian Ferron Notom deltaic complex, south-central Utah, U.S.A: Journal of Sedimentary Research, v. 82, p. 723–746.

CHAPTER 4

DEPOSITIONAL FACIES OF A MIXED-PROCESS INFLUENCED DELTAIC SYSTEM IN A STORMY RAMP SETTING: THE CRETACEOUS GALLUP SYSTEM, NEW MEXICO, U.S.A.

Abstract

Both modern and ancient depositional systems have shown that shoreline processes are more dynamic and complicated with mixed-energy domination. Classification of depositional processes in previous studies has been over simplistic and sandstone-biased. A detailed process-based facies analysis with a high-resolution sequence stratigraphic framework will help to decipher shoreline depositional evolution in space and time and to consequently distinguish deltaic versus non-deltaic shoreline deposition and link the deposition to sequence stratigraphic control. We measured 71 sections in a 68 km long outcrop belt of the Cretaceous Gallup Formation in the NW of the San Juan Basin. The work allows us to document five major environmental facies associations using sedimentological and iconological interpretation: offshore shelf, shoreline sandstones, deltas, coastal plain, and fluvial. Each facies association also comprises subordinate facies associations. Depositional facies interpretations, associated with the high-resolution sequence stratigraphic control, allow reconstructing paleogeography of parasequences, and these synchronous paleogeographic maps comprising various facies associations are critical to reveal Earth's surface processes and its evolutionary history. The results show that the Gallup Formation was deposited in a wave-dominated, river-influenced, and tide-affected mixed-process environment, contrasting with previous interpretations of a solely

wave-dominated environment. The dominant depositional processes are linked to cyclic shoreline trajectory and base-level-related shoreline morphology, although river input, climate, and storm intensity can influence deposition independently of relative sea level. The paleogeography and recognition of depositional processes below fair-weather wave base help to inherently distinguish deposition of wave-dominated deltas and non-deltaic shorefaces. This analysis also demonstrates an asymmetrical delta model formed by locally enhanced clockwise longshore currents. The study proves that evolution and variability of the dynamic and complicated depositional processes are predictable.

4.1 Introduction

The classic tripartite (wave, tide, and river) classification of deltaic deposition (Galloway, 1975) has been increasingly realized to be over simplistic inasmuch as shoreline processes are more dynamic and complicated with mixed-energy common in most depositional systems through time (Boyd, 1992; Willis, 2005; Plink-björklund, 2008; Ainsworth et al., 2011; Legler et al., 2014; Rossi & Steel, 2016; Van Cappelle et al., 2016, 2017; Rossi et al., 2017; Li et al., 2018; Peng et al., 2018).

Ainsworth et al., (2011) proposed a semiquantitative classification of deltas based on the relative importance of various depositional processes, known as the "WTF" classification scheme. However, in their examples, the percentages of sedimentary strucures used as the criteria to determine the relative processes are primarily derived from analysis of sand-dominated intervals. Those sandstones of shoreline deposition tend to possess similar sedimentary structures, independing on dominant processes: trough cross-bedding can be seen either in distributary channels of a fluvial-domianted delta, or

in the upper shoreface of a wave-dominated delta, or in the strandplain of a non-deltaic shoreface. In addition, sandstone-based analysis most likely leads the facies-model-driven interpretations towards wave domination since deposition of shoreline sandstones are mostly above fair-weather wave base. In contrast, facies of mudstone and heterolithic sections (sensu offshore transition and shelf) may be more diagnostic for the distinction of depositional processes, in that processes such as hyperpycnal and turbidity flows and tidal influence are preserved below fair-weather wave reworking and may provide a better record of the sediment delivery process (MacEachern & Pemberton, 1992; Bhattachyara & Giosan, 2003; Bhattacharya & MacEachern, 2009; Dashtgard et al., 2012).

Wave-dominated deltas and non-deltaic shorefaces (sensu fluviatile and nonfluivatile coastlines of Ainsworth et al., 2011) share similar facies characteristics and are not always distinguished in many previous studies, especially given the fact that shoreline protuberance is not a necessity for delta definition (Olsen et al., 1999; Hampson & Storms, 2003; Pontén & Plink-Björklund, 2009; Charvin et al., 2010; Hein et al., 2013; Van Cappelle et al., 2018). Although many wave-dominated deltas have non-deltaic shorefaces attach to them, and they can transit into each other over a short distance along strike, in fact, deltas—even wave-dominated—and non-deltaic shorefaces are deposited differently (Bhattacharya, 2010). The distinction can be more difficult where the sand-dominated updrift part of an asymmetrical delta is attached to a non-deltaic shoreface (Bhattacharya & Giosan, 2003). Determination of the influence of processes in ancient systems also relies on the paleogeography of the area and the size of paleorivers and fluvial drainage areas that existed during deposition. Hampson & Howell (2005)

attempted a quantitative analysis of shoreline morphology and river proportion and spacing to distinguish wave-dominated deltas and strandplains in the Cretaceous Book Cliffs of Utah. However, the method requires high-resolution sequence stratigraphic controls, and study areas must be greater than average river spacing along shorelines (e.g., 130 km in modern shoreline systems).

Although particular depositional facies are considered to be preferentially deposited during different stages of a transgressive–regressive (T–R) cycle: such as deltas and strandplains occurring during regressions, with estuaries and barrier island more likely to be deposited during transgressions (Boyd, 1992), the linkage between depositional environments and T–R cycles may be more complicated than initially thought, given the influence of accommodation over sediment supply ratios and coastal morphology (Ainsworth et al., 2008, 2011). The relationships between dominant depositional processes and systems tracts were suggested by Yoshida et al. (2007) to be a result of shelf width and coastal morphology such that waves are dominant in HST and tides tend to dominant in LST. However, the stratigraphic controls on shoreline processes and paleogeography remain underestimated, and further understanding requires more examples and more accurate sequence stratigraphic controls to generalize.

Despite extensive studies of the Cretaceous Gallup Formation, the interpretation of the depositional environments remains equivocal. The majority of previous studies interpreted the thick amalgamated marine sandstones as wave-formed strandplains, barrier islands, shorefaces, or beaches (Campbell, 1973, 1979, Molenaar, 1973, 1983; Mccubbin, 1982; Nummedal et al., 1989); the existence of other process (tide and fluvial)

is poorly documented (Campbell, 1971; Molenaar, 1973; Mccubbin, 1982; Jones et al., 1991; Nummedal & Molenaar, 1995; LoParco, 2011). This may reflect that older interpretations were largely focused on the description of 1D facies in the absence of process-based analysis and detailed sequence stratigraphic context. Lacking sequence stratigraphic control can particularly cause misinterpretation of depositional process of isolated sandstones, such as the sandstones in Figure 4 of Nummedal and Molenaar (1995).

Paleogeographic reconstructions are critical for understanding the temporal and spatial evolution of depositional systems (Bhattacharya & Walker, 1991; Kauffman & Caldwell, 1993; Wood, 2004; Hampson et al., 2011; Legler et al., 2014; Burton et al., 2016; Van Cappelle et al., 2016, 2018). However, paleogeographic analysis must have sequence stratigraphic controls to decipher the influence of those dynamic sedimentary processes on shoreline evolution and their lateral variabilities. The availability of a high-resolution sequence stratigraphic framework enables reconstruction of the paleogeography of synchronous stratigraphic units. It also enables stratigraphically-controlled facies analysis allowing us to understand the genetic relationships between depositional facies development and its relationship to sequence stratigraphic position (Yoshida et al., 2007; Jones et al., 2018).

In the present study, we aim to document the sedimentary facies of the Gallup Formation in detail and to interpret the depositional environments and reconstruct the paleogeography within a high-resolution sequence stratigraphic framework. This work will allow us to denote the evolution of mixed depositional processes within the system

and to unravel the distinction between wave-dominated deltaic deposits and shoreface deposits on the basis of sedimentary process analysis.

4.2 Geological Setting

From the Jurassic to the Tertiary, the collision between the Farallon and the North American plates and the subsequent subduction formed the Cretaceous North American foreland basin and the Western Interior Seaway (Decelles, 2004). The flexural and dynamic subsidence and loading of the foreland basin caused a series of eastward fold-and-thrust belts during the Sevier Orogeny (Liu & Nummedal, 2004). During the Campanian and Maastrichtian, tectonic deformation of the basin graded into thick-skinned basement-uplift of the Laramide orogeny and formed the San Juan Basin, exposing the Gallup Formation along the basin margin (Leva Lopez & Steel, 2015; Yonkee & Weil, 2015; Copeland et al., 2017). Sediments derived from the Sevier fold-and-thrust belt were transported eastward into the Western Interior Basin, forming a series of siliciclastic wedges of alluvial, coastal plain, and shallow marine deposits with an overall north–south-trending coastline (Fig. 4.1).

The northwest-southeast-striking Mogollon Highlands lay to the southwest, along present-day Arizona, New Mexico, and Mexico, and supplied sediment northeastwards into the basin (Bilodeau, 1986; Dickinson & Lawton, 2001; Lawton et al., 2003; Dickinson & Gehrels, 2008; Lawton & Bradford, 2011; Lawton et al., 2014; Szwarc et al., 2015; Fig. 4.1).

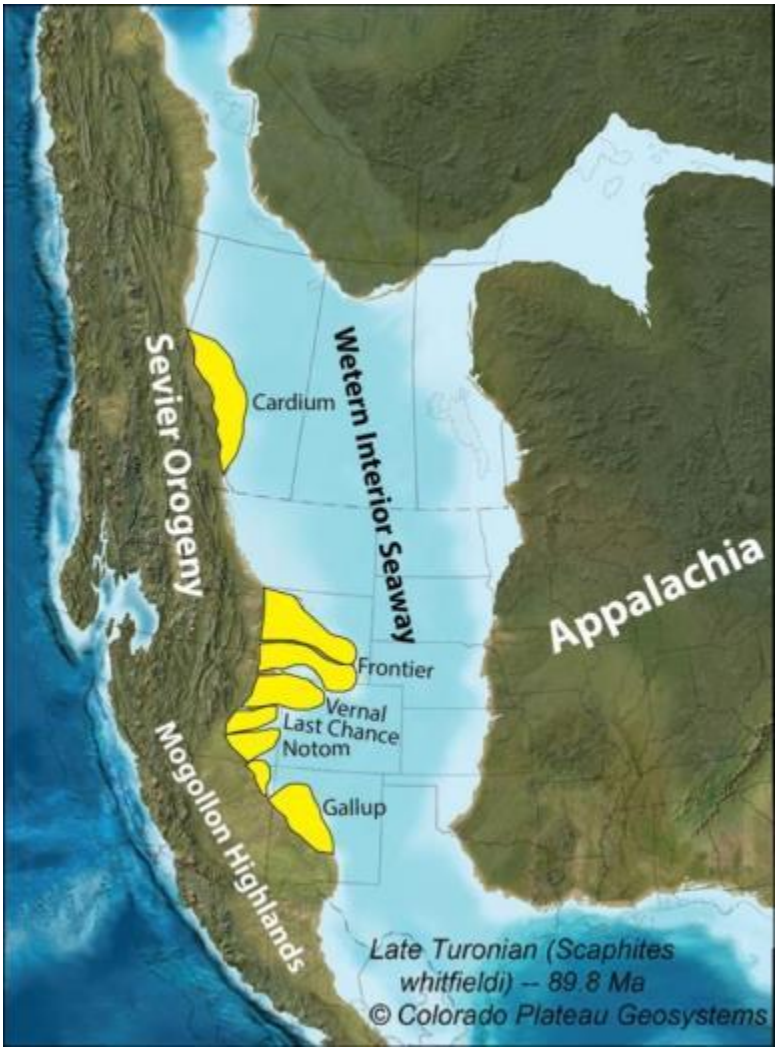

Fig. 4.1.–Regional paleographic map of the Cretaceous Western Interior Seaway (from Colorado Plateau Geosystems).

The Cretaceous Gallup Formation is one of the clastic depositional systems in the Seaway, deposited from late Turonian to early Coniacian (Nummedal & Molenaar, 1995). Predominantly shallow marine sandstones prograded towards the northwest with NW–SE oriented paleoshorelines (Campbell, 1971; Molenaar, 1973; Nummedal & Molenaar, 1995). The Gallup system consists of six distinct sandstone tongues interfingering with the Manco Shale (Nummedal & Molenaar, 1995). It conformably overlies the marine

Juana Lopez Member and unconformably underlies the marine Tocito Sandstone (Fig. 3.1). The depositional system was located around 30 °- 45 °N during the Late Cretaceous time indicating a subtropical warm and humid climate (Fricke et al., 2010; Hay & Floegel, 2012).

The Cretaceous Western Interior Seaway was formed in an active foreland basin and characterized as a semi-closed source-to-sink depositional system with robust mixed-energy controls. The seaway provides an ideal clastic depositional setting for a variety of studies regarding mixed-process dominance in depositional systems in space and time (Hampson & Storms, 2003; Yoshida et al., 2007; Hampson et al., 2011; Van Cappelle et al., 2018).

4.3 Dataset and Methods

A 68 km N–S oriented outcrop belt is located in northwest New Mexico along the flanks of the San Juan Basin (Fig. 3.3). Data used for this study constitutes 71 measured sedimentological sections and numerous photomosaic panels. Measured sections include lithology, grain size, sedimentary structures, bed thickness, paleocurrent directions, and trace fossils. Facies associations are described and interpreted based on these 1D vertical measured sections and 2D correlation of measured sections. 3D planview paleogeographic analysis is based on the combination of both 1D and 2D facies analysis within a sequence stratigraphic framework. Lateral variability of key facies is observed by tracing continuous outcrops and photomosaic panels between adjacent measured sections. Depositional facies and environmental associations are described and interpreted

using the practice described by Dalrymple (2010). Bioturbation intensity is characterized using the Bioturbation Index (BI) scheme of Taylor & Goldring (1993).

4.4 Facies Analysis

Five major depositional environmental facies associations have been identified in the Gallup system: offshore shelf, shoreline sandstones, deltas, coastal plain, and fluvial deposits. They are further subdivided into sixteen lithofacies associations: the offshore shelf facies association includes shelf and offshore transition; the delta facies association comprises prodelta, delta front, delta plain, and distributary channel and mouth bar; the shoreline sandstones consist of distal lower shoreface, proximal lower shoreface, upper shoreface, and foreshore; the coastal facies association constitutes barrier island, lagoon–bay fill, bayhead delta, and tidal inlet–delta; and the fluvial facies association comprise fluvial channel and bar and floodplain facies (Table 4.1; Fig. 4.2). Facies associations are arranged into various successions, such as upward-coarsening marine shelf–shoreline facies successions constituting shelf deposits at the base through lower-shoreface deposits and upper-shoreface deposits to foreshore deposits at the top. The shoreline sandstone is the dominant facies association, accounting for 38% of total facies associations (Fig. 4.3A). Proximal lower shoreface is the most common sandstone lithofacies association, comprising 40.7% of total marine sandstone thickness measured (Fig. 4.3B).

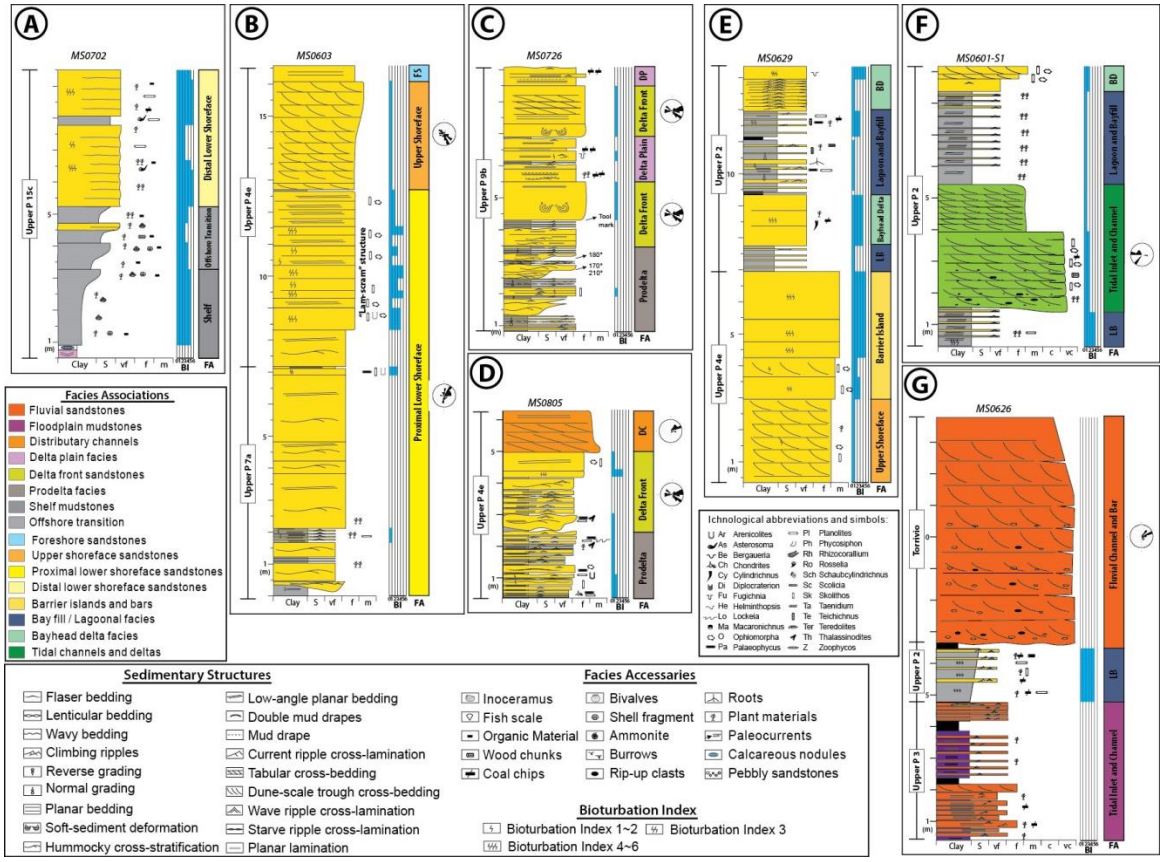

Fig. 4.2.– Measured sections illustrating representative facies associations, including grain size, sedimentary structures, bioturbation index (BI), and paleocurrent measurements of the Gallup Formation. (A) Shelf, offshore transition, and distal lower shoreface succession. (B) Proximal lower shoreface, upper shoreface, and foreshore succession. (C) Prodelta, delta front, and delta plain succession. Note this deltaic succession is most likely fluvial-dominated. (D) Prodelta, delta front, and distributary channel succession. (E) Succession of Upper shoreface, barrier island, lagoon or bayfill, and bayhead delta. (F) Section showing tidal inlet or channel embedded in lagoon or bayfill facies and capped by bayhead delta deposits. (G) Section showing fluvial channel and floodplain facies associations.

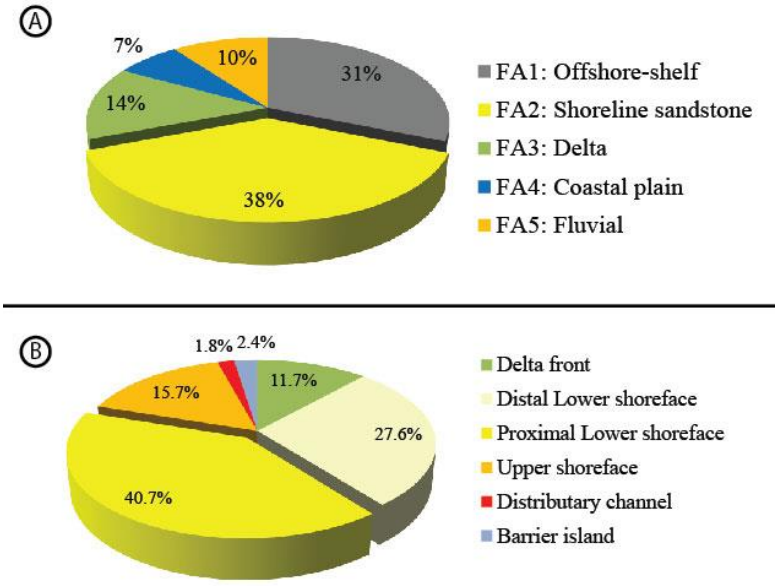

Fig. 4.3.–Facies association distribution charts. (A) Overall facies association distribution of the Gallup system. (B) Distribution of the marine sandstone lithofacies association.

4.4.1 Facies Association 1: Offshore shelf

Description.--- The shelf facies association has a thickness of up to 10 m above the lower bentonite and below shorefaces. It shows dark grey homogenous mudstones interbedded with centimeter-scale grey silty mudstones to muddy siltstones (Fig. 4.2A and 4.4A). Clay content can be up to 90%. Mudstones and siltstones show massive, laminated, and graded bedding. Thinly-bedded siltstones often show ripple cross-lamination. Centimeter-scale very-fine-grained sandstones are occasionally embedded as starved ripples. Bouma sequences (Tc – Te) are occasionally seen. Body fossils of ammonites, inoceramids, bivalves, and fish scales, associated with abundant organic matter, are common (Fig. 4.4B). Bioturbation intensity (BI) ranges from 0 to 6. The representative ichnogenera include *Chondrites*, *Palaeophycus*, *Planolites*, *Phycosiphon*, *Asterosoma*, *Teichichnus*,

Zoophycos, *Rosselia*, *Cylindrichnus*, and *Diplocraterion* (Fig. 4.4C), defining a *Zoophycos* to *Cruziana* ichnofacies (MacEachern et al., 2010).

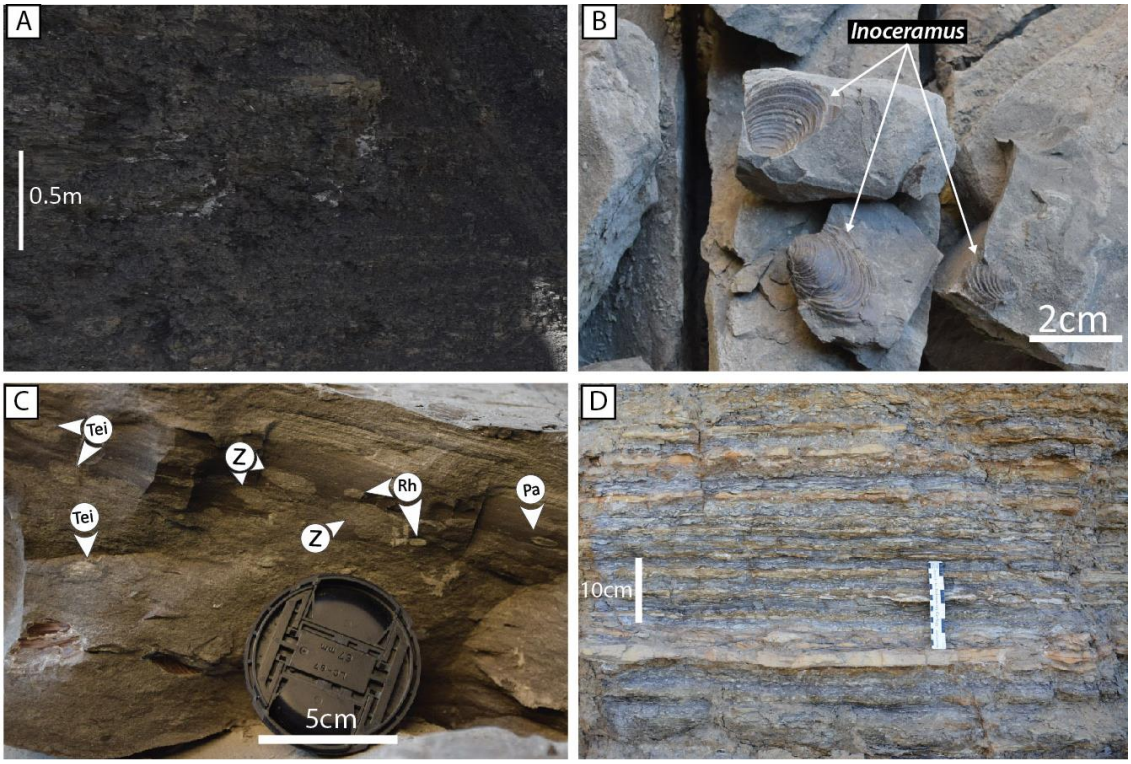

Fig. 4.4.–Photos of Facies Association 1. (A) Mudstones in a shelf section. (B) Inoceramus shell fragments in mudstones of shelf facies association (MS 0607). (C) *Zoophycos* dominated ichnofacies in shelf mudstones (MS 0607). (D) Bioturbated mudstone with thin-bedded very fined-grained sandstones and starved ripple laminated sandstones indicating offshore transition facies association (MS 0720).

The offshore transition facies genetically overlies shelf facies and commonly presents an upward-coarsening trend, the thickness of which varies from a few meters up to 8 m. It constitutes silty to sandy mudstones and sandy siltstones interbedded with thinly-bedded (1-5 cm) lower-very-fine-grained sandstones. Wave, combined-flow, and starved ripple cross-laminations are common. Relatively thick (around 5cm) sandstone beds are usually sharp and erosive based, and show hummocky-cross-stratification (HCS) grading into

wave ripple or combined-flow ripple cross lamination. Bouma sequences (Tb-Tc) are often seen throughout this facies succession. Sole marks are common. Mudstones contain graded beds and horizontal lamination; and otherwise are intensely bioturbated (BI of 0-6). Ichnogenera of *Chondrites*, *Palaeophycus*, *Planolites*, *Phycosiphon*, and *Asterosoma* define a *Cruziana* Ichnofacies. Abundant organic matter, body fossils of ammonites, inoceramids, and bivalves, and plant materials are common. Wood debris is seen locally (Fig. 4.2A and 4.4D).

Interpretation.--- Fine-grained sediment and the *Zoophycos–Cruziana* ichnofacies indicate deposition below fair-weather wave base in an open-marine shelf environment (MacEachern et al., 2010; Li & Schieber, 2018). Large storms may periodically reach this shelfal area to transport coarse sediment here and rework the preceding deposits into wave-dominated structures (Hampson et al., 2011; Li & Schieber, 2018).

Siltstones and thin-bed very-fine-grained sandstones, associated with ripple cross-lamination, indicate episodic influxes of coarser-grained sediment, probably during large storm events (Wright, 1977). Sharp-based sandstone beds with HCS are interpreted as storm beds. Bouma sequences indicate sediment gravity flows (e.g., turbidites). The alternation of high and low sedimentation rates indicates a transitional zone between inner shelf and distal lower shoreface (sensu the upper offshore of MacEachern et al., 1999).

4.4.2 Facies Association 2: Shoreline sandstones

Description.--- Distal lower shorefaces, 1 to 10 m thick, are made of muddy to silty lower- to upper-very-fine-grained sandstones. Sedimentary structures and trace fossils are difficult to identify as a result of intense bioturbation (BI of 5-6; Fig. 4.5A), and only the

remnant forms of ripple cross-lamination, low-angle cross-lamination, and HCS are seen locally. Distal lower shoreface most often exists as an isolated sandstone unit and can extend a great distance—up to 45 km in dip. Organic matter is ubiquitous. Inoceramids and bivalves fossils and shell fragment are also common.

Proximal lower shorefaces consist of 2-31 m thick upward-coarsening lower-very fine- to lower-fine-grained amalgamated sandstones. This sandstone succession includes the following sedimentary structures (from bottom to top): HCS, swaley-cross-stratification (SCS), planar to low-angle sub-planar-bedding, and wave or combined-flow ripple cross-lamination (Fig. 4.2B and 4.5B). HCS beds are typically 20-100 cm thick (i.e., regular to mega HCS). Abundant gutter casts are seen at the bases of HCS sandstones, and wave ripple cross-lamination often caps the HCS sandstones. Abundant plant materials and sporadic wood chunks are associated with the HCS (Fig. 4.5D). Tool marks are also commonly observed at the bottom of HCS sandstone beds. Mud drapes along HCS or planar bedding are occasionally seen. Higher up, HCS sandstones grade upward into horizontally laminated sandstones interbedded with bioturbated sandstones, showing the "lam-scram" structure (Fig. 4.5C). The laminated and bioturbated sandstone beds vary from 10-30 cm thick. In general, the grain size of laminated or bedded sandstones is slightly coarser than that of bioturbated sandstones in "lam-scram" packages. *Cruziana* constituting horizontal burrows, such as *Chondrites*, *Paleophycus*, *Planolites*, *Phycosiphon*, and *Asterosoma*, is the dominant ichnofacies (Fig. 4.5E). Bioturbation Index (BI) centers at 3-4 in the bioturbated sandstone intervals with BI of 5-

6 locally. Paleocurrents, measured from ripple lamination and tool marks, are oriented predominantly perpendicular to the paleoshoreline seaward (Fig. 4.2B).

Upper shorefaces gradually overlie proximal lower shorefaces. Contacts between the upper shoreface and lower shoreface are concordant and sharp, marked by an increase of grain size. Upper shorefaces range from lower-fine- to lower-coarse-grained—are predominantly upper-fine- to lower-medium-grained—dune-scale trough and tabular cross-bedded and planar-bedded sandstones (Fig. 4.2B and 4.5F). This facies association is generally coarsening and thickening upward. Individual beds are 30-300 cm thick, with cross-sets 20-40 cm thick. Bidirectional paleocurrents approximately parallel to the paleoshoreline show a dominant SE direction (Fig. 4.2B). Bioturbation intensity and diversity is generically low (BI of 0-3); intense bioturbation occurs locally. Marine trace fossils constituting *Ophiomorpha*, *Skolithos*, *Arenicolites*, and *Thalassinoides* define a *Skolithos* ichnofacies (Fig. 4.5G).

The foreshore consists of fine-grained planar- to sub-planar-bedded sandstones that gently dip seaward (Fig. 4B and 7H). Bioturbation is absent or sparse (BI of 0-1), with *Ophiomorpha* and *Skolithos* occasionally seen. Foreshore deposits are 10-40 cm thick and rarely seen in outcrops.

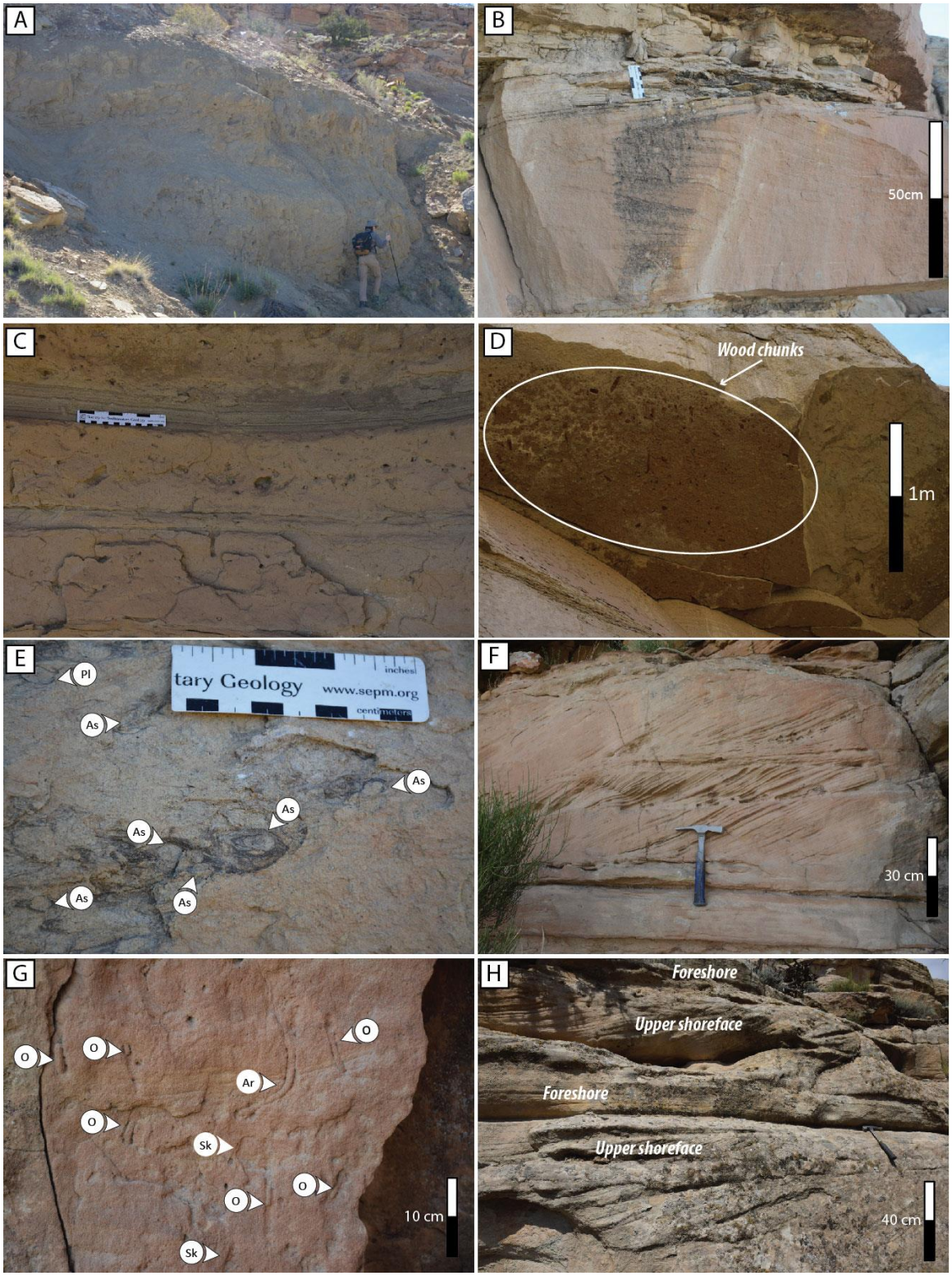
A
B
50cm
C
D
Wood chunks
1m
E
tary Geology
www.sepm.org
inches
centimeters
Pl
As
As
As
As
As
As
F
30 cm
G
O
O
O
O
Ar
Sk
O
O
Sk
10 cm
H
Foreshore
Upper shoreface
Foreshore
Upper shoreface
40 cm

Fig. 4.5.–Photos of Facies Association 2. (A) Distal lower shoreface constitutes very fine-grained intensely bioturbated sandstones. No obvious sedimentary structures. BI is high (BI of 5-6). Cryptic remnant sedimentary structures, such as hummocky-cross-stratification (HCS) and cross-lamination can be seen locally. Centimeter-scale thick ripple cross-laminated sandstones are occasionally seen at upper part of these facies successions. See the geologist for scale (MS 0520). (B) Very fine-grained HCS sandstones in the proximal lower shoreface facies association, indicating storm wave dominated depositional environments (MS 0714). (C) Laminated and bioturbated sandstone interbedding, known as the "lam-scram" structure, indicating high energy and low energy depositional environment alternating, typically representing the proximal lower shoreface facies association (MS 0609). (D) Abundant wood chunks with the size of a few centimeters along boundaries (bottom) of HCS sandstone bed, suggesting proximity to a river mouth (MS 0609). (E) Dominated trace fossils of proximal lower shorefaces include *Cruziana*, comprising *As* (*Asterosoma*) and *Pl* (*Planolites*). (F) Fine-grained dune-scale cross-bedded sandstones in the upper shoreface facies association. Cross-bedding indicates high energy environments that are constantly above fair-weather wave base (MS 0714). (G) Sandstones comprising *O* and *Sk* trace fossils, defining a *Skolithos* ichnofacies (MS 0805). (H) Fine-grained planner-bedded sandstones of the foreshore facies association interbedded with cross-bedded sandstones of the upper shoreface (MS 0607).

Interpretation.--- The very fine grain size and thorough bioturbation of the interpreted distal lower shoreface indicate deposition in an unstressed normal marine environment, below effective fair-weather wave base (MacEachern *et al.*, 1999; MacEachern *et al.*, 2010). The large volume of very-fine-grained sandstones indicates transport of sandy sediment by relatively high-energy processes (Wright, 1977). The cryptic sedimentary structures also imply that these units may be originally deposited by waves or storms, but completely bioturbated afterward. Such facies indicates wave influence overwhelming fluvial influence, resulting either from being distant from the delta that would allow

pervasive bioturbation or an increase in sea level that may bring the area from a wave- or storm-dominated environment down to a more quiescent open-marine environment.

HCS and SCS represent deposition during storms (Dott & Bourgeois, 1982; Walker *et al.*, 1983; Midtgaard, 1996). Amalgamated HCS and SCS beds suggest frequent and intensive storm events that eroded inter-storm deposits (Duke, 1985). Planar-bedding overlying HCS indicates a shoaling in water depth (Dumas & Arnott, 2006). When storms waned, wave ripples were formed by normal wave currents and overlie HCS beds (Duke *et al.*, 1991). Gutter casts were formed from erosion of the seabed by storm-generated currents in shore-norm directions and subsequent filling (Whitaker, 1973). The NE-dominated paleocurrent measurements suggest a nearly seaward-directed component of motion, combined with oscillatory waves, geostrophic flows, bottom currents, and downwelling coastal currents (Swift *et al.*, 1983; Duke *et al.*, 1991). The local abundance of terrestrial materials, such as wood chunks, may suggest proximity to terrestrial sediment sources (i.e., river mouths) with more fluvial influence. Mud drapes along HCS may suggest either rapid post-storm suspended deposition (Coates & Maceachern, 2009) or periodic and local tidal influence or even tidally-modulated storm deposits when storm energy subsided (Yang *et al.*, 2008; Legler *et al.*, 2014). The "lam-scram" beds are interpreted to represent an alternation of high-energy tempestites and low-energy fair-weather conditions, commonly occurring in an intermediate-energy shoreface (MacEachern & Pemberton, 1992). This facies indicates processes of tempestite emplacement during storms and post-storm recolonization of opportunistic suspension-

feeding ichnofauna during fair-weather periods, which most commonly occur in the upper part of the lower shoreface (MacEachern and Bann, 2008).

Trough and tabular cross-bedded sandstones in the upper shoreface facies association indicate the migration of subaqueous dunes that formed in response to longshore and onshore currents (Clifton *et al.*, 1971; Van Cappelle *et al.*, 2016). Low diversity *Skolithos* ichnofacies also suggests a high-energy environment above fair-weather wave base (MacEachern *et al.*, 2010).

Low-angle seaward dipping sandstone beds that overlie the upper shoreface represent foreshore deposition, which is interpreted to form in the swash zone, also known as intertidal zone, where waves break (McCubbin, 1982).

4.4.3 Facies Association 3: Deltas

Description.--- The prodelta association is mudstone dominated heterolithic facies (Fig. 4.6A). Thinly-bedded (1-10cm) very-fine-grained current and combined-flow ripple cross-laminated sandstones are intercalated locally. Thin-bed HCS and planar laminated very-fine-grained sandstones are occasionally seen (Fig. 4.2C, D and 4.6C). Graded beds and horizontal laminations are dominant (Fig. 4.6A and B). Bouma sequences, soft sediment deformation, loading structures, and microfaults are common structures (Fig. 4.6B and C). Thin-bed mudstones with high clay content and dark color are also observed locally (Fig. 4.6D). Abundant plant debris and wood chips are also often seen. Body fossils are rare. Bioturbation intensity and diversity are low (BI of 0-2). Identified trace fossils include *Chondrites*, *Planolites*, and *Palaeophycus*, belonging to *Cruziana* ichnofacies.

The delta front facies association constitutes upper-very-fine- to medium-grained sandstones, locally interbedded with thin-bed mudstones or siltstones. Massive bedding (i.e., structureless) and soft sediment deformation structures (e.g. "ball and pillow" structure) are prevalent and typically overlain by planar-bedded sandstones (Fig. 4.2C, D, and 4.6E). These beds vary from a few decimeters up to 2 meters thick. HCS, planar bedding, horizontal lamination, and wave, combined-flow, and current ripple cross-lamination are presented in fine-grained sandstones (Fig. 4.2C, D, and 4.6E); low-angle cross-bedding is seen in coarser-grained sandstones. Sandstone slumps in mudstones are observed locally (Fig. 4.6F). Abundant plant material, coal chips, and wood chunks are observed (Fig. 4.6G). Sole marks are often seen. The facies succession typically shows an upward-coarsening trend (Fig. 4.6E and I). The lateral correlation of this facies association appears to show clinoforms with high paleo-slopes (up to 0.002). Bioturbation is either absent or sparse (BI of 0-1) with *Planolites*, *Palaeophycus*, *Ophiomorpha*, *Skolithos*, *Thalassinoides*, *Arenicolites*, and *Rosselia*, defining a mixed *Cruziana* and *Skolithos* ichnofacies. Paleocurrent measurements show W–E oriented bidirectional trends with a dominant E to SE direction (Fig. 4.2C).

Distributary channels overlie delta front facies and comprise mostly granular upper-fine- to lower-coarse-grained and locally lower-very-coarse-grained dune-scale trough or tabular cross-bedded and locally planar-bedded sandstones (Fig. 4.6H and I). Sandstone beds are 1 to 2 m in thickness. Thinly-bedded (2 - 10cm) mudstones drapes are occasionally observed. Sandstone beds have sharp bases and show an upward-fining trend (Fig. 4.6H). Some sandstone beds show distinctive bar shapes with limited lateral extent

and unidirectional accretion (Fig. 4.6J). Abundant mud rip-up clasts, plant material, coal chips, and wood chunks are common (Fig. 4.6G). Bioturbation is absent to very low (BI of 0-1) with only *Skolithos* and *Ophiomorpha* observed. Paleocurrents are approximately perpendicular to the paleoshoreline in the seaward direction (Fig. 4.2D).

The delta plain is characterized by thinly-bedded very-fine- to fine-grained sandstones interbedded with carbonaceous siltstones and mudstones. Entire facies successions can be up to 1.5 m thick. Individual beds range from 2-20 cm thick (Fig. 4.2C and 4.6K). Horizontal lamination and ripple cross-lamination are most common (Fig. 4.6K). Cross-bedding and HCS are observed locally. Carbonaceous mud drapes are commonly seen. Abundant plant material, coal chips, and wood chunks occur along lamination and bedding surfaces. Bioturbation intensity and diversity are low (BI of 0-1) with *Asterosoma* and *Palaeophycus* identified locally.

Interpretation.--- The prodelta records the muddy section and basinward extension of the deltaic facies association. Horizontal lamination suggests deposition by suspension, which is the most common depositional process in distal areas. The commonly seen normal and inverse graded beds and Bouma sequences are interpreted to be deposited rapidly by hyperpycnal or turbidity flows, and thereby associated with river floods (Bhattacharya, 2010; Olariu *et al.*, 2010). The homogenous dark-colored mudstones are interpreted as fluid muds. Soft sediment deformation, loading structures, and microfaults are indicators of high sedimentation rates and the subsequent overpressure (Bhattacharya, 2010). Current and combined-flow ripples also reflect periodic sand transport with high sedimentation rates; while HCS sandstones imply storm influence. Fluid mud deposits

may indicate rapid mud transport along the seafloor by hyperpycnal flows (Bhattacharya & MacEachern, 2009). The abundance of plant and organic matter also suggests proximity to terrestrial sediment sources, such as river mouths. Low BI can be interpreted as deposition in stressed environments as a result of high sedimentation rates with river input (MacEachern *et al.*, 2010).

Sandy delta front facies possessing upward-coarsening trends reflect the progradational nature of deltas (Bhattacharya, 2010). Rapid sedimentation occurs in delta fronts as a result of flow deceleration. Massive bedding and soft sediment deformation indicate rapid deposition and unstable slope conditions. The facies of meter thick planar-bedded sandstones overlying massive sandstones is interpreted as deposition caused by river-flood-generated hyperpycnal flows (Olariu *et al.*, 2010). The co-existence of low-angle cross-bedding and current ripples also suggests cycles of waxing and waning flows (Mulder *et al.*, 2003). Slumps and soft sediment deformation can also be formed from shoreline failure (e.g., mouth bar failure) as a result of steep clinoforms, mechanical dewatering of sediment—due to salinity change, or pore pressure buildup (Bhattacharya, 2010; Olariu *et al.*, 2010). Large-scale soft sediment deformation can also result from earthquakes; however, limited lateral extent of these locally deposited “ball-and-pillows” likely rule out the interpretation of earthquake origin. Abundant terrestrial materials indicate proximity to the river mouth. The mix of fresh and sea waters and high sedimentation rates also explain the stressed bioturbation conditions. The dominant approximately shoreline-perpendicular paleocurrent direction, associated with the characteristics described above, suggest the delta front is most likely dominated by rivers.

The distributary channel facies association is interpreted by the observation of sharp-based cross-bedded sandstones with an obvious increase in grain size. The lack of scour bases may suggest the channels are small and shallow terminal distributary channels, subsequently filled by sandy bar deposits (e.g., mouth bar; Bhattacharya, 2010; Olariu & Bhattacharya, 2006). Bar-shape sandstones with unidirectional accretion represent downstream migration of mouth bar deposits. Abundant mud rip-up clasts and carbonaceous material suggest a high-energy environment and a connection to an upstream subaerial plain (Staub & Gastaldo, 2003). Low BI is interpreted to be a result of dynamic and high-energy depositional processes. The NE oriented paleocurrent direction is consistent with the direction of shoreline progradation.

The delta plain, comprising abundant carbonaceous material and carbonaceous mudstone drapes, indicates this facies association was either covered by or adjacent to subaerial vegetation (Staub & Gastaldo, 2003). Silty and muddy sediment suggests deposition in a low-energy environment. The rareness of trace fossils indicates a highly stressed environment (MacEachern *et al.*, 2010), and such stress is interpreted to be caused by low salinity in the delta plain environment.

4.4.4 Facies Association 4: Coastal plain

Description.--- Barrier islands are made of lower-fine- to upper-medium-grained sandstones. These sandstone beds locally contain dune-scale cross-bedding and planar bedding. This facies succession is most often capped by bioturbated sandstones with *Ophiomorpha*, *Skolithos*, *Palaeophycus*, and *Thalassinoides*, defining a *Skolithos* ichnofacies (Fig. 4.2E and 4.7A). Bioturbation diversity is low (only *Skolithos*

ichnofacies); bioturbation intensity is low (BI of 0-1) in cross-bedded sandstones and high (BI of 3-4) in bioturbated sandstones (Fig. 4.7A).

Lagoon and bay fill comprises mudstone and siltstone. This facies association ranges from 2 to 10 m in thickness and typically overlies barrier islands (Fig. 4.2E). Grey-mudstone-dominated heterolithic sections intercalate with thin-bed lower-very-fine- to lower-fine-grained sandstones. Ripple cross-lamination is commonly observed in sandstone and siltstone beds. Graded beds and horizontal lamination are seen in mudstones (Fig. 4.2E and F). Carbonaceous material (plant material, wood chips, and coal chips) are abundant (Fig. 4.7B). Roots are occasionally seen in thin-bed (5 cm) mudstones. Thin-bed (5-20 cm) coal seams are often embedded (Fig. 4.2F and 4.7B). The facies successions are often intensely bioturbated (BI of 0-5), but by limited ichnogenera, including *Teichichnus*, *Planolites*, *Palaeophycus*, and *Chondrites* (Fig. 4.7C).

Bayhead deltas consist of relatively thinly-bedded (up to 30 cm) lower-very-fine- to upper-fine-grained sandstones intercalated with thin-bed mudstones and siltstones. The successions show 80 cm to 5 m thick upward-coarsening trends (Fig. 4.2E, F, and 4.7D). Sandstones are either ripple cross-laminated to dune-scale cross-bedded or intensely bioturbated (BI of 0-5; Fig. 4.7D). The dominant trace fossils, *Ophiomorpha*, *Skolithos*, *Palaeophycus*, and *Thalassinoides*, represent a *Skolithos* ichnofacies. Abundant plant and organic matter, including wood chips, coal chips are common.

Tidal facies associations described here incorporate tidal inlet, tidal channel and bar, and tidal delta (*sensu* Boyd, 2010). This facies association comprises lower-fine- to lower-coarse-grained sandstones (Fig. 4.2F). Granules are seen locally at the bases of

tidal channels. Cross-bedding, ripple cross-lamination, and double mud drapes are the predominant sedimentary structures (Fig. 4.7E). Planar bedding, herringbone cross-bedding, and inclined-heterolithic-stratification (IHS) are locally observed (Fig. 4.7F and G). The successions mostly fine upward and locally coarsen upward. Plant material is abundant, and wood and coal chips are common. Bioturbation intensity varies from absent to high (BI of 0-4); bioturbation diversity is low, and only *Teichichnus*, *Ophiomorpha*, and *Skolithos* have been identified. Paleocurrents are approximately perpendicular to paleoshorelines, but dominantly landward (Fig. 4.2F).

Interpretation.--- Cross-bedding of the upward-coarsening succession of barrier island suggests deposition by longshore currents in a wave-dominated environment. These sandstone beds are interpreted as the product of reworking of upper shoreface sandstones (Van Cappelle *et al.*, 2018). This facies association grades into upper shoreface basinward and lagoon/bay fill landward. The bioturbated section at the top is interpreted as the post-depositional recolonization that is most likely related to marine incursion during transgression (McCubbin, 1982).

The muddy lagoon and bay fill association is interpreted to be deposited from suspension in a low-energy environment. Ripple cross-lamination may suggest periodic tidal processes (e.g., inlet or flood). Abundant carbonaceous debris and sporadic roots indicate deposition close to vegetation-covered areas of the coastal plain (Van Cappelle *et al.*, 2018). Despite the locally high bioturbation intensity, the low trace-fossil diversity indicates deposition in stressed, marginal marine environments with brackish salinity (MacEachern & Bann, 2008; Hampson *et al.*, 2011).

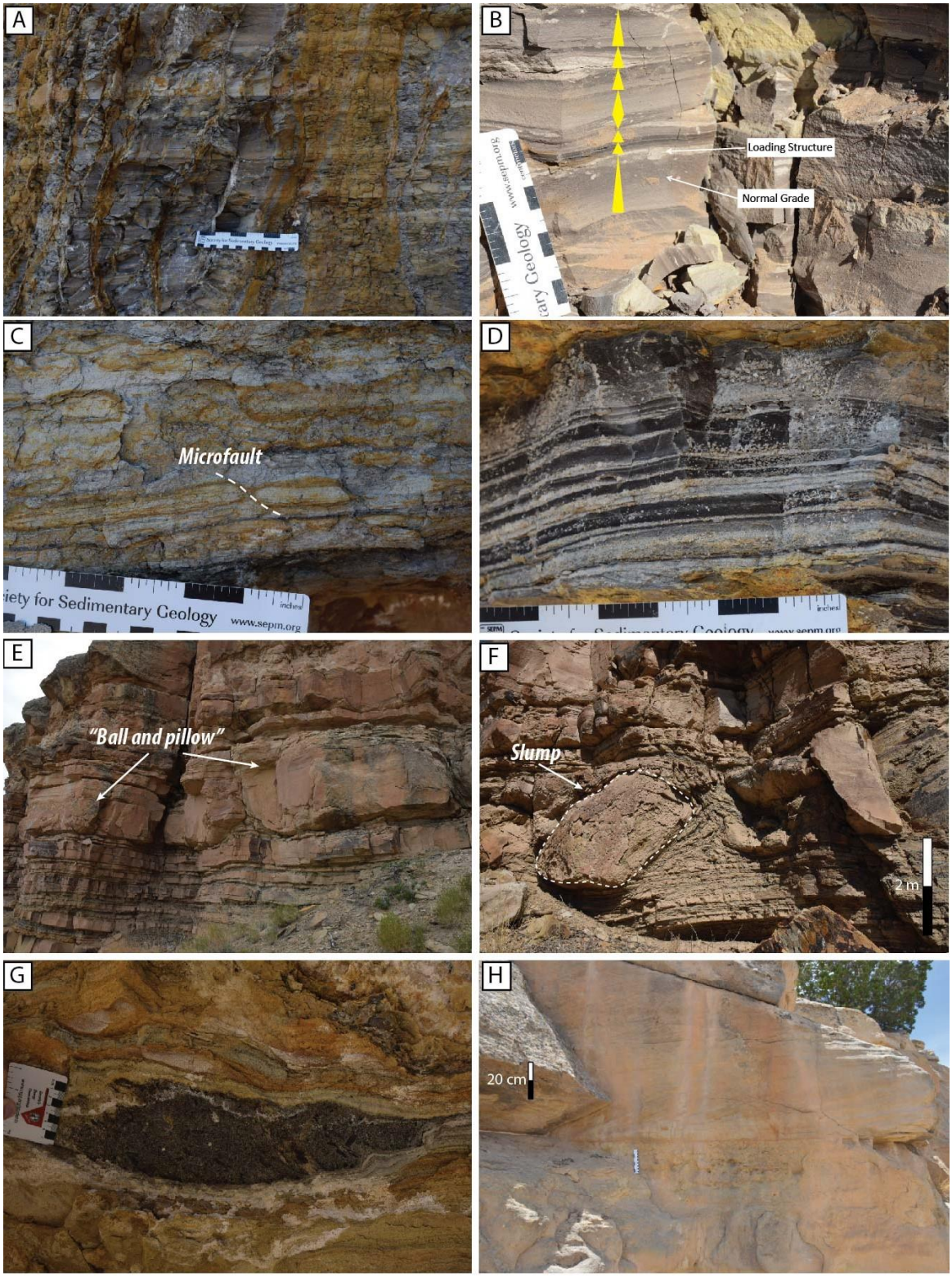
A
B
Loading Structure
Normal Grade
C
Microfault
D
E
"Ball and pillow"
F
Slump
2 m
G
H
20 cm

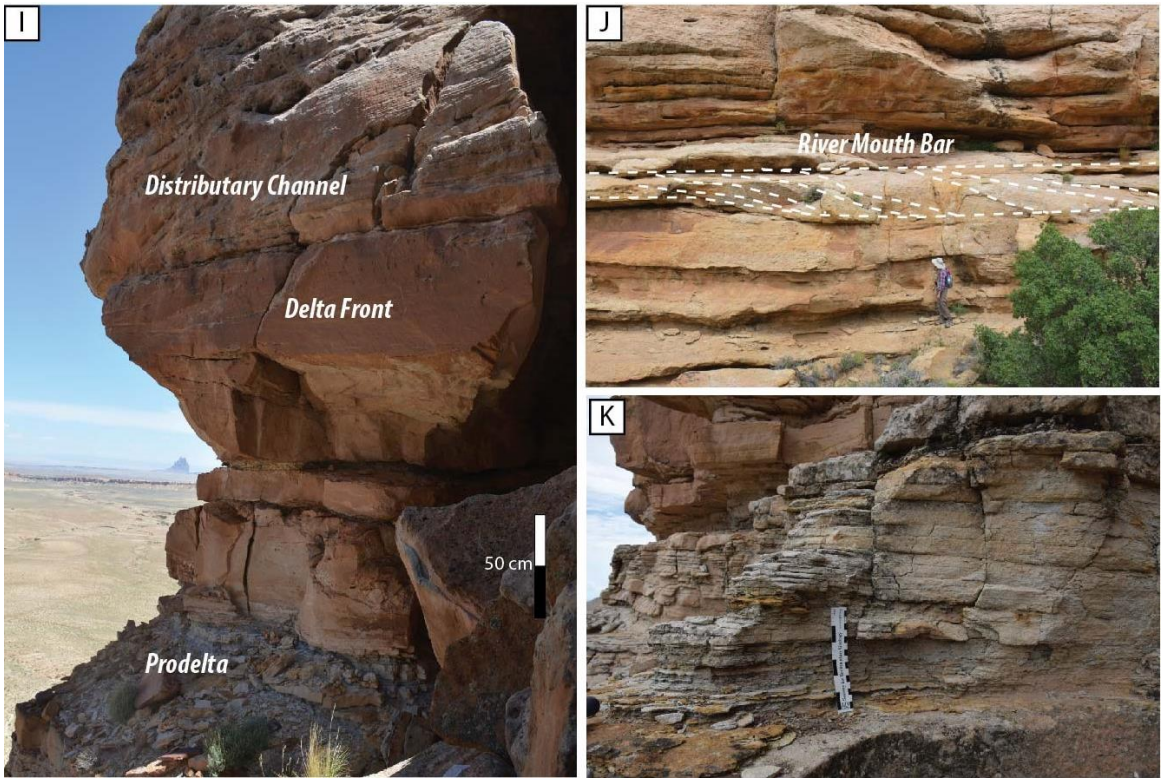

Fig. 4.6.–Photos of Facies Association 3. (A) Mudstones- and siltstones-dominated prodelta facies association shows grading beds with low bioturbation intensity, indicating high sedimentation rate environments (MS 0715). (B) Normal grade, inverse grade, and loading structures in the muddy and silty prodelta facies association (MS 0706). (C) Microfault in the prodelta facies association indicating overpressured deposits (MS 0714). (D) Fluid mud in the prodelta facies association suggesting mud deposition is resulted from hyperpycnal flows (MS 0729). (E) Upward coarsening and thickening succession of the delta front facies association with soft sediment deformation ("ball and pillow") structures at the top, indicating instable slope environments, typically seen in fluvial-dominated delta fronts. Note the heterolithic bottom part and the thick bedded top part (MS 0716). (F) Sandstone slumps indicating shoreline failure as a result of instable shoreline conditions in the delta front facies association (MS 0729). (G) Carbonaceous mudstones and abundant terrestrial material, such as plant and wood debris suggesting proximity to a river mouth (MS 0711). (H) The delta front facies association overlain by the distributary channel facies association. Note grain size increases in the distributary channels (MS 0602). (I) Coarse-grained dune-scale cross-bedded sandstones representing distributary channels that overlie shorefaces sandstones (MS 0716). (J) Downstream accretion of river mouth bars (MS0609). (K) The thinly-

beded delta plain facies association comprises laminated fine-grained sandstones interbedded with carbonaceous mudstones that contain abundant terrestrial material (MS 0726).

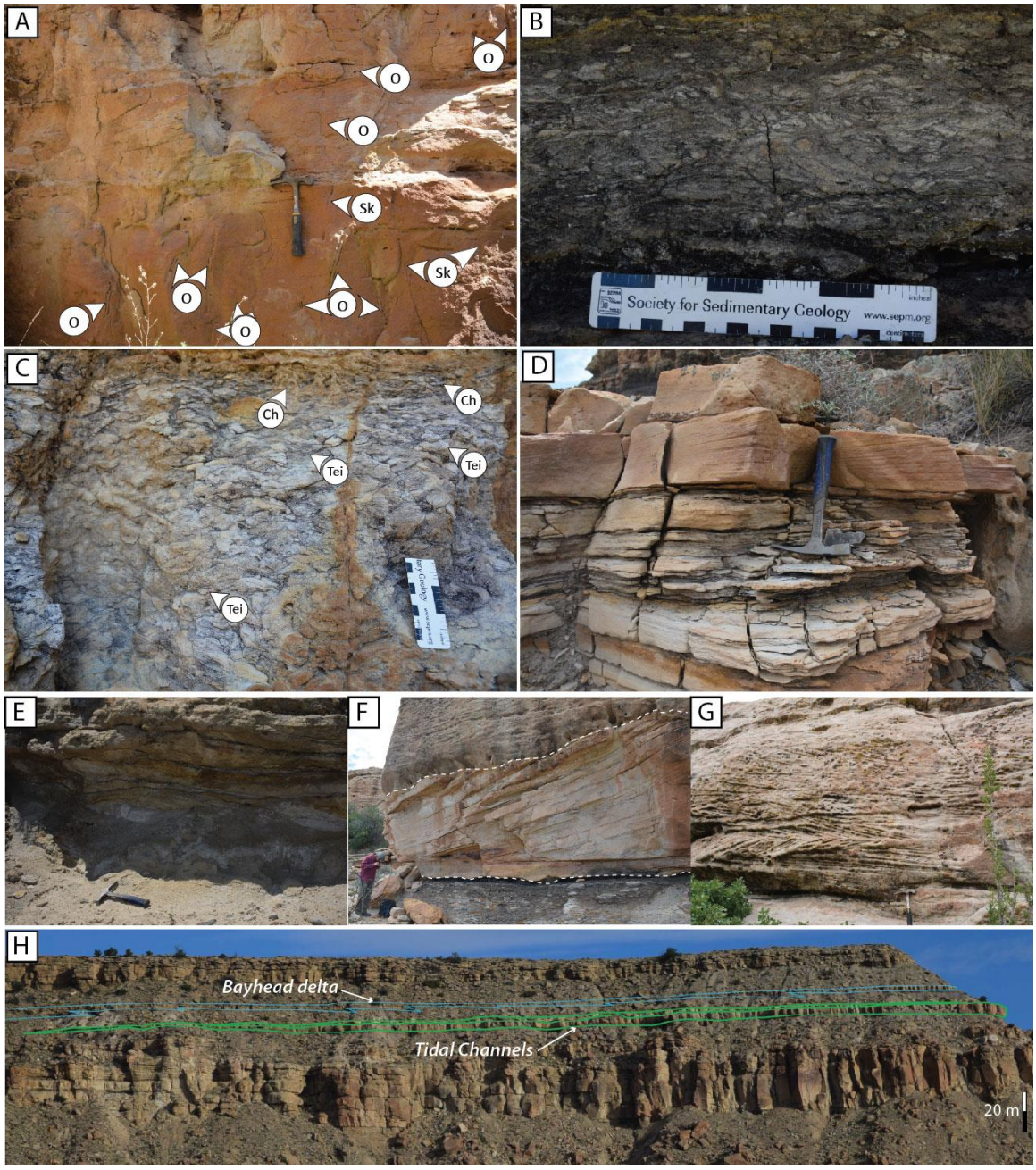

Fig. 4.7.–Photos of Facies Association 4. (A) Upper-fine-grained cross-bedded and bioturbated sandstones with *Ophiomorpha* dominated *Skolithos* ichnofacies. This suggests a relative low energy environment with less wave influence, interpreted as barrier island deposits with more

embayment (MS 0629). (B) Bioturbated siltstone indicating a brackish environment, representing the lagoon or bayfill facies association (MS 0713). (C) *Teichichnus* dominated intensely bioturbated sandy siltstone indicating low energy a brackish depositional environment, representing the lagoon or bayfill facies association (MS 0626). (D) Upward coarsening sandstone succession comprising thinly-bedded cross-bedded and laminated sandstones interbedded with carbonaceous mudstones, suggesting the bay-head delta facies association (MS 0626). (E) Double mud-drape and bioturbated coarse-grained sandstones representing the tide-influenced channel (MS 0607). (F) Inclined heterolithic stratification (IHS), associated with bioturbation along bedding surfaces, indicating tidally influenced channels in a brackish water environment (MS 0519). White dash lines indicate boundaries of the tidally influenced channel. (G) Herringbone structure indicates tidal influence (MS 0609). (H) Photo panel with outlines show the tidal inlet channel pinching out landward and overlying the bayhead delta (MS 0708 – MS 0604).

Bayhead deltas, also termed "lagoon-head deltas" by Kamola & Wagoner (1995), are a small-scale type of delta that develops at the landward end of a lagoon or bay (Bhattacharya, 2010; Aschoff *et al.*, 2018). Bayhead deltas are considered to be fluvial influenced, and depositional processes resemble that of a river delta. The upward-coarsening trend reflects a progradational nature during regression (Fig. 4.7H). The *Teichichnus*-dominated assemblage suggests a brackish water environment (MacEachern & Bann, 2008). The richness in terrestrial carbonaceous materials including roots also suggests proximity to a fluvial plain.

The upward-fining channelized successions with coarse sediment are interpreted as tidal inlet channels or tidally-influenced channels (Van Cappelle *et al.*, 2018; Gomez-Veroiza & Steel, 2010; Fig. 4.7H). This interpretation is further supported by the bidirectional but landward-dominated paleocurrents and the occurrence of double mud drapes. IHS sandstones with *Skolithos* ichnofacies trace fossils suggest channel bar migration in brackish water. Herringbone structures imply flood- and ebb-tidal currents

(Dalrymple & Rhodes, 1995). The upward-coarsening successions landward of the tidal channels are interpreted as flood tidal deltas. The abundance of carbonaceous plant material, associated with low bioturbation intensity and diversity reflects a low salinity stressed coastal environment (Kamola & Van Wagoner, 1995).

4.4.5 Facies Association 5: Fluvial deposits

Description.--- Channel facies of FA 5 range from 6 to 12 m thick and are characterized by up to 6 m thick multiple vertically-amalgamated upward-fining sandstone successions (Fig. 4.2G and 4.8A). These successions typically start with pebbly coarse-grained sandstones, often mixed with mud rip-up clasts, coal chips, and fossilized tree trunks, overlying sharp and erosive basal surfaces (Fig. 4.8B, C, and H). These coarse-grained sandstones grade upward into medium-grained dune-scale trough or tabular cross-bedded sandstones. The average thickness of the cross sets is around 20cm.

Floodplains vary from 1 to 6 m thick, and comprise carbonaceous and coaly mudstones with abundant plant materials, roots, and wood and coal chips. 5-50 cm thick sheet-like very-fine-grained current ripple cross-laminated sandstones and siltstones are intercalated with mudstones (Fig. 4.2G, 4.8D, E and G). Slickenside structures are observed locally (Fig. 4.8F). Coal beds are commonly observed, either within floodplain successions or underlying fluvial channels from a few centimeters to up 50 centimeters thick (Fig. 4.8D and G).

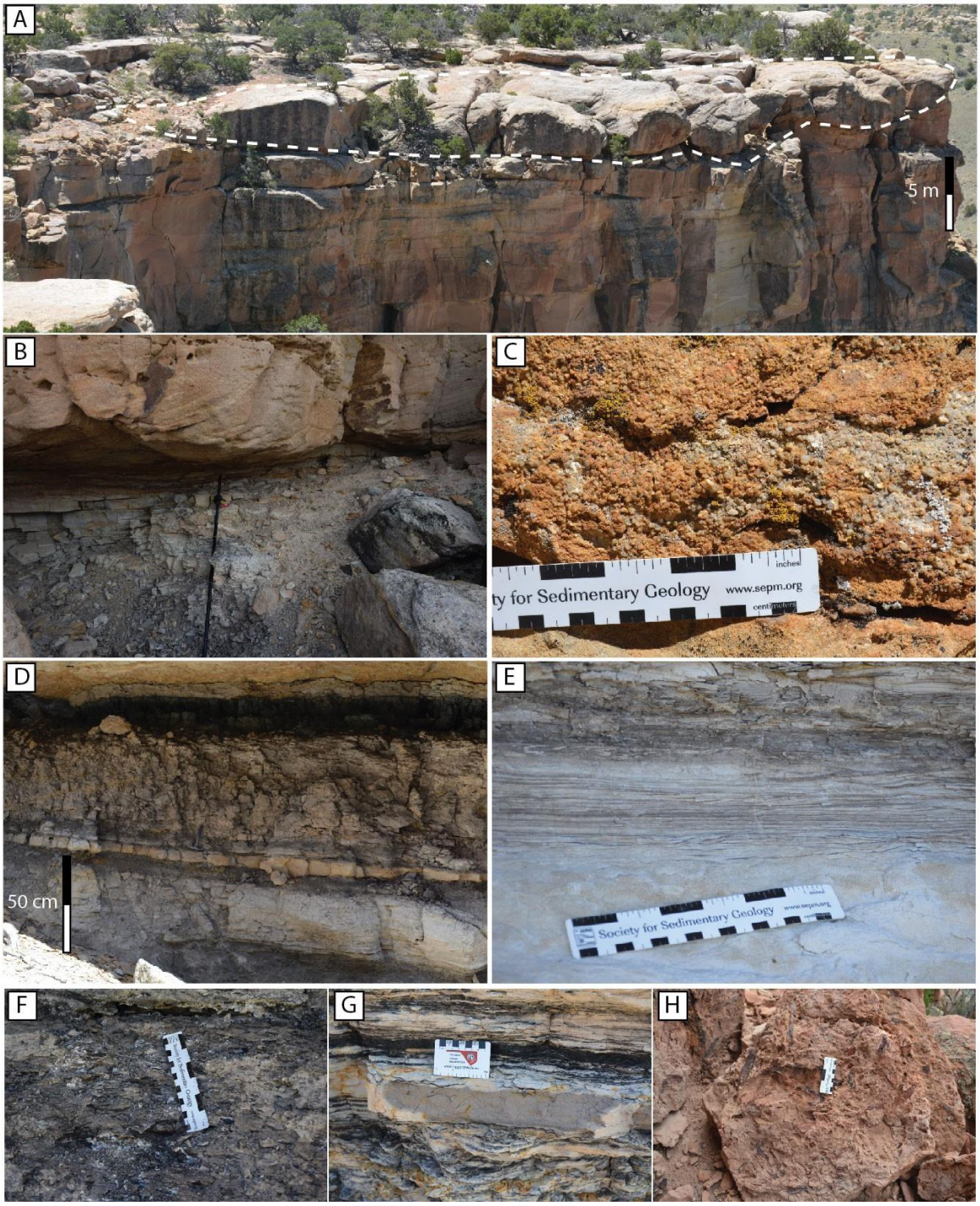

Fig. 4.8.–Photos of Facies Association 5. (A) Fluvial channels with lateral accretion bars incising into the underlying marine sandstones (MS 0714). (B) Coarse-grained fluvial sandstones incising into floodplain or coastal plain siltstones (MS 0726). (C) Very coarse-grained sandstones at the

bottom of fluvial channels (MS 0606). (D) The floodplain facies association constituting (from bottom to top) very fine-grained crevasse splay sandstones, natural levee sandstones to siltstones, floodplain mudstones, and a coal seam. (MS 0524). (E) Ripple-laminated siltstones to very fine-grained sandstones of natural levees in the floodplain facies association (MS 0520). (F) Slicken-sided mudstones in floodplain interpreted as subaerial exposed paleosols (MS 0713). (G) Roots and coal in the floodplain facies association (MS 0629). (H) Wood chunk debris in the floodplain facies association (MS 020).

Interpretation.--- Channelized coarse-grained sandstones with a variety of internal architectures are interpreted as fluvial channel bodies resulting from channel fill with sand and bar migration (Miall, 2014). The estimated river depth ranges from 3.6 to 6 m, based on an average cross-set thickness of 20 cm (Leclair & Bridge, 2001). The overall thickness of channelized sandstones suggests multi-story amalgamated fluvial deposition. Fluvial channels often erode directly into marine shoreface deposits.

Carbonaceous mudstones and siltstones are interpreted as floodplain deposits. Slickensided mudstones and coal beds indicate subaerial exposure and swampy environments. Thin sandstone beds with ripples are interpreted as either natural levee or crevasse splays, dependent on the thickness (levees are generically thin, and splays are relatively thick). Channel plugs may exist but cannot be distinguished from floodplain deposits (Hampson *et al.*, 2011).

4.5 Sequence Stratigraphy

We have identified key stratigraphic surfaces that establish the high-resolution sequence stratigraphic framework of the Gallup system: including flooding surfaces, sequence boundaries, maximum flooding surfaces, and ravinement surfaces (transgressive surface of erosion). Two bentonite layers have been found throughout most of the study area and

used as regional datums. These bentonite layers are considered to coincide with regional transgressions and maximum flooding events (Mitchum & Van Wagoner, 1991; Haq, 2014). The upper bentonite divides the Gallup system into lower and upper parts, and each part represents a composite sequence (Lin *et al.*, in revision).

The lower Gallup consists of six high-frequency depositional sequences, which are subdivided into ten parasequence sets and twenty-four parasequences. The upper Gallup comprises seven sequences, constituting sixteen parasequence sets and thirty-seven parasequences (Fig. 3.9; Lin *et al.*, in revision). Falling-stage systems tracts (FSST), lowstand systems tracts (LST), transgressive systems tracts (TST), and highstand systems tracts (HST) compose a full sequence; few sequences have all these four systems tracts preserved (Fig. 3.16). Four classes of shoreline trajectory are identified in the Gallup system: ascending regressive with decelerating rate, ascending regressive with accelerating rate, descending regressive, and transgressive (*sensu* Helland-Hansen & Martinsen, 1996). We also observed four classes of distinct geometric stacking patterns of parasequence sets: progradational–aggradational (PA), aggradational–progradational (AP), retrogradational (R), and degradational (D)(*sensu* Neal & Abreu, 2009).

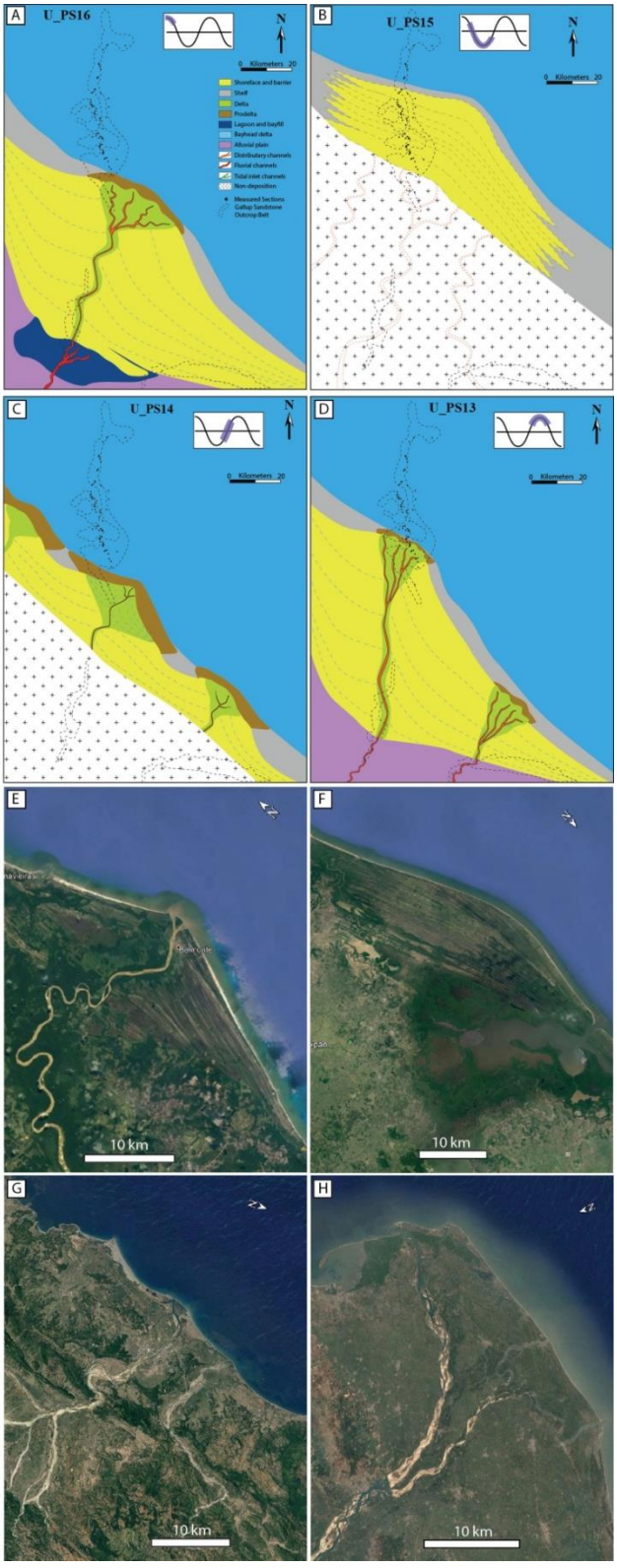
A
U_PS16
N
0 Kilometers 20
Shoreface and barrier
Shelf
Delta
Prodelta
Lagoon and bayfill
Bayhead delta
Alluvial plain
Distributary channels
Fluvial channels
Tidal inlet channels
Non-deposition
Measured Sections
Gallup Sandstone
Outcrop Belt
B
U_PS15
N
0 Kilometers 20
C
U_PS14
N
0 Kilometers 20
D
U_PS13
N
0 Kilometers 20
E
10 km
F
10 km
G
10 km
H
10 km

Fig. 4.9.–Paleogeographic evolution of the upper Gallup. Paleogeography of Parasequence Sets 16, 15, 14, and 13 show stratigraphic evolution during a relative sea-level cycle. (A) Parasequence Set 16 represents the highstand systems tract of Sequence 7. (B) Parasequence Set 15 shows the falling-stage and lowstand systems tracts of Sequence 6. (C) Parasequence Set 14 represents the transgressive system tract. (D) Parasequence Set 13 represents the highstand systems tract. (E) Google Earth map of the Brazilian Jequitinhonha Delta resembles the paleogeography of PS 16. (F) Google Earth map of the coast of Nayarit, Mexico represents the paleogeography of PS 15. (G) Google Earth map of the Padsan River, NW Philippines. This modern coastal morphology represents small-scale deltaic shoreline deposition that resembles the paleogeography of PS 14. (H) Google Earth map of the Godavari Delta is analogous to the paleogeography of PS 13.

4.6 Paleogeographic Reconstruction

The high-resolution sequence stratigraphic framework, associated with the detailed facies analysis, allows us to reconstruct the paleogeography of the Gallup system through its evolutionary history. In this paper, we use paleographic maps of four successive parasequence sets as examples to show the paleogeographic evolution through a full cycle of a stratigraphic sequence. Parasequence Set 16 of the upper part of Gallup represents the preceding HST, and Parasequence Set 15 - 13 represent the following FSST–LST, TST, and HST, respectively (Fig. 4.9).

4.6.1 Paleographic map of Parasequence Set (PS) 16

PS 16 represents the HST of Sequence 7. The deposition of this parasequence set is dominated by the mixed influence of waves and rivers. Landward, coastal plain and lagoonal deposits, associated with fluvial deposits are observed. Seaward, river-dominated and wave-influenced delta front deposits center at the shoreline, and wave-

dominated shorefaces are deposited at flanks of the delta front. Prodeltas were deposited in front of the delta front and laterally transit into offshore–shelf deposits (Fig. 4.9A).

The deposition shows a NE progradational trend. The co-existence of wave and river influence in the same parasequence set implies mixed depositional processes. During this HST, the river-dominated delta prograded towards the NE; whilst longshore currents reworked the sediment delivered into the system and dispersed it along the shoreline simultaneously. The river-dominated delta is most likely single-sourced; the sediment of the wave-dominated shorefaces is probably derived from multiple sources along the shoreline. A proposed modern analog of such paleogeography is the Brazilian Jequitinhonha Delta (Fig. 4.9E)

4.6.2 Paleographic map of Parasequence Set (PS) 15

PS 15 is interpreted as the FSST and LST of Sequence 6. The deposition shows a series of progradational to degradational parasequences that shifted the system basinward (Fig. 4.9B). A similar sequence stratigraphic model was discussed by MacEachern *et al.* (1999). Rivers may drive the progradation and degradation initially; but waves later overwhelmed the rivers' influence and dominated the late LST when relative sea level began to rise. Therefore, river-dominated delta front lobes were reworked into sheet-like and linear shorefaces. Sediment supply is considered to be high during the FSST; hence a depositional model of multiple feeding rivers is speculated (Fig. 4.9B). Such depositional-process-based model can be observed in the modern coast of Nayarit, Mexico, where the extensive and sheet-like sandstone bodies are most likely reworked from river-borne sediment during the post-glaciation transgression (Fig. 4.9F; Curray *et al.*, 1969).

4.6.3 Paleographic map of Parasequence Set (PS) 14

PS 14 represents the TST of Sequence 6. The shoreline migrated landward significantly from the time of PS 15. A series of small-size wave-dominated and river-influenced deltas were restricted at the shoreline as a consequence of the back-step (Fig. 4.9C). During the transgression, the shoreline shifted landward as a result of relative sea level rise. Sediment may be deposited into the system by rivers, but were largely reworked by waves. As landward-moving waves were the predominant control, the wave-dominated deltas of the TST show a more symmetrical geometry, with sediment dispersed to the sides of the river mouths (Fig. 4.9C). Similar small-scale wave-dominated deltas can be observed around the Padsan River, NW Philippines (Fig. 4.9G).

4.6.4 Paleographic map of Parasequence Set (PS) 13

PS 13 depicts the HST of Sequence 6. The shoreline had moved basinward. Similar to PS 16, river-dominated and prograding wave-influenced deltas were deposited at the shoreline, and wave-dominated shorefaces form flanking strandplains. A model of two deltaic lobes with separate feeding rivers has been interpreted in this HST (Fig. 4.9D). The modern Godavari Delta may be analogous in scale, morphology, and process to the paleogeography of PS 13 (Fig. 4.9H).

To summarize, during a fully developed sequence, the paleoshoreline moved back and forth as illustrated by Figure 4.9. Multiple rivers likely existed in the depositional system along the shoreline and dynamically interacted with waves and longshore currents. Paleogeographic reconstructions of the Late Cretaceous Western Interior Seaway of Van Cappelle *et al.* (2018) show a similar multiple-feeder model as a result of a relatively

short catchment distance. Such model was also proposed by Blum et al. (2013) for "Greenhouse" narrow shelves. The deposition of the HST is dominated by mixed energy of rivers and waves. The FSST–LST may be initially dominated by multiple rivers at the early stage, but the systems tract was reworked by waves as a result of a subsequent relative sea level rise. The deposition of the TST is dominated by waves along with the shoreline back-stepping. The straight/lobate shoreline with the absence of embayments favors wave's domination, although tides may dominate locally (Yoshida et al., 2007).

4.7 Discussion

4.7.1 Relationships between depositional facies and sequence stratigraphy

Genetic relationships between depositional facies associations and sequence stratigraphic positions have been hypothesized as a result of depositional processes governed by changes in shoreline morphology and regional bathymetry during relative sea level cycles (Dalrymple *et al.*, 1992; Porebski & Steel, 2006; Yoshida *et al.*, 2007). For example, wave-dominated shorefaces are thought to be more commonly deposited in the HST; whereas tides are commonly thought to dominate the LST and TST as a result of significant embayment caused by lower sea levels (Bhattacharya & Willis, 2001; Yoshida *et al.*, 2007; Legler *et al.*, 2014). In the present study, we have documented that depositional environmental facies associations are controlled by sedimentary processes that are related to sequence stratigraphic systems tracts and relative sea level positions. Table 4.2 summarizes these relationships. Among the 16 lithofacies associations, only shelf, offshore transition, distal, and proximal lower shoreface are present in all four systems tracts. By contrast, upper shorefaces, foreshores, and delta plains are only

observed in the HST. Coastal plain associations are only formed in the TST and HST. Deltaic deposits are notably missing in the LST.

Table 4.1. Summary of the relationships between facies successions and systems tracts of sequence stratigraphy in the Gallup system.

Systems Tracts / Facies Association	FSST	LST	TST	HST
Shelf	√	√	√	√
Offshore transition	√	√	√	√
Distal Lower shoreface	√	√	√	√
Proximal Lower shoreface	√	√	√	√
Upper shoreface				√
Foreshore				√
Prodelta	√		√	√
Delta front	√		√	√
Distributary channel and bar	√			√
Delta plain				√
Barrier island			√	√
Lagoon and bay fill			√	√
Bayhead delta			√	√
Tidal inlet and delta			√	√
Floodplain		√	√	√
Fluvial channel and bar		√	√	√

At some highstands of sea levels in the Cretaceous, the Western Interior Seaway can be as wide as 1000 km (Kauffman, 1977), and the shoreline of the western margin was fairly straight. Such open marine conditions and ascending regressive shoreline trajectory favor diverse depositional processes and allow for deposition of a variety of facies associations, ranging from coastal plain to marine shelf. The straight shoreline and wide seaway particularly favor waves to dominate, which may explain the observation of upper shorefaces and foreshores only in the HST. Although rivers are thought to be rejuvenated during the FSST, as a result of base level falls, channels and floodplains are predominantly deposited during the LST. This may indicate that channels were deposited and preserved as a result of channel "cut-and-fill" process during LST (Blum & Tornqvist,

2000). Nonetheless, such processes can also continue in the subsequent TST and HST, dependent on other factors, such as climates (*sensu* the "buffer zone" of Holbrook *et al.*, 2006).

Deltaic successions are mainly observed in FSST and HST due to their regressive nature. Previous studies have argued that deltas may be favored in the LST as a result of the processes of erosion, bypass, and progradation (*sensu* Posamentier & Vail, 1988; Van Wagoner et al., 1990; Plint & Wadsworth, 2003). Nevertheless, Porebski & Steel (2006) suggested that deltas can form at various localities in response to sea level changes. The lack of a shelf break in the WIS makes the FSST and LST hard to distinguish. Previously interpreted "lowstand deltas" more likely represent the deltaic deposits in the FSST (Plint, 1988; Bhattacharya, 1993; Ainsworth & Pattison, 1994; Bhattacharya & Willis, 2001; Plint & Wadsworth, 2003; Olariu et al., 2010). Plint & Wadsworth (2003) indicated in their Figure 22 that the "lowstand delta" of the Allomember E of the Dunvegan Formation shows offlapping and thereby implies a FSST. Deposition during FSST may be more significant than it has been documented in previous work, especially in the Cretaceous WIS (Ainsworth & Newall, 2000; Fitzsimmons & Johnson, 2000; Mellere & Steel, 2000; Plint & Nummedal, 2000). The LST appears to be more wave or tide dominated as a result of initial relative sea level rise, which may either hamper the formation of river-dominated deltas or rework river deltas into more wave-dominated shorefaces (Plint & Nummedal, 2000; Yoshida et al., 2007; Fig. 4.9B).

Within the same systems tract, depositional processes can also change independently of relative sea level, such that shoreface and delta front sandstones can both exist in a

HST. In this case, depositional processes are determined by a variety of factors, including fluvial channel locations, climate, and wave or storm intensity (Hampson & Howell, 2005). Away from river mouths, river influence decreases and is likely suppressed by wave influence (Bhattacharya & Giosan, 2003). Climate changes also influence the dominant processes of depositional systems by adjusting the sediment discharge and grain size of feeding rivers and by changing storm frequency and intensity (Holbrook *et al.*, 2006; Blum & Tornqvist, 2000; Fricke *et al.*, 2010).

Barrier islands and the associated lagoon or bay deposits were arguably interpreted to form during transgression, and their counterpart—strandplains form during regression (Boyd *et al.*, 1992). However, in this study, we documented that typical "transgressive" facies also deposited during regression (e.g., lagoonal deposits of Parasequence Set 7 and 4 were deposited during HST regression; Fig. 3.9; Table 4.2). The paleogeography of Parasequence Set 4 predicts barrier island – lagoon deposits associated with delta construction and progradation (Fig. 4.10). This also proves that lagoons, bays, and barrier islands are not necessarily strictly associated with transgressive systems, which is consistent with the predication of the asymmetric delta model proposed by Bhattacharya & Giosan (2003).

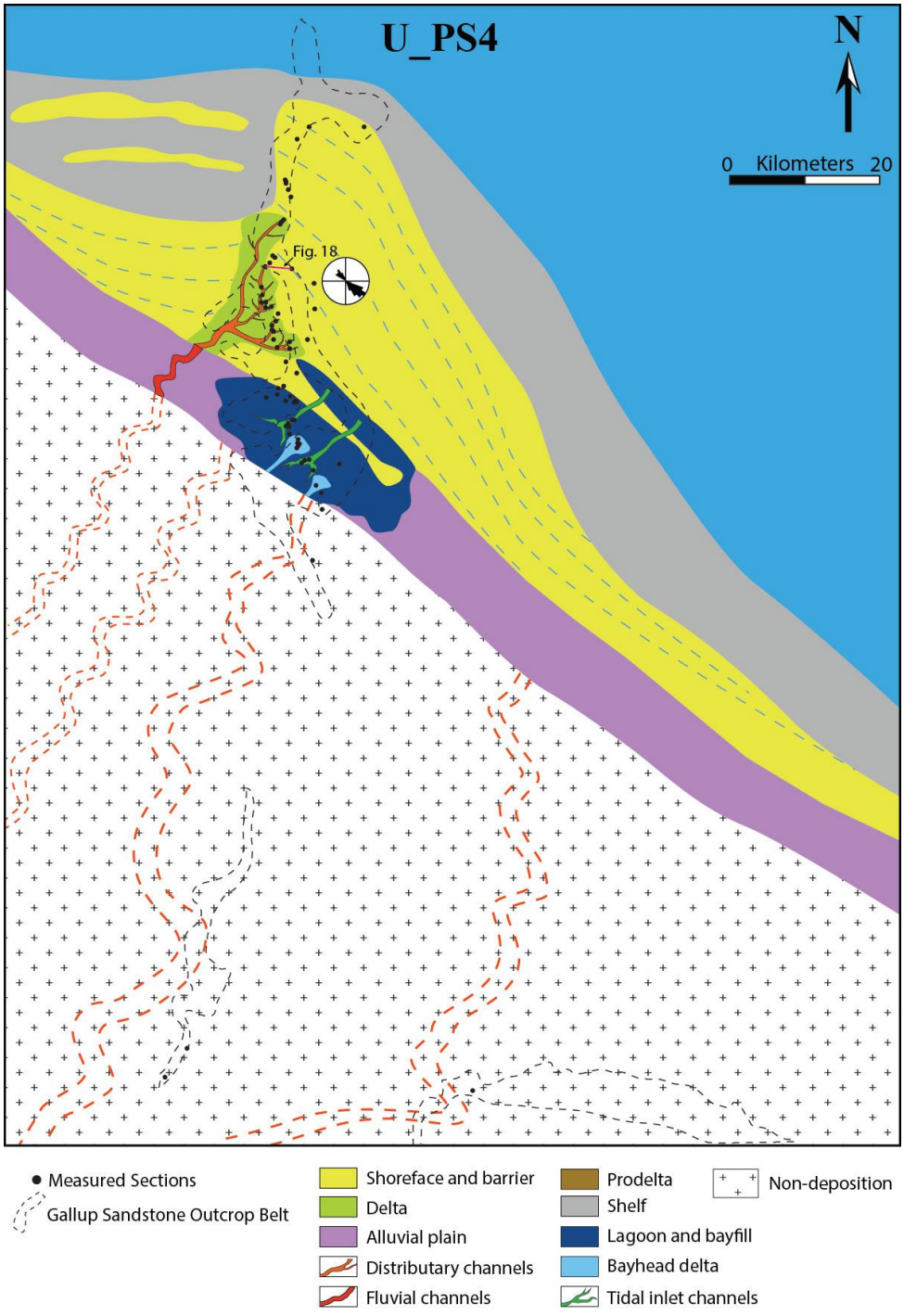

Fig. 4.10.–Paleogeographic reconstruction of Parasequence Set 4 of the upper Gallup system. The planview geometry matches a wave-influenced asymmetric delta model. The map also predicts the lagoon and bayfill deposition during regression.

4.7.2 Mixed-process dominated depositional system—river, wave, storm, and tide (tidal signature)

Depositional environments dominated by dynamic mixed-energy processes have been extensively documented in both modern and ancient systems (Boyd *et al.*, 1992; Anthony & Orford, 2002; Harris *et al.*, 2002; Bhattacharya & Giosan, 2003; Anderson *et al.*, 2004; Willis, 2005; Dalrymple & Choi, 2007; Yoshida *et al.*, 2007; Ainsworth *et al.*, 2008; Hampson *et al.*, 2008b; Yang *et al.*, 2008; Charvin *et al.*, 2010; Ainsworth *et al.*, 2011; Van Cappelle *et al.*, 2018). Such mixed-process-dominated deposition is particularly common in the Cretaceous Western Interior Seaway, owing to the active tectonic setting, shallow water depth, dynamic coastal morphology, and small drainage basins (Kauffman & Caldwell, 1993; Hampson & Howell, 2005; Hampson *et al.*, 2011; Van Cappelle *et al.*, 2018). Changes in the relative intensity of the depositional processes on a local scale can result in coexisting and lateral transition of multiple depositional environments along the same shoreline. Such changes can also occur along with stratigraphic evolution through time, manifested by vertical stratigraphic variation (Yoshida *et al.*, 2007).

In the Gallup system, changes in the mixture of processes can be observed throughout the temporal and spatial evolution. Based on the facies association distribution of the whole system (Fig. 4.3), the Gallup is characterized as a wave dominated, fluvial influenced, and tide affected depositional environment (Fig. 4.11; *sensu* Ainsworth *et al.*, 2011). Waves are the dominant force in most parasequences through the development of the system; fluvial is also dominant in particular parasequence sets (e.g., PS 13; Fig. 4.11). High-frequency sequence stratigraphic cyclicity has been documented and considered to

be controlled by Milankovitch Cycles (Lin *et al.*, in revision). The related high-frequency climate changes can modulate the dominance among depositional processes. For example, high precipitation brings rivers to flood and increases discharge, resulting in river dominated systems; on the contrary, waves can be intensified by winds, storms, and oceanic currents to overwhelm modest river input. Figure 4.12 demonstrates the temporal variations of dominant depositional processes and the associated facies changes. The parasequences show a transition from wave-dominated shoreface deposits in the lower part of the cliff, to river-dominated delta front deposits in the middle part, and to wave-dominated shoreface deposits in the upper part (Fig. 4.12A). The vertical evolution can be explained by lateral transition from a more symmetrical fluvial-dominated delta to a more asymmetrical wave-dominated shoreface (Fig. 4.12B).

Figure 4.9 shows the coexistence and the spatial variation of wave and fluvial influence along the same paleoshoreline within the same parasequence. Although the overall tidal proportion is insignificant quantitatively (Fig. 4.11), tidal signature has also been observed (Fig. 4.13) and can be dominant locally. The existence of double mud drapes or coal chips in HCS sandstones could indicate deposition in a tide-influenced storm-dominated lower shoreface environment (*sensu* Ainsworth *et al.*, 2011; Fig. 4.13A and B), resulting from temporary tidal resonance (Willis & Gabel 2001; Legler *et al.*, 2014; Van Cappelle *et al.*, 2018). Coal chips may be transported into the lower shoreface by distributary channels, in which case the environment was storm dominated with the influence of tides and rivers.

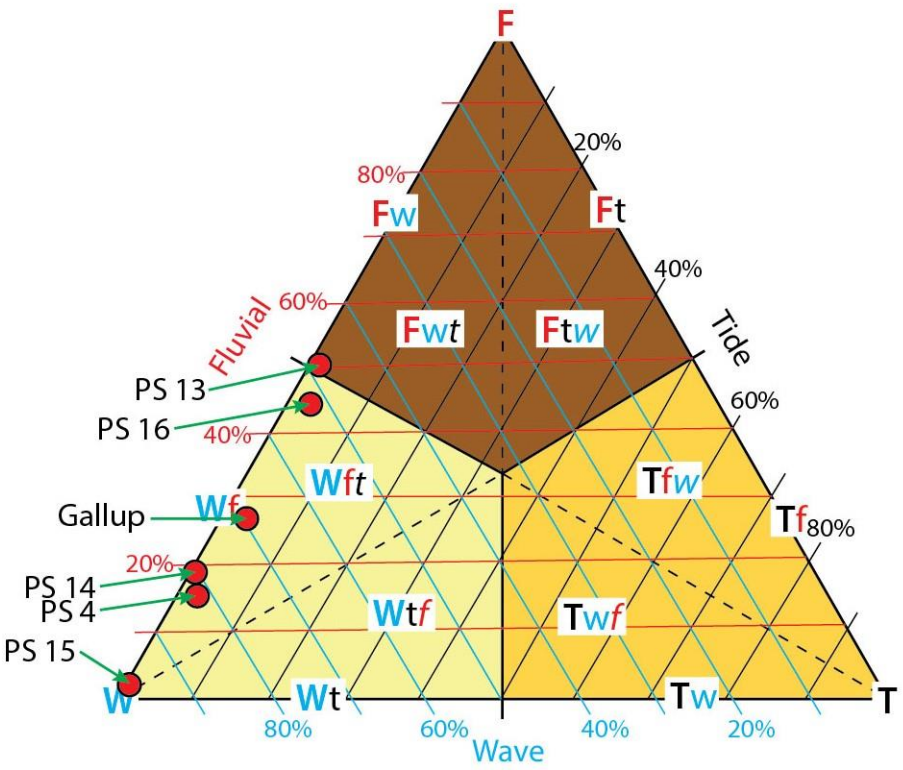

Fig. 4.11.–Upgraded tripartite classification of shallow marine depositional processes with various parasequence sets plotted on it (modified from Ainsworth *et al.*, 2011; the tripartite plot was originally from Galloway, 1977). Most parasequences of the Gallup system represent wave-dominated and mixed-process depositional environments.

An alternative interpretation could be deposition in a storm reworked tidally dominated environment (Dalrymple *et al.*, 2003; Van Cappelle *et al.*, 2018). The HCS has been documented in the intertidal zone of a tidal flat by Yang et al. (2008). The HCS can be generated by storms that were temporarily dominating and then overwhelmed by tidal influence after waning, draped by mud deposits. The mud-draped HCS sandstones may also infer a rapid storm reworking of proceeding tide-dominated delta deposits that allowed for preservation of the remnants of mud drapes.

Fig. 4.12.–Transition between delta and shoreface deposits. (A) An outcrop example showing vertical transition from a wave-dominated shoreface to a fluvial-dominated delta, and to a wave-dominated shoreface. The bottom part of the cliff shows shoreface deposits, and it then grades upward into deltaic deposits, which is subsequently overlain by shoreface deposits again. (B) Planview of the asymmetrical deltaic depositional model illustrating evolution from fluvial-dominated deltaic deposition to wave-dominated shoreface deposition, exemplified by (A) (modified from Bhattacharya & Giosan, 2003).

The double-mud-draped cross-bedding may represent tide-influenced wave-dominated shorefaces (Fig. 4.13C). Intense tidal reworking may modify wave-generated sedimentary structures (Legler *et al.*, 2014). Alternatively, it could be interpreted as the migration of subtidal bars (Boyles & Scott, 1982; Mellere & Steel, 2000; Willis & Gabel, 2001; Hampson *et al.*, 2008a). The preservation of tidal bar migration may reflect deposition in an environment protected from storm waves (Legler *et al.*, 2014).

The most common previous interpretations of the depositional environments of the Gallup are strandplains, barrier islands, and shorefaces. They are ubiquitously wave-generated with minimal influence of other processes. Based on McCubbin's (1982) paleogeographic analysis (his Fig. 48), Bhattacharya & Giosan (2003) speculated that the Gallup may represent an asymmetric deltaic system: the amalgamated beach ridges in the

southeast resemble the updrift sandy deposits, and the mud-dominated distributary plain represents the muddy downdrift. Our work further confirmed that the Gallup is a wave-dominated but strongly fluvial-influenced system (Fig. 4.11). The mixed processes of wave and river and the resulting paleogeography resemble the asymmetrical deltaic model (Fig. 4.9, 4.10; Bhattacharya & Giosan, 2003). The previous interpretations failed to address the mixed-process domination, partially because the lithostratigraphic correlation separated fluvial deposits from marine facies tracts (Nummedal & Molenaar, 1995). A new study on the sequence stratigraphy of the Gallup system has deciphered that some fluvial (Torrivio Member) and coastal deposits (Dilco Member) are synchronous to the Gallup age and coexist with Gallup marine facies (Lin *et al.*, in revision), indicating mixed depositional processes. Another key reason accounting for the misinterpretation may be ascribed to the fact that muddy and heterolithic successions below sand-dominated facies had received insufficient attention in previous studies. Those heterolithic successions record critical sedimentological and ichnological evidence to identify fluvial and tidal influence in areas below fair-weather wave base where shelf delivering mechanisms have a higher preservation potential (Bhattacharya & MacEachern, 2009; Dashtgard *et al.*, 2012).

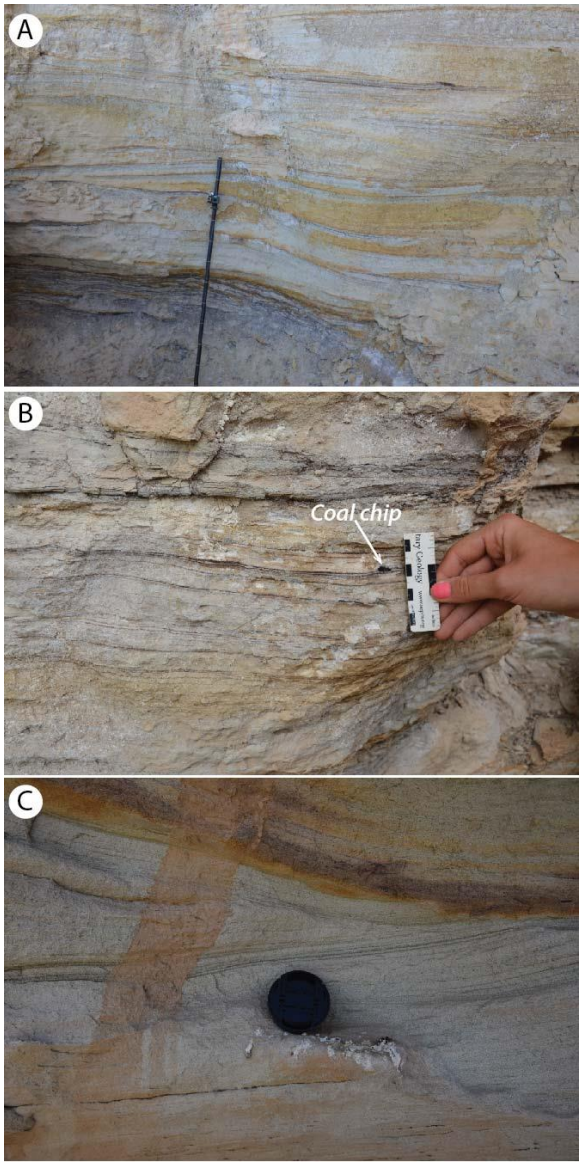

Fig. 4.13.–Photos showing examples of tidal influence. (A) Double mud drapes on very-fine-grained HCS sandstones showing tidal influence during storms (MS 0525). (B) Double mud drapes and coal chip co-existing with HCS indicating strong tidal and river's influence during Storms (MS 0730). (C) Double mud drapes on cross-bedded sandstones showing tidal influence (MS 0607).

4.7.3 Wave-dominated delta versus shoreface

The distinction of completely wave-generated non-deltaic shorefaces and wave-dominated delta deposits is controversial (Dominguez, 1996; Bhattacharya & Walker, 1992; Hampson & Howell, 2005). The recognition of the asymmetrical nature of strong wave-dominated deltas introduced more complication, in that shoreface deposits can be reworked from river mouth bars laterally and the updrift of deltas could be misinterpreted as non-deltaic shorefaces (Bhattacharya & Giosan, 2003). Although these two depositional environments are similar in some aspects: they are both wave-dominated and coarsening upward (Fig. 4.14); they both dip seaward as clinoforms and gradually transit into distal mudstone deposits, their depositional processes and characteristics are inherently different.

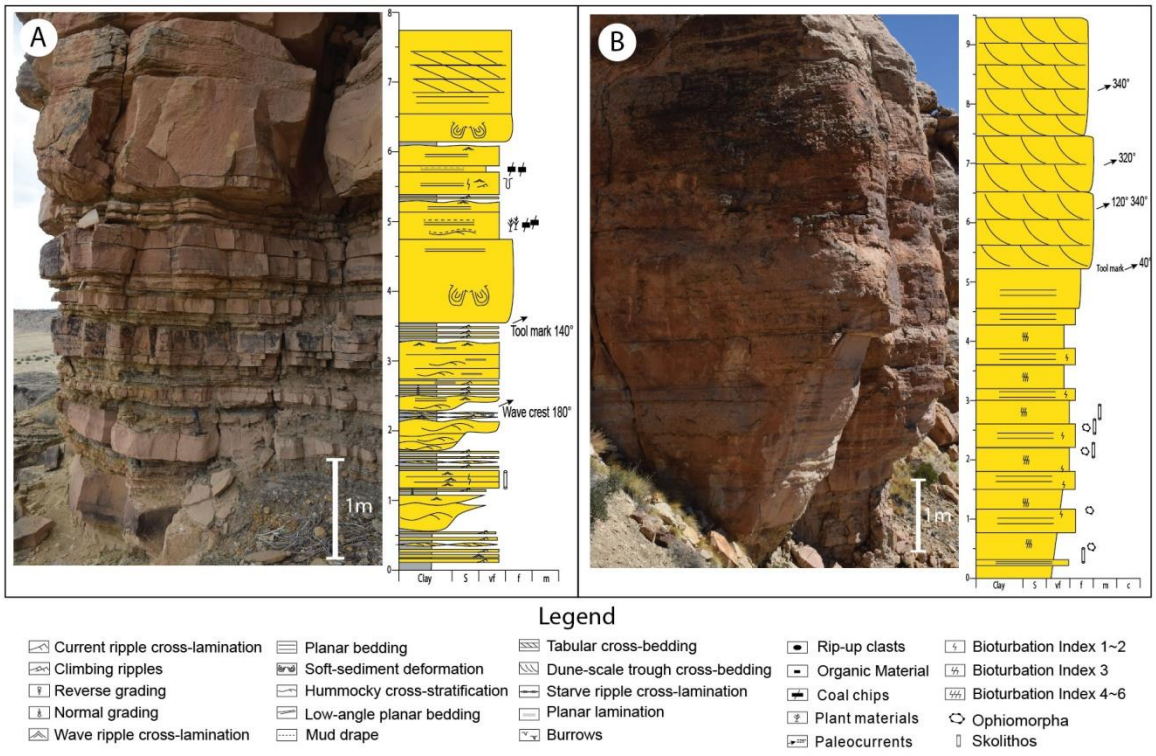

Fig. 4.14.–Two end-members of typical shoreline facies associations. (A) The fluvial-dominated and storm-influenced deltaic association (Parasequence 9b; MS 0726). (B) The wave-dominated and storm-influenced shoreface deposits (Parasequence 4e; MS 0713).

Shorefaces were extensively summarized as the deposits above fair-weather wave base (MacEachern & Pemberton, 1992; Walker & Plint 1992). The primary process in non-deltaic shorefaces is waves, either longshore currents or storms. Shorefaces are classified to storm-affected, storm-influenced, and storm-dominated, based on the intensity of storm waves (Dashtgard *et al.*, 2012). MacEarchern & Pemberton (1992) used a similar classification scheme to subdivide shorefaces into strongly storm-dominated (high energy), moderately storm-dominated (intermediate energy), and weakly storm-affected (low energy). The major sediment can be from multiple sources, either updrift or older delta deposits, or both. The vertical succession of non-deltaic shoreface is dominated by homogeneous sandstones with virtually no mudstones (Fig. 4.14B). The succession is interpreted to be formed by the amalgamation of beach ridges, above fair-weather wave base. Bioturbation intensity varies in a wide range, depending on storm severity. High BI (5-6) reflects unstressed conditions with minimal storm influence and slow sedimentation rates; low BI indicates stressed and erosive conditions as a result of storm waves, but needs to correspond to amalgamation of storm beds with HCS or SCS (MacEachern & Pemberton, 1992).

Deltas, on the other hand, are supposed to be built directly by or genetically associated with rivers, given their regressive nature (Bhattacharya, 2010). Even wave-dominated deltas must be fundamentally river influenced. Therefore, the definition has determined that deltas are singly sourced by their feeding rivers. In a wave-dominated

delta edifice, the sediment delivered by rivers has undergone significant wave reworking and been dispersed to the flanks of the river mouth, either symmetrically or asymmetrically, depending on wave strengths and directions (Bhattacharya & Giosan, 2003). Riverine sediment contains sand and mud; hence the lower part of a deltaic succession appears to be mudstone-dominated heterolithic (Fig. 4.14A). The proximity to the river mouth also allows for richness in terrestrial materials (debris of plant, coal, and wood). The absence of trace fossils indicates stressed conditions and high sedimentation rates in response to river's influence (MacEachern *et al.*, 2010).

Longshore currents can disperse sediment further away from river mouths and form sandy wave-dominated shorefaces or muddy chenier plains, resulting in lateral transitions from deltas to shorefaces. Similar lateral facies variations have been documented in both ancient and modern depositional systems (sensu asymmetrical delta model; Allison *et al.*, 2003; Bhattacharya & Giosan, 2003; Goodbred *et al.*, 2003; Giosan *et al.*, 2005, 2006; Hensen & MacEachern, 2007; Charvin *et al.*, 2010; Li *et al.*, 2011). We have also observed a similar transition in both vertical successions and paleogeographic reconstructions in the Gallup system. Figure 4.15 illustrates an outcrop example of such temporal and spatial facies variation. The left end of the outcrop shows a deltaic succession, in which the blocky sandstones at the top are interpreted as distributary channels and mouth bars, dipping and thinning rightward. The sandstones on the right side of the cliff are more homogeneous and less bedded than those on the left and thicken rightward, representing non-deltaic shoreface deposits. The shoreface onlaps onto the

delta edifice that reflects the transitional relationship and the lack of an intervening prodelta.

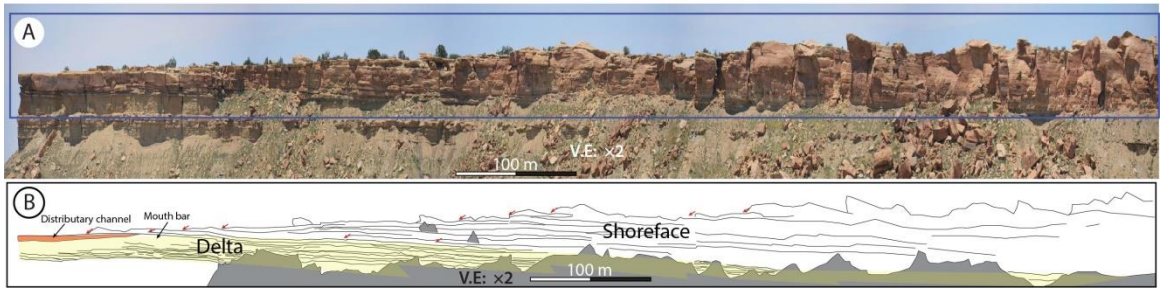

Fig. 4.15.–Photomosaic showing transition from a wave-dominated delta to a shoreface. (A) Outcrop cliff showing a lateral transition from the wave-dominated delta to the wave-formed shoreface. This photo was taken at the Rock Ridge point. Refer to Figure 4.10 for the photomosaic location. The blue box on (A) outlines the area of (B). (B) Bedding diagram illustrating internal facies architecture of the wave-dominate delta and shoreface. The yellow outline highlights the wave-dominated delta, and the white area represents the shoreface deposits. The shoreface onlaps onto the delta. Note the red arrows indicate onlapping points.

The paleogeographic map of Parasequence Set 4 of the upper Gallup system also illustrates the lateral facies variation (Fig. 4.10). Shorefaces are located on the southeast, and they transit into a river-dominated delta northwestward along the shoreline. The delta grades back into shorefaces further northwest. Based on the criteria discussed above, only the green triangle area of Figure 4.10 can be defined as deltas, and the yellow area is classified as shorefaces. Such lateral variation suggests an asymmetrical delta model (*sensu* Bhattacharya & Giosan, 2003) with downdrift deposits to the northwest and updrift deposits to the southwest. The longshore current can be implied to be northwest oriented, which is opposite to the counter-clockwise regional geostrophic current direction of the Western Interior Seaway (Erickson & Slingerland, 1990). The Gallup

system is the southernmost major clastic wedge along the west margin of the seaway and possesses a NW–SE oriented paleoshoreline (Fig. 4.1). Therefore, the Gallup system was influenced more by north-directed oceanic currents originating from the warm Tethys Sea and locally strengthened by the protection of a broad offshore bathymetric high (Leckie *et al.*, 1998). The NW–SE oriented shoreline may also have broken the prevailing southward waves and locally enhanced the northwestward longshore currents (Li *et al.*, 2018). Longshore currents with similar direction were also shown by McCubbin (1982).

Despite the domination of waves in shoreface deposition, it is unrealistic to deposit a thick and homogeneous upward-coarsening sandstone succession in the absence of the relatively high sediment supply basically derived from rivers (Hampson & Howell, 2005; Bhattacharya, 2010). However, if the criteria discussed above, such as point-source and low BI, cannot be met, the deposition may be distant enough from a river mouth to be interpreted as non-deltaic shorefaces rather than deltas in the strict sense (Bhattacharya, 2010). Also, based on planviews and paleographic maps of those modern (e.g., the Po, Paraiba do Sul, and Danube deltas) and ancient wave-dominated deltas, deltaic deposition generally presents protuberance to some extent in response to river influence (Fig. 4.9), as opposite to completely straight non-deltaic shorelines (e.g., the Nayarit coast; Clifton, 2006).

4.8 Conclusions

The Gallup system in NW New Mexico is one of the major progradational clastic wedges along the west margin of the Cretaceous Western Interior Seaway. The deposition of this

paralic depositional environment was controlled by a variety of processes and shows diverse environmental facies associations.

Five facies associations of the Gallup system have been identified, consisting of offshore shelf, shoreline sandstone, delta, coastal plain, and fluvial. These five depositional environmental facies associations can be further divided in to 16 lithofacies associations. The major facies are marine-dominated shoreline sandstones and offshore mudstones.

Genetic relationships between sequence stratigraphic systems tracts and facies associations show that particular facies are only favored in specific systems tracts. Only shelf, offshore transition, and lower shoreface are present in all four systems tracts. Upper shorefaces, foreshores, and delta plains are only formed in the HST. Coastal plain associations are not only observed in the TST but also the HST. Deltaic deposits are notably missing in the LST.

Paleogeographic reconstructions at parasequence scales depict depositional evolution in space and time, showing shoreline cyclic migration. The paleogeographic maps also show the dynamic mixed-process dominated deposition. Significant fluvial and tidal influence has been observed in association with wave and storm processes, contrasting previous interpretation of complete wave domination. Mudstone and heterolithic sections that represent distal facies below the wave base should be used to denote fluvial and tidal influence.

Vertical and lateral shoreline facies variations demonstrate transitions between deltaic and non-deltaic shoreface deposits. The distinction between shoreface and wave deltaic

sandstones has been clearly defined on the basis of key criteria, such as trace fossils and river input. Facies analysis also revealed an asymmetrical delta model in the Gallup system formed by locally enhanced clockwise longshore currents.

Acknowledgements

Thanks are given to Monica Wiercigroch, Sean Karner, and Andrew Stockford for their tremendous assistance in the field. We also would like to thank the Navajo Nation for permitting the field work and the Navajo people for allowing us to work on their lands. Funding for this project was generously supplied by NSERC Discovery Grant RPG IN05780-14 to Dr. Bhattacharya, by sponsors of the McMaster University Quantitative Sedimentology Laboratories (QSL) including BP and Inpex, and by the Susan Cunningham Research Chair in Geology. We also appreciate the AAPG "Martin D. Hewitt" Named Grant and the GSA Research Grant for their supports.

Field work on the Navajo Nation was conducted under a permit from the Navajo Nation Minerals Department. Any persons wishing to conduct geologic investigations on the Navajo Nation must first apply for, and receive, a permit from the Navajo Nation Minerals Department, P.O. Box 1910, Window Rock, Arizona 86515, and telephone number (928) 871-6587.

References

Ainsworth, R.B. and **Newall, M.J.** (1994) Forward stratigraphic modelling of foreced regressions: evidence for the genesis of attached and detached lowstand systems. In: *Sedimentary Responses to Forced Regressions* (Eds D. Hunt and R.L. Gawthorpe), *Geol. Soc. London Spec. Publ.*, **172,** 163–176.

Ainsworth, R.B. and **Pattison, S.A.J.** (1994) Where have all the lowstands gone? Evidence for attached lowstand systems tracts in the Western Interior of North America. *Geology,* **22,** 415–418.

Ainsworth, R.B., Flint,S.S. and **Howell, J.A.** (2008) Predicting coastal depositional style: influence ofbasin morphology and accommodation to sediment supply ratio within a sequence-stratigraphic framework. In *Recent Advances in Models of Shallow-Marine Stratigraphy* (Eds G.J. Hampson, R.J. Steel, P.M. Burgess, and R. W. Dalrymple), *SEPM Spec. Publ.,* **90,** 237–263.

Ainsworth, R.B., Vakarelov, B.K., and **Nanson, R.A.** (2011) Dynamic spatial and temporal prediction of changes in depositional processes on clastic shorelines: toward improved subsurface uncertainty reduction and management. *AAPG Bull.,* **95,** 267–297.

Allison, M.A., Kahn, S.R., Goodbred, S.L.Jr. and **Kuehl, S.A.** (2003) Stratigraphic evolution of the late Holocene Ganges–Brahmaputra lower delta plain. *Sed. Geol.,* **155,** 317–342.

Anderson, J.B., Rodriguez, A., Abdulah, K.C., Fillon, R.H., Banfield, L.A., McKeown, H.A. and **Wellner, J.S.** (2004) In: *Late Quaternary Stratigraphic Evolution of the Northern Gulf of Mexico Margin* (Eds J.B. Anderson and R.H. Fillon), *SEPM Spec. Publ.,* **79,** 1–23.

Anthony E.J. and **Orford, J.D.** (2002) Between wave- and tide-dominated coasts: The middle ground revisited. *J. Coastal Res.,* **36,** 8–15.

Aschoff, J.L., Olariu, C. and **Steel, R.J.** (2018) Recognition and significance of bayhead delta deposits in the rock record: a comparison of modern and ancient systems. *Sedimentology,* **65,** 62–95.

Bergman, K.M. and **Walker, R.G.** (1995) High-resolution sequence stratigraphic analysis of the Shannon Sandstone in Wyoming, using a template for regional correlation. *J. Sed. Res.,* **65,** 255–264.

Bhattacharya, J.P. (1993) The expression and interpretation of marine flooding surfaces and erosional surfaces in core; examples from the Upper Cretaceous Dunvegan Formation, Alberta foreland basin, Canada. In: *Sequence Stratigraphy and Facies Associations* (Eds H.W. Posamentier, C.P. Summerhayes, B.U. Haq and G.P. Allen), *Int. Assoc. Sedimentol. Spec. Publ.,* **18,** 125–160.

Bhattacharya, J.P. (2010) Deltas. In: *Facies Models 4* (Eds N.P. James and R.W. Dalrymple), *Geol. Assoc. Can., GEOtext,* **6,** 233–264.

Bhattacharya, J.P. and **Giosan, L.** (2003) Wave-influenced deltas: geomorphological implications for facies reconstruction. *Sedimentology,* **50,** 187–210.

Bhattacharya, J.P. and **MacEachern, J.A.** (2009) Hyperpycnal rivers and prodeltaic shelves in the Cretaceous Seaway of North America. *J. Sed. Res.,* **79,** 184–209.

Bhattacharya, J.P. and **Walker, R.G.** (1991) River-and wave-dominated depositional systems of the Upper Cretaceous Dunvegan Formation, northwestern Alberta. *Bull. Can. Petrol. Geol.,* **39,** 165-191.

Bhattacharya, J.P. and **Walker, R.G.** (1992) Deltas. In: *Facies Models: Response to Sea-Level Change* (Eds R.G. Walker and N.P. James), *Geol. Assoc. Can., GEOtext,* **1,** 157–177.

Bhattacharya, J. P. and **Willis, B. J.** (2001) Lowstand deltas in the Frontier Formation, Powder River Basin, Wyoming: implications for sequence stratigraphic models. *AAPG bull.,* **85,** 261–294.

Bilodeau, W.L. (1986) The Mesozoic Mogollon Highlands, Arizona: an Early Cretaceous rift shoulder. *The J. of Geol.,* **94,** 724–735.

Blum, M.D. and **Tornqvist, T.E.** (2000) Fluvial responses to climate and sea-level change: a review and look forward. *Sedimentology,* **47,** 2–48.

Blum, M., Martin, J., Milliken K. and **Garvin M.** (2013) Paleovalley systems: Insights from Quaternary analogs and experiments, *Earth-Sci. Rev.,***116,** 128–169.

Boyd, R. (2010) Transgressive wave-dominated coasts. In: *Facies Models 4* (Eds N.P. James and R.W. Dalrymple), *Geol. Assoc. Can. GEOtext,* **6,** 265–294.

Boyd, R., Dalrymple, R. and **Zaitlin, B.A.** (1992) Classification of clastic coastal depositional environments. *Sed. Geol.*, **80,** 139–150.

Boyles, J.M. and **Scott, A.J.** (1982) A model for migrating shelf-bar sandstones in upper Mancos Shale (Campanian), northwestern Colorado. *AAPG Bull.,* 66, 491–508.

Burton, D., Flaig, P.P. and **Prather, T.J.** (2016) Regional controls on depositional trends in tidally modified deltas: insights from sequence stratigraphic correlation and mapping of the Loyd and Sego Sandstones, Uinta and Piceance Basins of Utah and Colorado, USA. *J. Sed. Res.,* **86,** 763–785.

Campbell, C.V. (1971) Depositional model-upper Cretaceous Gallup beach shoreline, Ship Rock area, northwestern New Mexico. *J. Sed. Petro.* **41,** 395–409.

Campbell, C.V. (1973) Offshore equivalents of Upper Cretaceous Gallup Beach Sandstones, northwestern New Mexico. In: *Cretaceous and Tertiary Rocks of the SOuthern Colorado Plateau* (Ed J.E. Fassett), *Four Corners Geological Society Memoir Book*, 78–84.

Campbell, C.V. (1979) Model for beach shoreline in Gallup Sandstone (Upper Cretaceous) of northwestern New Mexico. In: *Circular 164, New Mexico Bureau of Mines & Mineral Resources.* pp. 1–32.

Charvin, K., Hampson, G.J. and **Gallagher, K.L.** (2010) Intra-parasequence architecture of an interpreted asymmetrical wave-dominated delta. *Sedimentology*, **57,** 760–785.

Clifton, H.E. (2006) A re-examination of facies models for clastic shorelines. In *Facies Models Revisited* (Eds. H.W. Posamentier and R.G. Walker), *SEPM, Spec. Publ.,* **84,** 293–337.

Clifton, H.E., Hunter, R.E. and **Phillips, R.L.** (1971) Depositional structures and processes in the non-barred high-energy nearshore. *J. Sed. Res.,* **41,** 651-670.

Coates, L. and **MacEachern, J.A.** (2009) The ichnological signatures of river- and wave-dominated delta complexes: differentiating deltaic and non-deltaic shallow marine successions, lower Cretaceous Viking Formation and upper Cretaceous Dunvegan Formation, west-central Alberta. In: *Applied Ichnology* (Eds J.A.

MacEachern, K.L. Bann, M.K. Gingras, and S.G. Pemberton), *SEPM, Short Course Notes,* **52,** 237–254.

Copeland, P., Currie, C.A., Lawton, T.F., and **Murphy, M.A.** (2017) Location, location, location: the variable lifespan of the Laramide Orogeny. *Geology,* **45,** 223–226.

Curray, J.R., Emmel, F.J. and **Crampton, P.J.S.** (1969) Holocene history of a strand plain, lagoonal coast, Nayarit, Mexico. In: *Coastal Lagoons, a Symposium* (Eds A.A. Castañares and F.B. Phleger), pp. 63–100. University Nacional Autonoma Mexico–UNESCO, Mexico.

Dalrymple, R.W. (2010) Interpreting sedimentary successions: facies, facies analysis and facies models. In *Facies Models 4* (Eds N.P. James and R.W. Dalrymple), *Geol. Assoc. Can. GEOtext,* **6,** 3–18.

Dalrymple, R.W. and **Choi, K.** (2007) Morphologic and facies trends through the fluvial-marine transition in tide- dominated depositional systems: a schematic framework for environmental and sequence-stratigraphic interpretation. *Earth-Sci. Rev.,* **81,** 35–174.

Dalrymple, R.W. and **Rhodes, R.N.** (1995) Estuarine dunes and bars. In *Geomorphology and Sedimentology of Estuaries* (Eds G.M.E. Perillo), *Amsterdam, Elsevier,* 359–422.

Dalrymple, R.W., Zaitlin, B.A. and **Boyd, R.** (1992) Estuarine facies models; conceptual basis and stratigraphic implications. *J. Sed. Res.,* **62,** 1130–1146.

Dalrymple, R.W., Baker, E.K., Harris, P.T., and **Hughes, M.G.** (2003) Sedimentology and stratigraphy of a tide-dominated foreland-basin delta (Fly River, Papua New Guinea). In: *Tropical Deltas of Southeast Asia: Sedimentology, Stratigraphy, and Petroleum Geology* (Eds F.H. Sidi, D. Nummedal, P. Imbert, H. Darman and H.W. Posamentier), *SEPM Spec. Publ.*, **76,** 147–173.

Dashtgard, S.E., Maceachern, J.A., Frey, S.E., and Gingras, M.K. (2012). Tidal effects on the shoreface : Towards a conceptual framework. *Sedimentary Geology* 279, 42–61.

Decelles, P.G. (2004). Late Jurassic to Eocene evolution of the Cordilleran thrust belt and foreland basin system, western USA. *Am. J. Sci.,* **304,** 105–168.

Dickinson, W.R. and **Lawton, T.F.** (2001) Tectonic setting and sandstone petrofacies of the Bisbee basin (USA–Mexico). *J. S. Am. Earth Sci.,* **14,** 475–504.

Dickinson, W.R. and **Gehrels, G.E.** (2008) Sediment delivery to the Cordilleran foreland basin: insights from U-Pb ages of detrital zircons in Upper Jurassic and Cretaceous strata of the Colorado Plateau. *Am. J. Sci.,* **308,** 1041–1082.

Dominguez, J.M.L. (1996) The São Francisco strandplain: a paradigm for wave-dominated deltas? In: *Geology of Siliciclastic Shelf Seas* (Eds M. De Baptist and P. Jacobs), *Geol. Soc. London Spec. Publ.*, **117,** 217–231.

Dott, R.H. and **Bourgeois, J.** (1982) Hummocky stratification: significance of its variable bedding sequences. *Geol. Soc. Am. Bull.*, **93,** 663–680.

Duke, W.L. (1985) Hummocky cross-stratification, tropical hurricanes, and intense winter storms. *Sedimentology,* **32,** 167–194.

Duke, W.L., Arnott, R.W.C. and **Cheel, R.J.** (1991) Shelf sandstones and hummocky cross-stratification: new insights on a stormy debate. *Geology*, **19,** 625–628.

Dumas, S. and **Arnott, R.W.C.** (2006) Origin of hummocky and swaley cross-stratification - The controlling influence of unidirectional current strength and aggradation rate. *Geology*, **34,** 1073–1076.

Erickson, M.C. and **Slingerland, R.** (1990) Numerical simulations of tidal and wind-driven circulation in the Cretaceous Interior Seaway of North America. *Geol. Soc. Am. Bull.*, **102,** 1499–1516.

Fitzsimmons,R. and Johnson, S. (2000) Foreced regressions: recognition, architecture and genesis in the Campanian of the Bighorn Basin, Wyoming. In: *Sedimentary Responses to Forced Regressions* (Eds D. Hunt and R.L. Gawthorpe), *Geol. Soc. London Spec. Publ.*, **172,** 113–162.

Fricke, H.C., Foreman, B.Z. and **Sewall, J.O.** (2010) Integrated climate model-oxygen isotope evidence for a North American monsoon during the Late Cretaceous. *Earth Planet. Sci. Lett.*, **289,** 11–21.

Galloway, W.E. (1975) Process framework for describing the morphologic and stratigraphic evolution of deltaic deposi- tional systems. In: *Deltas, Models for Exploration* (Ed. M.L. Broussard), Houston Geological Society, Houston. 87–98.

Giosan, L., Donnelly, J.P., Vespremeanu, E.I. and **Buonaiuto, F.S.** (2005) River delta morphodynamics: examples from the Danube delta. In: *River Deltas—Concepts, Models, and Examples* (Eds L. Giosan and J.P. Bhattacharya), *SEPM Spec. Publ.*, **83,** 87–132.

Giosan, L., Constantinescu, S., Clift, P.D., Tabrezd, A.R., Danish, M., and **Inam, A.** (2006) Recent morphodynamics of the Indus delta shore and shelf. *Cont. Shelf Res.,* **26,** 1668–1684.

Gomez-Veroiza, C.A. and **Steel, R.J.** (2010) Iles clastic wedge development and sediment partitioning within a 300-km fluvial to marine Campanian transect (3 m.y.), Western Interior Seaway, southwestern Wyoming and northern Colorado. *AAPG Bull.,* **94,** 1349–1377.

Goodbred, S.L, Jr., Kuehl, S.A., Steckler, M.S. and **Sarker, M.H.** (2003) Controls on facies distribution and stratigraphic preservation in the Ganges–Brahmaputra delta sequence. *Sed. Geol.,* **155,** 301–316.

Hampson, G.J. and **Howell, J.A.** (2005) Sedimentologic and geomorphic characterization of ancient wave-dominated deltaic shorelines: Upper Cretaceous Blackhawk Formation, Book Cliffs, Utah, USA. In: *River Deltas–Concepts, Models, and Examples* (Eds L. Giosan and J.P. Bhattacharya), *SEPM Spec. Publ.,* **83,** 131–154.

Hampson, G.J. and **Storms, J.E.A.** (2003) Geomorphological and sequence stratigraphic variability in wave-dominated, shoreface-shelf parasequences. *Sedimentology*, **50,** 667–701.

Hampson, G.J., Procter, E.J., and **Kelly, C.** (2008a) Controls on isolated shelf sandstone ridges in the Cretaceous Western Interior Seaway, northern Utah and Colorado, USA. In: *Recent Advances in Models of Siliciclastic Shallow-Marine*

Stratigraphy (Eds G.J. Hampson, R.J. Steel, P.M. Burgess, and R.W. Dalrymple), *SEPM Spec. Publ.*, **90,** 355–390.

Hampson, G.J., Rodriguez, A.B., Storms, J.E.A., Johnson, H.D., and **Meyer, C.T.** (2008b) Geomorphology and high-resolution stratigraphy of progradational wave-dominated shoreline deposits: impact on reservoir-scale facies architecture. In: *Recent advances in models of siliciclastic shallow-marine stratigraphy* (Eds G.J. Hampson, R.J. Steel, P.M. Burgess, and R.W. Dalrymple), *SEPM Spec. Publ.*, **90,** 117–142.

Hampson, G.J., Gani, M.R., Sharman, K.E., Irfan, N. and **Bracken, B.** (2011) Along-strike and down-dip variations in shallow-marine sequence stratigraphic architecture: Upper Cretaceous Star Point Sandstone, Wasatch Plateau, Central Utah, U.S.A. *J. Sed. Res.*, **81,** 159–184.

Hansen, C.D. and **MacEachern, J.A.** (2007) Application of the asymmetric delta model to along-strike facies variation in a mixed wave- and river-influenced delta lobe, Upper Cretaceous Basal Belly River Formation, Central Alberta. In: Applied Ichnology (Eds J.A. MacEachern, K.L. Bann, M.K. Gingras and S.G. Pemberton), *SEPM Short Course Notes,* **52,** 256–269.

Haq, B.U. (2014) Cretaceous eustasy revisited. *Global Planet. Change,* **113,** 44–58.

Harris, P.T., Heap, A.D., Bryce, S.M., Porter-Smith, R., Ryan, D.A. and **Heggie, D.T.** **(**2002) Classification of Australian clastic coastal depositional environments based upon a qualitative analysis of wave, tidal, and river power. *J. Sed. Res.*, **72,** 858–870.

Hay, W.W. and Floegel, S. (2012) New thoughts about the Cretaceous climate and oceans. *Earth-Sci. Rev.,* **115,** 262–272.

Hein, C.J., Fitzgerald, D.M., Cleary, W.J., Albernaz, M.B., Thadeu de Menezes, J. and Klein, A.H.D.F. (2013) Evidence for a transgressive barrier within a regressive strandplain system: Implications for complex coastal response to environmental change. *Sedimentology,* **60,** 469–502.

Helland-Hansen, W. and **Martinsen, O.J.** (1996) Shoreline trajectories and sequences; description of variable depositional-dip scenarios. *J. Sed. Res.,* **66,** 670–688.

Holbrook, J., Scott, R.W. and **Oboh-Ikuenobe, F.E.** (2006) Base-level buffers and buttresses: a model for upstream versus downstream control on fluvial geometry and architecture within sequences. *J. Sed. Res.,* **76,** 162–174.

Jones, C.R., Van Wagoner, J.C., Jennette, D.C., Nummedal, D. and **Riley, G.W.** (1991) Road log, day six: sequence stratigraphy and facies architecture of the Torrivio and Tocito sandstones Near Beautiful Mountain, Four Corners Platform, Northwestern New Mexico. In: *Sequence Stratigraphy Applications to Shelf Sandstone Reservoirs: Outcrop to Subsurface Examples* (Eds J.C. Van Wagoner, C.R. Jones, D.R. Taylor, D. Nummedal, D.C. Jennette, G.W. Riley), *AAPG Spec. Publ.,***25,** 1–39.

Jones, M.T., Dashtgard, S.E. and **Maceachern, J.A.** (2018) A conceptual model for the preservation of thick, transgressive shoreline successions: examples from the forearc Nanaimo Basin, British Columbia, Canada. *J. Sed. Res.,* **88,** 811–826.

Kamola, D.L. and **Wagoner, J.C.** (1995) Stratigraphy and facies architecture of parasequences with examples from the Spring Canyon Member, Blackhawk Formation, Utah. In *Sequences Stratigraphy of Foreland Basin Deposits* (Eds J.C. Van Wagoner and G.T. Bertram), *AAPG Mem.*, **64,** 27–54.

Kauffman, E.G. (1977) Geological and biological overview: Western Interior Cretaceous basin. *The Mt. Geol.*, **14,** 75–99.

Kauffman, E.G. and **Caldwell, W.G.E.** (1993) The Western Interior Basin in space and time. In: *Evolution of the Western Interior Basin* (Eds W.G.E. Caldwell and E.G. Kauffman), *Geol. Assoc. Can. Spec. Pap.*, **39,** 1–30.

Lawton, T.F. and **Bradford, B.A.** (2011) Correlation and provenance of Upper Cretaceous (Campanian) fluvial strata, Utah, USA, from zircon U-Pb geochronology and petrography. *J. Sed. Res.*, **81,** 495–512.

Lawton, T.F., Pollock, S.L. and **Robinson, R.A.J.** (2003) Integrating sandstone petrology and nonmarine sequence stratigraphy: application to the Late Cretaceous fluvial systems of southwestern Utah, USA. *J. Sed. Res.*, **73,** 389–406.

Lawton, T.F., Schellenbach, W.L. and **Nugent, A.E.** (2014) Late Cretaceous fluvial-megafan and axial-river systems in the Southern Cordilleran Foreland Basin: Drip Tank Member of Straight Cliffs Formation and adjacent strata, southern Utah, USA. *J. Sed. Res.*, **84,** 407–434.

Leckie, R.M., Yuretich, R.F., West, O.L.O., Finkelstein, D. and **Schmidt, M.** (1998) Paleoceanography of the Southwestern Western Interior Sea During the Time of the Cenomanian-Turonian Boundary (Late Cretaceous). In: *Stratigraphy and*

Paleoenvironments of the Cretaceous Western Interior Seaway, USA (Eds W.E. Dean and M.A. Arthur), *SEPM Concepts In Sedimentology And Paleontology,* **6,** 101–126.

Leclair, S.F. and **Bridge, J.S.** (2001**)** Quantitative interpretation of sedimentary structures formed by river dunes. *J. Sed. Res.*, **71,** 713–716.

Legler, B., Hampson, G.J., Jackson, C.A., Johnson, H.D., Massart, B.Y.G., Sarginson, M. and **Ravnas, R.** (2014) Facies Relationships and Stratigraphic Architecture of Distal, Mixed Tide- and Wave-Influenced Deltaic Deposits: Lower Sego Sandstone, Western Colorado, U.S.A. *J. Sed. Res.*, **84,** 605–625.

Leva Lopez, J. and **Steel, R.J.** (2015) Laramide signals and architecture of a widespread fluvial sand sheet: Canyon Creek Member, Southern Wyoming, USA. *J. Sed. Res.*, **85,** 1102–1122.

Li, W., Bhattacharya, J.P., Zhu, Y., Garza, D. and **Blankenship, E.** (2011) Evaluating delta asymmetry using three-dimensional facies architecture and ichnological analysis, Ferron 'Notom Delta', Capital Reef, Utah, USA. *Sedimentology*, **58,** 478–507.

Li, Y., Bhattacharya, J.P., Ahmed, S. and **Garza, D.** (2018) Re-evaluating the paleogeography of the river-dominated and wave-influenced Ferron Notom Delta, Southern Central Utah: an Integration of detailed facies-architecture and paleocurrent analysis. *J. Sed. Res.*, **88,** 214–240.

Li, Z. and **Schieber, J.** (2018) Detailed facies analysis of the Upper Cretaceous Tununk Shale Member, Henry Mountains Region, Utah: implications for mudstone depositional models in epicontinental seas. *Sed.Geol.,* , **364,** 141–159.

Lin, W., Bhattacharya, J.P. and **Stockford, A.** (2018) High-resolution sequence stratigraphy of the Late Cretaceous Gallup system, New Mexico, U.S.A. *J. Sed. Res.,* in review.

Liu, S. and **Nummedal, D.** (2004) Late Cretaceous subsidence in Wyoming: quantifying the dynamic component. *Geology*, **32,** 397–400.

LoParco, M.D. (2011) Application of the asymmetric wave-influenced delta model to the Cretaceous Gallup Sandstone in Shiprock, New Mexico, [MS thesis]: University of Houston, 68 p.

MacEachern, J.A. and **Bann, K.L.** (2008) The role of ichnology in refining shallow marine facies models. In: *Recent Advances in Models of Siliciclastic Shallow-Marine Stratigraphy* (Eds G.J. Hampson, R.J. Steel, P.M. Burgess and R.W. Dalrymple), *SEPM Spec. Publ.,* **90,** 73–116.

MacEachern, J. A. and **Pemberton, S. G.** (1992) Ichnological aspects of Cretaceous shoreface successions and shoreface variability in the Western Interior Seaway of North America. In: *Application of Ichnology to Petroleum Exploration, A Core Workshop* (Ed. S.G. Pemberton), *SEPM Core Workshop*, **17,** 57–84.

MacEachern, J.A., Zaitlin, B. and **Pemberton, S.G.** (1999) A sharp-based sandstone of the Viking Formation, Joffre Field, Alberta, Canada: criteria for recognition of transgressively incised shoreface complexes. *J. Sed. Res.,* **69,** 876–892.

MacEachern, J.A., Pemberton, S.G., Gingras, M.K., Bann, K.L., James, N.P. and **Dalrymple, R.W.** (2010). Ichnology and facies models. In: *Facies models 4* (Eds N.P. James and R.W. Dalrymple), *Geol. Assoc. Can. GEOtext,* **6,** 19–58.

McCubbin, D.J. (1982) Barrier-island and strand-plain facies. In: *Sandstone Depositional Environments* (Eds P.A. Scholle and D. Spearing), *AAPG Mem.* **31,** 247–279.

Mellere, D. and **Steel, R.J.** (2000) Style contrast between forced regressive and lowstand/ transgressive wedges in the Campanian of south-central Wyoming (Hatfield Member of the Haystack Mountains Formation). In: *Sedimentary Responses to Forced Regression* (Eds D. Hunt and R.L. Gawthorpe), *Geol. Soc. Lon. Spec. Publ.,* **172,** 141–162.

Miall, A.D. (1992) Sedimentology of a sequence boundary within the nonmarine Torrivio Member, Gallup Sandstone (Cretaceous), San Juan Basin, New Mexico. In *The Three-Dimensional Facies Architecture of Terrigenous Clastic Sediments and its Implications for Hydrocarbon Discovery and Recovery* (Eds A.D. Miall and N. Tyler), *SEPM Spec. Publ.,* **3,** 224–232.

Miall, A.D. (2014) The facies and architecture of fluvial systems. *Fluvial Depositional Systems, Springer, Cham*, 9–68.

Midtgaard, H.H. (1996) Inner-shelf to lower-shoreface hummocky sandstone bodies with evidence for geostrophic influenced combined flow, Lower Cretaceous, West Greenland. *J. Sed. Res.,* **66,** 343–353.

Mitchum, R.M. and **Van Wagoner, J.C.** (1991) High-frequency sequences and their stacking patterns: sequence-stratigraphic evidence of high-frequency eustatic cycles. *Sed. Geol.,* **70,** 131–160.

Molenaar, C.M. (1973) Sedimentary facies and correlation of the Gallup Sandstone and associated. In: *Cretaceous and Tertiary Rocks of the SOuthern Colorado Plateau* (Ed J.E. Fassett), *Four Corners Geological Society Memoir Book,* 85–110.

Molenaar, C.M. (1983) Major depositional cycles and regional correlations of Upper Cretaceous rocks, southern Colorado Plateau and adjacent areas. In: *Mesozoic Paleogeography of the West-Central United States* (Eds M.W. Reynolds and E.D. Dolly), *SEPM Rocky Mountain Symposium,* **2,** 201–224.

Mulder, T., Syvitski, J.P., Migeon, M.S., Faugères, J.C. and **Savoye, B.** (2003) Marine hyperpycnal flows: initiation, behavior and related deposits: A review. *Mar. Petrol. Geol.,* **20,** 861–882.

Neal, J. and Abreu, V. (2009) Sequence stratigraphy hierarchy and the accommodation succession method. *Geology,* **37,** 779–782.

Nielsen, L.H. and **Johannessen, P.N.** (2008) Are some isolated shelf sandstone ridges in the Cretaceous Western Interior Seaway transgressed, detached spit systems? In *Recent Advances in Models of Shallow-Marine Stratigraphy* (Eds G.J. Hampson, R.J. Steel, P.M. Burgess, and R. W. Dalrymple), *SEPM Spec. Publ.,* **90,** 333–354.

Nummedal, D. and **Molenaar, C.M.** (1995) Sequence stratigraphy of ramp-setting strand plain successions: the Gallup Sandstone, New Mexico. In *Sequences Stratigraphy*

of Foreland Basin Deposits (Eds J.C. Van Wagone and G.T. Bertram), *AAPG Mem.,* **64**, 277–310.

Nummedal, D., Wright, R., Swift, D.J., Tillman, R.W. and **Wolter, N.R.** (1989) Depositional systems architecture of shallow marine sequences. In *Cretaceous Shelf Sandstones and Shelf Depositional Sequences, Western Interior Basin, Utah, Colorado and New Mexico: Salt Lake City, Utah to Albuquerque, New Mexico, June 30-July 7, 1989* (Eds D. Nummedal and R.R. Remy), *International Geological Congress, Am. Geophys. Union, Guidebook to Field Trip,* **T119,** 35–80.

Olariu, C. and **Bhattacharya, J.P.** (2006) Terminal distributary channels and delta front architecture of river-dominated delta systems. *J. Sed. Res.,* **76,** 212–233.

Olariu, C., Steel, R.J. and **Petter, A.L.** (2010) Delta-front hyperpycnal bed geometry and implications for reservoir modeling: Cretaceous Panther Tongue delta, Book Cliffs, Utah. *AAPG Bull.,* **94,** 819–845.

Olsen, T.R., Mellere, D. and **Olsen, T.** (1999) Facies architecture and geometry of landward-stepping shoreface tongues: the Upper Cretaceous Cliff House Sandstone (Mancos Canyon, south-west Colorado). *Sedimentology,* **46,** 603–625.

Pemberton, S.G., Maceachern, J.A. and **Frey, R.W.** (1992) Trace fossil facies models: environmental and allostratigraphic significance. In *Facies Models; Response to Sea-Level Change* (Eds R.G. Walker, and N.P. James), *Geol. Assoc. Can., GEOtext,* **1,** 47–72.

Peng, Y., Steel, R.J. and Rossi, V.M. (2018) Mixed-energy process interactions read from a compound-clinoform delta (paleo-Orinoco Delta, Trinidad): preservation of river and tide signals by mud-induced wave damping. *J. Sed. Res.,* **88,** 75–90.

Plink-Björklund, P. (2008) Wave-to-tide process change in a Campanian Shoreline Complex, Chimney Rock Tongue, Wyoming/Utah. In: *Recent Advances in Models of Siliciclastic Shallow-Marine Stratigraphy* (Eds G.J. Hampson, R.J. Steel, P.M. Burgess and R.W. Dalrymple), *SEPM Spec. Publ.,* **90,** 265–291.

Plint, A.G. (1988) Sharp-based shoreface sequences and 'offshore bars' in the cardium formation of alberta: their relationship to relative changes in sea level. In: *Sea-Level Changes: An Integrated Approach* (Eds C.K. Wilgus, B.S. Hastings, C.A. Ross, H. Posamentier, J.C.G. Van Wagoner and St. C. Kendall), *SEPM Spec. Publ.*, **42.** 357–370.

Plint, A. G. and **Nummedal, D.** (2000) The falling stage systems tract: recognition and importance in sequence stratigraphic analysis. *Geol. Soc. London Spec. Publ.,* **172,** 1–17.

Plint, A. G. and **Wadsworth, J. A.** (2003) Sedimentology and palaeogeomorphology of four large valley systems incising delta plains, western Canada Foreland Basin: implications for mid-Cretaceous sea-level changes. *Sedimentology,* **50,** 1147–1186.

Pontén, A. and **Plink-Björklund, P.** (2009) Process regime changes across a regressive to transgressive turnaround in a shelf-slope basin, Eocene Central Basin of Spitsbergen. *J. Sed. Res.,***79,** 2–23.

Porebski, S.J. and **Steel, R.J.** (2006) Deltas and sea-level change. *J. Sed. Res.,* **76,** 1–14.

Posamentier, H.W. and **Vail, P.R.** (1988) Eustatic controls on clastic deposition II-sequence and systems tract models. In: *Sea-Level Changes: An Integrated Approach* (Eds C.K. Wilgus, B.S. Hastings, C.A. Ross, H. Posamentier, J. C.G.Van Wagoner and St. C. Kendall), *SEPM Spec. Publ.,* **42.**125–154.

Rossi, V.M. and **Steel, R.J.** (2016) The role of tidal, wave and river currents in the evolution of mixed-energy deltas: example from the Lajas Formation (Argentina). *Sedimentology,* **63**, 824–864.

Rossi, V.M., Perillo, M.M., Steel, R.J. and **Olariu, C.** (2017) Quantifying mixed-process variability in shallow-marine depositional systems: what are sedimentary structures really telling us? *J. Sed. Res.,* **87,** 1–15.

Staub, J.R. and **Gastaldo, R.A.** (2003) Late Quaternary sedimentation and peat development in the Rajang river delta, Sarawak, east Malaysia. In: *Tropical Deltas of Southeast Asia - Sedimentology, Stratigraphy, and Petroleum Geology* (Eds F. Hasan Sidi, D. Nummedal, P. Imbert, H. Darman and H. Posamentier), *SEPM Spec. Publ.,* **76,** 71–78.

Swift, D.J.P., Figueiredo Jr., A.C., Freeland, G.L. and **Oertel, G.F.** (1983) Hummocky cross-stratification and megaripples: a geological double standard. *J. Sed. Petrol.,* **53,** 1295–1317.

Szwarc, T.S., Johnson, C.L., Stright, L.E. and **Mcfarlane, C.M.** (2015) Interactions between axial and transverse drainage systems in the Late Cretaceous Cordilleran foreland basin: evidence from detrital zircons in the Straight Cliffs Formation, southern Utah, USA. *Geol. Soc. Am. Bull.,* **127,** 372–392.

Taylor, A.M. and **Goldring, R.** (1993) Description and analysis of bioturbation and ichnofabric. *J. Geol. Soc.,* **150,** 141–148.

Van Cappelle, M., Stukins, S., Hampson, G.J. and **Johnson, H.D.** (2016) Fluvial to tidal transition in proximal, mixed tide-influenced and wave-influenced deltaic deposits: Cretaceous lower sego sandstone, Utah, USA. *Sedimentology,* **63,** 1333–1361.

Van Cappelle, M., Ravnås, R., Hampson, G.J. and **Johnson, H.D.** (2017) Depositional evolution of a progradational to aggradational, mixed-influenced deltaic succession: Jurassic Tofte and Ile formations, southern Halten Terrace, offshore Norway. *Mar. Petrol. Geol.*,**80,** 1–22.

Van Cappelle, M., Hampson, G.J. and **Johnson, H.D.** (2018) Spatial and temporal evolution of coastal depositional systems and regional depositional process regimes: Campanian Western Interior Seaway, U.S.A. *J. Sed. Res.,* **88,** 873–897.

Van Wagoner, J.C., Mitchum, R.M., Campion, K.M. and **Rahmanian, V.D.** (1990) Siliciclastic sequence stratigraphy in well logs, cores, and outcrops: concepts for high-resolution correlation of time and facies. *AAPG Methods Explor. Ser.,* **7,** 55.

Walker, R.G. and **Bergman, K.M.** (1993) Shannon sandstone in Wyoming: a shelf-ridge complex reinterpreted as lowstand shoreface deposits. *J. Sed. Petro.,* **63,** 839–851.

Walker, R.G. and **Plint, A.G.** (1992) Wave and storm dominated shallow marine system. In: *Facies Models: Response to Sea-Level Change* (Eds R.G. Walker and N.P. James), *Geol. Assoc. Can., GEOtext,* **1,** 219–238.

Walker, R.G., Duke, W.L. and **Leckie, D.A.** (1983) Hummocky stratification: significance of its variable bedding sequences: discussion. *Geol. Soc. Am. Bull*. **94,** 1245–1 249.

Whitaker, J.H.M. (1973) Gutter casts, a new name for scour-and-fill structures-with examples from the Llandoverian of Ringerike and Malmöya, Southern Norway. *Norsk Geologisk Tidsskr,* **53,** 403–417.

Willis, B.J. (2005) Deposits of tide-influenced river deltas. In *River Deltas: Concepts, Models, and Examples* (Eds L. Giosan and J.P. Bhattacharya), *SEPM, Spec. Publ.,* **83,** 87–129.

Willis, B.J. and **Gabel, S.** (2001) Sharp-based tide-dominated deltas of the Sego Sandstone, Book Cliffs, Utah, USA. *Sedimentology,* **48,** 479–506.

Wood, L.J. (2004) Predicting Tidal sand reservoir architecture using data from modern and ancient depositional systems. In: *Integration of Outcrop and Modern Analogs in Reservoirs Modelling* (Eds G.M. Grammer, P.M. Harris and G.P. Eberli), *AAPG Mem.,* **80,** 45–66.

Wright, L.D. (1977) Sediment transport and deposition at river mouths: a synthesis. *Geol. Soc. Am. Bull.,* **88,** 857–868.

Yang, B., Dalrymple, R.W., Chun, S., Johnson, M.F. and **Lee, H.** (2008) Tidally modulated storm sedimentation on open-coast tidal flats, southwestern coast of Korea: distinguishing tidal flat from shoreface deposits. In *Recent Advances in Models of Siliciclastic Shallow-Marine Stratigraphy* (Eds G.J. Hampson, R.J. Steel, P.M. Burgess, and R.W. Dalrymple), *SEPM Spec. Publ.,* **90,** 161–176.

Yonkee, W.A. and **Weil, A.B.** (2015) Tectonic evolution of the Sevier and Laramide belts within the North American Cordillera orogenic system. *Earth-Sci. Rev.*, **150,** 531–593.

Yoshida, S., Steel, R.J. and **Dalrymple, R.W.** (2007) Changes in depositional processes-an ingredient in a new generation of sequence-stratigraphic models. *J. Sed. Res.*, **77,** 447–460.

CHAPTER 5

CONCLUSIONS

5.1 Research Conclusion

The research in this dissertation has achieved the primary goals and provided remarkable contributions. All the proposed hypotheses have been successfully examined.

Chapter 2 quantified sediment budgets using the fulcrum approach with the assumption of the total mass balance in a S2S system. Ancient trunk rivers are considered to be the prominent fulcrum candidates, and their paleohydrologic parameters can be used to estimate paleodischarge and instantaneous sediment volumes passing through them. In a given depositional duration, the total volume of sediment transported by a trunk river should reflect the volume of sediment derived from the catchment, as well as that of sediment accumulated in the basin. The sediment quantification of Allomember E of the Upper Cretaceous Dunvegan Alloformation using the fulcrum approach shows such a matching relationship. A range of estimated values has been applied to respect the uncertainty. The upper-range estimate of sediment delivered to the sink is 2.5 times the measured sediment-sink volume and suggests sediment escape on the shelf or sediment sequestration inland.

In Chapter 3, high-resolution sequence stratigraphy is firstly applied to the Late Cretaceous Gallup system in the light of advanced sequence stratigraphic analytical tools. Using bentonites as regional datums, thirteen depositional sequences (six in the lower Gallup and seven in the upper Gallup), comprising twenty-six parasequence sets and sixty-one parasequences are identified in the Gallup system. FSST, LST, TST, and HST

are depicted in a depositional sequence using parasequence stacking patterns and key surface recognition. The established high-frequency sequence stratigraphic framework successfully deciphered the relationship between the previously defined lithostratigraphic units and sequence stratigraphy and revealed the diachroneity of the lithostratigraphic members. The associated quantitative shoreline trajectory and accommodation succession analysis proposes a Milankovitch-dominated glacio-eustatic control on the high-frequency cyclicity of the Gallup system.

Chapter 4 documented the detailed depositional environmental facies associations of the Gallup system. The deposition of this paralic depositional environment was controlled by a variety of processes and shows diverse environmental facies associations. Based on analyses of 1D sedimentological measured sections and 2D correlation, five facies associations have been identified, consisting of offshore shelf, shoreline sandstone, delta, coastal plain, and fluvial. Genetic relationships between sequence stratigraphic systems tracts and facies associations have been found, which show that particular facies are only favored in specific systems tracts. High-resolution paleogeographic maps have been firstly reconstructed in the Gallup system. These paleogeographic maps with stratigraphic controls show the dynamic mixed-process dominated deposition. Significant fluvial and tidal influence has been observed in association with wave and storm processes. Transitions between deltaic and shoreface deposits have been depicted using the observation of vertical and lateral shoreline facies variations. The distinction between shoreface and wave deltaic sandstones has been clearly defined on the basis of key criteria, such as trace fossils and river input. An asymmetrical delta model in the Gallup

system has also been revealed. The asymmetrical delta may be formed by locally enhanced clockwise longshore currents, which further demonstrates the mixed-process depositional environment of the Cretaceous Western Interior Seaway.

5.2 Future Work

In the light of the significant contribution made by the research incorporated in this dissertation, more work is needed to further address remaining unknowns. The future research may focus on aspects as follows.

Outcrops provide the most continuous and visible data; however, they tend to be two-dimensional and lack three-dimensional extension. The high-resolution sequence stratigraphic framework established in this dissertation is based on 2D outcrop data with limited 3D resolution. Subsurface data can be used to remedy the lack of 3D coverage. San Juan Basin is one of the most petroliferous basins in the word, yielding tremendously large volume of subsurface data, particular well logs. Extended from outcrops, the sequence stratigraphic work needs to be tied to subsurface well log data for more advanced results. The combination of outcrop and well log data is ideal for such high-resolution study, as to the mutual benefit between the high-resolution visualization of outcrop data and the areal coverage of subsurface data.

The integration of subsurface data can also be applied to the paleogeographic reconstruction. With a 3D sequence stratigraphic framework, depositional facies can be analogized from outcrop analysis to well logs, resulting in a 3D distribution of various facies associations. Paleogeography can thereby be reconstructed using the areal distribution of faces with accurately-dated time slices.

Facies architectural analysis (architectural element scale) is also very important to completely understand depositional evolution and processes. The results can improve depositional models and provide insights into environmental facies morphologies. A facies architectural analysis of particular facies associations, such as distributary channels and river mouth bars of deltas and unit bars of fluvial systems will be of help in understanding their depositional processes and their relative dominance. The analysis will also help us to decipher the inherent differences regarding the deposition of various facies.

Drone technology has been increasingly applied into geological research. Preliminary work has shown the advantage of drone application in terms of continuously imaging outcrops and 3D stratal model building. Give the extensive and continuous outcrops around the San Juan Basin, a drone project can definitely improve outcrop imaging continuity and quality. This work will subsequently help to improve 3D prediction of sequence stratigraphy.

A well-established sequence stratigraphic framework provides chronological controls on sediment quantification of S2S systems. The linkage between sufficiently-documented upstream trunk channels and well-mapped downstream deltas or shorefaces in a parasequence that is dominated by Milankovitch precession cycles is used to apply the fulcrum analysis to estimate sediment budgets. We have mapped out forced regressive deltas and shorefaces with their linked upstream channels at various stratigraphic levels through time. It is worth examining the total sediment balance within a S2S system by comparing sediment delivered by channels and deposited in those basinal deposits to test

the quantitative approach (Lin & Bhattacharya, 2017), which can be applied to S2S basin analysis and hydrocarbon exploration, especially in the frontier basins with limited data.

Several researchers have realized and documented the problems of the conventional sequence stratigraphic model for coastal shallow marine realms (sensu Van Wagoner et al., 1988), such as the diachroneity of a composite sequence boundary that consists of a serious diachronous basal surfaces of incised channels (Strong & Paola, 2008; Bhattacharya, 2011; Holbrook & Bhattacharya, 2012; Lin et al., in revision), or even the composite SB ever existed (Pattison, 2018). It is urgent to incorporate all the documented examples from outcrop and subsurface data, integrated with advanced analytical approaches, such as shoreline trajectory and accommodation succession, to propose a new sequence stratigraphic model for shallow marine environments. The key work for defining a new sequence stratigraphic model falls on high-resolution sequence stratigraphic analysis of nonmarine to marine transition realms. Detailed sequence stratigraphic correlations of those nonmarine and their genetically related marine strata would help to decipher the temporal and spatial evolution and to develop the new model.

REFERENCES

Ainsworth, R.B., Vakarelov, B.K., and Nanson, R.A. (2011). Dynamic spatial and temporal prediction of changes in depositional processes on clastic shorelines: Toward improved subsurface uncertainty reduction and management. AAPG Bulletin, 95, 267–297.

Allen, P. A. (2008). From landscapes into geological history. Nature, 451, 274–276.

Bhattacharya, J.P. (2010). Deltas. In: Facies Models 4 (Eds N.P. James and R.W. Dalrymple), Geological Association of Canada, GEOtext, 6, 233–264.

Bhattacharya, J.P. (2011). Practical problems in the application of the sequence stratigraphic method and key surfaces: integrating observations from ancient fluvial-deltaic wedges with Quaternary and modelling studies. Sedimentology 58, 120–169.

Bhattacharya, J.P., Copeland, P., Lawton, T.F., and Holbrook, J. (2016). Estimation of source area, river paleo-discharge, paleoslope, and sediment budgets of linked deep-time depositional systems and implications for hydrocarbon potential. Earth Science Reviews, 153, 77–110.

Bridge, J.S. (2002) Characterization of fluvial hydrocarbon reservoirs and aquifers: problems and solutions, Asociación Argentina de Sedimentología Revista, 8, 87-114.

Coleman, J.D., and Wright, L.D. (1975). Modem river deltas: variability of processes and sand bodies. In: Deltas: Models for Exploration (Ed M.L. Broussard), Houston Geological Society, pp. 99–149.

Hilgen, F.J., Hinnov, L.A, Abdul Aziz, H., Abels, H.A, Batenburg, S., Bosmans, J.H. C., … Zeeden, C. (2015) Stratigraphic continuity and fragmentary sedimentation: the success of cyclostratigraphy as part of integrated stratigraphy. In: Strata and Time: Probing the Gaps in Our Understanding (Eds D.G. Smith, R.J. Bailey, P.M. Burgess, and A.J. Fraser), Geological Society, London, Spec Publ., 404, 157–197.

Holbrook, J.M., and Bhattacharya, J.P. (2012) Reappraisal of the sequence boundary in time and space: Case and considerations for an SU (subaerial unconformity) that is not a sediment bypass surface, a time barrier, or an unconformity. Earth-Science Reviews 113, 271–302.

Kauffman, E.G. and Caldwell, W.G.E. (1993) The Western Interior Basin in space and time. In: Evolution of the Western Interior Basin (Eds W.G.E. Caldwell and E.G. Kauffman), Geological Association of Canada, Spec. Pap., 39, 1–30.

Lin, W. and Bhattacharya, J.P. (2017) Estimation of source-to-sink mass balance by a fulcrum approach using channel paleohydrologic parameters of the Cetaceous Dunvegan Formation, Canada, Journal of Sedimentary Research, 87, 97–116.

Miall, A.D. (1985). Architectural-element analysis: a new method of facies analysis applied to fluvial deposits, Earth Science Reviews, 22, 261-308.

Miall, A.D. (2013). Sophisticated stratigraphy. In: The web of geological sciences: Advances, impacts and interactions (Ed M.E. Bickford), Geological Association of America, Spec. Pap., 500, 169-190.

Miller, K.G. et al. (2005). The Phanerozoic Record of Global Sea-Level Change. Science, 310, 1293–1398.

Mitchum, R.M., Vail, P.R., and Thompson, S. (1977). Seismic stratigraphy and global changes of sea level, Part 2: The depositional sequence as a basic unit for stratigraphic analysis: Section 2. Application of seismic reflection configuration to stratigraphic interpretation. In Seismic Stratigraphy-Applications to Hydrocarbon Exploration (Ed C.E. Payton), AAPG Memoir 62, 53–62.

Pattison, S.A.J. (2018) Using classic outcrops to revise sequence stratigraphic models : Reevaluating the Campanian Desert Member (Blackhawk Formation) to lower Castlegate Sandstone interval , Book Cliffs , Utah and Colorado , USA. Geology, 46, 1–4.

Sageman, B.B., Rich, J., Arthur, M.A., Birchfield, G.E., and Dean, W.E. (1997) Evidence for Milankovitch periodicities in Cenomanian-Turonian lithologic and geochemical cycles, Western Interior U.S.A. Journal of Sedimentary Research, 67, 286-302.

Steel, R.J., and Milliken, K.L. (2013) Major advances in siliciclastic sedimentary geology, 1960-2012. In: The web of geological sciences: Advances, impacts and interactions (Ed Bickford, M.E.), Geologicl Society of America, Spec. Pap., 500, 121-167.

Strong, N. and Paola, C. (2008) Valleys that never were: Time surfaces versus stratigraphic surfaces, Journal of Sedimentary Research, 78, 579-593.

Sømme, T.O., and Jackson, C. a L. (2013). Source-to-sink analysis of ancient sedimentary systems using a subsurface case study from the Møre-Trøndelag area of southern Norway: Part 2 - sediment dispersal and forcing mechanisms. Basin Research, 25, 512–531.

Tuttle, M.L.W., Charpentier, R.R., and Brownfield, M.E., (1999) The Niger Delta petroleum system: Niger Delta Province, Nigeria, Cameroon, and Equatorial Guinea, Africa: US Department of the Interior. US Geological Survey.

Tyler, N. and Finley, R.J., (1991) Architectural controls on the recovery of hydrocarbons from sandstone reservoirs. In The three-dimensional facies architecture of terrigenous clastic sediments, and its implications for hydrocarbon discovery and recovery (Eds A.D. Miall and N. Tyler), SEPM, Concepts and models in sedimentology and paleontology, 3, 1-5.

Vakarelov, B.K., Bhattacharya, J.P., and Nebrigic, D.D. (2006) Importance of high-frequency tectonic sequences during greenhouse times of Earth history, Geology, 34, 797–800.

Van Cappelle, M., Hampson, G.J., and Johnson, H.D. (2018). Spatial and temporal evolution of coastal depositional systems and regional depositional process regimes : Campanian Western Interior Seaway , U. S. A. Journal of Sedimentary Research 88, 873–897.

Van Wagoner, J., Posamentier, H.W., Mitchum, R.M., Vail, P.R., Sarg, J.F., Loutit, T.S., and Hardenbol, J. (1988). An overview of the fundamentals of sequence stratigraphy and key definitions. In Sea-Level Changes – An Integrated Approach (Eds C.K. Wilgus, B.S. Hastings, C.A. Ross, H. Posamentier, J. Van Wagoner, C.G. and St. C. Kendal), SEPM, Spec Publ., 42, 39–45.

Yoshida, S., Steel, R.J. and Dalrymple, R.W. (2007) Changes in depositional processes-an ingredient in a new generation of sequence-stratigraphic models. Journal of Sedimentary Research 77, 447–460.